The effect of modulating the dystrophic skeletal muscle environment on donor satellite cell engraftment

Bruno Doreste Gonzalez

UCL Great Ormond Street Institute of Child Health

University College London

Thesis submitted to University College London in fulfilment of the requirements for the title of Doctor of Philosophy

June 2018

I, Bruno Doreste Gonzalez, confirm that the work presented in this thesis is my own. Where information has been derived from other sources, I confirm that this has been indicated in the thesis.

Abstract

Satellite cells derived from normal donor mice contribute to muscle regeneration and restore dystrophin expression when transplanted into dystrophin-deficient mice (*mdx*$^{nu/nu}$). However, unless the local host muscle environment has been modulated with high doses of gamma-radiation to incapacitate host satellite cells, but maintaining a functional niche, donor satellite cell engraftment is negligible. This work aimed to determine the cells and pathway(s) within host muscle which are responsible for mediating the radiation-induced effect.

I first investigated whether this effect was mediated by apoptotic cells, by quantifying the percentage of TUNEL positive cells in muscles at basal levels and at different time points after irradiation. There was a correlation between the percentage of TUNEL positive cells and the time for optimal engraftment in *mdx*$^{nu/nu}$ host muscles. This suggests that apoptotic cells within host muscle might be mediators of the radiation-induced promotion of donor satellite cell engraftment.

Then I performed a series of co-transplantation experiments to determine whether different cell preparations within the pre-irradiated *mdx*$^{nu/nu}$ muscle would enhance donor satellite cell transplantation. Three cell preparations (satellite cells, monocytic cell suspension, and single myofibres) were isolated from pre-irradiated *mdx*$^{nu/nu}$ donors and grafted with donor *3F-nLacZ-2E* satellite cells into *mdx*$^{nu/nu}$ hosts. None of these preparations significantly enhanced donor satellite cell engraftment in non-irradiated hosts.

Finally, I performed RNA sequencing on differentially treated muscles to investigate possible signalling pathways involved in enhancing satellite cell

engraftment in pre-irradiated muscles. This revealed a phenotype consistent with type I and type II interferon responses after irradiation, leading to the secretion of the IL-6 family of cytokines. Further investigation confirmed an upregulation of LIF in pre-irradiated muscle. Overall, my findings suggest that irradiation of host muscle alters the inflammatory phenotype and elicits the secretion of the IL-6 family of cytokines, which are powerful regulators of satellite cell proliferation and differentiation.

Impact Statement

One of the key limiting factors in the development of cell therapies for muscular dystrophies such as Duchenne Muscular Dystrophy (DMD) is the poor engraftment of donor satellite cells within the host muscle. Prior research by Boldrin et al 2012 and Morgan et al 2002, has shown that host muscle pre-irradiation is capable of dramatically increasing the efficiency of satellite cell and myoblast transplants within skeletal muscle, leading to the generation of large amounts of muscle of donor origin.

This radiation induced effect is dose, dose-rate, and time dependent. Furthermore, complete ablation of the host's satellite cells inhibits the enhancement of donor cell engraftment. Together, this suggests that the radiological damage within the host muscle is triggering an active process that promotes satellite cell proliferation within the host tissue. However, no obvious signs of inflammation are observed in irradiated muscles (up to 25Gy). This project aimed to determine what changes occurred within irradiated muscles to mediate this effect, and determine which cells are responsible.

The research within this thesis suggests that lethally damaged cells (TUNEL positive), either apoptotic or senescent, increase within the host dystrophic muscle at the time points when satellite cell engraftment is enhanced. TUNEL positive cells are located within the muscle stroma, not the post-mitotic myofibres or satellite cells, as there were no TUNEL positive nuclei within the basal lamina. The increase in TUNEL positive cells post-irradiation did not occur in irradiated non-dystrophic muscles, and engraftment in pre-irradiated non-dystrophic host muscles is negligible.

Co-transplantation experiments indicate that neither pre-irradiated satellite cells nor single muscle fibres alone are able to enhance engraftment of donor satellite cells within non-irradiated host muscles. Conversely, single cell suspensions from pre-irradiated muscles show a trend towards an enhanced engraftment efficiency, although this was not statistically significant. Further research on the cell types necessary to enhance donor satellite cell engraftment may lead to protocols where satellite cells are grafted with other cell types (for example, senescent fibroblasts) to facilitate their engraftment in skeletal muscle.

RNA-sequencing was performed in mdx nude muscles, collected 3 days after irradiation, irradiation and grafting, or irradiation and sham injection. Gene-set enrichment analysis suggests the activation of an inflammatory response, with a strong role for interferon gamma and alpha. Network analysis indicates a prominent role for interferon regulatory factors, IL-6, and Toll-like receptors. Together, these are consistent with a tissue specific inflammatory response due to the release of Damage Associated Molecular Patterns from lethally damaged cells, or that host irradiation leads to the presence of senescent cells within the tissue. Senescent cells are known to secrete a cocktail of inflammatory cytokines known as the Senescence Associated Secretory phenotype, which may also promote donor cell engraftment.

Together this research highlights the importance of damaged cells in modulating the host muscle environment to become receptive to stem cell transplants. Further dissection of the key inflammatory cytokines released will inform further research to enable the translation of cell therapies for DMD into the clinic.

Acknowledgements

I am extremely thankful to my supervisors, Prof. Jennifer Morgan and Dr Silvia Torelli, for their guidance, support, and saintly patience throughout my PhD. Their experience and knowledge has been of invaluable help throughout this project. Importantly, I would like to thank them for making my PhD a thoroughly enjoyable, pleasant, and memorable experience that I am certain would be the envy of many PhD students.

I must also express my gratitude to all the members, past and present, of the Dubowitz Neuromuscular Unit for the advice and support. In particular, I would like to thank Dr Jinhong Meng for all our informal discussions, as well as the wealth of tacit knowledge that I have acquired by working alongside her during the past 4 years. Additionally, I would like to express my gratitude to Dr Jacob Ross, not only for his help during the co-transplantation experiments, which was pivotal in allowing their execution, but also for his advice, support, patience, and friendship.

A special thank you to all my friends for their support and encouragement. I would like to extend a special mention to my friends Sarah Hester and Lucy Congreve. Importantly, I would also like to thank my dear friend, Dr Catherine Ennett, whose friendship, unwavering support, and incomparable wit have kept me in good spirits throughout this project.

Most importantly, words cannot express my gratitude to my family, especially parents, for their unconditional support, for sacrificing so much to ensure I could pursue my ambitions, and for striving to provide me with the best opportunities in life.

Finally, I would like to thank Muscular Dystrophy UK for providing the funding required to carry out this work.

Author's Presentations and Publications

Presentations

- 44th European Muscle Conference, Warsaw, Poland, 21st -25th September 2015. Poster presentation – "Cellular Compartments responsible for the augmentation of satellite cell engraftment within dystrophic skeletal muscle"
- Neuromuscular Translational Research Conference, 13th November 2015, Poster Presentation, Title: "Cellular Compartments responsible for the augmentation of satellite cell engraftment within dystrophic skeletal muscle"
- UK Neuromuscular Translational Research Conference, 2017 - Poster Presentation. Title: "Understanding how ionising radiation enhances satellite cell engraftment in mdxnu/nu skeletal muscle"
- Developmental Neuroscience Seminar Series, Wednesday 26th April 2017 Title: "The Effect of Modulating the Dystrophic Muscle Environment on donor stem cell engraftment"

Publications

- Doreste B., Torelli, T., and Morgan, J.E., (2018) 'The role of damaged cells within pathological skeletal muscle in promoting the engraftment of transplanted stem cells' – In preparation of publication
- Boldrin, L., Ross, J. A., Whitmore, C., Doreste, B., Beaver, C., Eddaoui, A., Pearce, D. J., and Morgan, J. E. (2017) 'The effect of calorie restriction on mouse skeletal muscle is sex, strain, and time dependent', *Scientific Reports,* 7(1). doi: 10.1038/s41598-017-04896-y.

Table of Contents

List of Figures

List of Tables

List of Abbreviations

- **^{137}Cs:** Caesium, isotope 137
- **BINGO:** Biological Networks Gene Ontology (BINGO) Tool
- **cDNA:** Copy DNA
- **Corr p-value:** Corrected p-value
- **COX2:** Cyclooxygenase 2
- **DAMPs:** Damage Associated Molecular Patterns
- **DAPI:** 4', 6-diamidino-3-phenylindole
- **DDR:** DNA Damage Response
- **DMD:** Duchenne Muscular Dystrophy
- **DMEM:** Dulbecco's Modified Eagle Medium
- **DNA:** Deoxyribonucleic Acid
- **dsDNA:** double stranded DNA
- **dsRNA:** Double Stranded RNA
- **EDL:** Extensor Digitorus Longus
- **EP4:** Prostaglandin Receptor 4
- **ES:** Enrichment Score
- **FBS:** Foetal Bovine Serum
- **FDR q-val:** False Discovery Rate q-value
- **FDR:** False Discovery Rate
- **FWER:** Familywise-error rate

- **GFP:** Green Fluorescent Protein
- **GO:** Gene Ontology
- **GSEA:** Gene Set Enrichment Analysis
- **Gy:** Gray
- ***Ifi204:*** Interferon Activated Gene 204
- ***Ifng*/INFγ:** Interferon Gamma
- ***IL-6:*** Interleukin 6
- **IQR:** Interquartile Range
- **IR:** Irradiation
- ***Irf7*:** Interferon Regulatory Factor 7
- **LIF/*Lif*:** Leukaemia Inhibitory Factor
- **M*dx*$^{nu/nu}$:** mdx nude mouse
- **mRNA:** Messenger RNA
- **MyD88:** Myeloid differentiation primary response protein 88
- **NES:** Normalised Enrichment Score
- **NFκB:** nuclear factor kappa-light-chain-enhancer of activated B cells
- **NOM p-value:** Nominal p-value
- **Padj:** Adjusted p-value
- **PAMPs:** Pathogen Associated Molecular Patterns
- **Pax7:** Paired box 7
- **PBS:** Phosphate Buffered Saline
- **PC1:** Principal Component 1
- **PC2:** Principal Component 2

- **PCA:** Principal Component Analysis
- **PCR:** Polymerase Chain Reaction
- **PFA:** Paraformaldehyde
- **PGE_2:** Prostaglandin E_2
- **PPR:** Pattern Recognition Receptors
- **RiN:** RNA Integrity Number
- **RNA-seq:** RNA Sequencing
- **RNA:** Ribonucleic Acid
- **RNS:** Reactive Nitrogen Species
- **ROS:** Reactive Oxygen Species
- **RT-qPCR:** Reverse Transcriptase Quantitative Polymerase Chain Reaction
- **SASP:** Senescence Associated Secretory Phenotype
- **SEM:** Standard Error of the Mean
- **STRING:** Search Tool for the Retrieval of Interacting Genes/Proteins
- **Sv*:*** Sievert
- **TA:** Tibialis Anterior
- **TLR/*Tlr*:** Toll-like Receptor
- **TNFα:** Tumour Necrosis Factor Alpha
- **TUNEL:** Terminal Deoxynucleotidyl Transferase dUTP Nick End Labeling
- **WT:** Wild Type
- **X-Gal:** 5-bromo-4-chloro-3-indolyl-ß-galactopyranoside

Chapter 1 - Introduction

1.1) Introduction

Skeletal muscle is a highly specialised tissue consisting of striated, post-mitotic myofibres that act to generate force and movement. Normally skeletal muscle has a low turnover, but possesses a remarkable capacity for growth, and regeneration upon injury and during pathological conditions. The regeneration of skeletal muscle is mediated by muscle stem cells – termed satellite cells – which upon activation proliferate to produce myoblasts. These myoblasts fuse and differentiate to repair or replace damaged myofibres and replenish the stem cell pool (reviewed by Relaix & Zammit 2012).

Cell therapies provide a promising avenue for the treatment of muscle wasting conditions such as Duchenne Muscular Dystrophy (DMD). However, muscle is remarkably hostile to the grafting of donor cells and the tissue must first be experimentally altered to permit their successful engraftment of cells, and the formation of muscle of donor origin. The pre-irradiation of host muscles with high localised doses of ionising radiation (x-rays or gamma-radiation) has proven to be the most successful avenue to generate a host muscle environment that enhances the grafting of myoblasts (Morgan et al. 2002) and satellite cells (Boldrin et al. 2012) generating a high number fibres of muscle of donor origin (Morgan et al. 2002; Boldrin et al. 2012; Collins et al. 2005).

This chapter will provide an overview of the structure of skeletal muscle, its regeneration mediated by satellite cells, potential therapies for DMD with a focus on cell therapies, as well as the nature of radiobiological injuries and a potential way by which this form of injury is able to augment satellite cell engraftment.

1.2) Skeletal Muscle Structure

Skeletal or striated muscle is a highly specialised tissue that is responsible for the movement of the skeleton, tongue, and diaphragm. It is predominantly composed of elongated bundles of myofibres – termed fasciculi - that contract to generate directional force. Individual myofibres are separated by a delicate sheath of collagenous tissue called the endomysium. Each fasciculus is surrounded by a loose collagenous sheath called the perimysium, and the several fasciculi that make each muscle are encased in a denser sheath called the epimysium. These connective tissues are continuous with those of the tendons and muscle attachments, and supply muscle with nerves and blood vessels (Thakali et al. 2012).

The functional unit of skeletal muscle is the long cylindrical muscle fibre that generates force by contraction. Each myofibre is filled with myofibrils composed of thousands of sarcomeres that contain the actin and myosin filaments that interact to produce force. These myofibres are multinucleated, and are formed by the fusion of many myoblasts during embryonic and foetal development (Mintz & Baker 1967; Zammit & Beauchamp 2001). These fibres do not replicate and are considered post-mitotic.

The post-mitotic nature of myonuclei was first demonstrated by Stockdale and Holtzer, who cultured embryonic chick muscle cells in ^{3}H-thymidine. The

radioactive thymidine was rapidly incorporated into the nuclei of mononucleate myoblasts, but only detected in the nuclei of multinucleated myotubes after they had been generated by fusion of the already labelled mononucleate cells (Stockdale & Holtzer 1961). The first observation that muscle could be formed by the differentiation of mononucleate cells is commonly attributed to Harrison (1910) who, by performing early tissue culture experiments, reported that cross-striated fibres were generated from myoblasts emanating from tadpole myotome explants (Harrison 1910). However, in this work the fusion of myoblasts was not directly observed. Later, the *in vitro* formation of myotubes by fusion of mononucleate precursors was observed directly in clonal cultures of chick embryo myoblasts (Konigsberg 1961, 1963); by using time-lapse photography (Cooper & Konigsberg 1961); and by the co-culturing of ^{3}H-thymidine labelled and unlabelled rat myoblasts (Yaffe & Feldman 1965).

These *in vitro* observations were recapitulated in the generation of chimeric mouse embryos from homozygotic paternal strains expressing different isoforms of the metabolic enzymes nicotinamide-adenine dinucleotide phosphate (NADP)-dependent isocitrate dehydrogenase (Mintz & Baker 1967) and glucose phosphate isomerase (GPI) (Gearhart & Mintz 1972). The formation of heteromeric isoforms of these enzymes in the chimeric muscles demonstrated that nuclei derived from both parental strains shared the same cytoplasm in mosaic myofibres (Mintz & Baker 1967; Gearhart & Mintz 1972). In adult tissues a similar mechanism was demonstrated by labelling rat muscles with ^{3}H-thymidine, only the mononucleated precursors incorporated the radioactive label. When the labelled muscles were removed, minced, and grafted into non-labelled rats the multinucleated myofibers

of the hosts were labelled, demonstrating that mononucleated cells differentiated into myofibres in adult muscles (Snow 1978). Furthermore, using different isoenzymes of malate dehydrogenase, Partridge et al. (1978) showed that when donor myoblasts expressing only one isoform were grafted into the muscles of hosts expressing a different isoform of the enzyme, it led to the expression of heteromeric enzymes, demonstrating the fusion of muscle precursor cells with host muscles (Partridge et al. 1978).

Together, these studies showed that throughout developmental myogenesis and adult regeneration, muscle fibres form from mononucleated precursors, and muscle fibres themselves are post-mitotic. The origin of these mononucleate precursors (myoblasts) in adult muscle are discussed in the following section (1.3).

1.3) Satellite Cells

1.3.1) Satellite Cells as Endogenous Muscle Stem Cells

Although it was demonstrated that muscle regeneration needs a pool of mononucleate precursors, termed myoblasts, that divide, fuse, and differentiate to repair or produce multinucleated muscle fibres (section 1.2), their origin remained unknown. Using electron microscopy to image frog muscle fibres, Mauro (1961) discovered a type of cell closely associated with the muscle fibre, that was located

between the sarcolemma (muscle fibre membrane) and the basal lamina which sheaths the whole fibre (figure 1.1).

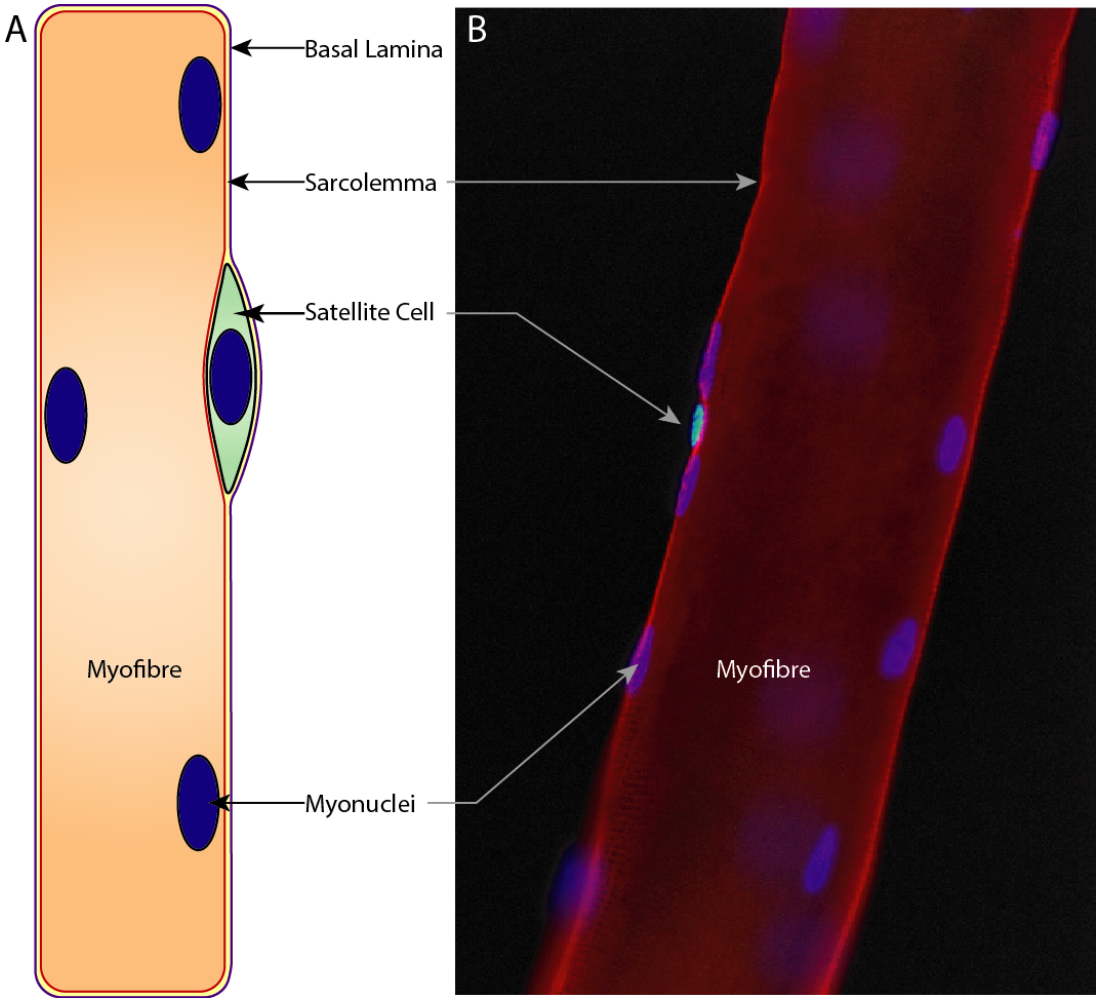

Figure 1.1: Localisation of the satellite cell. A) Schematic representation of a single muscle fibre with an associated satellite cell between the sarcolemma (red) and the basal lamina (purple). B) Immunofluorescent image of a single muscle fibre stained for dystrophin to mark the localisation of the sarcolemma (red), Pax7 (green) marking the nuclei of the satellite cell, and nuclei stained blue (DAPI).

These cells had an extremely small cytoplasm leading to them to acquire the shape of the nucleus, with the cell protruding inwards, towards the multinucleated muscle fibre. He chose to call them satellite cells and hypothesised that they may be dormant myoblasts, which are deployed in the event of damage into the multinucleated fibre (Mauro 1961). The same month Katz (1961) observed the same cells, also in the frog. They were subsequently observed in human, cat, dog (Ishikawa 1966), mouse and fruit bat skeletal muscles (Muir et al. 1965; Venable 1966). The lack of continuity between the satellite cell cytoplasm and that of the muscle fibre was also confirmed, as the satellite cells were shown to be resistant to the osmotic swelling of their associated myofibre (Muir et al. 1965). Several studies in rodents confirmed the involvement of satellite cells in muscle growth and regeneration (Moss & Leblond 1971; Bischoff 1975; Cardasis & Cooper 1975; Konigsberg et al. 1975; Snow 1978). However, their role as muscle stem cells remained in question, in particular in light of the description of bone marrow cells with myogenic potential (Ferrari et al. 1998; LaBarge & Blau 2002). This question was finally resolved when in 2005 Collins et al. performed grafts of single intact donor myofibres (with their associated satellite cells) from *3F-nLacZ-2E* mice (section 2.1.3) into radiation-ablated tibialis anterior (TA) muscles of mdx-nude mice (section 2.1.2). The satellite cells from these muscle fibres, as few as 7 per transplanted fibre, were able to generate over 100 new myofibres containing thousands of myonuclei. These transplanted satellite cells were capable of vigorous self-renewal, expanding in number and repopulating the host muscle with new, donor derived satellite cells. Following experimental injury, the donor-derived satellite cells proliferated extensively and formed large clusters of myofibres even after repeated rounds of injury (Collins et al. 2005). This cemented

the role of satellite cells as the endogenous muscle stem cell, with the ability to give rise to extensive progeny, differentiate, and self-renew.

Although satellite cells have been traditionally identified by their position between the sarcolemma and basal lamina, a variety of molecular markers are available that have make their identification much easier such as Pax7 (Seale et al. 2000), CD34 and the *Myf5nLacZ* reporter (Beauchamp et al. 2000), caveolin-1 (Volonte et al. 2004), calcitonin receptor (Gnocchi et al. 2009), M-cadherin (Irintchev et al. 1994), syndecan-3 and -4 (Cornelison et al. 2001), integrin α7 (Blanco-Bose et al. 2001), and integrin ß1 (Sherwood et al. 2004). However, most of these markers are also expressed in other types of cells, and markers such as CD34 and M-cadherin only mark subsets of satellite cells. For these reasons Pax7 remains the most useful marker for the identification of quiescent satellite cells in a range of animals from fish to humans (reviewed by Kuang & Rudnicki 2008).

1.3.2) Signalling Pathways Regulating Satellite Cell Proliferation, Differentiation, and Self-Renewal

Traditional master regulators of development and growth, including Notch, Wnt, and Sonic Hedgehog signalling have all been implicated in the regulation of satellite cell function.

Notch3 is expressed in quiescent satellite cells, particularly the Myf5-Cre and ROSA26-YFP, which display a high ability to proliferate and produce large amounts of muscle of donor origin (Kuang et al. 2007; Fukada et al. 2007). Satellite cells also express Notch-1 and its inhibitor Numb, while in response to injury its ligand Delta-1 is activated and Numb expression decreases, and this correlates with increases in

satellite cell proliferation (Conboy et al. 2003). Furthermore, foetal myogenic progenitors and postnatal satellite cells are ablated if Notch signalling is impaired through the conditional knockout of RBP-J, a master down-stream mediator of Notch signalling (figure 1.2), in mice (Vasyutina et al. 2007). Similarly, if Delta-1 is ablated, the number of muscle progenitor cells in mouse embryos is severely depleted due to early differentiation of muscle progenitors (Schuster-Gossler et al. 2007). Augmentation of Notch signalling through the ablation of Stra13 in mice ($Stra13^{-/-}$) lead to defects in regeneration marked by the persistence of necrotic myofibres, increased numbers of mononuclear cells, and fibrosis. Primary myoblasts from $Stra13^{-/-}$ mice also exhibited enhanced Notch activity, increased proliferation, and defective differentiation (Sun et al. 2007). In contrast, suppression of Notch signalling by elevated expression of Numb correlates with increased myogenic differentiation *in vitro* (Conboy & Rando 2002). Therefore, Notch signalling is involved in the regulation of quiescence and stem cell status, and the inhibition of differentiation in satellite cells (figure 1.2).

Wnts are powerful morphogens and Wnt/ß-catenin signalling is involved in embryonic morphogenesis and the regulation of adult stem cells function in many systems (Kléber & Sommer 2004). Quiescent satellite cells express Frizzled 7 (Fzd7) and signalling through the Wnt7a/Fzd7 planar-cell-polarity pathway drives the symmetric expansion of satellite cells, but did not affect the growth or differentiation of myoblasts. Wnt7a overexpression in vivo enhanced muscle regeneration and increased satellite cell numbers, while its ablation led to a significant decrease in satellite cell number after regeneration (Le Grand et al. 2009). Over expression of Wnt7a has also been associated with myofibre hypertrophy after regeneration,

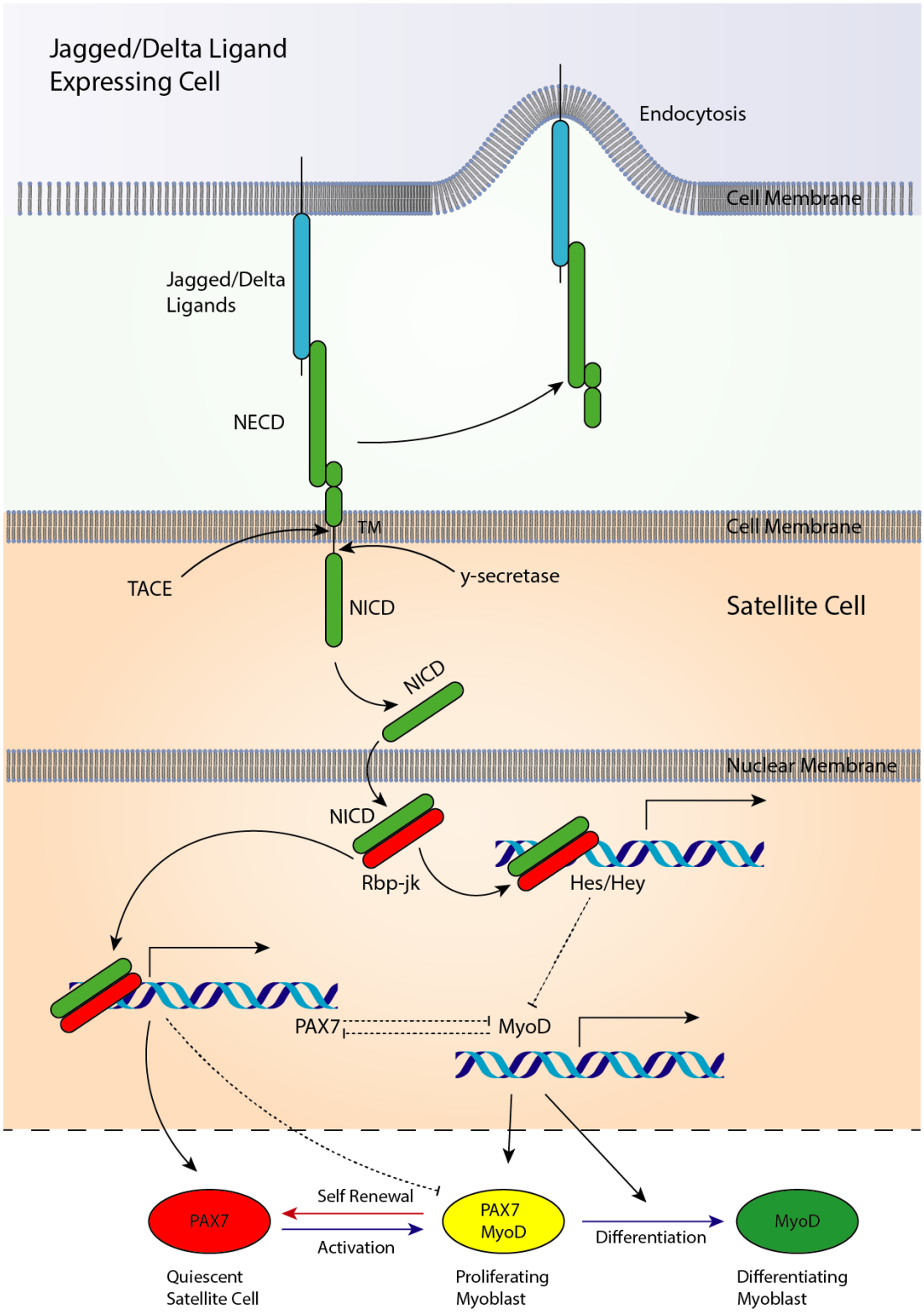

Figure 1.2: Notch signalling pathway regulating satellite cell quiescence, proliferation, and differentiation. Notch receptors are single pass transmembrane proteins, composed of a functional extracellular domain (NECD), a transmembrane domain (TM), and the intracellular domain (NICD). Upon binding to the members of

the Delta-like or Jagged family of ligands the NECD is cleaved from the TM-NICD (*figure 1.2 continued)* domain by TACE (TNF-α ADAM metalloprotease converting enzyme). The NECD remains bound to its ligand and the complex undergoes endocytosis/recycling within the signal sending cell. The NICD in the signal receiving cells is cleaved from the TM by γ-secretase, which releases the NICD. This allows translocation of the NICD to the nucleus where it associates with the transcriptional coactivator Rbp-Jk, resulting in the subsequent activation of the canonical Notch target genes Hes/Hey. In satellite cells, it also mediates Pax7 transcription. Hes/Hey proteins inhibit MyoD transcription. Therefore, Notch activation upregulates Pax7 to promote satellite cell renewal while inhibiting MyoD to block myogenic differentiation. Pax7 upregulation and MyoD downregulation leads to withdrawal from the cell cycle, while the reciprocal inhibition between Pax7 and MyoD further amplifies Notch signalling. Conversely, during activation, satellite cells rapidly downregulate Notch signalling, allowing the expression of MyoD and entry into the cell cycle. During the myoblast amplification phase, high Notch activity in Pax7 expressing myoblasts allows them to remain undifferentiated and replenish the satellite cell pool.

independently from any effects on myoblast proliferation and differentiation, but by instead activating the anabolic Atk/mTOR signalling pathway (von Maltzahn et al. 2011).

The remodelling of the stem cell niche by satellite cells expressing fibronectin also appears to play a role in Wnt7a signalling and satellite cell expansion (Bentzinger et al. 2013). Syndecan-4 (Sdc4) and Fzd7 form a co-receptor complex in satellite cells, and binding of fibronectin to Sdc4 stimulates the ability of Wnt7a to induce the symmetric expansion of satellite cells (figure 1.3). Recently-activated satellite cells remodel their niche by transiently expressing high levels of fibronectin. If fibronectin is knocked down in primary cultures, the ability of satellite cells to repopulate the satellite cell niche is impaired. *In vivo* overexpression of fibronectin with Wnt7a dramatically enhances the expansion of satellite cells in regenerating muscle. This shows that activated satellite cells remodel their niche through autologous expression of fibronectin, which provides a feedback loop to enhance Wnt7a signalling through the Fzd7/Sdc4 co-receptor complex, demonstrating that Wnt7a regulates homeostatic levels of satellite cells during regenerative myogenesis (Bentzinger et al. 2013). Additionally, Wnt7a/Fzd7 can also act on muscle growth and repair to increase the polarity and directional migration of murine satellite cells and human myogenic progenitors through the activation of Svl2 and the small GTPase Rac1 (Bentzinger et al. 2014a). Furthermore, these effects can be employed to potentiate myogenic cell transplantations into dystrophic muscles. This was achieved by exposing cultured primary myoblasts to Wnt7a for 3 hours before transplantation, which led to significant improvements in tissue dispersal and engraftment of donor

cells (Bentzinger et al. 2014a). Taken together this suggests that Wnt7a stimulates the symmetric expansion of satellite cells, their polarity and motility, and is able to directly induce myofibre hypertrophy through Atk/mTOR signalling (figure 1.3). Other Wnt family members may also be involved in the regulation of satellite cell function. For example, by studying single myofibres cultured *in vitro* it has been shown that overexpression of Wnt1, Wnt3a, or Wnt5a causes a dramatic increase in satellite cell proliferation, while exposure to Wnt4 or Wnt6 diminishes proliferation (Otto et al. 2008).

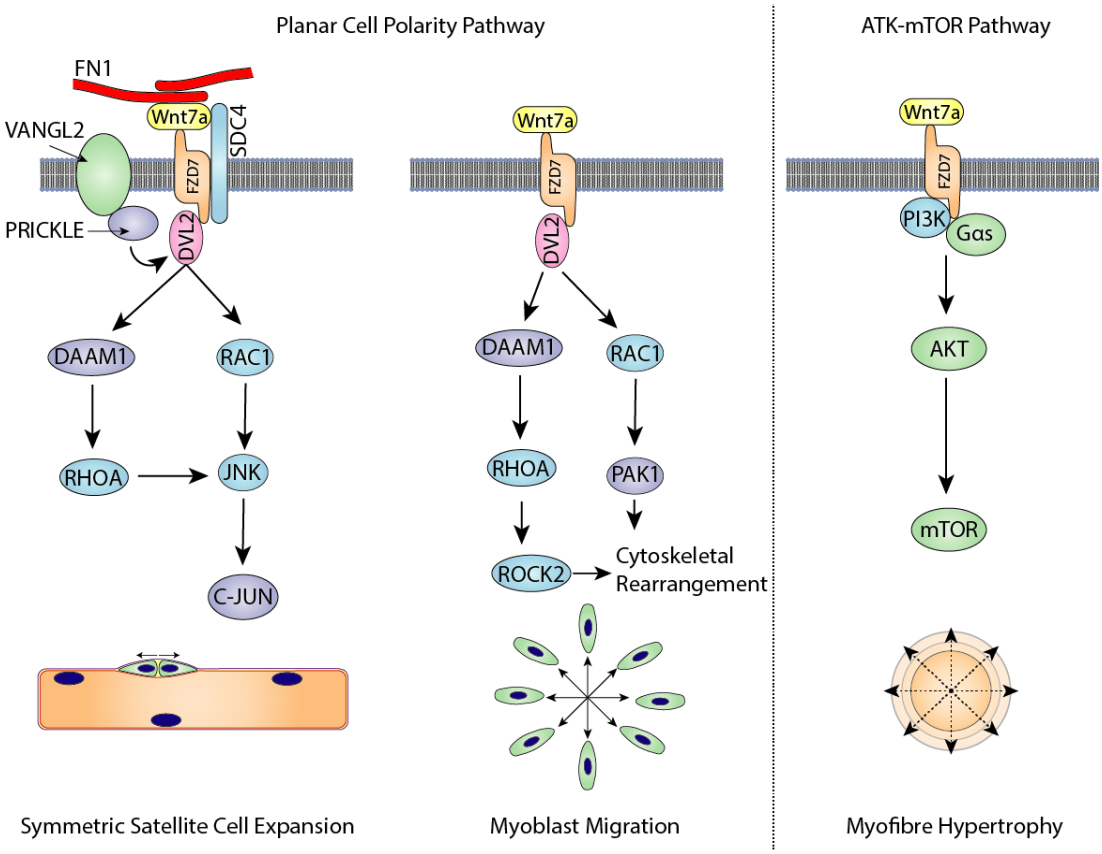

Figure 1.3: Wnt7a induces the symmetric proliferation of satellite cells in conjunction with Fibronectin (FN1), syndeca-4 (SDC4), and Vangl2 through the planar cell polarity pathway (left). In myogenic progenitors Wnt7a also facilitates RAC1 mediated cell polarization and migration. Fusion of myogenic precursors

(figure 1.3 continued) exposed to Wnt7a with myofibres activates the AKT-mTOR pathway, leading to myofibre hypertrophy. Figure adapted from (Bentzinger et al. 2014b).

The Sonic Hedgehog (Shh) pathway is also involved in the control of satellite cell function (figure 1.4). In mammals, there are 3 homologous hedgehog genes: Sonic (*Shh*), Desert (*Dhh*), and Indian hedgehog (*Ihh*). Signalling through the Shh pathways occurs by binding to its receptor Patched1 (Ptch1) which activates the transmembrane protein smoothened (Smo), in turn activating Gli1, Gli2, or Gli3, which then translocate to the nucleus to regulate target gene expression (figure 1.4) (reviewed by: Choudhry et al. 2014). In adult murine muscle regenerating after ischaemia reperfusion injury Shh and Ptch1 are upregulated (Pola et al. 2003), suggesting a role in muscle regeneration. Furthermore, it has been shown to promote satellite cell and C2C12 immortalised myoblast cell line (Yaffe & Saxel 1977; Blau et al. 1983) proliferation, and prevents their differentiation into multinucleated myotubes. Under conditions of serum starvation-induced apoptosis, Shh signalling is also able to inhibit caspase 3 to act as a pro-survival factor (Koleva et al. 2005). In primary chicken myoblast cultures and the mouse C2C12 myogenic cell line, Shh also promotes proliferation, which is reversed by the blockade of the Shh signalling pathway with a chemical inhibitor (cyclopamine). The expression of Shh and that of its downstream molecules also localise adjacent to Pax7 cells in adult muscle sections. It has been shown that Shh signalling acts via the phosphorylation of Atk to enhance myoblast proliferation through the PI3K/Atk pathway (Elia et al. 2007). Furthermore, insulin growth factor-1 (IGF1) has been shown to act synergistically with Shh and Smo to stimulate the expression of myogenic regulatory factors, to

increase the activation of PI3K/Akt, and MAPK/ERK pathways (Madhala-Levy et al. 2012). Inhibition of Shh signalling after injury reduces the required upregulation of Myf5 and MyoD and impairs angiogenesis. This results in reduced satellite cell numbers at the site of damage, and an increased fibrotic and inflammatory reaction, which results in impaired muscle regeneration (Straface et al. 2009).

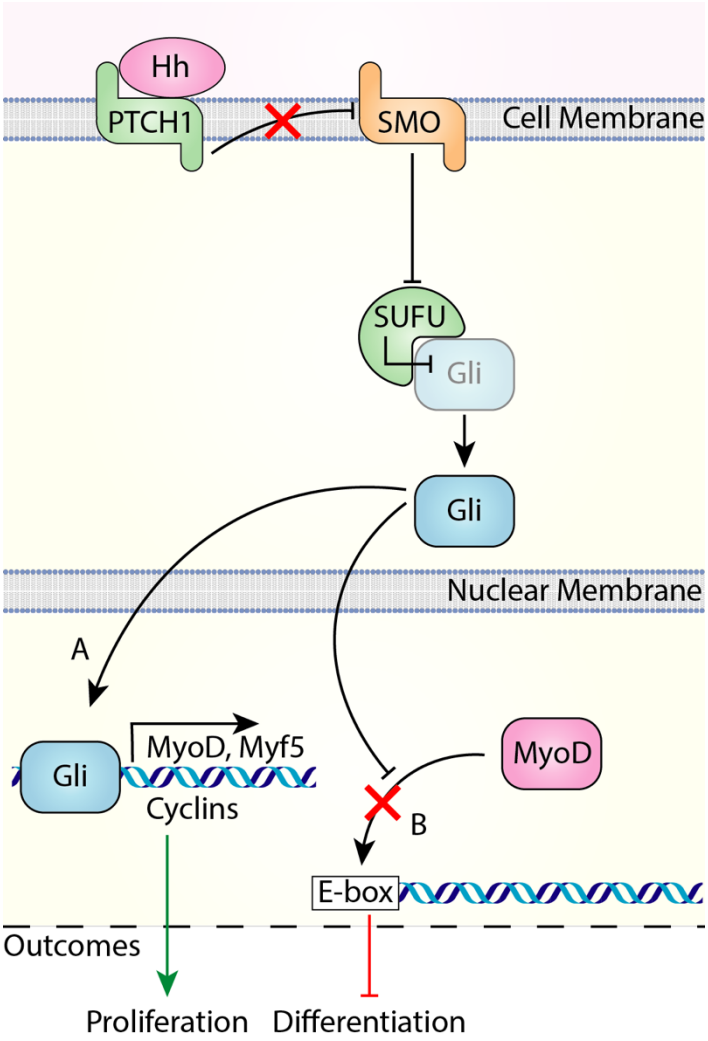

Figure 1.4: Simplified model of Shh signalling in myogenesis. Binding of Hedgehog (Hh) to its ligand Pathed1 (PTCH1) releases the inhibition of Smoothened (SMO). Consequently, SMO is able to block SUFU, preventing the degradation of the Gli family. Gli proteins translocate to the nucleus where they mediate the activation of the MyoD family (*Myod, Myf5*) and cyclins (A). Simultaneously, the Gli family prevents the basic Helix Loop Helix (bHLH) factors from forming heterodimers with E proteins, binding DNA (E-boxes), and activating muscle gene transcription (B). Inhibition of differentiation, and the Shh mediated activation of cyclins leads to the proliferation of myogenic precursors.

Many other factors and signalling molecules also regulate satellite cell function, for example nitric oxide, which incidentally is produced in response to radiation damage (section 1.6), is able to stimulate satellite cell proliferation and their fate in such a way that it prevents the exhaustion of the reserve pool under conditions of severe muscle damage in mice, and the genetic or chemical inhibition of nNOS in skeletal muscle fibres is sufficient to induce a progressive reduction of the regenerative capacity of murine muscles. The increases in satellite cell proliferation appear to be dependent on two pathways, cGMP and the non-canonical Wnt pathway (Wozniak & Anderson 2007; Buono et al. 2012). Other factors such sphingosine 1 phosphate, which induces mouse satellite cells to enter the cell cycle (Nagata et al. 2006), fibroblast growth factor (DiMario et al. 1989; DiMario & Strohman 1988), and insulin-like growth factor (IGF-1) (Hill & Goldspink 2003) all play a part in the regulation of satellite cell proliferation and muscle regeneration. Other signals are also involved in controlling satellite cell function, including stromal cell-derived factor (SDF-1) that binds to chemokine receptors CXCR4 and CXCR7 on myogenic cells to promote differentiation (Melchionna et al. 2010) and M-cadherin that is involved in satellite cell quiescence (Irintchev et al. 1994) and fusion into myotubes (Charrasse et al. 2007). Additionally, other cells within the skeletal muscle may impact satellite cells, for example smooth muscle cells and fibroblasts secrete angiopoietin 1 that is involved in maintaining satellite cell quiescence and self-renewal (Abou-Khalil et al. 2009), or pro-inflammatory macrophages that promote myoblast proliferation *in vivo* (Bencze et al. 2012). However, the control of satellite cell quiescence, activation, proliferation, differentiation, and self-renewal within adult skeletal muscle has yet to be fully understood.

1.4) DMD and Potential Therapies

1.4.1) Duchenne Muscular Dystrophy

Duchenne Muscular Dystrophy (DMD) is the most commonly inherited paediatric muscle disorder. It is an X-linked genetic progressive and degenerative myopathy characterised by characterised by muscle wasting and weakness, which leads to the loss of motor functions in puberty, cardiac and respiratory involvement, and premature death (Mercuri & Muntoni 2013). DMD occurs at a rate of 1:5000 male births (Mendell et al. 2012; Moat et al. 2013) and arises due to random mutations in the dystrophin gene, with 65% of causative mutations consisting of intragenic deletions, 6-10% by intragenic duplications, and 30-35% are point mutations (figure 1.5) (Nallamilli et al. 2014).

The pathology is caused by the absence of dystrophin (figure 1.5), or the synthesis of functionally impotent versions of the protein, which is a critical component of the dystrophin glycoprotein complex which has both mechanical, stabilizing, and signalling roles in mediating the interactions between the cytoskeleton, sarcolemma, and the extracellular matrix (Lapidos et al. 2004). The importance of this protein is highlighted by the pathological features that appear in its absence. Patients are normally diagnosed by the age of 5 and present with muscle weakness, altered gait, muscle pseudohypertrophy, difficulty ambulating, and abnormally high serum levels of creatine kinase, which is an indicator of ongoing muscle degeneration. This muscle degeneration is visible as focal groups of necrotic fibres (Decary et al. 2000; Reinig et al. 2017). As the disease progresses muscle

weakness extends in proximal to distal manner due to repeated rounds of muscle degeneration and regeneration that

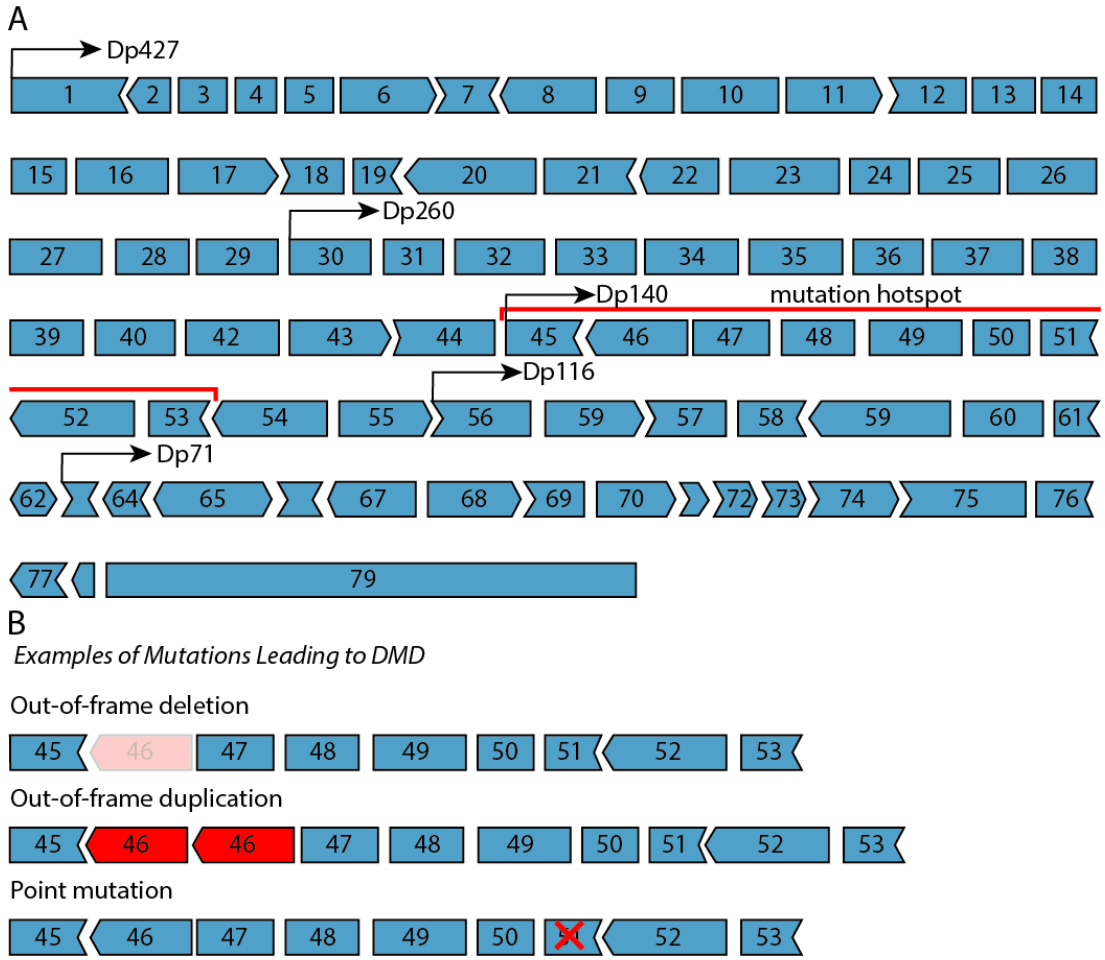

Figure 1.5: A) Structure of the dystrophin gene, including the positions of promoters for different isoforms. The full-length dystrophin (Dp427) has 3 tissue specific promoters, and is expressed in skeletal muscle, brain, and Purkinje cells. The Dp260 isoform is mainly expressed in retina; Dp140 has a promoter in intron 44 and is present in the CNS and kidney; Dp116 has an intron 55 promoter and is predominantly found in Schwann cells. Dp71 is expressed from an intron 62 promoter and plays an important role within the CNS. The area most susceptible to mutations in DMD is highlighted in red (mutation hotspot). B) Examples of mutations leading to the absence of dystrophin, including out-of-frame deletions (65%), duplications (6-10%), and point mutations (30-35%).

eventually deplete the regenerative capacity of skeletal muscle. As a consequence, the contractile tissue is replaced by fibrotic and adipose tissue (figure 1.6) and patients loose ambulation by age 13 (Mercuri & Muntoni 2013). The disease also presents with dilated cardiomyopathy after age 10, which is observed in almost all patients by age 18, with congestive heart failure or sudden death occurring in 20% of patients (Hsu 2010; Mercuri & Muntoni 2013). Degeneration of the diaphragm muscles leads to respiratory complications that eventually require patients to be mechanically ventilated, and these respiratory problems normally culminate in the death of the patient on the third decade of life. Depending on the localisation of the dystrophin mutation patients may also present with cognitive impairment (Anderson et al. 2002). Although there is currently no cure for DMD, significant advances have been made in the development of therapies to target the disease which are discussed in the following sections.

1.4.3) Exon Skipping Agents

Exon skipping is an RNA-based approach to remove mutated or additional exons during mRNA splicing, allowing the restoration of the open reading frame, which in turn allows for the expression of a shorter but partially functional dystrophin (Fairclough et al. 2011; Goyenvalle et al. 2011). Exon skipping relies on antisense oligonucleotides (AONs), chemically synthesised single–strand DNAs, typically 20-30 nucleotides in length, designed to hybridise with a complementary sequence of pre-mRNA. (Arechavala-Gomeza et al. 2012). While several chemistries exist for the development of AONs, the two in clinical development for DMD are 2'O-methylphoshorothioate oligoribonucleotide (2'OMe) and phosphorodiamidate morpholino oligomers (PMO). 2'OMe AONs bind to albumin, showing high plasma

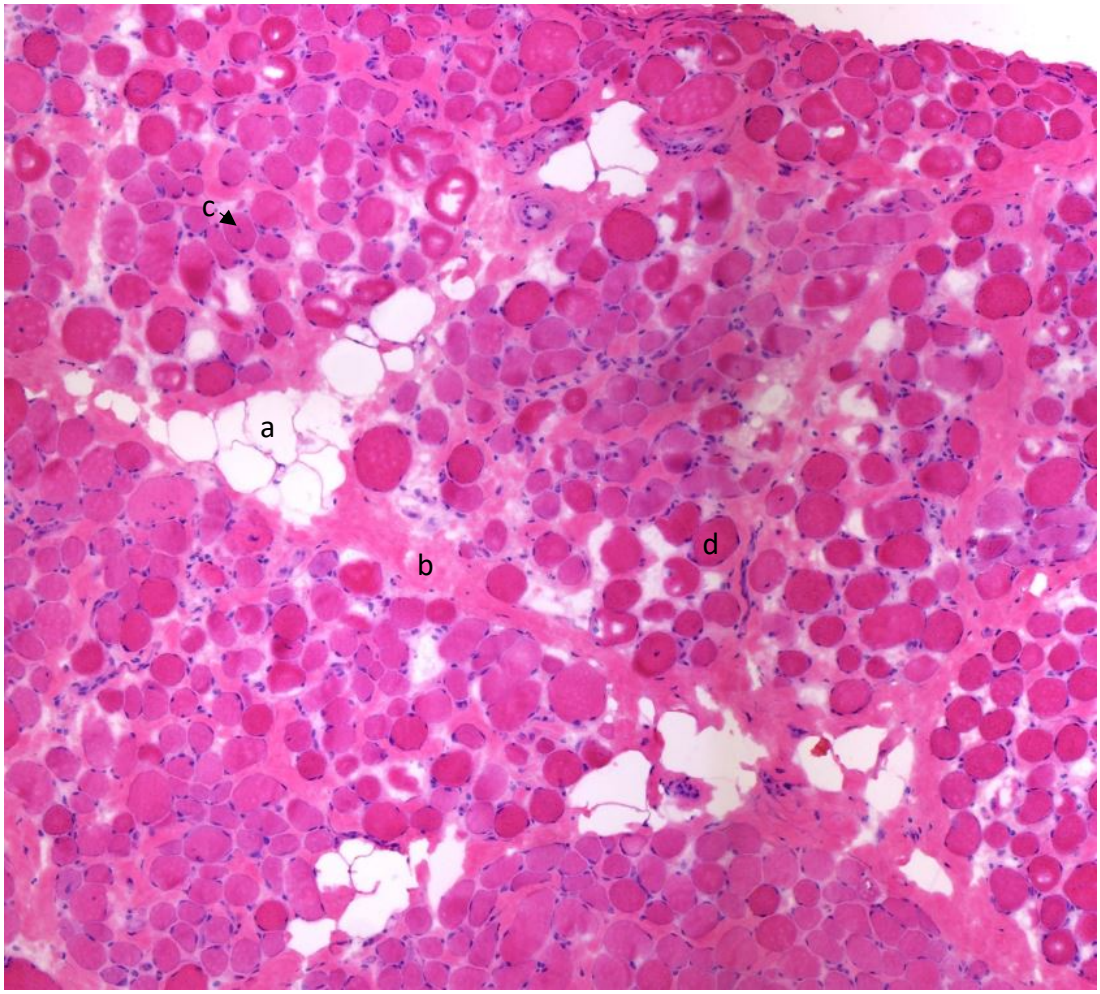

Figure 1.6: Representative image of the muscle pathology of a DMD patient. A large variation in fibre size is observed, along with centrally nucleated fibres (c) indicating muscle regeneration. Large areas of fat deposition (a), fibrotic tissue (b).

concentrations and longer half-lives than PMOs, however this protein binding has been shown to trigger activation of the immune system, anaphylaxis, hypotension, or antiarrhythimic effects in preclinical and clinical studies (Muntoni et al. 2008). PMOs are not metabolised and are resistant to endonucleases (Amantana et al. 2007); they are rapidly removed from the bloodstream and do not bind to serum proteins, which is the likely why they have not been associated with the side effects of 2'OMe. A particularly successful PMO has been the development of the PMO Eteplirsen, designed to skip exon 51 in DMD patients, representing the largest group

(13%) of DMD patients (Aartsma-Rus et al. 2009), which has shown significant increases (52% and 43% under different dose regimes of 30 and 50mg/kg respectively) in dystrophin expression, which translated in clinical improvements with patients displaying a slower rate of decline in ambulation after 3 years (Mendell et al. 2013; Mendell et al. 2016). This has become the first therapy targeting the root cause of DMD to receive conditional FDA approval (https://www.fda.gov/NewsEvents/Newsroom/PressAnnouncements/ucm521263.htm).

1.4.4) Viral Mediated Gene Therapy

There are three types of viral vectors that have primarily been used for research into treatment of muscular dystrophies: adenoviral, adeno-associated viral, and lentiviral vectors (Goyenvalle et al. 2011), although the large size of the dystrophin cDNA has made their use challenging (Fairclough et al. 2011).

Lentiviral vectors are a class of retroviral vectors that stably integrates transgenes into the genomes of quiescent and non-quiescent cells (Kafri et al. 1997; Li et al. 2005). Integration into the host genome, however, can cause insertional mutagenesis leading to the potential activation of proto-oncogenes (Beard et al. 2007; Hacein-Bey-Abina et al. 2003) although at low frequency. Additionally, they have not been shown to achieve widespread transduction of tissues *in vivo* (Kafri et al. 1997; MacKenzie et al. 2005). For example, when used for intramuscular delivery of mini- or micro- dystrophins, they successfully transduce and cause stable retention of transgenes in myogenic stem cells and muscle fibres, but the efficiency is too low for clinical use (Kimura et al. 2010; Kobinger et al. 2003). Consequently they have been mainly use for the stable transduction of myogenic stem cells or stem cell

progenitors and mesoangioblasts which are then used for autologous transplantation (Li et al. 2005; Bachrach et al. 2004; Sampaolesi et al. 2006). Traditionally, truncated but partially functional forms of dystrophin have been packaged into lentiviral vectors, working under the assumption that the dystrophin cDNA is too large to package into viral vectors. However, recent developments by Counsell et al., have shown that it is possible to package loads of more than 15000 base pairs into lentiviral vectors, allowing for the packaging and delivery of full length dystrophin cDNA into DMD myoblasts, which expressed dystrophin at the sarcolemma after differentiation (Counsell et al. 2017).

In contrast to lentiviral vectors, adenoviral vectors do not integrate into the host genome, have reasonably large carrying capacities, are easily produced at high titres (Goyenvalle et al. 2011), although they are more effective in transducing immature or regenerating muscles (Larochelle et al. 2010). However, testing in non-human primates showed the triggering of acute lethal toxicity consistent with the activation of the innate inflammatory response, the severity of which was dose dependent, and independent of viral gene expression (Brunetti-Pierri et al. 2004). Furthermore, in a pilot study to treat an 18 year old male for ornithine transcarbamylase deficiency using an adenoviral vector there was a systemic inflammatory response syndrome 18 hours after gene transfer, leading to his death 98 hours following gene transfer (Raper et al. 2003). These two reports have severely set back the development of adenoviral vectors due to their high immunogenicity.

Adeno-associated viruses are single-stranded DNA paroviruses, and accordingly require a helper virus for replication and assembly (Muzyczka 1992). However, recombinant forms of these viruses (rAAV), despite carrying no viral genes,

can be produced at high titres in the absence of a helper virus and infect both replicating and non-dividing cells (Podsakoff et al. 1994). Stable expression of transgenes following intramuscular rAAV injections has been reported of up to 2 years in mice (Kessler et al. 1996), over 17 months in dogs (High et al. 1999; Monahan et al. 1998), and humans (Manno et al. 2003). Recently rAAV vectors have been employed for successfully skipping dystrophin exons 6 to 8 of the golden retriever muscular dystrophy (GRMD) , dog model of Duchenne Muscular dystrophy, which showed stable expression of dystrophin in myofibres up to 3.5 months after treatment in a dose dependent manner, with up to 80% of myofibres expressing dystrophin at the highest dose and showing clinical improvement (Le Guiner et al. 2014). Additionally, there are several ongoing human clinical trials to treat neuromuscular disorders using AAV-based gene therapy. These include safety studies on the transfer of a mini-dystrophin construct (Mendell, Campbell, et al. 2010); alpha-sarcoglycan expression in patients with limb-girdle muscular dystrophy (Mendell, Rodino-Klapac, et al. 2010); and follistatin gene transfer in patients with Becker muscular dystrophy (Mendell et al. 2015; Al-Zaidy et al. 2015). These vectors have attracted much attention for the treatment of muscular dystrophies for the ability of several serotypes to be efficiently extravasated from capillaries and infect the underlying muscle, which would permit the ability to develop gene therapies that would work through systemic delivery (Goyenvalle et al. 2011).

1.4.5) Utrophin Upregulation

Utrophin is an autosomal analogue of dystrophin, with an 80% similarity between the two proteins (Kleopa et al. 2006). In utero, utrophin is prevalent in developing foetal muscles, but by the end of gestation utrophin expression is

downregulated and dystrophin upregulated, becoming the prevalent of the two proteins in adult musculature. In adult muscle, utrophin can still be found at the neuromuscular and myotendonous junctions, and is upregulated during muscle repair (Ricotti et al. 2016). In DMD, utrophin expression is increased, but not to an extent that would provide any alleviation of the clinical symptoms (Guiraud et al. 2015). Considering the similarity between utrophin and dystrophin, some studies are seeking to evaluate whether utrophin is an effective substitute for dystrophin in DMD patients. *In vivo* studies in the *mdx* mouse showed that a 2-fold increase in utrophin levels can prevent muscular dystrophy symptoms (Tinsley et al. 1998). Utrophin modulators seek to increase utrophin expression, and ezutromid is a compound that has been shown to increase utrophin production in *mdx* mice, leading to improvements in strength and reducing muscle fatigue following forced exercise (Tinsley et al. 2011). In a phase I trial, paediatric patients received 100mg/kg 3 times/day and showed increased utrophin in skeletal and cardiac muscle (Ricotti et al. 2016). This has led to a phase II trial which is currently ongoing (Clinicaltrials.gov identifier NCT02858362). In addition to ezutromid, another utrophin modulator is in development (SMT022357), an oral second generation utrophin modulator that has shown to decrease muscle damage in *mdx* mice (Guiraud et al. 2015).

1.4.6) Read-through Agents (Ataluren)

In about 10-15% of patients with DMD have a nonsense mutation (Pichavant et al. 2011), which introduces a premature stop codon into the dystrophin mRNA, leads to the translation of a truncated, non-functional protein. PTC124, or Ataluren, was first discovered as a candidate in a chemical library screen that selectively induces ribosomal breakthrough of premature, but not normal termination codons.

When applied to primary muscle cells from humans and mdx mice containing dystrophin nonsense alleles it promoted dose-dependent dystrophin production (Welch et al. 2007). Furthermore, when given to *mdx* mice, it promoted dystrophin production, which also exhibited proper membrane localization of dystrophin and associated proteins. The restoration of dystrophin expression was also associated with a rescue in functional strength deficit characteristic of the *mdx* mice within 2-4 weeks of drug exposure (Welch et al. 2007). Following clinical trials demonstrated that ataluren was active and safe in humans, inducing increases dystrophin expression (measured by immunofluorescence in muscle biopsies pre- and post-treatment) in 23 of 38 subjects (Finkel et al. 2013). Further studies showed promising results, with patients given 40mg/kg three times a day showed improvements in their ability to walk, as measured by the 6 minute walking distance test (Bushby et al. 2014). Phase 3 randomised, double-blind, placebo-controlled clinical trials showed that ataluren was able to improve the rate of decline in patients with a 6 minute walking distance of 300m or more to less than 400m (McDonald et al. 2017). The European Medicines Agency granted Ataluren a conditional approval to market within the EU, and further long-term observation studies are currently ongoing (ClinicalTrials.gov Identifier: NCT02369731).

1.5) Progress in Cell Mediated Therapies for Muscular Dystrophies

Conceptually, stem cell therapies would be an ideal treatment for recessive muscular dystrophies, such as DMD, in which muscle fibres are lost as a result of a genetic mutation. To break the cycles of degeneration and regeneration in DMD,

dystrophin has to be restored to the muscle fibre membrane. This could be achieved by stem cell treatments with donor cells from a normal individual (allograft), or by extracting cells from the patient, restoring dystrophin expression *in vitro* and grafting them back into the patient (autograft). Ideally, whatever stem cell is used, it must be expandable *in vitro* without losing their stem cell properties, be immune-privileged, be systemically deliverable, survive, proliferate, and migrate upon arrival within the host muscle to maximise the area treated, differentiate into host muscle fibres to repair or replace damaged or lost fibres, express dystrophin once incorporated into the host muscle, and most importantly, be able to replenish the satellite cell pool with functional stem cells, so that when future rounds of degeneration occur they can activate to repair and maintain the fibre, sustaining dystrophin expression (Meng, Muntoni, et al. 2011).

Myoblasts, the progeny of satellite cells, were the first candidate for the development of cell therapies to treat muscular dystrophies. They can be easily expanded in culture (Allen et al. 1985; Bischoff 1986) and form muscle after intramuscular injection into the *mdx* mice (Huard et al. 1994; Partridge et al. 1989). However, they have several disadvantages, most notably that they regenerate skeletal muscle far less efficiently than freshly isolated satellite cells (Montarras et al. 2005), and studies into the kinetics of myoblast transplantation show that most die shortly after intramuscular injection (Jonathan R Beauchamp et al. 1999). In addition, myoblasts are not systemically deliverable, severely hindering their potential as a whole body therapy for DMD (Dellavalle et al. 2007) and show limited migration, mainly causing muscle regeneration along the needle track of engraftment (Moens et al. 1996) meaning it would be necessary to inject each muscle

to obtain an effective treatment. Attempts have been made to improve the migratory capacity if intramuscularly delivered myoblasts, including the overexpression of follistatin in human myoblasts transplanted into mouse muscles (Benabdallah et al. 2009); heatshock treatment of cells prior to engraftment (Bouchentouf et al. 2004); co-injection of monkey myoblasts with bFGF or IGF-1 (Lafreniere et al. 2009); and the use of an enriched laminin environment (Silva-Barbosa et al. 2008). However, none of these treatments have shown improvements that would be significant in clinical terms. Furthermore, the failure of previous clinical trials investigating myoblast transplantation for DMD (Gussoni et al. 1997; Mendell et al. 1995; Miller et al. 1997; Tremblay et al. 1993) have led to decreasing interest in myoblast transplantation for DMD, despite recent encouraging data regarding improved methods for myoblast transplantation, by using high density injection protocols where myoblast delivery occurs through a series of parallel injections (Skuk et al. 2007; Skuk et al. 2006; Skuk et al. 2004).

However, other cell types may offer alternatives for the development of cell therapies for DMD. Mesoangioblasts or pericytes are blood-vessel associated stem cells of embryonic origin, arising from the dorsal aorta (Minasi et al. 2002) or of post-natal origin (Dellavalle et al. 2007) respectively. It has been shown that in mouse models of limb-girdle muscular dystrophy (alpha-sarcoglycan null mice) intra-arterial delivery of mesoangioblasts into dystrophic host mice reconstitutes skeletal muscle, restoring both functional and morphological features of the dystrophic phenotype (Sampaolesi et al. 2003). When human pericytes are grafted into SCID-mdx mice, pericyte-derived cells colonised the host muscles, generating fibres expressing human dystrophin, whilst cells derived from DMD patients and transduced to express

a dystrophin construct also gave rise to dystrophin positive fibres *in vivo* (Dellavalle et al. 2007). Mouse-derived pericytes have been reported to replenish the satellite cell pool (Dellavalle et al. 2011), however transplantation of human pericytes derived from DMD patient muscle into *mdx*$^{nu/nu}$ hosts have failed to replicate these findings (Meng, Adkin, et al. 2011) highlighting that the need for further research is necessary to prepare pure populations that maintain their phenotype in culture and make a robust contribution to skeletal muscle regeneration.

Another promising cell type has been the discovery of circulating cells expressing CD133 in humans, a well characterised marker of haematopoietic stem cells (Handgretinger & Kuçi 2013). When these cells are co-cultured with either myogenic cells, or with Wnt producing cells, they are able to undergo myogenic differentiation. This has also been observed *in vivo* after intra-arterial and intra-muscular transplantation into the *SCID/mdx* mouse model (Torrente et al. 2004). Furthermore, CD133 cells from DMD patients have been isolated, and via exon skipping, dystrophin expression was corrected (Benchaouir et al. 2007). When these cells were intra-muscularly and intra-arterially grafted into the *SCID/mdx* mouse they contributed to the formation of dystrophin positive fibres within the mouse host (Benchaouir et al. 2007). Furthermore, when grafted into cryoinjured *Rag2*$^{-/-}$*/γ-chain*$^{-/-}$*/C5*$^{-/-}$ mice, human CD133 cells showed a greater regenerative capacity when compared to human myoblasts, as measured by an increased in the number of muscle fibres expressing human proteins and human cells located in a satellite cell position, and dispersion within the tissue (Negroni et al. 2009). In any cell therapy the reconstitution of the stem cell pool is essential. Meng et al. 2014 showed that some human CD133 cells are located underneath the basal lamina of human muscle

fibres, a position traditionally associated with satellite cells. In culture these CD133 cells derived from human muscle are multipotent, capable of forming myotubes and reserve satellite cells *in vitro*. When transplanted intramuscularly into irradiated and cryodamaged, or cryodamaged tibialis anterior muscles of *Rag2*$^{-/-}$/γ-*chain*$^{-/-}$/*C5*$^{-/-}$ mice, they also contributed to extensive muscle regeneration and satellite cell formation. Furthermore, some donor-derived satellite cells expressed MyoD, indicating that they were activated. After these muscles were reinjured, CD133 cell grafted muscles produced more newly regenerated fibres muscle of donor origin than non-reinjured muscles, indicating the ability of human CD133 cells to replenish a functional satellite cell pool within skeletal muscle, giving rise to functional muscle stem cells able to respond to injury (Meng et al. 2014). Their ease of isolation from blood and their high myogenic potential *in vivo*, combined with their ability to replenish the muscle stem cell pool, make them highly attractive for clinical application. However, they do occupy a very small fraction of the mononuclear population of blood, which might limit their application.

Other muscle specific cells with the capacity to produce skeletal muscle have also been recently identified. Mitchell et al. (2010) discovered a population of muscle resident stem cells which are located in the interstitium of skeletal muscle, expressing the cell stress mediation PW1 but no other markers of muscle stem cells such as Pax7. PW1^{+}/Pax7^{-} interstitial cells (PICs) have been shown to be myogenic *in vitro* and efficiently contribute to muscle regeneration *in vivo* as well as generating satellite cells and PICs after intramuscular transplantation. Furthermore, they are not derived from the satellite cell lineage, making them a new and anatomically identifiable population of muscle progenitors (Mitchell et al. 2010). Furthermore,

PICs haven been shown to express markers of pluripotency (Oct3/4, Sox2, and Nanog), be self-renewing with over 60 population doublings, and can generate both striated and smooth muscle *in vivo* without producing any tumours (Cottle et al. 2017). However, their systemic deliverability has not yet been tested.

Additionally, muscle progenitor cells derived from induced pluripotent stem cells primed towards a myogenic lineage have also shown some promise in grafting experiments. Magli et al (2017) induced the transient expression of Pax7 in human iPSCs, committing them to a myogenic lineage. By identifying surface expression markers (CD54, SDC2, and integrin α9ß1) specific to muscle progenitor cells, they successfully isolated the muscle progenitor cell population, which when grafted into cardiotoxin injured muscles they formed muscle fibres of donor origin, marked by the detection of human dystrophin and human Lamin A/C positive myonuclei. Furthermore, they observed the persistence of cells occupying the satellite cell position and co-expressing human Lamin A/C and the muscle stem cell marker M-cadherin, for up to 10 months after grafting. This indicates not only that these muscle progenitors could contribute to host muscle regeneration, but also reconstitute the satellite cell pool (Magli et al. 2017). Although in its infancy, muscle precursor cells derived from induced pluripotent stem cells could be a viable way of producing muscle specific stem cells for the treatment of muscular dystrophies.

Finally, satellite cells themselves have an extraordinary myogenic capacity, with as few as 7 satellite cells being able to give rise to over 100 muscle fibres, while at the same time functionally repopulating the satellite cell niche (Collins et al. 2005). Furthermore, single luciferase-expressing satellite cells transplanted in mouse muscles are capable of extensive proliferation, contributing to muscle fibres and the

satellite cell niche, highlighting their extraordinary capacity for muscle regeneration and self-renewal (Sacco et al. 2008). When larger numbers of freshly isolated satellite are grafted into pre-irradiated skeletal muscle, they are also able to produce hundreds of fibres of donor origin, reconstitute the satellite cell niche and participate in further rounds of degeneration and regeneration (Collins et al. 2005; Boldrin et al. 2012). However, only small numbers of satellite cells can be derived from muscle, and they are only effectively contribute to muscle regeneration when freshly isolated, as they rapidly lose their myogenic capacity when cultured *in vitro* (Montarras et al. 2005), limiting the ability to expand them for therapeutic use.

Current models of cell transplantation rely on inflicting a round of muscle degeneration to enhance the contribution of donor cells to the host muscle by a variety of agents, including myotoxins (notexin and cardiotoxin), barium chloride, and cryodamage. Interestingly mouse satellite cells seem only produce significant levels of muscle of donor origin after the host muscle has been subjected to large, acute doses of gamma radiation, and the effect is dose and time dependent, which is discussed further at the end of section 1.6.4 (Boldrin et al. 2012). Muscle irradiation at these dosages (18Gy and 25Gy) produces no obvious histological damage to the musculature, and no abnormal signs of inflammation are observed in pre-irradiated *mdx*$^{nu/nu}$ hosts. However, understanding the mechanisms by which ionising radiation affects skeletal muscle may allow the eventual development of pharmacological interventions that may simulate the graft enhancing effects of irradiation without its numerous deleterious side effects. The ways by which ionising radiation affect biological molecules, and the pathology of radiation injury is discussed in the following section (1.6).

1.6) Biological Effects of Radiation

1.6.1) Background

Radiation is classified into two major forms: ionising and non-ionising. Environmentally most of the radiation is non-ionising, such as visible light, or electromagnetic radiation associated with radio waves and microwaves, and UV as their energy is insufficient to produce ionisations. However, the interaction of ionising radiation (IR) with biomolecules is much more aggressive than non-IR due to the ability of IR to induce atom ionisation (that is the ability to displace or remove electrons from an atom). The major types of IR are alpha (helium nuclei) and beta (electrons) particles, X-rays, and gamma rays (high energy photons). Alpha and beta radiation can be easily blocked by physical barriers such as a sheet of paper or an aluminium sheet, while X- and gamma rays are significantly more penetrating (Parker et al. 1978). Therefore, environmental exposure to gamma rays induces a greater degree of biological damage than alpha or beta radiation. However, all four types of radiation have the potential of causing significant cellular damage (DeVita et al. 2015). The international unit for the measure of absorbed radiation dose is the Gray (Gy), defined as joules absorbed per kilogram of mass (J/Kg). Since equal doses of IR elicit different effects depending on the source and properties of the biological target, the unit Sievert (Sv) is used to express the equivalent dose. Individuals receive on average 2.4mSv per year of IR from natural sources, and while natural sources of gamma rays exist, such as potassium 40 (K-40), gamma rays most widely used in research are provided by manmade sources such as Cobalt-60 (Co-60) and Caesium-137 (Cs-137) (Reisz et al. 2014). For the purpose of this project a Cs-137 source of

gamma radiation was used to irradiate host muscles, and therefore the focus of this section will be primarily on the interactions of gamma rays with biological systems, illustrating how exposure to gamma radiation initiates damage within the cell, how it propagates, and some examples of chemical modifications and their biological consequences.

1.6.2) Radiolysis of Water and the formation of Reactive Oxygen Species

Biological tissues are mostly composed of water. The effects of gamma radiation of cellular water evolve in phases. In the initial physical phase, lasting 10^{-16} seconds, energy from the gamma photons is deposited on water molecules, causing the ejection of an electron ($\mathbf{e^-_{aq}}$) leaving a positively charged species of H_2O^+ (Parker et al. 1978; Singh & Singh 1983):

$$\mathbf{H_2O} \longrightarrow \mathbf{e^-_{(aq)}} + \mathbf{H_2O^+}$$

In the second physiochemical stage (lasting about 1μs) the ions react with other water molecules to form new species. The positive H_2O^+ ion dissociates leaving a hydrogen ion and a hydroxyl free radical (Parker et al. 1978; Singh & Singh 1983):

$$\boldsymbol{H_2O^+ \longrightarrow H^+ + {}^{\bullet}OH}$$

The aqueous electron ($\boldsymbol{e^-_{(aq)}}$) reacts with another water molecule to form a hydrogen free radical ($H^{\bullet}$) and a hydroxyl ion (OH^-) (Parker et al. 1978):

$$\boldsymbol{H_2O + e^- \longrightarrow H_2O^-}$$

$$\boldsymbol{H_2O^- \longrightarrow H^{\bullet} + OH^-}$$

The $\boldsymbol{OH^{\bullet}}$ radicals can also react to produce hydrogen peroxide (H_2O_2) which is a powerful oxidizing agent (Parker et al. 1978):

$$\boldsymbol{OH^{\bullet} + OH^{\bullet} \longrightarrow H_2O_2}$$

Organic (R) radicals ($R^{\bullet}$) are also formed In the presence of oxygen, which is present within the cells, additional reactive species are formed including peroxy radicals ($RO^{\bullet}_2$), superoxide anions (O_2^-), and singlet oxygen ($^1O_2$) as follows (Singh & Singh 1983):

$$\boldsymbol{R'^{\bullet} + O_2 \longrightarrow R'O_2^{\bullet}}$$

$$\boldsymbol{e^-_{aq} + O_2 \longrightarrow O^-_{2(aq)}}$$

$$\boldsymbol{H + O_2 \rightarrow HO_2^{\bullet} \xleftrightarrow{H_2O} O_{2(aq)}^{\bullet -} + H^+_{(aq)}}$$

$$\boldsymbol{R'RH^{\bullet} + O_2 \longrightarrow {}^1O_2 + R'RH}$$

Subsequent chemical cascades can affect the intracellular stoichiometry of these reactive species and generate additional cell damaging agents. For example, metal catalysis by intracellular ferrous or cuprous ions can convert $\boldsymbol{O_2^{\bullet -}}$ and H_2O_2 into additional amounts of $^{\bullet}OH$ (Singh & Singh 1983)

In a separate process $\boldsymbol{O_2^{\bullet -}}$ couples with endogenous nitric oxide ($^{\bullet}NO$) forming the peroxynitrite anion ($ONOO^-$). This is just one of the reactions leading to the formation of reactive nitrogen species (RNS), other RNS formed as a result from radiation damage also include oxynitrous acid (ONOOH), nitrogen dioxide ($NO_2^{\bullet}$), and dinitrogen trioxide (N_2O_3). The increased formation of RNS and the generation of additional ROS are extremely harmful to the cells, as their reaction products are in many cases more reactive with biological molecules than their precursors. Direct radiation damage of biomolecules is also rapidly initiated with the deposition of energy on, and subsequent breaking of, S-H, O-H, N-H, and C-H bonds (Reisz et al. 2014).

1.6.3) Propagation of IR-induced ROS and RNS

The initial and direct production of ROS during radiation exposure is still low compared to the levels produced by normal metabolism, for example it has been estimated that the intracellular production of H_2O_2 is equivalent to 0.1mM/min under conditions of reperfusion injury (Turrens et al. 1991). Radiation induced levels of these agents is estimated to be much lower, for example at a dose of 2Gy it is estimated that only 0.1μM of H_2O_2 is produced (Ward 1994). However, it has been shown that the amount of ROS generated from primary ionisation events are further propagated via the intracellular activation of ROS-producing systems in the mitochondria (Leach et al. 2001; Azzam et al. 2012; Narayanan et al. 1997). For example, Manganese superoxide dismutase (SOD2) is a nuclear encoded and mitochondrially located antioxidant enzyme that converts mitochondrially derived superoxide into hydrogen peroxide. Using mouse embryonic fibroblasts (MEFs) from SOD2(+/+), SOD2(+/-), and SOD2(-/-) mice Du et al. showed that after irradiation the increases in intracellular ROS were similar 24h after irradiation in all cell lines. However, 72h after irradiation SOD2(-/-) MEFs showed an increase in intracellular ROS levels which associated with increased accumulation of DNA damage. These results showed that long after the initial radiological insult, a metabolic redox-response regulates the levels of DNA damage produced (Du et al. 2009).

B9 hamster cells with mutations in the gene coding for the electron transport chain protein succinate dehydrogenase subunit C (SDHC) show increases in steady-state levels of $O_2^{\bullet-}$ and H_2O_2. When exposed to radiation (5-50cGy) they display significantly decreased clonogenic survival compared to wild type B9 cells. However, this increased radiosensitivity can be reduced by transfection with human SDHC, as

well as by blocking the electron transport chain, or the overexpression of antioxidant enzymes prior to exposure to ionising radiation, demonstrating that increased ROS generation by the mitochondria significantly contributed to radiosensitivity and cell survival (Aykin-Burns et al. 2011).

Rats exposed to 8Gy of whole body gamma radiation displayed an increased activity of cytochrome oxidase and NADH-cytochrome c reductase, decreased antioxidant activity, and increased lipid peroxidation, and malonaldehyde concentrations (a marker of oxidative stress) in liver mitochondrial fractions (Kergonou et al. 1981). Irradiation of A549 adenocarcinomic human alveolar basal epithelial cells (Giard et al. 1973) induced a time dependent increase in mitochondrial ROS production, increased mitochondrial membrane potential, and promoted respiration and ATP production suggesting the upregulation of the electron transport chain function after irradiation (Yamamori et al. 2012). Similarly, increases in the expression of NADPH oxidase have been reported after 10Gy irradiation of rat brain microvascular endothelial cells, and its inhibition to a decrease in IR-generated ROS (Collins-Underwood et al. 2008). Furthermore, the inhibition of NADPH oxidase in irradiated (6.5Gy) haematopoietic stem cells after total body irradiation of mice reduced the increase in ROS production, oxidative DNA damage, and DNA-double strand breaks, and the number of cells presenting unstable chromosomal aberrations in the clonal progeny of irradiated haematopoietic stem cells (Pazhanisamy et al. 2011). In human Jurkat T cells, the dramatic increases in ROS production and DNA damage after irradiation (2.5Gy) could be inhibited in the presence of rotenone, a mitochondrial respiratory chain inhibitor (Choi et al. 2007). Together these findings indicated that although IR can induce ionisation events that lead to the generation

of ROS, the initial insult is propagated and amplified by the mitochondria within the cells.

The propagation of IR effects is also achieved through nitrosative stress mechanisms. A study showed that γ irradiation (2-50Gy) of murine bone marrow cells (D2XRII) stimulated the expression of nitric oxide synthase 2 (iNOS) and the iNOS dependent release of •NO 24 hours after irradiation. Furthermore, bone marrow cells from C57BL/6J mice showed increases in 3-nitrotyrosine (a product of tyrosine nitration) *in vivo*, while non-irradiated P1JL26 haematopoietic stem cells co-cultured with previously irradiated D2XRII cells for 1 or 4 hours showed similar increases in 3-nitrotyrosine, suggesting that the nitrative/oxidative stress can be transferred from irradiated to non-irradiated cells, probably due to the release of nitric oxide by irradiated cells (Gorbunov et al. 2000). Elevated levels of iNOS, nitrate, and nitrite as a consequence of radiation exposure have been associated with radiation-induced epithelial dysfunction in the colon, in the absence of an inflammatory response, in 10Gy irradiated C57BL/6 mice (Freeman & MacNaughton 2000). Furthermore, •NO is the endogenous precursor to the peroxynitrite anion ($ONOO^-$) (Beckman & Koppenol 1996) which itself is the precursor to other powerful secondary reactive nitrogen species such as NO_2• (Beckman et al. 1990).

The activation of ROS and RNS producing pathways in response to initial ionisation events exacerbates the physical alterations already induced by ionising radiation and illustrates that the global production of ROS induced by IR can selectively alter cellular signalling and a host of metabolic pathways. The increases in ROS and RNS in turn may impact physiological processes such as cell proliferation, cell cycle arrest, senescence, and apoptosis.

1.6.3) Examples of Chemical Alterations Caused by ROS and their Biological Consequences

1.6.3.1) Interactions with DNA

The interaction of radiation with the cell nucleus has been established as the primary mechanism responsible for the genotoxic effects of radiation. In the early 70's Munro showed that a significantly higher dose of radiation is needed to kill Chinese Hamster fibroblasts when the alpha or x-ray radiation is targeted at the cytosol rather than the cell nucleus (Munro 1970). Damaging events of IR alone to the DNA include the deleterious alteration of bases and sugars, cross-link formation, single- and double-strand breaks (Lyngdoh & Schaefer 2009; Thompson 2012). Of the water radiolysis products, the hydroxyl radical is the most common and most damaging to nucleic acid molecules. Double-strand breaks in particular, originate from the reactivity of •OH radicals at nearby ribose sites, ultimately leading to strand breaks through subsequent radical pathways which occur at high frequency and randomly along the DNA backbone (Reisz et al. 2014; Singh & Singh 1983), as shown in figure 1.7. Both the nucleobases and deoxyribose are susceptible to •OH mediated damage. The OH radical attacks purine nucleobases at carbons 4, 5, and 8, generating reactive radicals that lead to a variety of products, with the most common being 8-hydroxypurines, specifically 8-oxodG (figure 1.8, product B), which serves as a well-known hallmark of oxidative DNA damage (Reisz et al. 2014). *In vivo* this oxidative damage is illustrated by elevated levels of 8-oxodG in mouse kidney in response to 20Gy IR even 24 weeks after treatment (Robbins et al. 2002). Pyrimidines are also highly susceptible to •OH addition, particularly at carbons 5 and 6 (figure 1.9),

generating pyrimidine glycols in the presence of O_2 (Fujita & Steenken 1981). Nucleobase modifications continue, eventually leading to strand breakages in the DNA backbone. Furthermore, the extent of radiation induced DNA damage is dramatically increased in the presence of bivalent metal ions (Cu^{2+}, Fe^{2+}) (Ayene et al. 2007).

The immediate cellular response to this DNA damage is the activation of the DNA damage response (DDR) which ultimately leads to the repair of nucleic acid damage or the initiation of cell death pathways. These breaks are detected by two major pathways, which include the Mre11-Rad50-Nbs1 (MRN) complex, which rapidly recognises DNA DSBs where it acts to recruit and assist ATM (mutated in ataxia-telangiesctasia (A-T)) which in turn phosphorylates all three members of the MRN complex, to initiate down-stream signalling that give rise to cell cycle control, DSB repair, DNA replication fork restart, telomere maintenance, and ultimately cell survival or apoptosis (reviewed by: Lavin et al. 2015; D'Amours & Jackson 2002; van den Bosch et al. 2003). Evidence for the implication of the MRN complex in the DDR comes from patients with mutations in these genes. RAD50 deficiency has been described to cause severe microcephaly, mental retardation, 'bird-like' face, and short stature, while the patient cells were characterised by chromosomal instability, radiosensitivity, failure to induce DNA damage induced MRN foci, impaired radiation induced activation and downstream signalling through ATM. Their cells were also impaired in the G1/S cell-cycle-checkpoint activation and displayed radioresistant DNA synthesis (absence of a steep component of inhibition of DNA synthesis in a dose-response curve when the rate of DNA synthesis is plotted against radiation dose) and G2 phase accumulation (Waltes et al. 2009). Cells from human MRE11

mutants also show hypersensitivity to IR, radioresistant DNA synthesis, and the abrogation of ATM dependent events (Stewart et al. 1999). ATM is also activated by irradiation in a IR-induced ROS dependent manner (Guo et al. 2010). In addition to modifying crucial cell cycle checkpoint proteins, ATM also mediates the phosphorylation of Kap1, promoting heterochromatin relaxation and increasing the efficiency of DNA repair (Goodarzi et al. 2008).

The other pathway recognising DSBs is non-homologous end joining (NHEJ) which operates throughout the cell cycle but is particularly important in the G1 phase. Ku70 and Ku80 are the essential sensors for DNA free ends in repair by NHEJ (Merkle et al. 2002). Once bound to DNA ends these proteins recruit DNA-dependent protein kinases (DNA-PKcs), the XRCC4/Ligase 4 heterodimer, CLF, and PAXX protein to complete the process of DSB repair (Ochi et al. 2015). Other sensors and transducers in the DDR also include the BRCA1/2 proteins, checkpoint kinases (Chk1/2) and poly(ADP-ribose) polymerase (Reisz et al. 2014).

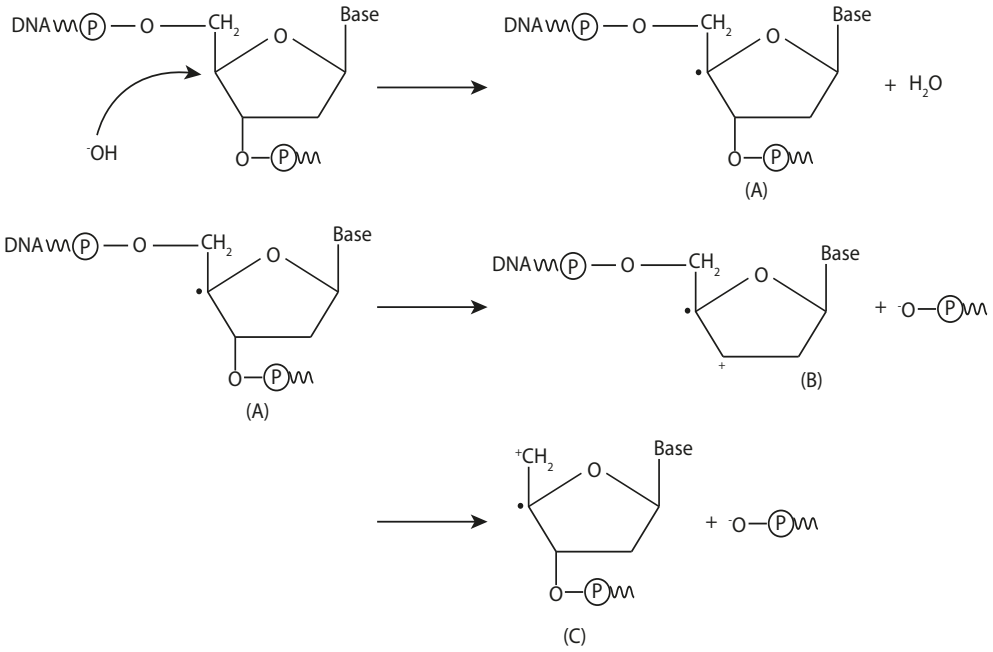

Figure 1.7: •OH radical attack on the sugar moiety of DNA can lead to strand breaks as shown above. The Radicals B and C undergo further reactions leading to the elimination of the second phosphate group as well.

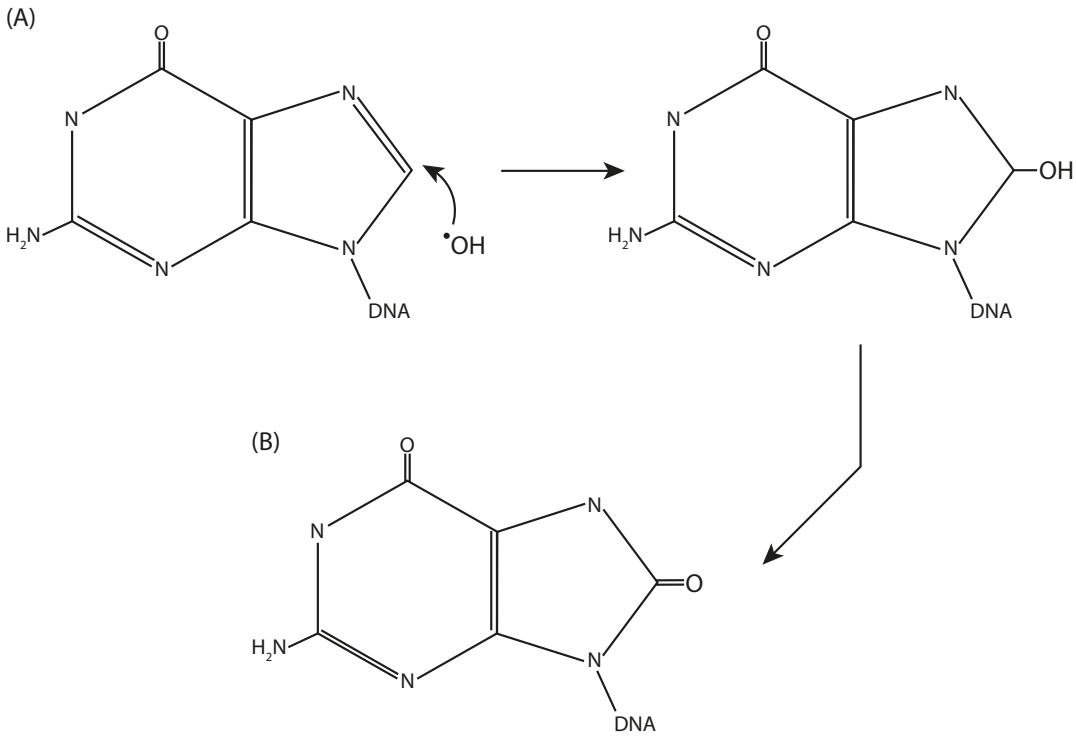

Figure 1.8: Guanine (A) is attached at carbon 8 by a hydroxyl radical, leading to the formation of 8-oxodGuanine.

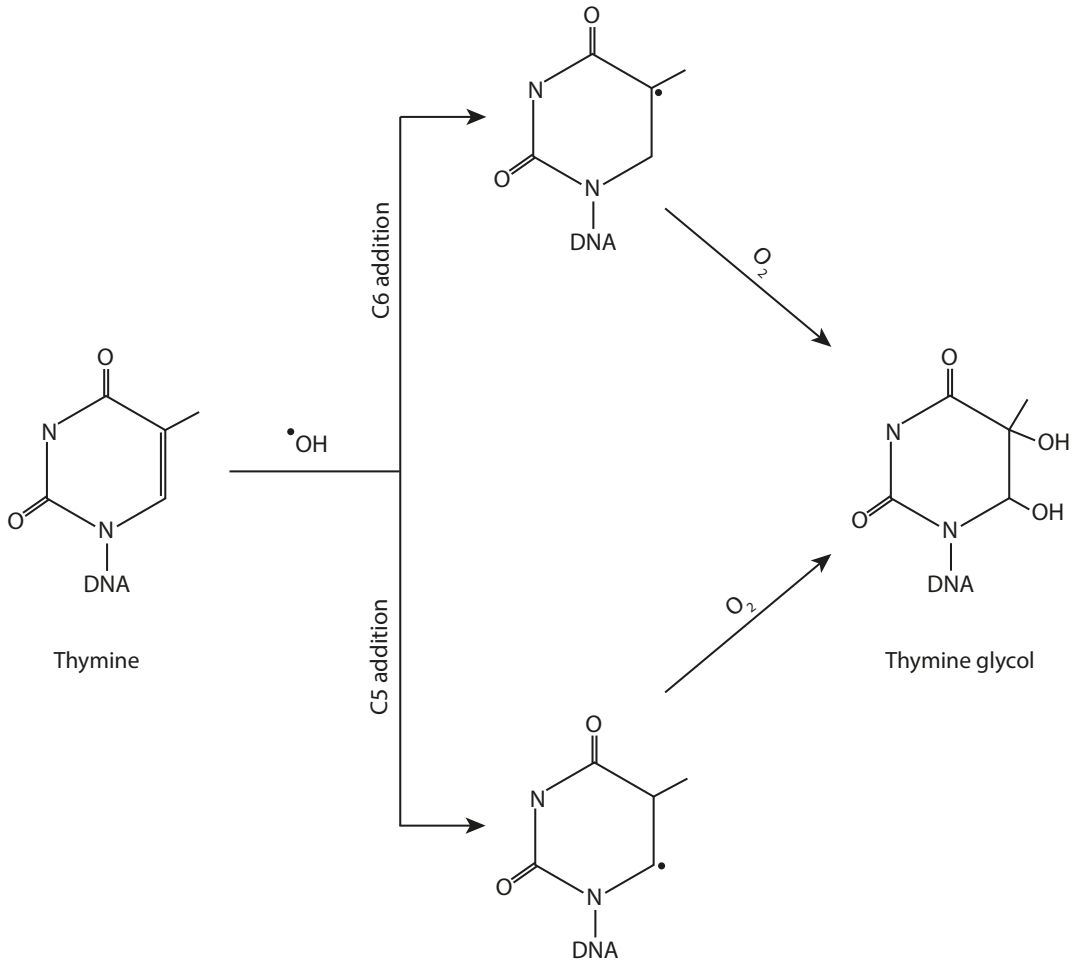

Figure 1.9: Addition of the •OH radical to thymine carbons 6 and 5, leading to the formation of thymine glycol in the presence of oxygen, which can react further to produce other compounds.

1.6.3.2) Interactions with Lipids

Traditionally, DNA damage has been considered the main event leading to cell death after IR. However, although IR can directly affect lipids, radiation induced ROS presents a major mechanism of damage to the lipid component of cell membranes which are significantly exposed to the cellular aqueous environment (Stark 1991). Radiation-induced $^{\bullet}OH$ leads to the formation of a peroxyl radical, which is terminated with the formation of a lipid hydroperoxide (LOOH) and the isomerisation of arachidonic acid to a cis-trans structure shown in the top path of figure 1.10. Moreover, the addition and subsequent ejection of a thiyl radical ($RS^{\bullet}$) also leads to the cis-trans isomerisation in the presence of oxygen (bottom path, figure 1.10) (Reisz et al. 2014; Stark 1991). Lipid peroxidation in turn can increase membrane permeability, disrupt ion gradients, and other transmembrane processes, as well as altering the activity of membrane associated proteins (Corre et al. 2010).

Sphingolipids are one of the for major classes of membrane lipids and participate in the rigidity and stability of the outer cell membrane, and are now considered bioactive lipids involved in numerous biological functions, in particular ceramide being involved in the regulation of signal transduction of directing protein organisation (Corre et al. 2010). Ceramide can be generated by sphingomyelin hydrolysis. Under conditions of IR mediated stress acidic sphingomyelinase (ASMase) re-localises from the lysosomal compartment to the cell membrane in a variety of cells including lymphoblasts (Santana et al. 1996), endothelial cells (Haimovitz-Friedman et al. 1994), and in tumour cells such as Burkitt's lymphoma (Michael et al. 1997), and prostate tumours (Kimura et al. 2003). ASMase then mediates the rapid hydrolysis of sphingomyelin to ceramide in a DNA damage independent manner

minutes after IR damage (Haimovitz-Friedman 1994). A second wave of ceramide accumulation occurs several hours later in a DNA damage dependent manner which activates the *de novo* synthesis of ceramide by activation of the ceramide synthase enzyme (Corre et al. 2010). Increases in ceramide levels within the cell membrane lad to the formation of lipid platforms or rafts. These lipid rafts are used to sort proteins and spatially reorganise receptors and intracellular signalling molecules. For example, death receptors (Trail, CD95, TNF, TRAIL, CD40), toll-like receptors (TLR2, 4, 5) and cytokine receptors (IL-1R) are able to cluster within these ceramide enriched domains, leading to a high density of receptors in a small area of the membrane, which leads to the enhancement of signal transmission into the cell. This clustering also limits lateral diffusion, and therefore stabilises the interactions of receptors with their ligands (Bollinger et al. 2005; Corre et al. 2010). For example, in many cancers epidermal growth factor receptor (EGFR) is overexpressed, and small molecule tyrosine kinase inhibitors targeting EGFR have shown clinical efficacy in lung and colon cancers, but not in breast cancer cell lines. When EGFR expressing breast cancer cell lines, which were resistant to tyrosine kinase inhibitors, were depleted of cholesterol, therefore altering the formation of lipid rafts, they became sensitized to EGFR specific tyrosine kinase inhibitors (Irwin et al. 2011). In the squamous cell carcinoma cell line SCC61, gamma-irradiation induces the reorganisation of plasma membrane rafts and leads to radiation-induced apoptosis in a ceramide dependent manner. In the radioresistant counterpart cell line SQ20B, this mechanism is defective and leads to the activation of the EGFR survival pathway, showing that lipid raft integrity is involved in the triggering of apoptotic cell death and/or survival pathways. In M624 melanoma cells, exposure to UV leads to the increase in ceramide

within lipid rafts, and this is associated with the aggregation of the Fas-receptor, which required to trigger UV-induced apoptosis (Elyassaki & Wu 2006). Furthermore, when in ASMase-invalidated lymphoblasts from patients suffering from Niemann-Pick disease and resistant to radiation induced apoptosis, ASMase was re-expressed, their radioresistance disappeared (Santana et al. 1996). Together, this shows that the effects of ROS on lipid metabolism is capable of heavily modifying signalling pathways in irradiated cells, determining their eventual fate.

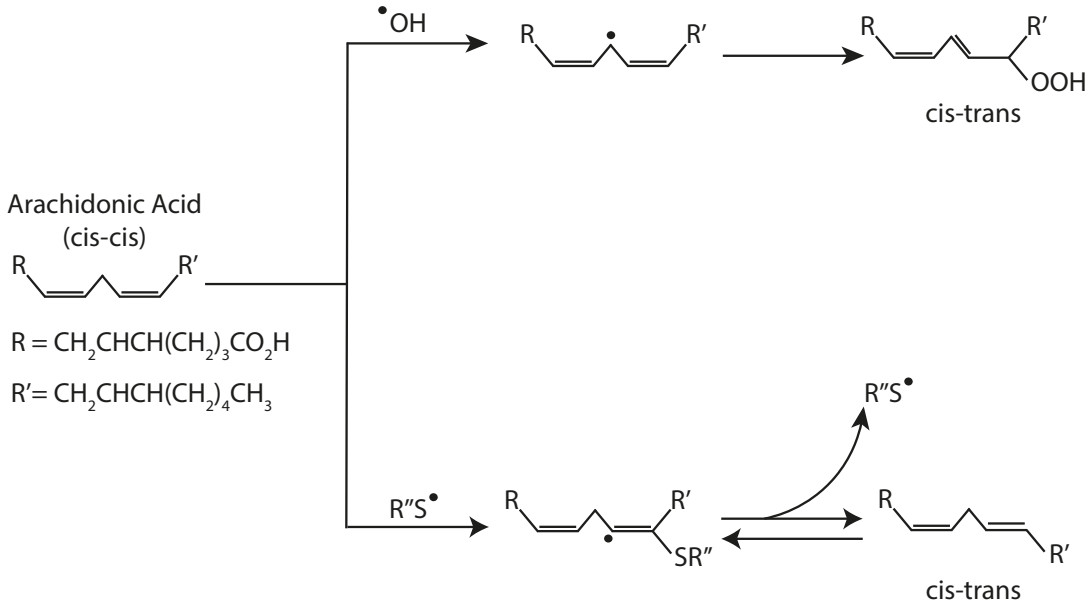

Figure 1.10: Hydroxyl (•OH) attack to arachidonic acid leads to the formation of a peroxyl radical (top path) which is terminated with the formation of a lipid hydroperoxide (LOOH) and its isomerisation to a cis-trans structure. Alternatively, thiyl radical (R''S•) addition and ejection in the presence of oxygen leads to the cis-trans isomerisation of arachidonic acid.

1.6.3.3) Interactions with Proteins

Proteins are also prominently targeted by IR, inducing changes in expression, activity, as well as oxidative or reductive post-translational modifications. There are a multitude of oxididative modifications that may occur to proteins after irradiation, including direct amino-acid oxidations, for example of cysteine and methionine, the oxidative cleavage of protein backbones and modification of amino-acid side chains with the OH radical interacting with each of the 20 standard amino acids (Reisz et al. 2014), and the carbonylation of proteins such as TGFß (Ehrhart et al. 1997; Jobling et al. 2006).

The ROS induced modifications of proteins have been shown to be involved in the progression of many disease states after radiation therapy. These include: diabetes (Yang et al. 2011); the activation of inflammatory cascades (Spychalowicz et al. 2012); the nitrosylation of cysteine thiols has also been shown to increase sensitivity to septic shock (Liu et al. 2004); Alzheimer's disease (Hensley et al. 1996); and elevated levels of protein carbonylation in the white and gray matter of multiple sclerosis patients (Bizzozero et al. 2005). Additionally, they have been involved in many cancers, for example, the activation by ROS of pathways such as NF-κB, p53, HIF-α, or the ß-catenin/Wnt pathway (Reuter et al. 2010). Together, this highlights that irradiation can not only affect DNA as traditionally thought, but the subsequent increases in ROS can lead to protein modifications that may impact on key cellular pathways.

1.6.4) Radiation Injury in Skeletal Muscle

Skeletal muscle is remarkably resistant to radiation injury, however the pathology of radiation injuries in skeletal muscle are poorly understood, with few published reports. The most striking effects of severe radiation injury to skeletal muscle are described by Gestner et al. (1954) who carried out studies on the effects of extremely high acute doses of x-ray irradiation in both frog (*Rana pipiens*) and rabbits. Their report makes for an interesting read, however the doses employed are brutal compared to the radiation doses used in this project. Isolated frog gastrocnemious muscles were subjected to radiation at a rate of 60Gy per minute (6000rad). During irradiation the work capacity, twitch, and force production of each muscle was measured, while the contralateral controls were also subjected to the same tests but without exposure to irradiation. Regarding work capacity, they report that the muscles functioned normally for the first 8 to 10 minutes, followed by a sudden decrease in the contraction length of irradiated muscles which progressed steadily to 0. The muscles also failed to return to their resting length during relaxation. After 15 minutes, the muscles were completely exhausted and failed to produce twitches. In contrast muscle fatigue in non-irradiated controls occurred within 20 to 40 minutes following the start of the stimulation. Measuring twitch during irradiation showed similar early fatigue onset: in all experiments, irradiated muscles remained normal for 10 minutes of irradiation, then the amplitude of the twitch began to dampen and disappeared within the subsequent? 15 to 20 minutes. On the other hand, control muscles showed either normal or slightly decreased amplitude after this time? (Gerstner et al. 1954). Frog muscles fixed immediately

after 2 hours of irradiation showed no pathological features, even with doses of up to 4800Gy. However, after 8 hours they observed acute destructive lesions of the myoplasm, including the breaking up of single muscle fibres or small groups of fibres, the nuclei were either absent or displayed fragmentation (karyorrhexis), and the sarcolemma was severely damaged (Gerstner et al. 1954).

Their studies in *in vivo* rabbits focused on a dose of 720Gy to the hindlimb muscles of 5 male rabbits, at a dose rate of 12Gy/minute. Within 30 minutes following exposure the animals fully recovered from anaesthesia, and spontaneous activity was normalised. Examination of the irradiated legs revealed slight swelling and a decrease in sensitivity to pin-prick. After 8 hours swelling of the hindlimb increased and extended to adjacent areas, sensitivity to pin-prick injury became pronounced and loss of coordination was observed during rapid motion. By 24 hours the swelling was exacerbated, and there was a complete loss of sensitivity and motion of the irradiated hindlimbs. 72 hours after irradiation gangrene and infection began to take hold. Histologically the legs showed oedema, particularly in subcutaneous tissues and to a lesser extent in muscles. After 24 hours, haemorrhages became visible and by 72 hours gross muscle necrosis was apparent. 12 hours following irradiation, the muscle fibres were swollen, with a loss of cross-striations, and broken into amorphous masses with an abundant inflammatory exudate. Haemorrhages were observed by 24 hours, and after 3 and 6 days large arteries were showing extensive necrosis of their walls and thrombi in the lumen (Gerstner et al. 1954).

It must be taken into account that this brief report by Gerstner et al. used brutal doses of radiation that are not employed in current research (720Gy used by

Gerstner, in contrast the research in this thesis employs 18Gy or 25Gy), but it does highlight that although skeletal muscle is highly radioresistant compared to other tissues, requiring doses of over 500Gy to trigger the observed damage, it can still be gravely affected as a result of radiation injury. The early onset of fatigue and work capacity is probably mediated by damage to cell membranes (section 1.6.3.2), including mitochondrial membranes, leading to the disruption of ATP production, and increases in membrane permeability leading to the loss of ion gradients required for signal transduction of both the nervous system (loss of sensitivity) and muscle contraction. The increases in membrane permeability of skeletal muscle fibres were shown in *in vitro* cultured single muscle fibres, which showed an increased efflux of calcein dye after a dose of 16Gy of gamma radiation (Canaday et al. 1994), however this was not observed *in vivo* after 18Gy of x-ray irradiation by Pagel & Partridge 1999. However, these dosages are much lower than those used by Gerstner et al. 1954. Additionally, the observation of necrosis in arterial walls illustrates the damage that radiation can inflict on endothelial cells, leading to internal haemorrhaging. Therefore, when considering damage to skeletal muscle by radiation, it must be taken into account that different cell types within the tissue may have different levels of radiation resistance, reacting differently to the same dosage.

Pagel and Partridge (1999) carried out an excellent comparison of the effects of an acute dose of X-ray irradiation (18Gy) in the C57Bl/10ScSn mdx/mdx mouse and their non-dystrophic control the C57Bl/10ScSn +/+ mouse. They observed that 18Gy doses irradiation of skeletal muscle caused no acute or chronic damage to muscle fibres (figure 1.11). Furthermore, in dystrophic mice irradiated at a young age irradiation appeared to have a protective effect, delaying the onset of the mdx

pathology. They hypothesise that this might be due to the disabling of the stem cell pool, which prevents myofibres growth to a threshold where damage may occur. However, in mdx mice they observed a loss in muscle mass and fibre number when compared to non-irradiated contralateral muscles, but this was likely due to myofibre necrosis and the inhibition of regeneration (figure 1.11) by the ablation of satellite cells (C. . Pagel & Partridge 1999). A more recent study by Hardee et al. (2014) used 8 week old female C57Bl/6 mice which had their hindlimb muscles exposed either to a single dose of 16Gy or four doses of 4Gy (4x4Gy). They reported that 16Gy but not 4x4Gy decreased total muscle protein and RNA content. Neither the fractioned dose or the 16Gy dose altered overall body weight, hindlimb grip strength, or TA or gastrocnemius muscle mass. However, the 16Gy dose did decrease protein and RNA content in the gastrocnemius, but not when exposed to 4x4Gy. In the TA, both radiation treatments lead to an increase in the number of fibres displaying centrally located nuclei (>0.4% compared to control muscles at <0.2%), indicating an increase in muscle degeneration. Increases in extracellular matrix volume was also observed, but only in the 16Gy treatment group. Neither treatment altered any of the muscle signalling pathways tested by western blot related to growth and remodelling (pERK1/2$^{T202/Y204}$, p-p38$^{T180/Y182}$, p-Akt^{S473}, and p-Akt^{T308}) compared to non-irradiated controls. They also assessed the effects of irradiation on oxidative stress, showing that the 4x4Gy treatment increased the expression of 4-hydroxynonenal (a protein marker of oxidative stress), but not at 16Gy. Interestingly they did seem to observe a differential effect of radiation on fibre type. Both 16Gy and 4x4Gy decreased the mean cross-sectional area (CSA) of type IIB myofibres. The 16Gy dose also decreased mean CSA of type IIA fibres, whilst simultaneously increasing the incidence of type

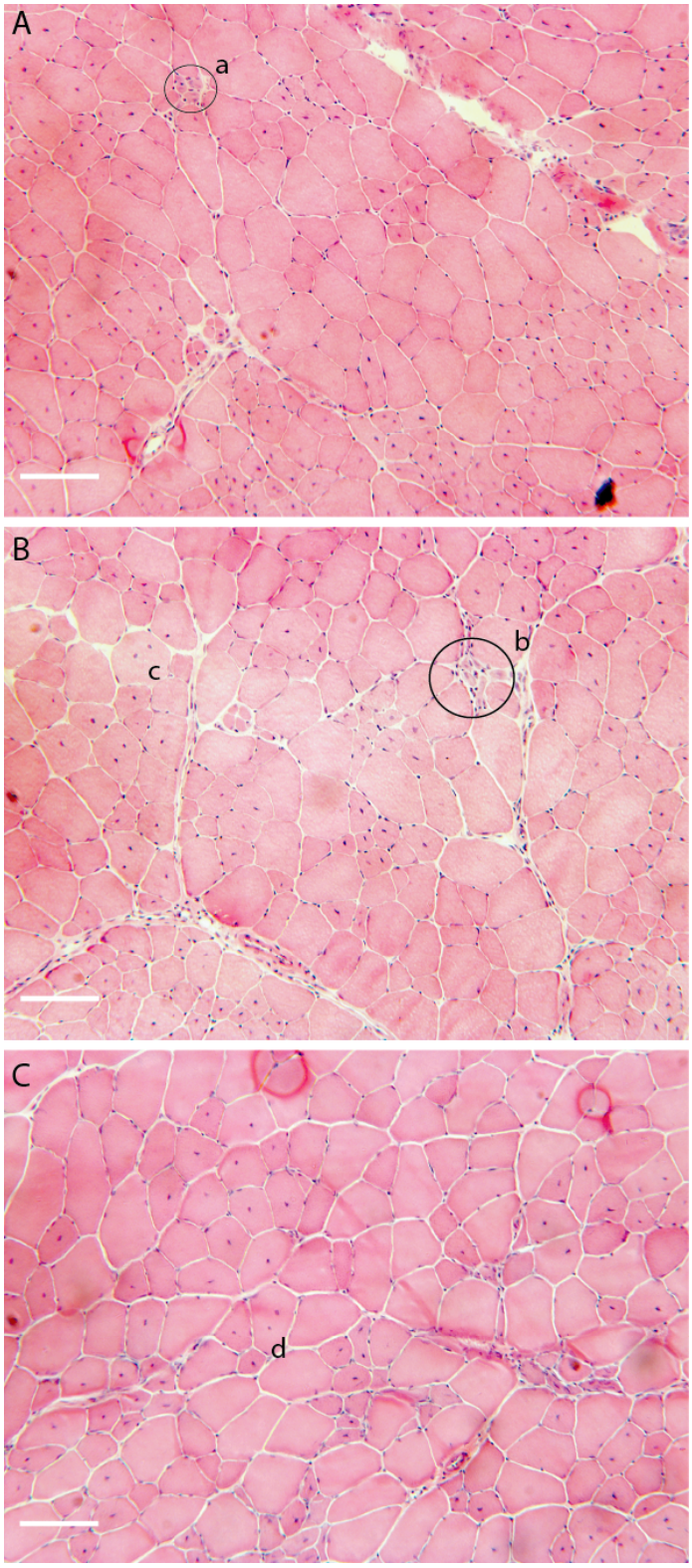

Figure 1.11: Representative H&E staining of *mdx*$^{nu/nu}$ TA muscles. A) Non-IR control; B) 3 hours post 25Gy irradiation; C) 1-month post 25Gy irradiation. There is no obvious pathology in the irradiated muscles compared to controls. In control and 3 hour irradiated sections areas of regenerating fibres are visible (a and b). After irradiation areas of myofibre regeneration are not visible, but large centrally nucleated regenerated fibres (c and d) are observed from prior rounds of regeneration. Scale bars: 100µm

IIA and IIB fibres, while the 4x4Gy regime only increased the incidence of type IIB fibres. Both treatments also decreased the frequency and mean CSA of muscle fibres with low succinate dehydrogenase activity but not those with high succinate dehydrogenase content, showing that the oxidative capacity of the myofibres affects its susceptibility to radiation damage. Together this shows that radiation damage to myofibres depends on their ability to tolerate oxidative stress, with type IIA glycolytic fibres being more susceptible to radiation damage, while type IIA oxidative fibres were more resilient to radiation damage in the 4x4Gy dosage.

Although reports on the specific pathology of radiation damage in skeletal muscle are sparse, skeletal muscle irradiation was historically employed to block the replication of satellite cells responsible for the growth and regeneration of the tissue. Gulati (1987) excised mouse EDLs and subjected them to different doses of irradiation (6.5Gy, 20Gy, and 100Gy), grafting them back into the animals after irradiation to study the effects of radiation on muscle regeneration. This research showed a dose dependent inhibition of regeneration. Muscles exposed to 6.5Gy (650rad) were able to regenerate with no morphological difference compared to non-irradiated controls. In both groups the majority of myofibres, except a thin outer rim, underwent degeneration. 4 days later the presence of activated satellite cells and myoblasts was observed. By 7 days these myoblasts fused into myotubes with centrally located nuclei. By 30 days regeneration was complete and the muscles consisted of uniformly sized myofibres resembling normal muscle. 4 days after 20Gy irradiation a myogenic zone of myoblast was observed between the outer surviving myofibres and the inner ischemic ones, yet to undergo degeneration. 7 days later this increased and some myotube formation was seen. By 30 days the number and

size of regenerated myotubes was considerably less than controls with increases in connective tissue fibrosis. 4 days after a 100Gy dose muscles were divided into 3 zones, outer surviving myofibres, a myogenic zone of myoblasts, and an inner zone of ischemic degenerated fibres. At 7 days the myogenic zone had increased in size, but no myotubes were observed, and the area consisted mainly of undifferentiated cells with heterochromatic or vesicular nuclei, fibroblasts, and macrophages. No formation of myotubes was observed, and at 30 days the muscle consisted mainly of collagenous connective tissue and had decreased in size, showing that at 100Gy muscle regeneration is completely ablated (Gulati 1987). These results showed that in all cases early regeneration was still seen (appearance of myoblasts) highlighting the radioresistance of quiescent satellite cells. However, myotube formation was inhibited, suggesting that irradiation is inhibiting the later stages of regeneration, probably by reducing the pool of satellite cells, and therefore myoblasts, required for muscle regeneration (Gulati 1987). Robertson and Papadimitriou (1992) subjected mice to whole body irradiation (16Gy) to ablate the bone marrow (but protected the right leg from radiation), and compared their muscle regeneration with those mice subjected to only local doses of irradiation (16Gy). This allowed them to conclude that myofibre repair was mediated by proliferating myoblasts and not infiltrating leucocytes, but the clearance of necrotic tissue was dependent on leucocyte infiltration (Robertson et al. 1992). Rosenblatt and Parry (1993) showed that after irradiation of rat skeletal muscles, sufficient to ablate the satellite cell population (25Gy), compensatory hypertrophy of overloaded muscles was impaired (Rosenblatt & Parry 1993). Irradiation has also been used to study the degenerative component. By irradiating the *mdx* muscles with high local doses of ionising radiation before the

onset of myopathy (3 weeks of age) the satellite cell pool is ablated, preventing muscle regeneration and therefore allowing the isolation of the degenerative aspects of the disease, as the loss of muscle fibres is not counteracted by regeneration (Quinlan et al. 1995; Quinlan et al. 1997; Wakeford et al. 1991; Weller et al. 1991).

Subsequently, irradiation was used to ablate the satellite cell niche in skeletal muscle, allowing researchers to investigate the contribution of donor myoblasts to muscle regeneration without interference from endogenous satellite cells. During the course of these cell grafting experiments it was noticed that when endogenous regeneration was blocked by applying local doses of X-rays (Wakeford et al. 1991), implanted new-born myoblasts took over the host muscle to a greater extent than in non-irradiated muscles (Morgan et al. 1990). Myoblasts derived from C57Bl/10 mice were also confirmed to produce more dystrophin positive fibres and migrate more when the dystrophic host muscle had been pre-irradiated (Morgan et al. 1993). In 2002 Morgan et al. showed that pre-irradiation of host muscles enhanced the ability of C2C12 cells to form tumours in host muscles in a dose dependent manner, with 4.5Gy and 9Gy being suboptimal and 18Gy being effective. Furthermore, they showed that enhanced grafting efficiency of H2K 18 conditionally immortal mouse myoblasts was also dependent on the host strain, with enhanced engraftment in the *mdx*$^{nu/nu}$ and *C5*$^{-/-}$*/ gamma-chain*$^{-/-}$*/Rag2*$^{-/-}$ mice but not in the *beige/nu/Xid* mouse. When the authors tested candidate growth factors (bFGF, FGF-6, FGF-4, HGF, MMP2, MMP-9) that might explain this enhancement no significant increases were observed (Morgan et al. 2002). In a similar manner to myoblasts, freshly isolated satellite cells produce significantly more muscle of donor origin when grafted into pre-irradiated

hosts, but fail to produce significant amounts of muscle of donor origin in non-irradiated, notexin, $BaCl_2$, or cryo- injured muscles (Boldrin et al. 2012).

In 2012 Boldrin et al. investigated the effects of different pre-treatment regimes on satellite cell engraftment. In non-treated muscle controls, very little muscle of donor origin (dystrophin positive and X-gal positive) was formed by grafted satellite cells (mean=11 dystrophin positive fibres; SEM: ±4). In contrast, pre-irradiation of the host muscles produced large amounts of muscle of donor origin when the host had been pre-irradiated (18Gy) 3 days before (mean fibres of donor origin: 589; SEM: 149), or immediately before grafting (mean fibres of donor origin: 418; SEM: ±83). In contrast, after other host muscle injury regimes such as notexin, cardiotoxin, or cryodamage, no significant difference in the amount of muscle of donor origin was seen between treated and non-treated muscles, and was in all cases significantly less than the amount of muscle produced in pre-irradiated muscles, with at least 50 times more muscle fibres of donor origin than in non-treated groups and at least 10 times more than in muscles injured with barium chloride. Satellite cells grafted into pre-irradiated muscles also produced significantly more donor satellite cells, allowing reconstitution of the stem cell niche. It may be tempting to attribute these findings to a case of niche depletion by irradiation and replenishing by the grafting of donor satellite cells. However, Boldrin et al. clearly demonstrated that if the endogenous satellite cells are fully ablated by increasing the radiation dose to 25Gy and grafting cells 3 days later, almost no donor derived regeneration occurred. They then tested if a 25Gy dose would permit satellite cell engraftment immediately after irradiation, when host satellite cells are still present, and this yielded large amounts of muscle of donor origin. Together, they suggested that it is not only the

depletion of satellite cells that enhances donor cell engraftment, but that a functional or receptive niche was also required, and this arose in a dose and time dependent manner. This suggests an active modulation of the satellite cell niche after irradiation that renders the muscle permissible for cell grafting. While they attempted to perform cytokine arrays to determine what factors may be mediating this effect, they found no differences between irradiated and non -irradiated muscles (Boldrin et al. 2012).

However, delivering heavy doses of radiation is not a viable way to modulate patient muscles in the clinic. But understanding how irradiation renders the muscle receptive for cell grafting could lead to the development of pharmacological interventions that may allow the enhancement of cell grafting in the clinic, without the negative effects of radiation injuries. Therefore, it is the aim of this project to elucidate how ionising radiation creates a permissive environment for satellite cell grafting. In the next section a potential mechanism of action is discussed.

1.7) Potential Role for Apoptosing Cells in the Augmentation of Satellite cell engraftment

As discussed in section 1.6, ionising radiation can lead to the alteration of a wide number of cellular compartments, from DNA, to mitochondria, lipid bilayers, and protein modifications. This opens up a wide range of possibilities as to how irradiation may be enhancing donor satellite cell engraftment. However, one constant feature of radiation damage is the induction of cell death, and there is a large body of evidence suggesting that lethally damaged cells can have pro-mitotic effects on their adjacent non-damaged counterparts. This is termed apoptosis

induced proliferation. Therefore, this project will begin by investigating how lethally damaged cells may affect satellite cell engraftment.

1.7.1) Evidence for Apoptosis Induce Proliferation

One possible pathway for the irradiation induce augmentation of satellite cell engraftment could lie in a widely conserved mechanism termed apoptosis induced proliferation, whereby damaged or dying cells secrete mitogenic signals to adjacent cells to compensate for their eventual loss. Since the widely accepted impact of radiation and ROS production is the loss of cell viability, mitotic inactivation, and cell death, leading to tissue damage this could present a viable research avenue.

The ability to repair and replace damaged tissues (up to varying levels of loss) is a feature common to all metazoan organisms (Birnbaum *et al.,* 2008; Gurtner *et al.,* 2008). Initially it was thought that the first responders to tissue injury and the mediators of regeneration were neutrophils and macrophages. Although vital for wound repair, it has been observed in *PU.1* knockout mice, which lack neutrophils and macrophages, that wound healing could still proceed. This indicates that macrophages and neutrophils are not indispensable for repairing tissue injuries and that the damaged tissue alone is sufficient to trigger wound repair without the need for immune system mediation (Cooper *et al.,* 2005; Martin *et al.,* 2003).

Apoptosis induced or compensatory proliferation is a widely observed phenomenon, first described *in-vivo* in *Drosophila* by Haynie and Bryant in 1977. They observed that the wing imaginal disks (sacs of epithelial cells found in the *Drosophila* larvae that become adult structures such as eyes, wings, and limbs) exposed to 1500rad (15Gy) of radiation, depleting up to 60% of the cells, fully

recovered their size and shape, giving rise to morphologically normal adult structures, thus demonstrating that cells adjacent to the damaged tissue could proliferate and compensate for the loss of irradiated cells.

Recent research has shown that if cells are triggered to induce pro-apoptotic genes by irradiation or heat shock, but kept alive by inhibition of executioner caspases (for example by the baculovirus P35 protein), there is an increase cell proliferation in adjacent tissues, leading to hypertrophic growths in adult subjects (Fan and Bergmann 2008; Kondo *et al.,* 2006; Ryoo and Bergmann 2012; Perez-Garijo *et al.,* 2004).

Although the term compensatory proliferation is not an adequate term for these experiments, since apoptosis in these cells has been artificially inhibited, the phenomenon has also been observed in normal cells (Smith-Bolton R. K., *et al.,* 2009; Fan and Bergmann 2008; Perez-Garijo *et al.,* 2004). Furthermore, it is phylogenically conserved, examples include the regeneration of the head in the Hydra mediated by the secretion of Wnt3a from the dying cells (Galliot and Chera 2010); regeneration in planarian worms, able to form whole individuals from the smallest of body parts (Rink *et al.,* 2009); and the early stages of tail regeneration in *Xenopus Laevis* (Tseng et al. 2007). In all cases apoptotic cells play a crucial role in tissue repair.

In mammalian models, it was shown that mouse embryos exposed to mitomycin C would decrease up to 10% in size. 48 hours later these embryos would recover their full size through a compensatory growth program (Snow *et al.,* 1979). Furthermore, accelerated tumour repopulation after radiotherapy is not a new concept (Withers *et al.,* 1988; Hopewell *et al.,* 2003). The observations have also

indicated that the rate of repopulation is directly proportional to the escalation of radiation treatment. These observations can be tracked back as early as 1956 where Revesz described how mixing irradiated tumour cells with non-irradiated cells lead to an increase in the number of successful tumour grafts in mice, compared to those transplanted without any irradiated cells (Revesz *et al.,* 1956).

Further confirmation of this process was provided by Li *et al,* (2010), who demonstrated that mouse embryonic fibroblasts (MEFs) that are irradiated with a lethal dose (18Gy) could induce the proliferation of a variety of rodent cells such as murine epidermal keratinocyte progenitor cells (EKCs), neural stem cells, and mesenchymal stem cells. Further testing in-vivo confirmed that if EKCS are subcutaneously engrafted, they will only proliferate when co-transplanted with a population of lethally irradiated MEFs (Li *et al.,* 2010)

Following this, a series of experiments by the same authors showed that if the mouse hind-limbs are irradiated (18Gy), EKCs will again proliferate if transplanted subcutaneously, while in non-irradiated controls no proliferation is observed. They further confirmed their findings by using Caspase 3 and Caspase 7 knockout mice, demonstrating that the effects of radiation are abrogated if Caspases are inhibited. Additionally, normal tissue regeneration, following skin excision wounds and partial hepatectomies, was also reduced, providing a molecular link between apoptosis and the release of mitogenic signals from damaged cells (Li *et al.,* 2010).

This provides further credence to recent investigations carried out in murine nude mdx muscle by members of our group, showing that irradiation of host muscle enhanced the tumourgenicity of engrafted immortalised myogenic cells (C2C12)

(Morgan *et al.,* 2002); it is also probable that the same mechanism is responsible for mediating the enhanced engraftment of satellite cells observed by Boldrin *et al.,* 2012.

Together, this provides evidence indicating that, just as observed in lower organisms, apoptotic cells in mammals might be able to secrete caspase dependent factors that stimulate tissue regeneration and cell proliferation. Since the major outcome of radiation damage is cell death, it is reasonable to hypothesise that the effects we are observing in satellite cell transplantation experiments are simply a way of exploiting this signalling pathway to enhance satellite cell grafting efficiency, where the dying cells provide mitotic signals to the donor cells. Elucidating and artificially mimicking or inducing these pathways without the need for radiological damage could provide a significant step forward for the development of cell transplantation techniques for the treatment of muscular dystrophies.

1.7.2 Potential Mechanism for Apoptosis Induced Proliferation

Lessons from cancer biology, such as the signalling mechanisms that modulate tumour repopulation and resistance to traditional therapies, can provide insights for how lethally damaged cells within the pre-irradiated muscle may modulate the survival and proliferation of satellite cells.

Familial adenomatous polyposis (FAP) is a condition characterised by hundreds of benign colonic polyps, some of which eventually progress to colon cancer. This condition is caused by mutations of the *APC* gene, a tumour suppressor that along with Axin, GSK3ß and CK1 compromise the destruction complex which limits the

accumulation of stable, typically proproliferative ß-catenin. Waddell & Loughry (1983) observed that polyps were largely eradicated in FAP patients that had been administered sulindac, a non-steroidal anti-inflammatory drug (NSAID), shown in earlier studies to inhibit chemically induced polyps in rats (Pollard & Luckert 1980; Pollard & Luckert 1981). NSAIDs act by the inhibition of COX ennzymes, and thereby the synthesis of prostaglandins. Ten years later, the efficacy of sulindac in repressing colorectal adenoma in FAP was confirmed by a controlled clinical trial (Giardiello et al. 1993). Taking into account that FAP is caused by defects in Wnt signalling, and NSAIDs target prostaglandins, this raised a potential mechanism of overlap between prostaglandin signalling and Wnt signalling.

The link between prostaglandin synthesis and Wnt signalling began to be dissected when Castellone et al. (2005) using colorectal carcinoma cells *in vitro, demonstrated* that prostaglandin E_2 (PGE_2) increased the activation of Tcf/Lef transcription factors and activated components of the canonical Wnt signalling pathway. PGE_2 treatment induced the loss of phosphorylation of ß-catenin and increased its nuclear accumulation. Furthermore, the nuclear accumulation of ß-catenin was essential for the activation of Tcf/Lef and the increase in proliferation (Castellone et al. 2005). This allowed the identification of PGE_2 as the prostaglandin responsible for the cross-talk between Wnt signalling and prostaglandins.

ß-catenin normally forms a complex with axin, CK1, GSK-3ß, and APC. GSK-3ß and CK1 phosphorylate ß-catenin, which triggers its ubiquitin dependent degradation. Therefore, inhibition of ß-catenin phosphorylation can occur either by the inactivation of CK1 and GSK-3ß; the inability of APC to enhance the interaction of

axin and ß-catenin; or mutations in the phosphorylation sites of ß-catenin itself (Buchanan & DuBois 2006).

On the other hand, PGE_2 is a ligand for a family of G protein coupled receptors (EP1-4) (Tsuboi et al. 2002), which modulate distinct kinase pathways including proto-oncogene tyrosine-protein kinase SRC, PI3K/ATK and PKA (Buchanan & DuBois 2006). By studying downstream pathways from the EP receptors Castellone et al. (2005) showed that the activation of Tcf/Lef was not due to signalling via the PKA/c-AMP pathway. Instead, this process appeared to be dependent on the association of the $G_{\alpha s}$ subunit of the EP receptors (present in EP2 and 4) with the regulator of G protein signalling domain of axin (RGS) and the over expression of RGS domain of axin inhibited the PGE_2 induced proliferation. The RGS domain is also the site of APC binding to axin, so the binding of $G_{\alpha s}$ to axin would lead to the displacement of APC and loss of ß-catenin phosphorylation, leading to the increased accumulation and nuclear translocation of ß-catenin. Furthermore, Castellone et al also showed that if HEK293T cells were induced to ectopically express the EP2 receptor, GSK-3ß was phosphorylated at serine 9, leading to the inhibition of its kinase activity via the Atk/PKB pathway. This showed that the interplay between PGE_2 and Wnt signalling required two components: the binding of $G_{\alpha s}$ to axin, and the phosphorylation of GSK-3ß via Atk (figure 1.12).

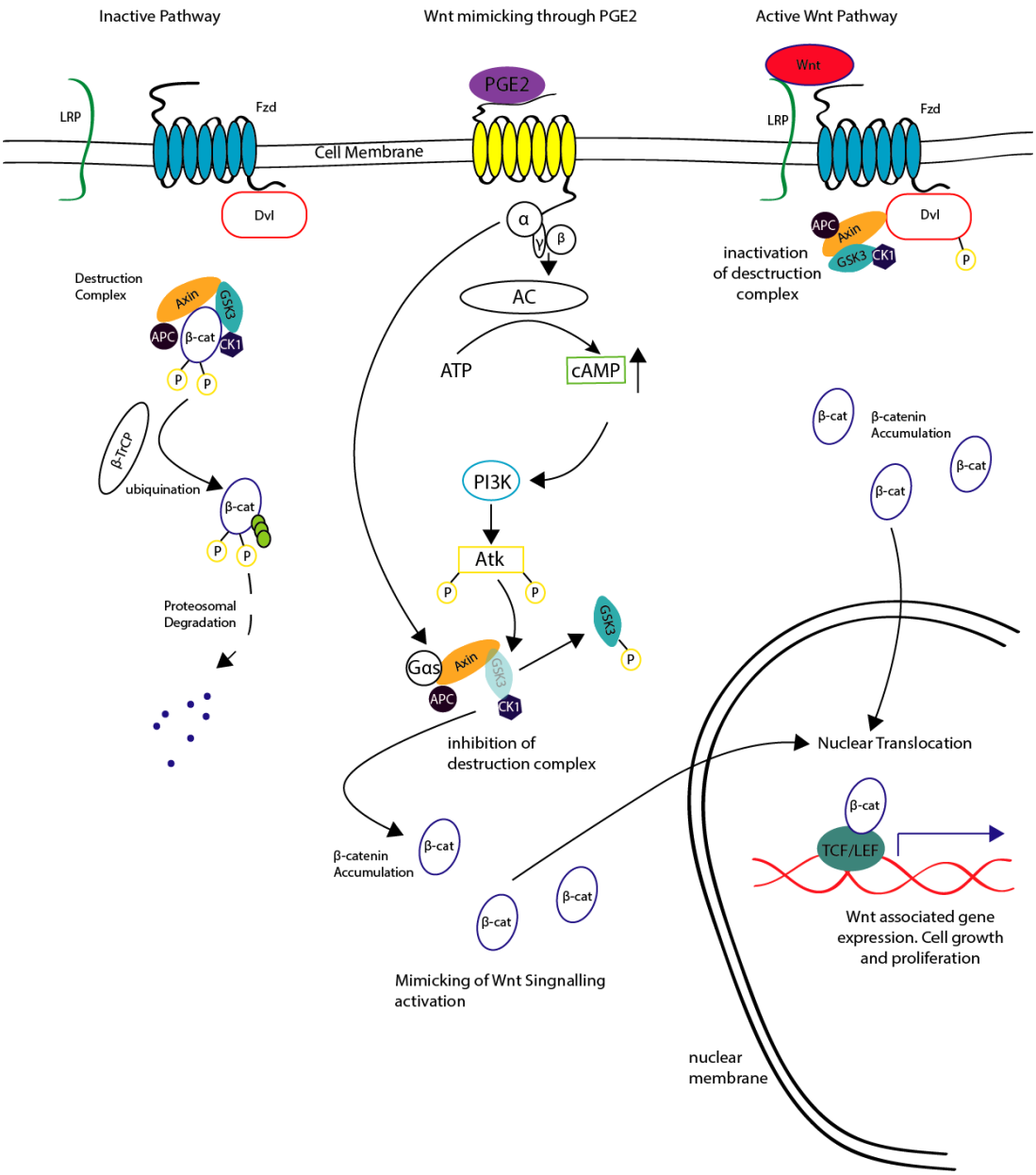

Figure 1.12: Schematic representation of the cross talk of the PGE_2 receptor with the Wnt signalling pathway. The Wnt signalling pathway is shown in both its inactive state (left) and in its activated form (right). The PGE_2 receptor is able to increase Wnt signalling via the association of the $G_{\alpha s}$ subunit to Axin, and the phosphorylation of GSK3 via ATK signalling. This in turn inhibits the ß catenin destruction complex, leading to the accumulation of ß-catenin and its nuclear translocation.

However, the observation by Castellone et al related to cancer biology. To address whether this interplay between Wnt and PGE_2 signalling is conserved in stem cells and regeneration, Goessling et al. (2009) performed a series of experiments to demonstrate a conserved and widely used stem cell and regeneration pathway in which Wnt and PGE_2 collaborate to stabilize ß-catenin. The authors studied the development of long-term repopulating haematopoetic stem cells (HSCs). Definitive HSCs are derived during embryogenesis from the aorta-gonad-mesophoros region, and subsequently colonize foetal and adult haematopoietic organs, and are marked by the expression of the Runx1 transcription factor (Galloway & Zon 2003; Dzierzak 2005). As a prelude to their 2009 paper, the research group screened a panel of biologically active compounds to test their effects on stem cell induction of Aorta-gonad-mesonephros (AGM) region of zebrafish embryos. They found that stabilized derivatives of PGE_2 enhance the number of Runx1 positive cells, while COX2 inhibitors (indomethacin) block their proliferation. Wnt signalling is a well-established regulator of adult bone marrow haematopoiesis (Malhotra & Kincade 2009) and has roles in stimulating liver regeneration (Goessling et al. 2008). Taking into account the studies into the interplay of PGE_2 and Wnt signalling in colon carcinoma cells, the authors set out to determine whether these two pathways interact *in vivo* during HSC development.

Using a zebrafish line carrying a ß-catenin responsive reporter, they found that Wnt signals in the AGM region are enhanced by the addition of stabilized PGE_2, or supressed by the addition of COX inhibitors. The proliferation seemed to be enhanced by Wnt8 expression, but blocked by the addition of indomethacin.

Therefore, their proliferation is dependent on Wnt signalling, and has an interplay with PGE_2 to promote cell survival and cell proliferation. They also showed that the modulation of Wnt signalling by PGE_2 converged on the stabilisation of ß-catenin, and is mediated by the cAMP/PKA signalling (Goessling et al. 2009). They also showed that this pathway is also involved in zebrafish liver and fin regeneration, and that it appears to be phylogenetically conserved in the generation of HSCs derived from mouse embryonic stem cells *in vitro*, and to enhance the survival and repopulating activity of bone marrow-derived progenitors grafted into pre-irradiated mice (Goessling et al. 2009).

Irradiation of cells, as discussed previously (section 1.6), mainly triggers apoptosis which is mediated by executioner caspases, and caspases 3 and 7 have been shown to enhance the activity of calcium independent phospholipase A_2 ($iPLA_2$), the activity of this enzyme increases the release of arachidonic acid (Zhao et al. 2006) which is a precursor to the synthesis of PGE_2 (Langenbach et al. 1995). Based on these observations Li et al. (2010) tested whether irradiation of wild-type mouse embryonic fibroblasts (MEFs) led to increases in arachidonic acid release. They found this to be the case, and furthermore, they showed that it was dependent on the activity of caspase 3, as in caspase 3 deficient MEFs the release of arachidonic acid was significantly reduced. This was also shown to be caspase 3 dependent, with caspase 3 mediating the cleavage of $iPLA_2$. Further examination showed that this led to increases in the amount of PGE_2 present in the supernatant of pre-irradiated wild type MEFs, while it was reduced in caspase 3 deficient MEFs. *In vitro* pre-irradiated MEFs placed into silicone cylinders and implanted subcutaneously, caused vascular

growth into the MEF embedded silicone cylinders. Knocking down $iPLA_2$ significantly reduced the vascularisation of these constructs, whereas the exogenous expression of $iPLA_2$ in caspase 3 mutant MEF cells again stimulated host tissue growth into the silicone cylinders. These experiments (discussed in section 1.7.1) then provided evidence that, like in cancer studies, PGE_2 is released as a consequence of radiological damage in a caspase 3 dependent manner, and leads to the proliferation of adjacent non-irradiated cells, potentially through the inhibition of the ß-catenin destruction complex via cross talk with downstream signals from EP receptors.

This represents one example of how dying cells may stimulate tissue regeneration by the release of mitogenic signals. However, these findings linking apoptosis to a secretory phenotype that may augment cell proliferation can be understood via recent developments in the understanding of cellular senescence and the senescence associated secretory phenotype (SASP), which will be discussed in the following section.

1.8) Cellular Senescence and the Senescence Associated Secretory Phenotype

1.8.1) Senescence and the DNA Damage Response

One of the first observations derived from the culture of primary cells explanted from human tissue was that these cells, unlike those derived from tumours, do not proliferate indefinitely, but that they are instead "mortal". Hayflick & Moorhead (1961) were the first to report that normal cultured cells stop dividing after a limited amount of passages. They divided this into 3 phases: Phase I exhibits a period of little proliferation before the first passage, during which the culture is established and a confluent sheet is formed; phase II is characterised by rapid cell proliferation; and phase III during which proliferation gradually grinds to a complete halt. Commenting on the possible causes for the arrest in cell proliferation, Hayflick (1965) hypothesised that "The finite lifetime of diploid cell strains *in vitro* may be an expression of senescence at the cellular level".

Consistent with Hayflick's hypothesis, it is now known that when human cells are propagated in culture, telomeres (protective chromosomal termini) are progressively shortened, causing cells to ultimately reach their "Hayflick Limit". This is termed replicative senescence. Telomeres are shortened with each primary cell division due to the failure of DNA polymerase to completely replicate the lagging strands, reflecting the replicative history of a primary cell (Harley et al. 1990).

Senescent growth arrest is often triggered by a persistent DNA damage response (DDR) caused by intrinsic (oxidative damage, telomere attrition, hyper proliferation) or extrinsic (ionising radiation, chemotherapeutic drugs) factors. For

example, during the replicative senescence of human fibroblasts the progressive telomere shortening leads to the exposure of uncapped double stranded chromosome free ends, which is regarded by the DDR machinery as DBS. Therefore, senescence is associated with a persistent DDR arising from irreparable DNA damage, which in turn make this pathway of particular interest within the context of pre-irradiated host muscles.

The exposure of single stranded DNA or the generation of DNA DSBs are also powerful activations of the DDR, as they compromise the structural stability of chromosomes. Single strand or double strand breaks are sensed by specialised complexes (eg, MRM complex, section 1.6.3.1) that recruit and activate the protein kinases ataxia telangiectasia Rad3-related (ATR) or ataxia telangiectasia mutated (ATM) respectively, at the site of the DNA damage (Shiloh 2006; Goodarzi et al. 2008).

The c terminus of NB1 in the MRM complex recruits the apical ATM kinase to the DSB lesion, where it undergoes autophosphorylation. Activation of ATM leads to the phosphorylation of the histone H2AX. At the sites of DNA damage γH2AX (the phosphorylated form of H2AX) recruits MDC1, leading to the additional recruitment of the MRM complex, which amplifies ATM activity, creating a positive feedback loop. Crucial to the maintenance of this feedback loop are the mediator of DNA-damage checkpoint 1 (MDC1) and the p53-binding protein 1 (53BP1) which facilitate the recruitment of ATM to γH2AX (figure 1.13) (Shiloh 2006; d'Adda di Fagagna 2008).

If single stranded DNA breaks are exposed, the single stranded DNA-binding replication protein A (RPA) binds to them, generating a signal for ATR recruitment, which is then boosted by a complex composed of RAD9, RAD1, and HUS1, and by

topoisomerase II-binding protein 1 (TOPBP1), an amplifier of ATR kinase activity (d'Adda di Fagagna 2008) (figure 1.13).

To engage DDR factors that function far from the site of DNA damage, a certain ATM or ATR activity threshold must be exceeded. When substantial DNA damage causes this threshold to be exceeded, the checkpoint kinase 2 (CHK2) is activated by ATM phosphorylation, leading to its spread along the nucleoplasm, and in turn spreading DDR signalling. Similarly, ATR phosphorylates CHK1 (figure 1.13). Ultimately, these converge on decision making factors such as p53 and the cell-division cycle 25 (CDC25) phosphatases. DNA damage induced CDC25 inactivation leads to a rapid cell cycle arrest, while phosphorylation of p53 by DDR kinases leads to its stabilization, and induction of p21 (figure 1.13), a cyclin depended kinase inhibitor, which in turn blocks CDK2 activity, resulting in hypophosphorylated Rb (Retinoblastoma Protein, a tumour suppressor) which leads to cell cycle exit (Herranz & Gil 2018; d'Adda di Fagagna 2008).

If the stress that triggers senescence is transient, p53 induction can instead trigger a quiescent state and activate DNA repair processes, and upon resolution of the stress the cell may re-enter the cell cycle. However, if the damage or stress is persistent additional signals will trigger the activation of the tumour suppressor $p16^{INK4a}$, and inhibitor of CDK4 and CDK6, contributing to a long-term cell cycle arrest. It has been suggested that p21 plays a role in the initiation of senescence, while $p16^{INK4a}$ maintains a durable growth arrest (Herranz & Gil 2018; d'Adda di Fagagna 2008).

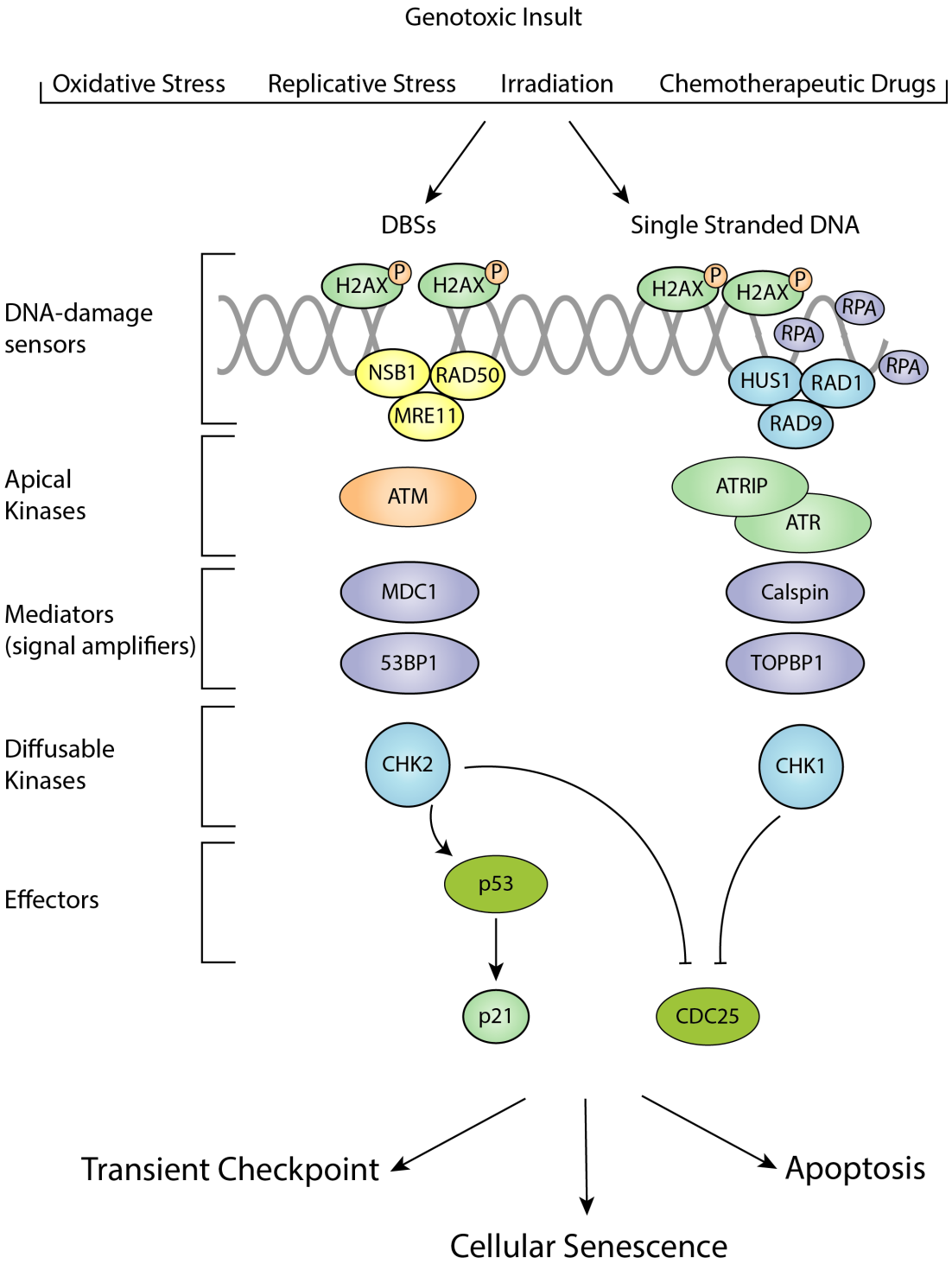

Figure 1.13: Activation of the DNA Damage Response (DDR) by DSBs and/or by the exposure to single stranded DNA coated in RPA. DSBs are sensed by the MRE11-RAD50-NBS1 (MRN) complex, which recruits ATM through the c terminus of NSB1. ATM is phosphorylated, which in turns leads to H2AX phosphorylation (γH2AX), which leads to the recruitment of MDC1 and the amplification of ATM activity and spread of γH2AX along the DSB. This leads to a to a positive feedback loop which

(figure 1.13 continued) augments ATM activity. Additionally, γH2AX also leads to the recruitment of 53BP1 which also binds to MDC1 directly. Single stranded DNA instead recruits the heterodimeric complex compromising ATR and its DNA binding subunit ATRIP. ATR activity is boosted by the RAD9-HUS1-RAD1 complex and TOPBP1, which is a target of ATR phosphorylation, and Calspin which is required for CHK1 phosphorylation. CHK1 and CHK2 are responsible for DDR signalling in regions distant from the DNA-damage site. Finally, p53 and CDC25 phosphatases interface the DDR pathway with the core of the cell cycle progression machinery. p53 induces cell-cycle arrest by activating p21 transcription, which blocks cyclin-dependent kinases (CDK) to halt cell cycle progression. CDC25 is important for normal cell cycle proliferation, as it activates CDKs. CHK1/CHK2 dependent phosphorylation of CDC25 at Ser216 mediates its nuclear export and destruction, causing cell cycle arrest. Depending on the level of DNA damage and persistence of the DDR, cells may either undergo a transient cell cycle arrest to enable the repair of the damage, undergo apoptosis, or enter a protracted DDR-induced cell cycle arrest (cellular senescence).

1.8.2) Non-cell autonomous effects of senescence

Cellular senesce was originally considered to be a cell intrinsic effect. However, increasing evidence has shown that senescent cells have the ability to signal and influence their surrounding environment, which is of particular interest when considering the impact of host muscle pre-irradiation in the augmentation of satellite cell engraftment.

Senescent cells produce a complex mixture of soluble and insoluble factors, collectively called the Senescence Associated Secretory Phenotype (SASP) (Coppé et al. 2010; Rodier et al. 2009). SASP is a general term given to the combination of cytokines, chemokines, extracellular matrix proteases, growth factors and other signalling molecules that are secreted by senescent cells, and whose specific composition varies depending on the cell type and the inducer of senescence (reviewed by Herranz & Gil 2018). The existence of the SASP was initially reported after microarray analysis of senescent human fibroblasts undergoing replicative senescence, which expressed inflammatory genes similar to those found in the early stages of wound repair (Shelton et al. 1999). Further work by Campisi and colleagues characterised this response in depth and showed a functional role for this phenotype in tumorigenesis (Krtolica et al. 2001; Coppé et al. 2008; Rodier et al. 2009).

For example, Krtolica *et al* (2001) showed that senescent human fibroblasts were able to stimulate premalignant and malignant, but not normal, epithelial cells to proliferate in culture when senescent cells compromised 10% if the fibroblast population. This effect was robust regardless of the mechanisms used to induce senescence (either replicative exhaustion, oncogenic RAS, $p14^{ARF}$, or hydrogen peroxide treatment). Furthermore, when senescent cells were co-injected into Nude

(*nu/nu*) mice with either HaCAT (immortalised human keratinocyte cell line (Boukamp et al. 1988)) or SCp2 (mouse mammary epithelial cell line (Desprez et al. 1998)) cells *in vivo* they stimulated the hyperproliferation and neoplastic progression, respectively, of HaCAT and SCp2 cells. Using HA(Pk) cells (a tumorigenic derivative of HaCAT cells) and MDA231 (an aggressive human breast cancer cell line (Cailleau et al. 1978)) they showed that senescent fibroblasts greatly accelerated and facilitated tumorigenesis *in vivo.*

Similarly, Coppé and colleagues showed that normal human fibroblasts, epithelial cells, and epithelial tumour cells subjected to either replicative senescence or high doses of X-rays (10Gy) secreted a complex mixture of inflammatory and immune-modulatory cytokines and chemokines (eg. IL-6, -7, -8, MCP-2, MIP-3); growth factors (Hepatocyte Growth Factor, and IGFBPs); shed cell surface molecules such as TNF receptors; and survival factors (Coppé et al. 2008).

Importantly, Coppé *et al* also laser captured epithelial tumour cells from patient biopsies before and after chemotherapy to determine whether chemotherapeutic agents were able to induce SASP *in vivo.* Their findings showed increased levels of p16INK4a and p21 mRNAs, commonly upregulated in senescent cells, and significantly lower levels of proliferation associated mRNAs encoding Cyclin A, MCM-3, and PCNA, while also showing higher levels of mRNAs encoding for SASP components (IL-6, IL-8, IL-1ß, GM-CSF, GRO-α, and IGFBP-2). Indicating that the SASP is not limited to cultured cells but can also occur when human cells undergo senescence *in vivo.* Furthermore, the secreted factors in conditioned media from senescent fibroblasts were able to stimulate an epithelial to mesenchymal transition (EMT) in two nonaggressive human breast cancer cell lines (TD47D and ZR75.1). The

EMT confers invasive and metastatic properties on epithelial cells, and is important step in cancer progression, which presages the transition of *in situ* carcinomas to potentially fatal invasive cancers. These results support the idea that the paracrine activities of the SASP can promote cell proliferation and promote malignant phenotypes in nearby premalignant or malignant cells, as well as inducing an EMT and enhancing basement membrane invasion (Coppé et al. 2008). These findings are of particular interest when compared to the findings of Morgan et al. (2002), which indicated that hindlimb irradiation was able to promote a tumorigenic phenotype in grafted C2C12 cells. This could have been mediated by an increase in senescent cells within the host muscle tissue, and the resulting SASP promoting the tumorigenesis of grafted C2C12 cells.

In 2015, Le Roux and colleagues published results of an investigation to determine the possibility that the endocytic adaptor Numb can mediate myogenic cell communication in skeletal muscle. The results showed that deletion of *Numb/Numbl* in satellite cells leads to impaired regeneration, marked by increased inflammation and fibrosis. Importantly, they evaluated senescence in wild-type and *Numb:Numbl* mutant mice after cardiotoxin injury.

In wild-type and mutant mice they observed an increase in SAßGal^{+} cells post injury, and these cells were not cycling (Ki67^{-}) suggesting they had undergone senescence. In wildtype mice, over half of the cells expressed the endothelial marker vascular endothelial growth factor receptor 2 (Flk-1), with only a subset of SAßGal^{+} cells expressing the macrophage surface marker F4/80. Furthermore, SAßGal^{+} did not express Pax7, Tcf4, or the pericyte marker NG2. This increase in SAßGal^{+} cells in wildtype mice was transitory, decreasing from 3.5 SAßGal^{+} cells per unit area at 10DPI

to 0.15 cells per unit area at 21DPI, and no SAßGal^{+} cells were observed during homeostasis (Le Roux et al. 2015). This transitory senescence observed in wild-type mice is reminiscent of the beneficial action of senescent fibroblasts and endothelial cells during wound healing (Demaria et al. 2014).

Le Roux and colleagues also identified a second type of senescence exclusive to *Numb:Numbl* mice, that persisted until regeneration was virtually complete (21DPI). The supernumerary of SAßGal^{+} cells could be rescued by antioxidant treatment between 5DPI-10DPI, which resulted in the number of SAßGal^{+} cells returning to levels similar to controls and rescued the regeneration phenotype. This lead the authors to suggest that *Numb* mutant specific senescent cells act in a paracrine manner to recruit macrophages and sustain inflammation, leading to increases in fibrosis. In contrast, in wildtype mice, a transitory senescence was required for wound regeneration in skeletal muscle (Le Roux et al. 2015) consistent with previous reports on the role of senescent cells in wound healing (Demaria et al. 2014). The transitory appearance of senescent cells, and their associated secretory phenotype that acts to increase inflammation, could therefore be beneficial to the engraftment of satellite cells. The transitory nature of these senescent cells is also in agreement with the time dependent effect of radiation in augmenting satellite cell engraftment (Boldrin et al. 2012).

The same research group later published research investigating the role of the SASP in mediating *in vivo* reprogramming in skeletal muscle (Chiche et al. 2017a). The efficiency of *in vivo* reprogramming to both pluripotency and lineage switching (Abad et al. 2013; Srivastava & DeWitt 2016) appears to show increased efficiency in organs such as pancreas, liver, and kidney, while skeletal muscle has traditionally

proven refractory. Notably, *in vivo* reprogramming in the liver and pancreas is more efficient when combined with injury (Heinrich et al. 2015). The transient induction of cellular senescence after tissue injury in skeletal muscle (Le Roux et al. 2015) lead Chiche and colleagues to investigate whether the increase in senescent cells, and their associated secretory phenotype, within the muscle tissue would be beneficial in inducing *in vivo* reprogramming within skeletal muscle.

Using the i4F-A mouse, which carries a doxycycline inducible (DOX) cassette with *Oct4, Sox2, Klf4,* and *c-Myc* (Abad et al. 2013) they show that cardiotoxin injury to the TA of these mice, induces senescence in the muscle and drives *in vivo* reprogramming, leading to the formation of dysplasias and teratomas *in vivo.* Furthermore, by crossing the i4F-A mouse with the *Dmd*$^{mdx\text{-}geo}$ mouse (a mouse model of DMD) and dosing them with DOX, the most severely affected muscles (TA and diaphragm) were those most likely to develop teratomas. This showed that increases in senescent cells either by acute or chronic injury enable *in vivo* reprogramming. Notably, the researchers demonstrate that Nanog positive cells were frequently in close proximity to senescent cells (SAßGal positive, Ki67 negative, p19^{Arf} positive) cells, which were more abundant. Additionally, there was a strong correlation between the number of senescent cells and the number of Nanog positive cells. The group also showed that the administration of senolytic compounds reduced the number of Nanog positive cells, and the administration of neutralising antibodies to IL-6 (a critical member of the SASP) also reduced *in vivo* reprogramming (Chiche et al. 2017a).

Furthermore, the group used 10Gy hindlimb irradiation (8-week-old i4F-A) mice to increase the proportion of senescent cells within the tissue. After cardiotoxin

injury and DOX treatment, irradiated TAs displayed a higher proportion of Nanog positive cells than non-irradiated counterparts at 12 weeks. This finding also supports the finding that irradiation of skeletal muscle can induce a population of senescent cells within the tissue (Chiche et al. 2017a).

Taken together, this suggests that the SASP plays a critical role in tissue regeneration within skeletal muscle, and the cytokines within it, such as IL-6 (Coppé et al. 2010) play a critical role in mediating the regenerative process. It is therefore possible that host tissue irradiation triggers extensive DNA damage within the host muscle, leading to the accumulation of senescent cells. The paracrine signalling from these senescent cells may in turn enhance the proliferation and engraftment of donor satellite cells (Boldrin et al. 2012).

1.9) Aims of this study

1.9.1) Overall Aim

Elucidate how ionising radiation is able to modulate the dystrophic host towards an environment that enhances satellite cell engraftment.

1.9.2) Specific Aims

1) Determine if there are increases in the number of TUNEL positive cells (section 2.5.4), where TUNEL staining marks DSBs which are characteristic of IR induced senescent cells and apoptotic cells, at the time points after irradiation where satellite cell engraftment is enhanced in mdx nude hosts.
2) Investigate if pre-irradiation is effective when applied to non-dystrophic hosts and how does this correlate with the numbers of TUNEL positive cells within the tissue at different time points after irradiation.

3) Investigate which cellular component of skeletal muscle is critical to mediate this effect.
4) Determine what pathways are altered in response to muscle radiation injury that could enhance satellite cell engraftment.

Chapter 2 - Materials and Methods

2.1) Mouse Strains

2.1.1) Ethics Approval and Animal Work

Mice were bred and experimental procedures carried out in the Western Laboratories, Biological Services Unit, University College London, Great Ormond Street Institute of Child Health, in accordance with the Animals (Scientific Procedures) Act 1986. All experiments were carried out under Home Office Licence (PIL: I944ABC23). All mice employed in the following experiments were between 3 and 4 weeks of age.

2.1.2) mdx nude

The *mdx* mouse originally arose as a spontaneous mutation in the X-linked dystrophin gene of an inbred colony of C57BL/10ScSn mice (Bulfield et al. 1984). This recessive mutation led to a general absence of dystrophin, with the exception of revertant fibres, as seen in DMD patients (Hoffman et al. 1987). Female homozygotes and male hemizygotes present with high levels of serum pyruvate kinase and creatine kinase, as seen in DMD patients, as markers of muscle degeneration. Further histological examination of mdx muscles showed myopathic lesions similar to those of DMD, including the presence of necrotic and degenerating fibres, increased variability in fibre size, and macrophage infiltration (Bulfield et al. 1984).

Mdx muscle growth lags behind that of wild type (WT) mice prior to any visible pathology, their fibres being smaller, with fewer myonuclei than those of WT relatives. At 3 weeks of age the *mdx* muscles enter a degenerative stage of myonecrosis, accompanied by subsequent regeneration that leads to the complete

replacement of existing muscle over the following weeks. At maturity their fibres become larger and hypernuclear compared to WT mice. With increasing age their fibres become branched and split, which is a major contributing factor to the muscle hypertrophy observed in *mdx* mice (Duddy et al. 2015).

For the purpose of cell transplantation experiments, the *mdx* mouse model was crossed with the nude mouse (Partridge et al. 1989). The nude (*nu)* mouse arose as a spontaneous mutation first reported by Flanagan (Flanagan 1966) and although this hairless mutant had a reduced lifespan, its importance was not realised until Pantelouris (Pantelouris 1968) reported the absence of a thymus in adult homozygote nude mice, in contrast to wildtype of heterozygous counterparts. (Pantelouris & Hair 1970) showed that the mutation caused dysgenesis of the thymus, and not as previously believed, its complete absence. The developmental failure of the thymus in homozygotes leads to the absence of T-cells and a partial defect in B cell development, robbing them of cell mediated immunity. This immunodeficiency made the nude mice ideal hosts for transplantation experiments.

Partridge *et al.,* (1989) bred *mdx* mice on to a 129/ReJ background (homozygous for the GPI-$1s^a$ isoenzyme allotype, rather than the GPI-$1s^b$ of C57BL/10) to follow the contribution of donor C57Bl/10 cells to mosaic muscle fibres. To prevent graft rejection these mice were then crossed onto the *nude* background (NU-$Foxn1^{nu}$), giving rise to the $mdx^{nu/nu}$ mouse (Partridge et al. 1989).

The colony was maintained by crossing nude heterozygous females ($nu^{+/-}$) with homozygote males ($nu^{+/+}$), as homozygote females suffer from reduced fertility and are prone to lactational failure. Homozygote offspring can be easily identified by their lack of hair (Fogh & Giovanella 1978).

2.1.3) 3F-*nLacZ*-2E

The 3F-*nlacZ-2E* transgenic mouse carries seven copies of a construct consisting of a 2kb sequence upstream of the myosin light chain (MLC)-3F transcriptional start site, *nlacZ*-SV40 poly(A) in frame in the second MLC3F specific exon, followed by 1kb of MLC3F sequence 3' of the *nlacZ* gene, and a 260-bp 3' MLC1F/3F enhancer. ß-gal expression faithfully recapitulates fast myosin expression in the nuclei of fast myofibres, but is absent in the nuclei of slow fibres and satellite cells (Kelly et al. 1995; Beauchamp et al. 2000). Genotyping to distinguish positive littermates from heterozygote pairs was performed by the detection of ß-gal staining in the muscle of tail tip biopsies.

2.1.4) $C5^-$/ γ chain deficient/ $Rag2^-$

The $C5^-$/ γ chain deficient/ $Rag2^-$ mice (C5) are severely immune-deficient but non-dystrophic, and thus were employed to determine if the irradiation mediated enhancement of satellite cell engraftment required a dystrophic environment. They contain 3 knockouts; the Complement Component 5 gene, the recombinase activating gene 2, and the common cytokine receptor γ. Their phenotype is characterised by a complete absence of T lymphocyte, B lymphocyte, and NK cell function(Goldman et al. 1998; Mazurier et al. 1999) whilst their muscles are still able to regenerate normally after injury (Brimah 2004). It has also been established that these mice are suitable hosts for mouse and human myoblast transplantation, which are well tolerated and produce donor derived muscle after direct injection into the TA (Morgan *et al.*, 2002; Brimah 2004; Ehrhardt *et al.*, 2007; Meng *et al.*, 2015). However, the immunocompromised background of these mice is different from that

of the *mdx*$^{nu/nu}$ mouse, which may affect the results of experiments comparing mdx$^{nu/nu}$ mice and C5 mice. However, the mdx$^{nu/nu}$ mouse available within western laboratories has been historically cross bred in house, and it is therefore not possible for the researcher to obtain the same nude mouse strain without the dystrophic phenotype. As C5 mice were readily available as a non-dystrophic immunocompromised background, these were used for the experiments.

2.1.5) ßactinGFP

The transgene in the ßactinGFP transgenic mouse (C57BL/6-Tg(CAG-EGP)1310Osb) is composed of cDNA encoding EGFP from the jellyfish *Aequoria Victoria*, downstream of the 'GAG' promoter. The GAG promoter consists of the cytomegalovirus immediate early (CMV-EI) enhancer, followed by a 1.3kb sequence including the promoter, first exon, and first intron of the chicken ß-actin gene, with the 3' splice junction sequence replaced by the rabbit ß-haemoglobin gene, followed by the rabbit ß-haemoglobin polyadenylation signal and 3' flanking sequence (Okabe et al. 1997). The transgene was introduced into fertilised C57Bl/6 donor eggs, and it integrated on Chr14D1. The founder progeny was backcrossed for 11 generations. GFP positive littermates exhibit bright green GFP expression in all areas without hair, which was used for genotyping. Although muscle fibres express GFP, quiescent satellite cells from these mice in our colony do not express it, in contrast to similar models such as the ßactin GFP mouse (Cerletti et al. 2008), however they begin expressing GFP upon activation and differentiation.

2.1.6) CD1

Young, outbred male CD1 mice were used for positive control tissues, including ovary, thymus, and small intestine. Pseudo pregnant females are routinely used by Western Laboratories for breeding purposes, and young males are largely marked for stock reduction. Tissues were obtained from these surplus mice.

Table 2.1: Summary of Mouse Strains Used	
Strain	Reasons for use
mdx nude	Immunocompromised model of DMD is used as a host for cell transplantations
C5$^-$/ γ chain deficient/ Rag2$^-$	Immunocompromised non-dystrophic mouse used to determine if irradiation is able to enhance satellite cell engraftment in non-dystrophic mice. This model was used due unfeasibility of obtaining nude mice with the same genetic background as the mdx nude mice developed in house
3F-nLacZ-2E	These mice were primarily used as satellite cell donors, allowing for the detection of muscle of donor origin by two markers, X-gal staining and dystrophin staining. This is due to the presence of revertant fibres within mdx muscles which may stain positively for dystrophin.
ßactinGFP	GFP positive mice were employed as satellite cell donors for grafts into non-dystrophic mice, allowing the use of GFP as a marker for tissue of donor origin, since as dystrophin staining would not allow the differentiation of endogenous muscle over muscle of donor origin in non-dystrophic hosts.
CD1	Outbred wildtype mouse employed for the collection of control tissues

2.2) Animal Protocols

2.2.1) Host Muscle Irradiation

Host mice (either *mdx*$^{nu/nu}$ or C5) had their hindlimbs irradiated using a Siemens TD-200 γ irradiator. Mice were anaesthetised via a subcutaneous injection of Hypnorm (79µl/ml fentanyl citrate, 2.5mg/ml fluanisone, Janssen-Cilag Ltd) and Hypnovel (Midazolam 1.25mg/ml, CP Pharmaceuticals Ltd), diluted in sterile water at a ratio of 1:1:4 respectively.

For hindlimb irradiation, custom made holders were employed. These consisted of an upper plastic chamber to hold the mice, attached to a 4cm thick base made of lead encased in plastic, to shield the bodies from irradiation. The upper chamber has 2 openings, leading to a protruding plastic platform that is devoid of lead shielding. For hindlimb irradiation, anaesthetised mice were placed in the upper plastic chamber, surrounded by sterile cotton wool to avoid hypothermia, and secured with labelling tape, ensuring the tail was protected by the lead shielding. The hindlimbs were stretched and passed through the openings in the upper chamber taped to the unshielded plastic platform (ensuring that the Tibialis Anterior was exposed (figure 2.1). The blocks containing the mice were placed inside the irradiator, and the irradiation time was set according to the manufacturer's instructions. The time required for the desired dose (18Gy or 25Gy) was compensated for on a monthly basis to account for the half-life of Cs-137.

Once the irradiation time had elapsed, the mice were removed from the irradiator and placed on a heated blanket, where they were allowed to recover from the anaesthetic before returning them to their respective cages.

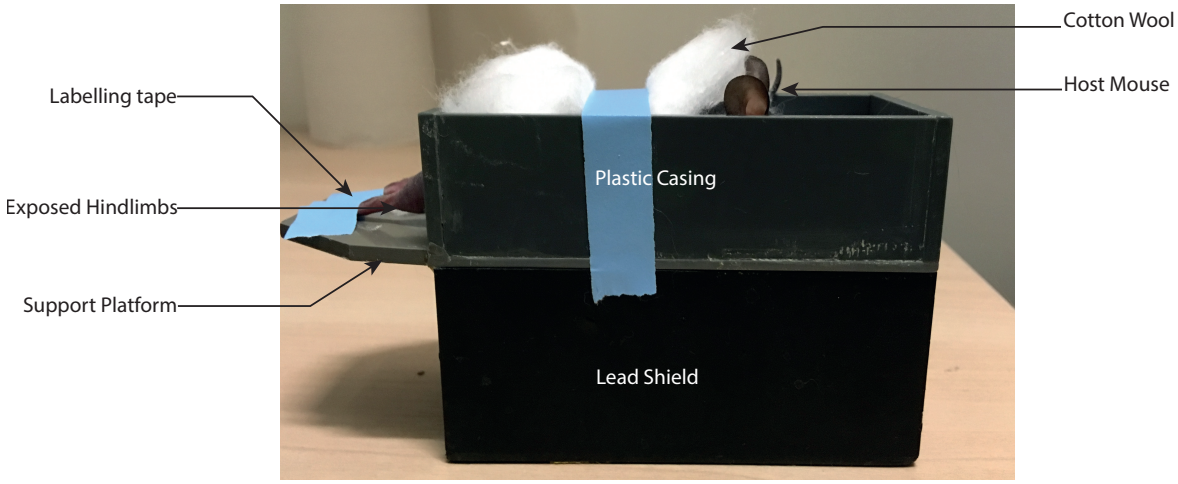

Figure 2.1: Preparation of a mouse for hindlimb irradiation. The mouse is placed in a support base with lead shielding to protect the body and tail from irradiation. The hindlimbs are exposed through an opening in the shielding and fixed in position.

2.2.2) Cell Grafting Procedure

All cells were grafted using 10µL PCR micropipettes (Drummond 5-000-1001-x10) whose end was pulled over the flame of a Bunsen burner using forceps and then trimmed to an adequate size under a dissection microscope to create a needle tip.

The mice were first placed under isoflurane anaesthesia, on top of a sterile drape placed over a heated electric blanket, and the hindlimbs taped with the TA facing upwards by rotating the leg, using the tibial crest as an anatomical reference point. The skin was sterilized with 70% ethanol, if required (in C5 hosts) the fur overlying the TA was shaved using a #22 scalpel. A small incision was performed on the skin above the TA using a #11 scalpel, big enough to allow the PCR pipette to pass through. 5µL of donor satellite cell suspension (approximately 400 cells) were pipetted using a sterile pipette tip and a Gilson pipette on to a sterile petri-dish lid and then taken up into the PCR micropipette. The pipette was then inserted through the incision into the TA to deliver the satellite cells.

For single fibre co-transplantation experiments, single muscle fibres from pre-irradiated *mdx*$^{nu/nu}$ donors were prepared according to sections 2.3.1.2 and 2.3.1.3. Muscle fibres were carried to the theatre in a horse serum coated Petri-dish containing plating medium. Two muscle fibres were first collected from the suspension culture using the glass micro-pipette and injected into the muscle, followed by injecting *3FTGnLacZ* satellite cells as described above.

For single cell suspension co-transplants, pre-irradiated *mdx*$^{nu/nu}$ muscles were enzymatically disaggregated according to section 2.4.2. Satellite cells were prepared from *3FTGnLacZ* donors and their total volume adjusted to give 400 cells in 3µL. 2µL of the single cell suspension (approximately $1.5x10^4$ cells) was mixed with 3µL of satellite cell suspension and taken up into a pulled PCR micropipette for injection into the TA. The mice were allowed to recover from anaesthesia on a heated blanket and returned to their cages.

2.2.3) Grafting Satellite Cell with LIF

To determine if LIF was a key mediator in augmenting satellite cell engraftment in pre-irradiated hosts (as described in section 2.2.1), freshly isolated satellite cells from 3F-nLacZ-2E (section 2.3.1) were grafted into the TA of *mdx*$^{nu/nu}$ mice divided into 2 experimental groups and 2 control groups:

- 3-day 18Gy pre-irradiated positive controls, where satellite cell engraftment is viable
- 5-day 18Gy pre-irradiated hosts, at time point after irradiation LIF expression is restored to non-irradiated control levels
- Non-irradiated hosts
- Non-irradiated hosts grafted with satellite cells incubated with LIF for 1 hour prior to transplantation and grafted in culture media containing 10ng/ml of murine LIF (PEPROTECH, catalogue number: 250-02; Lot number: 031271).

TAs were collected 4 weeks after transplantation, frozen according to section 2.4.1, cryosectioned (section 2.4.3), stained for X-gal (section 2.5.3) and dystrophin (2.5.2.1) and the amount of muscle of donor origin quantified according to section 2.6.4.1.

2.3) Primary Cell Isolations

2.3.1) Single Fibre and Satellite Cell Isolation

Single fibre isolations have been described previously, and detailed protocols are available from Boldrin & Morgan (2013), and Collins & Zammit (2009). A video protocol is also available from Pasut et al. (2013).

2.3.1.2) Muscle Dissection and Digestion

Donor mice varied depending on the host employed for transplantation experiments, using the *3F-nLacZ-E* for *mdx*$^{nu/nu}$ hosts and the *ßactinGFP* for *C5* hosts. The mice were euthanized by a schedule 1 procedure (cervical dislocation followed by decapitation).

Once euthanized, the mice were placed face up onto a support board, with the hind-limbs stretched out. The tail was passed under the hindlimb to be dissected and pulled towards the anterior end, to rotate the hip and allow easier access to the tibialis anterior (TA) and the extensor digitorus longus (EDL). The skin was sterilised with 70% ethanol. For the dissection procedure a dissection microscope can be used.

An incision was then performed from the upper side of the dorsal side of the paw, running along the skin above the tibial crest and up to the knee joint. The skin was then retracted to expose the underlying muscle. At this point the TA is clearly visible, and the EDL rests just beneath it. To extract the EDL, the fascia above the TA was removed using forceps (#5). The four tendons of the EDL were located on the dorsal side of the paw, and cut on the proximal side to their insertions on the base of the third phalanx of digits two and five. The

TA tendon was cut proximal to its insertion on the first cuneiform and proximal end of the first metatarsal.

Firmly gripping the tendons of the EDL and TA with forceps, the tendons were eased away from the underlying bone and musculature, and then used to pull the TA and EDL towards the proximal end. The EDL is visible just under the TA. Then the EDL was separated from the TA towards the distal side of the hind-limb. The TA was cut at the proximal end, to reveal the proximal EDL tendon beneath it as it goes into the knee joint, which was then severed.

Once the proximal end of the EDL tendon is cut, the EDL can then be gently pulled out of the hindlimb and placed in 2ml of collagenase solution (Collagenase Type 1, Sigma C0130, adjusted to 250CDU/ml) in DMEM (Gibco 41966-029) with penicillin (100 units/ml) streptomycin (100µg/ml), 2% by volume Glutamax (Gibco 35050-038), passed through a 0.2µm filter). The muscles were incubated in the collagenase solution for 1-2hrs at 35°C with regular agitation (15 minute intervals). The precise time depends on both the age and size of the mouse and the activity of the batch of enzyme used. The digestion is complete when the muscle looks less defined and slightly swollen, with hair-like single fibres seen coming away from the edge of the muscle.

2.3.1.3) Single Fibre Isolation

For single fibre isolations, 4 Petri-dishes per EDL were prepared at least 30min prior to the procedure (50mm deep, single vent, VWR cat 391-2022); these were coated with neat horse serum (Gibco 16050-098) to prevent the fibres from attaching to the surface. After coating, the dishes were filled with 8ml of DMEM with 2% Glutamax (Gibco 35050-038), 1% penicillin (100 units/ml) streptomycin (100µg/ml) (Sigma P4458) (final concentration: penicillin: 100 units/ml; streptomycin: 100 ug/ml; L-glutamine 4mM) (washing medium). Additionally, 2 types of pipettes are prepared:

- A wide bore pipette, made by cutting a glass Pasteur pipette using a diamond pen and heat polishing the cut end using the hottest part of a Bunsen burner flame. The opening at the end of the pipette was approximately 3.5mm.
- A heat-polished Pasteur pipette, bent at a 45˚ degree angle for ease of manipulation

Both pipettes were washed with 70% ethanol, then a rubber pipette filler was attached to the end of each pipette. The glass pipettes were rinsed in DMEM with 10% horse serum.

Using the wide bore pipette, each EDL was removed from its collagenase digest and placed in a pre-warmed Petri-dish. The dishes containing the remaining EDLs were then placed back in the incubator, removing only 1 EDL at a time for single fibre isolation.

The Petri-dish containing one EDL was then placed on a stereo dissecting microscope inside a laminar flow hood, and the EDL repeatedly taken up and released using the wide bore pipette for trituration. This procedure result in highly refractive, hair-like myofibres being released from the muscle, along with hypercontracted dead fibres, fat droplets, tendon, and other debris from the muscle. Using the small heat-polished and bent Pasteur pipette single liberated myofibres were collected and transferred to a new Petri-dish containing washing medium, taking care not to collect hypercontracted myofibres or debris. The collected myofibres should be smooth and free of any debris. Once isolated they were serially transferred through 2-3 further Petri dishes with DMEM to ensure that any contaminating endothelium, cells, and collagenase are removed. The final dishes containing single myofibres were then stored in the incubator at 37°C 5% CO_2.

2.3.1.4) Satellite cell stripping

The isolated single muscle fibres were transferred and pooled into a Petri-dish containing plating medium (DMEM/,2% L –Glutamine, 1% Penicillin-Streptomycin, supplemented with 10 % horse serum and 0.5 % chicken embryo extract). The satellite cells

were released by physical trituration for 5 minutes using a 19G needle mounted on a 1ml syringe. The cell suspension was then passed through a 40µm cell filter to remove hypercontracted fibres. Counting of stripped satellite cells is very difficult, due to large amounts of similarly sized debris and the very small size of satellite cells, however since the number of satellite cells per-fibre is known, counting the number of fibres used allows the number of satellite cells to be estimated (Boldrin & Jennifer E Morgan 2013; Collins et al. 2005).

To reduce the volume of medium containing stripped satellite cells, two rounds of centrifugation are required. The first was done at 240*g* for 15 minutes at 4°C to collect larger cells. This is followed by a second centrifugation at 600*g* for 20min at 4°C to collect smaller cells. The pellet was then re-suspended in the desired volume of plating medium.

2.3.1.5) Satellite cell irradiation

For the purpose of co-transplantation experiments, some satellite cells were irradiated using a Siemens TD-200 γ irradiator. The satellite cell collected as described in section 2.3.1.4 were placed in suspension on ice in a small polystyrene box. This box was placed on the shelf of the irradiator and the exposure time adjusted to a total dose of 18Gy, adjusting for the half-life of Cs^{137}.

2.3.2) Single Cell Suspension prepared from pre-irradiated donors

For single cell co-transplant experiments, a single cell suspension was prepared from the hindlimbs of *mdx*$^{nu/nu}$ mice pre-irradiated with 18Gy 3 days beforehand.

After culling the mice, the skin was washed with 70% ethanol and all the hindlimb muscles were dissected and placed in cold DMEM on ice.

In a laminar flow hood, the muscles were washed in phosphate buffered saline (PBS) and transferred to a Petri-dish with 2ml of collagenase II solution (Collagenase II (500 u/mL, (Sigma C0130) in 2ml DMEM, 4mg/ml). Using forceps and a #22 disposable scalpel, the

muscles were finely minced into a slurry, taking care to remove as much non-muscle tissue as possible. The muscle fragments were incubated at 37°C for 30 minutes. After digestion in collagenase II, the muscle fragments were crushed using the flat end of a sterile 5ml syringe plunger to create a 'sludge'.

5ml of cold sterile PBS containing 10% foetal bovine serum (FBS, GIBCO 10270-106) was then added to the muscle preparation and transferred to a 50ml falcon tube. Another 5ml of PBS/10%FBS was used to rinse the dish and added to the falcon tube. The suspension was then shaken vigorously and the volume made up to 50ml with PBS/10% FBS. The suspension was then centrifuged at room temperature at 600*g* for 5 minutes. The supernatant was then discarded, the pellet resuspended in PBS/10% FBS and centrifuged again at 600g. The pellet was then resuspended in 1ml of a collagenase D/Dispase II solution (collagenase D (Roche Diagnostics ref: 11088866001) 1.5u/ml and Dispase II (Roche 14549000) 2.4u/ml). The suspension was incubated for 1 hour at 37°C, and triturated by pipetting up and down with a 1ml Gilson pipette every 15 minutes.

After 1 hour the suspension was placed on ice. 50ml of PBS/10%FBS were added, and the suspension triturated by repeated pipetting. The suspension was then filtered through a 40µm cell strainer and centrifuged at 1500rmp for 5 minutes in a ALC PK130 centrifuge. The supernatant was then removed to a new falcon tube and centrifuged at 2500rpm for 5 minutes. The pellets were mixed and resuspended in 1ml of plating medium (in preparation for co-transplant experiments) and kept on ice. The number of live cells/ml was counted by staining a 2µL aliquot of the cell suspension with 2µL of 0.4% trypan blue (Invitrogen T10282), placed on counting slides (Bio-Rad 145-0011) on a TC20 automated cell counter (Bio-Rad). Two counts were made for each cell suspension and the average was used to adjust the live cell concentration to $7.5x10^3$ cells/µL for grafting (2µL per graft, equivalent to $1.5x10^4$ cells).

2.4) Histology

2.4.1) Unfixed Tissue

Gum Tragacanth (6% w/v, Sigma G1128-500)) was slowly dissolved in sterile water (3-4hrs) and heated overnight at 60°C in a waterbath, allowed to cool, and stored at 4°C.

Muscle or other tissues were bisected transversely and mounted in 6% Gum Tragacanth on cork disks and immediately frozen in liquid N_2 cooled isopentane (VWR 103616V). Once frozen, they were placed into liquid nitrogen, and then kept at -80°C until they were sectioned.

2.4.2) Immersion Fixation

When muscles were grafted with *ßactinGFP* donor satellite cells, the muscles had to be fixed prior to freezing to preserve GFP expression. The muscles were removed and fixed in cold 4% paraformaldehyde (PFA) dissolved in PBS (section 2.5.1.1) overnight at 4°C. After fixation, the tissues were prepared for cryopreservation by dehydration in a 30% (w/v) sucrose (Fisher S/860053) in PBS overnight at 4°C. Finally, the muscles were bisected transversely and mounted in 6% Gum Tragacanth on cork disks and immediately frozen in liquid N_2 cooled isopentane, then transferred to a -80°C freezer until cryosectioning.

2.4.3) Cryosectioning

Muscles were cut into serial 10µm transverse sections on a Bright (OTF 5000) or Leica (CM1850 UV) cryostat and collected on polylysine coated slides (VWR 631-0108). 10 slides of serial sections were prepared, meaning that each section on each slide was 100µm apart from the previous one. For immersion fixed muscles, SuperFrost Plus slides (VWR 631-0107) were used to aid attachment. In cases where a higher resolution was needed (eg. TUNEL assay, section 2.5.4) sections were cut at 7µm and captured on polylysine coated slides. After sectioning slides were stored at -80°C until required.

2.5) Staining of Tissues

2.5.1) Fixation

If muscles were not fixed before sectioning they were fixed before staining, except for staining using a dystrophin custom made P7 antibody (Lu et al. 2005).

2.5.1.1) Paraformaldehyde

4% PFA was prepared by slowly dissolving 40g of paraformaldehyde powder (Sigma P6148-500G) in 1l of pre-warmed (60°C) PBS, in a fume hood. Concentrated 10M NaOH was added dropwise until the powder had dissolved and the solution was clear. The pH was adjusted to 7.4 by adding 30% HCl or 10M NaOH. The solution was filtered to remove impurities and aliquoted into 20ml universals in a fume hood and stored at -20°C.

Sections were fixed in 4% PFA for 10 minutes at room temperature, followed by 3 washes in PBS.

2.5.1.2) Glutaraldehyde

Sections were fixed in cold 0.5% glutaraldehyde (Sigma G5882-50ml) for 10-20 minutes on ice, followed by rinsing and washing with cold 2mM $MgCl_2$ (Fluka 63064) in PBS.

2.5.1.3) Fixing single muscle fibres

Single muscle fibres were isolated as described in section 2.3.1.3, collected using a small heat polished pipette and placed into a horse serum coated 2ml round bottom tube (Eppendorf 0030 123.344) in as small a volume of media as possible. The tubes were then filled with 4% PFA and the fibres were fixed for 10 minutes at room temperature. After fixation as much PFA as possible was removed using a Pasteur pipette, trying not to disturb the fibres. The fibres were then washed in PBS/Tween (0.025%) (Tween 20 Sigma P1379-100ml) at room temperature for 5 minutes, and washed another 3 times (5 minutes in) PBS. The fibres were then stored at 4°C in PBS until needed.

2.5.2) Immunohistochemistry

2.5.2.1) Staining of muscle sections

Slides containing muscle sections were removed from -80°C storage and allowed to defrost at room temperature, then rehydrated in PBS for 5 minutes. After appropriate fixation (if required) the samples were permeabilised with 0.5% Triton-X-100 (Bio-Rad 161-0407) in PBS for 5 minutes at room temperature. The slides were washed 3 times in PBS for 10 minutes and then blocked with 10% Goat Serum (Sigma G9023-5ml), and when using mouse-anti mouse antibodies with Mouse-on-Mouse block (Vector Laboratories, MKB-2213), for 1 hour at room temperature to block endogenous mouse IgG. The primary antibody was diluted to the appropriate concentration (details of primary antibodies are in table 2.2), added directly to the slides, and allowed to incubate at room temperature in a humidified chamber for 2 hours. Slides were washed in PBS three times for 10 minutes and the incubated in with the appropriate fluorophore conjugated secondary antibody (table 2.2) at room temperature for 1 hour and protected from light. The slides were then washed 3 times in PBS for 10 minutes at room temperature before mounting with glass coverslips and Hydramount (National Diagnostics HS-106) containing DAPI (10µg/ml).

2.5.2.2) Staining of single muscle fibres

PFA fixed and PBS washed single muscle fibres (section 2.5.1.3) were retrieved from 4°C storage and as much PBS as possible was removed using a Pasteur pipette. The fibres were permeabilised with 0.5% Triton-X-100 (Bio-Rad 161-0407) in PBS for 5 minutes and then washed 3 times in PBS.

After removing as much PBS as possible the remaining volume was measured. An equal volume of 20% Goat Serum (Sigma G9023-5ml) in PBS was added (diluting it to 10% Goat Serum) for 1 hour, after which the primary antibodies were added directly to the

blocking solution at the appropriate concentration (table 2.2) and incubated at 4°C overnight.

The fibres were washed 3 times in PBS and the secondary antibodies were added in 10% Goat Serum, and incubated for 1 hour at room temperature. Finally, the fibres were washed 3 times in PBS, transferred to a goat serum coated Petri-dish. Using a dissection microscope and #5 forceps the fibres were collected and transferred to polylysine coated slides for mounting in Hydromount with DAPI (10µg/ml).

Table 2.2 - Antibodies							
Primary Antibodies					Secondary Antibody		
Antibody Against	Host Species	Cat. #	Supplier	Dilution	Antibody	Cat. #	Dilution
Pax7	Mouse	AB_528428	DSHB	1:100	AlexaFluor 488, Goat anti-Mouse IgG1	A21121	1:1000
EP4	Rabbit	ab93486	Abcam	1:100	AlexaFluor 594, Goat anti-Rabbit	A11037	1:1000
Laminin	Rabbit	L9393	Sigma Aldrich	1:500	AlexaFluor 594, Goat anti-Rabbit	A11037	1:1000
GFP	Rabbit	A6455	Invitrogen	1:1000	Alexa Fluor 488, Goat anti-Rabbit	A11034	1:1000
Dystrophin	Rabbit	Custom*	N/A	1:500	AlexaFluor 594, Goat anti-Rabbit	A11037	1:1000

*Note: Custom made P7 primary antibody against Dystrophin (Lu et al. 2005)

2.5.3) X-gal staining for localisation of ß-gal activity

Sections from muscles that were grafted with *3FTGnLacZ* donor satellite cells were first stained for ß-gal activity to detect areas of muscle of donor origin. Sections were fixed

in 0.5% glutaraldehyde (2.5.1.2), rinsed in cold 2mM $MgCl_2$ on ice for 10 minutes and incubated in detergent containing 2mM $MgCl_2$, 0.02% (v/v) IPEGAL CA-630 (Sigma 13021-50ml), and 0.01% (w/v) sodium deoxycholate (Sigma D6750-10G) in PBS for 10 minutes on ice.

X-gal solution was prepared by adding 1ml of X-gal stock (40mg/ml X-gal (Sigma B4252) in DMSO prepared in a glass beaker) to 40ml of X-gal diluent (2mM $MgCl_2$, 0.01% Sodium deoxycholate, 0.02% NP40, 5mM $K_3Fe(CN)_6$ (Sigma P8131), 5mM $K_4Fe(CN)_6$ (Sigma P9387) in PBS). The slides were incubated in either a Coplin jar or in a humidified chamber overnight in X-gal solution at 37°C. Finally, they were rinsed in PBS, followed by distilled water, and mounted in Hydromount with glass coverslips. The bright blue reaction product of X-gal localises ß-gal activity in the nucleus or cytoplasm of cells.

To check that donor mice were X-gal positive, the tip of the tails was removed and the skin removed. The tail tips were then incubated overnight in X-gal solution at 37°C; the bright blue colour around the tail muscles indicates that the donor mouse was indeed a *3FTGnLacZ* mouse.

2.5.4) TUNEL Staining

To stain apoptotic cells in muscle tissues a TUNEL staining method was used. This was done using the "ApopTag® Fluorescein *In Situ* Apoptosis Detection Kit" (Millipore S110), which is based on detecting DNA fragmentation that occurs during apoptosis. The kit relies on detecting DNA strand breaks by enzymatically labelling the free 3'-OH termini by using terminal deoxynucleotidyl transferase (TdT) which catalyses template independent addition of nucleotide triphosphates to the 3'-OH ends of single stranded or double stranded DNA (Gavrieli et al. 1992). The added nucleotides form an oligomer composed of digoxigenin labelled nucleotides and unlabelled nucleotides in a random sequence which is then detected by a fluorescein conjugated anti-digoxigenin antibody. The system allows the fluorescent detection of high concentrations of 3'-OH ends that are localised in apoptotic

bodies. However, the ability of this technique to stain apoptotic cells is questionable, as other environmental and cellular processes may yield double DNA strand breaks (DSBs) that will be stained by the TUNEL assay, such as necrosis, cellular senescence, and DSBs caused by exposure to ionising radiation (section 1.3.6.1)

The kit was used according to the manufacturer's instructions, using 7µm serial sections at least 100µm apart. After dioxigenin staining, the samples were stained for laminin (table 2.1) prior to mounting to identify the localisation of apoptotic nuclei in the muscle, finally the slides were mounted in Hydromount mounting media containing DAPI (10µg/ml). The stained samples were stored at -20°C until required.

For quantification of TUNEL staining, 3 randomly selected areas per muscle sample were imaged (x40). All three areas corresponded to different sections to prevent imaging the same area twice. They were randomly selected with the microscope out of focus and viewing DAPI staining. The total number of DAPI positive nuclei and TUNEL positive nuclei (co-localising with DAPI) were counted, and the results presented as a percentage of the total number of nuclei. From each muscle, the 3 counts from each randomly selected area were taken and the mean percentage value employed for data analysis.

For positive controls, sections from wax embedded receding rat mammary gland (provided with the kit) were used. Additionally, to test the efficacy of the kit on frozen tissues, I used sections from CD1 new born mouse thymus as positive controls, since about 5% of thymocytes developing in the thymus are normally removed by apoptosis, meaning the tissue should exhibit high levels of TUNEL staining (Surh & Sprent 1994; Klein et al. 2014).

2.6) Microscopy

2.6.1) Light Microscopy

Bright-field microscopy of sections was performed with a Leica DM4000B microscope and captured using MetaMorph® software (Molecular Devices Inc).

2.6.2) Fluorescence Microscopy

Fluorescence microscopy was performed using a Leica DM4000B microscope and captured using MetaMorph® software (Molecular Devices Inc). For scanning full sections, the Scan Slide function was used by determining the top right hand corner and bottom left hand corner of the area to be scanned. The images were then stitched together to form a composite image of the entire transverse section using the MetaMorph® software.

2.6.3) Confocal Microscopy

Stained samples were imaged in a Zeiss LSM 710 confocal microscope using a 63x Plan-Apochromat NA 1.4 WD 190µm Oil immersion objective and controlled using the Zen 2009 software. Each image was composed of the average of 16 scans.

2.6.4) Quantification of fibres of donor origin

2.6.4.1) Fibres of donor origin from 3FTGnLacZ satellite cells

Fibres of donor origin in host muscles grafted with *3FTGnLacZ* satellite cells were quantified by first identifying areas of muscle of donor origin by identifying x-gal positive areas. Serial sections were then stained for dystrophin and the section with the largest amount of dystrophin positive area was imaged with the "scan slide" function on Metamorph. Using the count tool on Adobe Photoshop (CC 2015) dystrophin positive fibres that coincided with x-gal positive areas on serial sections were counted. Small and separated groups which did not co-localise with x-gal positive areas, and without positive dystrophin staining along the full cell membrane were omitted, as these are likely to be revertant fibres.

2.6.4.2) Fibres of donor origin from B5GFP satellite cells

GFP stained muscle sections were imaged using the scan slide function. Three channels were captured, including DAPI, GFP, and texas-red. Texas-red was used to measure the average background fluorescence from PFA fixation; only GFP positive fibres exceeding

background level auto fluorescence were counted using the count tool on Adobe Photoshop CC (2015).

2.6.3) Image Processing

Minor modifications to brightness, contrast, and pseudo-colouring of images were performed using Fiji (NIH) or Photoshop CC 2015, all modifications were applied to the whole image. Quantification was performed by using the count tool included in Photoshop. Figures and images were arranged using either Photoshop CC 2015 or Illustrator CC 2015 (Adobe).

2.7) RNA Sequencing

2.7.1) Sample Preparations

RNA sequencing was performed on the TAs of 3-4 week old male mdx$^{nu/nu}$ mice. Four groups of samples with 3 biological replicates were used, and consisted of:

1. Non-Irradiated: (Non-IR) These consisted of non-irradiated, non-treated controls
2. 3 Days post 18Gy irradiation: At this time after this dose of irradiation, the muscle niche is permissive for satellite cell engraftment (Boldrin et al. 2012). *Mdx$^{nu/nu}$* mice had their hindlimbs irradiated as described in to section 2.2.1
3. Grafted: These samples consisted of a cohort of *mdx$^{nu/nu}$* mice whose hindlimbs had been irradiated according to section 2.2.1. Three days after 18Gy irradiation, donor *3FTGnLacZ* satellite cells were grafted into the TA as described in section 2.2.2, and grafted muscles were collected 2 days after grafting
4. Sham Injected: mouse hindlimbs were irradiated with 18Gy, TA muscles were sham injected with plating media 3 days after irradiation, and collected 2 days after the sham injection

The TA muscles were dissected and placed in sterile RNAse free DNAse free Eppendorf tubes and immediately snap frozen in liquid N_2 and kept at -80°C until required.

2.7.2) RNA Extraction

RNA extractions were performed using the *mir*Vana™ Isolation Kit (Ambion AM1560) according to the manufacturer's instructions. Briefly the muscles were removed from the -80°C freezer and were crushed to a fine powder using a liquid N_2 cooled mortar and pestle on a bed of dry ice. The muscle powder was transferred to an Eppendorf tube with x10 volume of lysis binding buffer (i.e. 50mg TA in 500µL) and homogenised using a ULTRA-TURRAXT8 (S8N-8G) homogeniser (IKA WERKE) on ice and then processed according to the manufacturer's instructions. RNA was eluted in RNAase free water and stored at -80°C until further use.

2.7.3) RNA Concentrations Quality Control

The quality and concentration of the extracted RNA was first assessed using a NanoDrop 1000 spectrophotometer (Thermo-Scientific) ensuring the A_{260}/A_{280} value was approximately 2.0. A value lower than 1.8 is indicative of protein contamination as aromatic proteins have a strong absorbance at 280nm. A large absorbance at 220nm and 270nm is also indicative of contamination, typically from reagents used in the isolation procedure (TRIzol, phenol, or chaotrophic salts).

The integrity of the extracted RNA was determined using the 2200 TapeStation system (Aligent G2964AA), RNA ScreenTape (Aligent 5067-5576) and the Aligent TapeStation software. This system is based on capillary gel electrophoresis and measures the ratio between the intensity of 28S and 18S RNA bands in the gel image. The ratio between these two measurements is derived using the RiN algorithm and determines the RNA integrity from a scale of 0-10. For RNA-sequencing a RiN value larger than 8.0 is required. This ensures that the quality of the RNA to be sequenced is sufficient to ensure reliable results.

2.7.4) RNA-sequencing and Raw Data Analysis

RNA samples were aliquoted in DNase free RNase free sterile Eppendorf tubes (catalogue number: 022431021), packed on dry ice, and shipped to Dr Peter White at The Research Institute at Nationwide Children's Hospital, Ohio (http://genomics.nchresearch.org/contact.html). Their research group performed further quality controls, and DNA digestion prior to sequencing. RNA sequencing was performed at 50 million 150bp paired end reads to maximise the accurate alignment of RNA reads.

They also analysed the raw data. Their parameters were set so each sample was aligned to the GRCm38.p4 assembly of the mouse reference from NCBI, using version 2.5.1b of the RNA-Seq aligner STAR (Dobin et al. 2013), and features were identified from the GFF file included with the assembly genome from NCBI. Coverage counts were calculated using HTSeq (Anders et al. 2015) and differentially expressed features were calculated using DESeq2 (Love et al. 2014). The spreadsheets that were returned to me contained features with an absolute fold change >= 2 and an adjusted FDR p-value <= 0.10, and also quality control PCA, volcano, MAV plots, alignment counts and read lengths.

2.7.5) Network Analysis Using Cytoscape

2.7.5.1) Creating a network of protein-protein interactions

Differentially expressed protein coding genes were queried using the STRING database (von Mering et al. 2003; Szklarczyk et al. 2015; Szklarczyk et al. 2017) using version 10.5 (available at http://string-db.org/) and accessed through Cytoscape (Version 3.5.1) to create a functional protein-protein association network. The confidence of interactions was set at 0.4, or medium, on the string database. In every network a small subset of genes showed no interactions with the remainder of the network, and these were excluded from network analysis.

2.7.5.2) Network Centrality Measures - Definitions

2.7.5.2.1) Eigenvector

To define the Eigenvector Centrality, the definition of Degree Centrality, one of the simplest centrality measures, must be understood. The Degree (κ) of a given node ν is simply the number of nodes adjacent to ν, where adjacent means directly connected. Nodes adjacent to ν are termed first neighbours. Therefore, degree is simply the number of connections, or edges, a node has to its first neighbours. Although simple, it can be very illuminating. In a social network, for instance, it would be reasonable to suppose that individuals who have connections to many others might have more influence, more access to information, or more prestige, than those with a fewer number of connections. In biologicals networks, proteins with a very high degree are interacting with several other signalling proteins, suggesting a central regulatory role, that is they are likely to be regulatory hubs. Depending on the protein the degree might, for example, indicate a central role in amplification (kinases), or the regulation of gene expression (transcription factors).

A natural extension of degree centrality is the Eigenvector centrality, first proposed by Bonacich 1987. In the case of degree centrality, one centrality point is awarded for each directly connected neighbour of ν. However, not all neighbours are equivalent. In many cases a vertex's importance in a network is increased by having connections to other vertices that are themselves important. This is the basis for Eigenvector centrality. Instead of awarding just one point for each first neighbour, eigenvector centrality gives each vertex a score proportional to the sum of the scores of its neighbours. Therefore, a vertex may have a large Eigenvector because the vertex has many neighbours or because it has important neighbours, or both. For example, an individual in a social network can be important by this measure because they know a lot of people (even though those people may not be important themselves) or knows a few highly influential people. In biological networks, a protein with high eigenvector is a protein interacting with several important proteins (regulating them or

being regulated by them), thus suggesting a central super-regulatory role or a critical target of a regulatory pathway. A low eigenvector would instead indicate a peripheral protein, interacting with few and not central proteins. The Eigenvector centrality has previously been used to identify and predict gene-disease associations (Ozgur et al. 2008) and to identify hubs in protein-protein interaction networks (Zotenko et al. 2008). A variant of this algorithm is used by Google's Page Rank Algorithm (Newman 2010; Scardoni & Laudanna 2012).

2.7.5.2.2) Stress

The stress of a node is measured by the number of shortest paths passing through a node. To calculate stress, all the shortest paths in a network are calculated, and then the number of shortest paths passing through a particular node v are counted. The stress of a node in a biological network can indicate the relevance of a protein as functionally capable of holding together communicating nodes. The higher the stress the higher the relevance of the node in connecting regulatory molecules. However, due to the nature of this centrality, it is possible that stress simply indicates a molecule that is heavily involved in cellular processes but is not relevant in maintaining communications between other proteins, as it is possible that two nodes may be connected by means of other shortest paths not passing though v. This measure can be complementary to Betweenness.

2.7.5.2.3) Betweenness Centrality

Betweenness centrality is similar to stress, however the measure is more elaborated and informative than stress on its own. Its first formal definition was provided by Freeman (1977). Supposing we have a network with information flowing around it from vertex to vertex along the edges, for example, in a social network messages, news, or rumours being passed from one person to another. Initially the assumption is made that every pair of vertices in the network exchanges a message with equal probability per unit time and that messages always take the shortest path through the network, or one such path chosen at random if there are several. After a suitably long time, many messages would have passed

between each pair of vertices. Since messages are passing through each geodesic path at the same rate, the number of messages passing through a particular vertex is simply proportional to the number of geodesic paths on which the vertex lies on. This number of geodesic paths is what is termed Betweenness centrality, or Betweenness for short (Newman 2010).

Vertices with high Betweenness centrality may have considerable influence within a network by virtue of their control over the flow of information passing between other vertices. The vertices with the highest Betweenness centrality are those through which the largest number of messages pass. If they are removed, they will also cause the most disruption in communications between other vertices, as they lie within the paths taken by the largest number of messages.

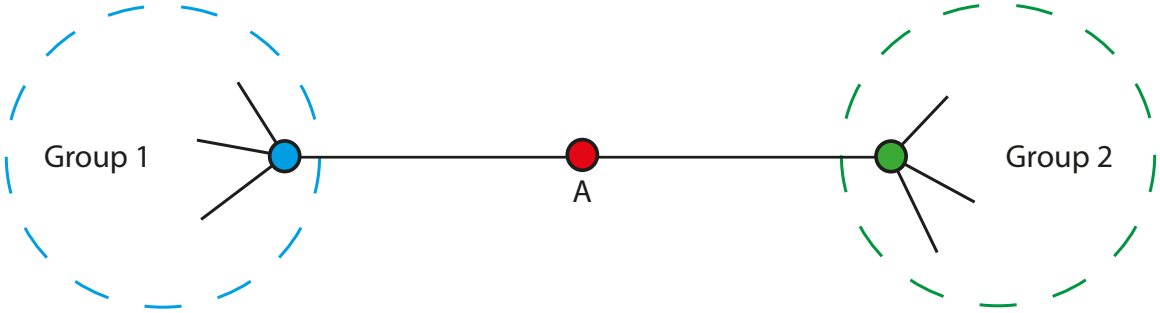

Figure 2.2: In this sketch of a network, node 'A' lies on a bridge joining two groups of other nodes. All paths between these groups must pass through A, so it has a high Betweenness centrality even though its degree is low. Therefore, node 'A' essential for maintaining the communication of this network.

Therefore, if a node A lies on a bridge joining two groups (1 and 2) of other vertices, all messages from group 1 must pass through vertex A to reach group two, and vice-versa (figure 2.2). Therefore, node A has a high Betweenness centrality even though its degree is low. Proteins with high Betweenness centrality have been termed "bottlenecks" for their role as key connector proteins with essential properties (Barabási et al. 2011).

In a biological network, this measure can indicate the importance of a protein as being capable of holding together communicating proteins. The higher the value the higher the relevance of that particular node as an organizing regulatory molecule. It essentially

indicates the capability of that protein to bring in communications from distant proteins, and are likely crucial to maintaining the functionality and coherence of signalling mechanisms (Newman 2010; Scardoni & Laudanna 2012). For example, in the yeast genome proteins with a low degree but high Betweenness centrality are abundant (Joy et al. 2005), and this finding is not explained by algorithms used to explain the scale-free property of protein-protein interaction networks where low connectivity proteins also have low Betweenness. The findings by Joy et al., (2005) indicate a modular network structure, and proteins with high Betweenness but low degree act as links between these modules. Joy et al also found that proteins with a high Betweenness are likely to be essential, and that their evolutionary age is positively correlated to their Betweenness centrality (Joy et al. 2005).

2.7.5.2.4) Closeness Centrality

The closeness of a node ν is calculated by computing the shortest path between node ν and all other nodes in the network (the number of edges along the path) then calculating the average. By this measure, vertices with a low average distance to all other nodes in the network will have better access to information or ability to directly influence all other nodes in the network. However, the mean distance is not a centrality measure in the same sense as the remaining centrality measures, since it gives high values to less central nodes, which is the opposite of the other centrality measures. Therefore, it is common to calculate the inverse of the mean distance. This inverse is called the closeness centrality (Newman 2010).

Biologically, a node with a high closeness centrality will be functionally relevant to several other proteins, but with the possibility of being irrelevant for a few other proteins. However, a high closeness value can be determined by the presence of a few nodes very close to node ν, with other much more distant, or by the fact that all nodes are generally very close to ν. Likewise, the value can be lowered by having a few nodes very distant from ν whilst the remainder are generally quite close to node ν. Therefore, closeness must always

take into account eccentricity (section 2.7.5.2.5), so a node with a high eccentricity and high closeness is very likely to be central in the network (Scardoni & Laudanna 2012)

Closeness centrality has been used to identify the top central metabolites in genome-based large scale metabolic networks (Ma & Zeng 2003), and to compare unicellular and multicellular eukarya to rank pathways and obtain a perspective on the evolution of metabolic organisation (Mazurie et al. 2010). It has been suggested as the best centrality measure that can be used to extract the metabolic core of a network (da Silva et al. 2008).

2.7.5.2.5) Eccentricity

The eccentricity of a node ν is calculated by computing the shortest path between node ν and all other nodes in the network, then the longest of these shortest paths (K) is chosen and its inverse is calculated ($1/K$). By this method if a node ν has a high eccentricity it means that all other nodes are in close proximity to ν. In contrast if the eccentricity is low, there is at least one node (and all of its neighbours) that is far from ν. Therefore, eccentricity is a more meaningful measure if its high compared to the average eccentricity of the network, calculated by averaging the eccentricity values of all nodes in the network. In biological terms this can be translated as the easiness of a protein to be functionally reached by all other proteins in the network. A protein with a high eccentricity compared to the average eccentricity of the network will be more easily influenced, or will easily influence, the activity of all other proteins in the network, and thus can readily perceive changes in the concentration of other enzymes or molecules that they are linked to (Scardoni & Laudanna 2012; Chavali et al. 2010)

2.7.5.3) Identifying major network regulators

The values for each centrality, and their network average, were calculated using the CentiScape app version 2.2 (Scardoni et al. 2009) for Cytoscape version 3.5.1. After each node had their centrality values computed, network filters were applied to select only nodes with Eigenvector, Betweenness, Closeness, Stress, and Eccentricity values above the network

average. Taken together this would amount to selecting nodes which are highly influential (Eigenvector), which are also essential in maintaining network communications (Betweenness and Stress), and can easily influence most nodes in the network (eccentricity and closeness centrality). The nodes matching values above the network average for all centralities were exported into a new network, this sufficed to extract hubs in small networks (control vs 3 day irradiated). However, when applied to larger networks too many nodes remain for a clear view of the top network regulators. Therefore only the nodes above 75th percentile of the observed distribution in each network was selected as the definition of a "high score" is network-specific and is less biased than the application of an arbitrary score cut-off for all data-sets (Azuaje, 2014). This was calculated by pasting all centrality values for each node into graph-pad Prism 7 and determining the column statistics for each centrality measure. This returns the minimum, 25% percentile, median, 75% percentile and maximum values for each centrality. The few nodes matching all the necessary thresholds were considered the major regulatory hubs of the network.

2.7.5.4) Gene Ontology Analysis of major network regulators using BINGO

To gauge the probable biological functions of the major network regulators identified by topological network analysis, the isolated top network regulator network was selected and used as the input for BINGO. BINGO is a tool to determine which Gene Ontology (GO) categories are statistically overrepresented in a set of genes or a subgraph of a biological network (Maere et al. 2005). Overrepresentation was assessed using a Hypergeometric test with a Benjamini & Hochberg False Discovery Rate correction, to a significance level of $p<0.001$. The selected ontology file was "GO_Biological_Process" and the species annotation was set to *Mus musculus.* To obtain the gene ontology tables outside the Cytoscape environment the saved results (.bng files) were changed to .txt and opened in Microsoft Excel for Mac (version 15.26).

2.7.6) Gene Set Enrichment Analysis (GSEA)

Cytoscape allowed me to separate the major network regulators and determine their probable biological functions. However, to obtain a more detailed understanding of what pathways may be represented in the network and integrate gene expression, data Gene Set Enrichment Analysis (GSEA) was performed using the open source GSEA analysis software (version 3.0) developed by the Broad Institute and UC San Diego (Subramanian et al. 2005; Mootha et al. 2003). This method focuses on gene set that is groups of genes sharing common biological functions, chromosomal localisations, or regulation. The gene sets use for the analysis are based on prior biological knowledge about biochemical pathways or co-expression. The software determines whether these defined sets of genes show statistically significant and concordant differences between two biological states. As a reference dataset, the molecular signatures database (MSigDB) hallmark gene set collection was used. Each hallmark in the collection consists of a "refined" gene set, derived from multiple founder sets, that emphasises genes that display co-ordinate expression and represent a well-defined biological process (Liberzon et al. 2015).

RNA-seq data were provided with a calculated overall fold change in expression for each gene, but not for each gene in each biological replicate individually, which is what is required for GSEA analysis. However, for each sample the number of reads for each gene was provided, however these had a very wide variation from 0 to thousands of reads. Therefore, I derived a value (v) from the number of reads (r) recorded for each gene in each biological replicated. Where:

$$\boldsymbol{v = Log_2(r + 1)}$$

This gives a set of values within a range that is easy to represent and interpret visually and proportional to the levels of expression of each gene within each sample. The data sets for each comparison were then loaded on the GSEA software for analysis. The following parameters were selected or altered from the default options:

- Gene sets database: *h.all.v.6.0.symbols.gmt (Hallmarks)*
- Number of Permutations: *1000*
- Phenotype labels: manually entered with "*create an on-the-fly phenotype*", manually assigning sample IDs to their respective treatment groups
- Permutation Type: This was changed from phenotype to *gene_set*. This was required due to the small number of samples, and although it provides a lower reliability than the phenotype option, it is useful for hypothesis generation and guidance (Subramanian et al. 2005)
- Chip platform: *GENE_SYMBOL.chip*
- Min Size: Exclude smaller sets: *10* – sequencing data did not return large data sets of differentially expressed genes so the threshold was lowered from 15 to 10

The data were then analysed and the GSEA software returned the reports for each enriched gene set in the uploaded gene list, along with heat-maps specific for each over-represented pathway. The values returned by GSEA are fully described by Subramanian *et al.*, (2005), and a brief description for interpretation is provided below, the abbreviation used for each statistic is shown in brackets:

- Enrichement Score (ES): The degree to which this gene set is overrepresented at the top or bottom of the ranked list of genes in the expression dataset.
- Normalised Enrichement Score (NES): By normalising the enrichment score GSEA accounts for differences in gene set size and in correlations between gene sets and the expression dataset. The normalised enrichement score can be used to compare analysis results across gene sets
- Nominal *P* value (NOM p-val): Estimates the statistical significance of the enrichement score for a single gene set. As it is not adjusted for gene set size and multiple hypothesis testing its of limited value when comparing gene sets. If the value is 0.0 it indicates the actual p value is less than 1/number of

permutations. All the analysed dataset were performed with 1000 permutations, and therefore it will indicate the p value is smaller than $1x10^{-3}$

- FDR q-value (FDR q-val): The estimated probability that the NES represents a false positive finding
- Familywise-error rate (FWER): A more conservative estimated probability that the normalised enrichment score represents a false positive finding.

Although all these statistics are provided in the results chapter, the guide to use the GSEA software provided by the broad institute recommends focusing on the FDR statistic.

2.8) RT-qPCR pathway focused plates for validation of RNA-seq results

The main pathway identified through analysis of the RNA-seq data were all related to type I interferon signalling and interferon gamma signalling. Therefore, the results were further validated by performing a series of pathway-focused RT-qPCR plates for interferons and receptors (RT^2 profiler arrays, interferons and receptors, PAMM-064Z, SAB Bioscience) containing 84 genes related to interferon signalling. For these experiments, I analysed 4 groups of samples with 3 biological replicates, all of which were from 3 to 4 week old male *mdx*$^{nu/nu}$ mice different from those used for sequencing. They consisted of:

- 3 Days after 18Gy – at this stage the muscle niche is permissive for donor satellite cell engraftment (Boldrin et al. 2012). Mouse hindlimbs were irradiated according to section 2.2.1
- 3 Hours after 25Gy – this is a different dose regime where donor satellite cells engraftment is successful immediately after irradiation (Boldrin et al. 2012). Under these conditions the niche is receptive to satellite cell engraftment. Mice were irradiated according to section 2.2.1

- 3 Days after 25Gy – These muscles have an hostile niche that does not allow satellite cells to engraft (Boldrin et al. 2012)
- Non-irradiated – controls used for the normalisation of all other samples.

The TAs were collected at the appropriate time points and immediately frozen in liquid nitrogen. The right TA was used for RNA extractions, whilst the left TA was reserved for protein quantifications.

2.8.1) RNA extraction

TAs were homogenised in tubes containing ceramic beads (Precellys 03961-1-002) and lysis reagent (QIAzol® Lysis Reagent) in a Precellys 24 Homogenizer at 5700rpm with a x2 30 second cycle at room temperature. Once homogenised, the RNA was extracted using the RNeasy Microarray Tissue Mini Kit 50 (Qiagen 73304) according to the manufacturer's instructions. Quality control for the RNA was performed according to section 2.7.3.

2.8.2) cDNA synthesis

Once the RNA was isolated, it was diluted to ensure all samples had a concentration of 100ng/µL, and 0.5µg of RNA was used to synthesise cDNA. The synthesis was performed using the RT^2 First Strand Kit (Qiagen 330401) following the manufacturer's instructions.

2.8.3) RT^2 Profiler Arrays

Since the RT^2 profiler arrays are supplied with qPCR plates pre-loaded with primers, the procedure was relatively simple and carried out according to the manufacturer's instructions. For each sample 1350µL of RT^2 SYBR Green Mastermix (Qiagen 330522) were mixed with 102µL of the cDNA synthesis reaction and 1248µL of RNase-free water and dispensed into their corresponding plate. 1 plate was used per sample. The plates were then sealed, centrifuged at 435g, and run on an Applied Biosystems Step One Plus qPCR machine with 1x10 minute 95°C cycle to activate *Taq* Polymerase, 40 cycles of 15 seconds at 95°C, and 1 minute at 60°C for fluorescence data collection. Once all the qPCR plates were run the data

were collected, and the threshold for every plate was set at the same value (0.05). The data were exported to Excel and analysed using an online software provided by the manufacturer.

2.9) Comparison of RNA-seq and Array Samples by RT-qPCR

To enable comparisons between the samples used for RNA sequencing and those used for pathway-focused arrays, qPCRs were performed for some of the genes of interest. These were done using the iTaq™ Universal Probes One-Step Kit (Biorad 172-5141) on MicroAmp Fast Optical 96 Well Reaction plates (Applied Biosystems 4346906) according to the manufacturer's instructions. All results were normalised to Actin, which was observed to be a stable House Keeping Gene in the qPCR arrays. Probes used were purchased from Thermo-Fisher Scientific and are shown in table 2.3.

Table 2.3: Primers used for RT-qPCRs	
Probe against:	Catalogue Number:
Actb (House Keeping Control)	Mm02619580_g1
Ifng	Mm01168134_m1
LIF	Mm01168134_g1
IRF7	Mm00516793_g1
Ifi204	Mm00492602_m1

2.10) RT-PCR

RT-PCRs were performed using the OneStep RT-PCR kit (Qiagen 210210) according to the manufacturer's instructions. RNA was extracted as detailed on section 2.8.1. For testing the expression of the EP4 receptor primers were designed using NCBI Primer Blast. The selected primer consisted of the following sequence:

- Forward Primer (5' to 3'): GCTTGACAAGTTCCGCACTG
- Reverse Primer (3' to 5'): ATGGTACCTGTAGGGTGGG

This spanned a 121bp sequence of the prostaglandin E_2 receptor EP4 mRNA. The PCR product was amplified and separated on a 1.5% agarose gel (Invitrogen Ultrapure™ Agarose 16500-500) with 1% by volume SYBR® Safe (Invitrogen S33102) at 70V for 1 hour and visualised using the GenoSmart UV illuminator (VWR).

2.11) Statistical Analysis

TUNEL assay results were analysed using a one-way ANOVA with a Tukey's multiple comparisons test.

Results from cell grafting experiments with more than 2 groups were analysed using a Kruskall-Wallis test with a Dunn's multiple comparisons test. If only two groups were compared a Mann-Whitney test was employed.

Gene expression data from qPCRs were analysed using a one-way ANOVA, comparing all experimental groups to the non-irradiated control, using a one-way ANOVA and a Fisher's LSD.

Chapter 3 - An investigation of the cells within irradiated host muscle that are responsible for the augmentation of donor satellite cell engraftment

3.1) Introduction

3.1.1) Background

Ionising radiation induces several pathological features in irradiated cells, such as cell death, chromosomal aberrations, DNA damage, mutagenesis, and carcinogenesis. It was previously thought that the damage incurred by the cell was a consequence of direct ionisation of cell structures, in particular DNA, or as an indirect consequence of the production of reactive oxygen species from the radiolysis of water. However, cells damaged by ionising radiation can have similar effects on neighbouring non-irradiated cells, a mechanism called the bystander effect. This can induce a reduced capacity for clonogenic survival (Mothersill & Seymour 1997); chromosomal aberrations (Lehnert et al. 1997); apoptosis (Prise et al. 1998); and altered gene expression at the RNA level of neighbouring cells (Rzeszowska-Wolny et al. 2009). The bystander effect demonstrates the ability of cells lethally damaged by irradiation to significantly alter surrounding non-irradiated cells.

However, lethally damaged cells also possess the ability to induce changes in their local environment that would be conducive to an increase in the proliferation of their neighbouring cells to aid in wound healing. This process is known as apoptosis-induced proliferation; whereby dying cells are able to trigger the surrounding cells to proliferate to compensate for their impending loss and thus begin tissue repair. The first evidence of this was work by Hayine and Bryant (Haynie & Bryant 1977) who demonstrated that 60% of precursor cells in the developing wing of *Drosophila Melanogaster* embryos could be eliminated by irradiation, and yet extra cell divisions within the surviving cells gave rise to a normal functioning adult wing. Subsequent work showed that in *Drosophila* embryonic epithelial tissues, the induction of apoptotic cell death is able to induce proliferation of surrounding cells. If the irradiated cells are kept in an 'undead' state, by the inactivation of effector caspases through the forced expression of baculoviral protein P35, they can trigger hypertrophic growths and changes in tissue morphology due to changes in the secretory phenotype of the 'undead' cells signalling to surrounding cells (Huh et al. 2004). Characterised examples of these secretory changes include the release of Decapentaplegic (Dpp) and Wingless (Wg) (Huh et al. 2004; Ryoo et al. 2004; Fan & Bergmann 2008) which are the mammalian equivalent to Bone Morphogenic Proteins (BMPs) and Wnt signalling respectively. These are also well recognised mediators in tissue development, cell proliferation, and morphogenesis (Ryoo et al. 2004; Huh et al. 2004; Fan & Bergmann 2008; Martin et al. 2009).

In mammals, one of the most notable characteristics of wound healing and tissue regeneration is the infiltration of immune cells to the wound site (Haertel et al. 2014; Müller et al. 2012). This inflammatory reaction precedes regeneration, and

inflammatory cells disperse once the regeneration process is complete. Therefore, it was long assumed that tissue regeneration required proliferative signals released by the inflammatory cells.

However, *PU.1* (Spi1 Proto-Oncogene) knockout mice, which lack the inflammatory cells associated with wound healing, are capable of fully repairing damage to their skin (Martin et al. 2003). This indicates that there must be something intrinsic within the wounded tissue that can also stimulate the re-growth of the damaged tissue. Based on these observations Li et al. (Li et al. 2010) demonstrated in vitro and in vivo how lethally pre-irradiated cells are able to trigger the proliferation of adjacent cells by the caspase dependent activation of calcium-independent phospholipase A_2 ($iPLA_2$). This enzyme is involved in the production of prostaglandins: in their model it is the subsequent production of prostaglandin E_2 (PGE_2) after irradiation which promotes progenitor cells proliferation (Li et al. 2010). Following this study, a series of reports studying mammalian pancreatic, bladder, and melanoma cancer cell lines have confirmed the role of the PGE_2 signalling pathway in tumour repopulation following radiotherapy and chemotherapy (Kurtova et al. 2015; Huang et al. 2011; Donato et al. 2014).

Previously *mdx*$^{nu/nu}$ mouse muscles were pre-irradiated as a means of blocking endogenous regeneration and studying myofibre loss (Wakeford et al. 1991). However, when myoblasts from new-born mice were grafted into these pre-irradiated muscles, they integrated to a greater extent than in non-irradiated muscles (Morgan et al. 1990). Furthermore, most myoblasts die quickly after injection into the host muscle, and only a small subpopulation of precursors go on to rapidly proliferate and generate myofibres of donor origin (Jonathan R Beauchamp et al.

1999). Donor myoblast proliferation occurs only within irradiated and not in non-irradiated, host muscle (Jonathan R Beauchamp et al. 1999). It was later shown that the irradiation of the host skeletal muscle triggers a pro-tumorigenic environment that enables transplanted immortal C2C12 myogenic cells to rapidly proliferate and form tumours within the host muscle (Morgan et al. 2002), matching previous observations on apoptosis induced proliferation. Boldrin et al. showed that after 18Gy or 25Gy irradiation there is a sharp decrease in the number of satellite cells present in the *mdx*$^{nu/nu}$ mouse muscle, but not in non-dystrophic mice. When low numbers (approximately 400 satellite cells per injection) of freshly isolated satellite cells are transplanted into these irradiated muscles, these few cells are able to give rise to large number of fibres of donor origin (mean: 589 SEM: ± 149) (Boldrin et al. 2012). This indicates that the grafted donor satellite cells must proliferate rapidly in the host muscle to allow the production of high numbers of fibres of donor origin.

The results reported by Boldrin *et al.,* placed into context with the wide body of evidence for apoptosis-induced proliferation, lead me to hypothesize that apoptosing cells within the pre-irradiated host *mdx*$^{nu/nu}$, in particular satellite cells, might be releasing mitotic signals that allow grafted donor cells to rapidly proliferate and then differentiate to produce fibres of donor origin, whilst simultaneously repopulating the satellite cell niche.

3.1.2) Aims

1. Determine if the PGE_2 receptor EP4 is expressed in satellite cells
2. Determine whether there is significantly more apoptosis in *mdx*$^{nu/nu}$ host muscles in conditions where donor cell engraftment is optimal

3. Quantify the percentage of apoptotic cells in non-dystrophic mouse muscle
4. Determine whether the levels of apoptotic cells correlate with donor engraftment efficiency between mouse strains
5. Co-transplant pre-irradiated satellite cells, single myofibres, and a monocytic cell suspension to determine which pre-irradiated cell preparation is able to enhance donor satellite cell engraftment

3.2) Aim 1: Determine if the PGE_2 receptor EP4 is expressed in satellite cells

For PGE_2 to have any effect on satellite cell engraftment, its receptor (EP4) must be expressed on the surface of satellite cells. To determine if the EP4 receptor transcript is being expressed in skeletal muscle, an RT-PCR was performed according to section 2.10. Some of the tissues known to express EP4 are the kidneys, uterus, and small intestine (Yokoyama et al. 2013). These were obtained from CD1 mice and used as positive controls for the RT-PCR as shown in figure 3.1a. Muscles from CD1 and *mdx*$^{nu/nu}$ mice were also used, in both cases both wild type (CD1) and *mdx*$^{nu/nu}$ muscles show a band corresponding to the presence of the EP4 receptor mRNA.

To confirm its expression at the protein level on satellite cells, single muscle fibres and their associated satellite cells were isolated from 3F-nLacZ-2E mice according to section 2.3.1.3, fixed according to section 2.5.1.3, and stained according to section 2.5.2.2. Stained fibres were imaged according to section 2.6.3.

Single muscle fibres express the EP4 receptor along the surface of the fibre membrane (figure 3.1 C and G). Satellite cells associated with the myofibre, marked by Pax7 expression co-localising with DAPI, also express the EP4 receptor on their surface, as seen in figure 3.1 C and G, with the EP4 staining surrounding the entire satellite cell. This indicates that, if PGE_2 is released after irradiation by dying cells, satellite cells would have the capability of responding to this signalling lipid.

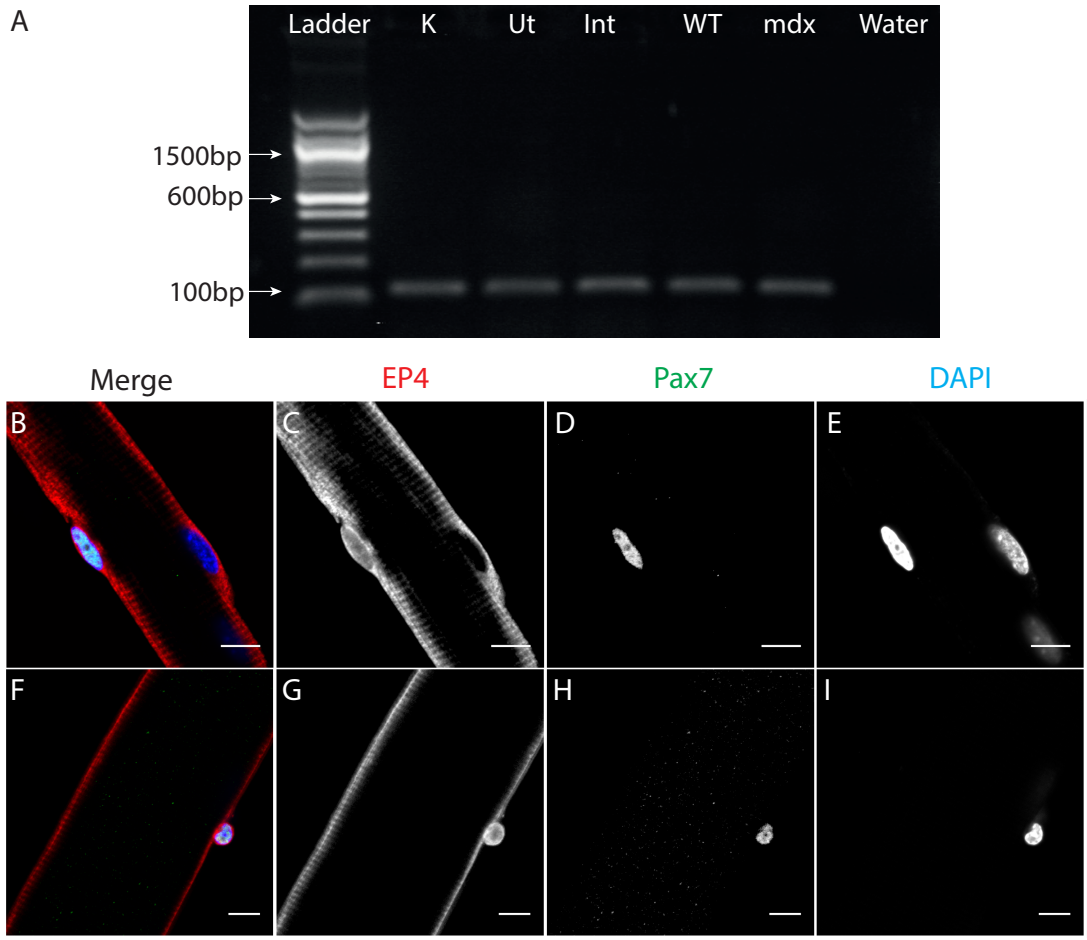

Figure 3.1: The PGE_2 receptor EP4 is expressed in muscle and localises to the surface of muscle fibres and the membrane of satellite cells. A) RT-PCR for the EP4 receptor shows expression in positive control tissues: Kidney (K), uterus (Ut), and intestine (Int). Wild type (WT) and *mdx*$^{nu/nu}$ skeletal muscle also show a band consistent with the presence of the EP4 receptor mRNA. B-I) Confocal imaging of single mouse (3FTGnLacZ) muscle fibres stained for the EP4 receptor, Pax7, and DAPI, showing Pax7 (D and H) co-localizing with DAPI (E and I) and expressing the EP4 receptor on the cell membrane of Pax7 positive cells, as well as along the surface of the myofibres (C and G). All scale bars = 10µm.

3.3) Aim 2: Determining whether there is significantly more apoptosis in mdx$^{nu/nu}$ host muscles at times of enhanced engraftment

The time point at which satellite cell engraftment is enhanced in a pre-irradiated host muscle has been shown to be dependent on the dose of γ-radiation delivered to the host tissue. After 18Gy, engraftment is enhanced up to 3 days after irradiation. One month after irradiation the beneficial effects are lost and donor satellite cell engraftment becomes negligible. A higher dose of 25Gy constricts this window for engraftment. After a dose of 25Gy, engraftment is possible immediately after, and the grafting procedure is normally done 3 hours after irradiation. However, 3 days later the host muscle environment is no longer permissive for donor satellite cell grafting (Boldrin et al. 2012). If apoptotic cells are mediating the enhanced engraftment, then it would be expected that there would be higher numbers of lethally damaged cells within host muscles at the time points that allow for a successful graft.

To test this hypothesis, the muscles of *mdx$^{nu/nu}$* mice were irradiated under both irradiation regimes (18Gy and 25Gy) and collected at the points where engraftment is successful (3 days and 3 hours respectively), and the points where engraftment is no longer viable (1 month and 3 days respectively). Using TUNEL staining (section 2.5.4) the percentage of TUNEL positive cells was determined.

Positive controls for TUNEL staining are shown on figure 3.2. Wax embedded receding mammary gland sections were provided by the manufacturer, new-born

thymus was used to test the effectiveness of the kit on frozen sections, and non-dystrophic *3F-nLacZ-2E* skeletal muscle was used to test its effectiveness in skeletal muscle tissue. Both the receding mammary gland and thymus stained extensively for TUNEL positive cells as expected. Non-dystrophic skeletal muscle showed no staining, as expected in a stable post-mitotic tissue.

Figure 3.3 shows representative images of untreated *mdx*$^{nu/nu}$ muscles (A-D); muscles collected 3 days after 18Gy irradiation, where the host muscle is permissive for donor satellite cell engraftment (E-H); and 1 month after 18Gy irradiation (I-L) where donor satellite cell engraftment is no longer viable.

Figure 3.4 shows a similar time-course for the group of mice under the 25Gy irradiation regime, with untreated muscles (A-D); muscles collected 3 hours after irradiation, where donor satellite cell engraftment is enhanced (E-F); and muscles collected 3 days after 25Gy irradiation (I-L) where satellite cell engraftment is no longer viable.

Under both irradiation regimes, no TUNEL positive nuclei are observed under the basal lamina, marked by Laminin staining (figures 3.5), suggesting that the TUNEL positive nuclei are neither satellite cells or myonuclei.

Untreated muscles, which are not permissive for donor satellite cell engraftment, had a mean of 0.261% (SEM: ±0.7897) TUNEL positive cells (figure 3.6). However, at the time points after irradiation where engraftment is enhanced, the levels of apoptotic nuclei increased significantly compared to untreated controls (figure 3.6). Three days after irradiation, the percentage of apoptotic nuclei was significantly increased from basal levels to 2.42% (SEM: ± 0.4429; p=0.0024), and 3 hours after a dose of 25Gy a similar increase in the percentage of apoptotic nuclei was observed,

having increased to 2.52% (SEM: ±0.6067; p=0.0016). In both cases this represents a 10-fold upregulation in the proportion of dying cells within the tissue at the time points corresponding to the host muscle being permissive to donor satellite cell engraftment. There was no significant difference between the percentage of TUNEL positive nuclei 3 days after 18Gy and 3 hours after 25Gy (p= 0.9996).

1 month after 18Gy irradiation, satellite cell engraftment is no longer viable (Boldrin et al. 2012), this correlates with a reduction in the amount of TUNEL positive nuclei, compared to the time points where grafting is permissive, to 0.773% (SEM: ±0.2783; n=4) which is not significantly different to the levels in untreated muscles (p=0.808) but is significantly lower than the levels observed 3 days after 18Gy (p=0.0386) or 3 hours after 25Gy (p=0.0264). Similarly, 3 days after 25Gy, where the host muscle is no longer permissive for engraftment, the levels of TUNEL positive nuclei are reduced to 0.328% (SEM= ±0.2242; n=3) which is significantly lower than 3 hours after 25Gy (p=0.0142) and 3 days after 18Gy (p=0.0203) but is not significantly different from the levels observed in untreated muscles (p=0.9948). Furthermore, there is no statistically significant difference between the levels of TUNEL positive cells at the time points after irradiation where satellite cell engraftment is no longer permissive (1 month after 18Gy vs 3 days after 25Gy, p=0.9784).

Taken together, these results indicate that the percentage of TUNEL positive nuclei within skeletal muscle positively correlates with the time points after irradiation, regardless of dose, at which satellite cell engraftment is enhanced in *mdx*$^{nu/nu}$ hosts.

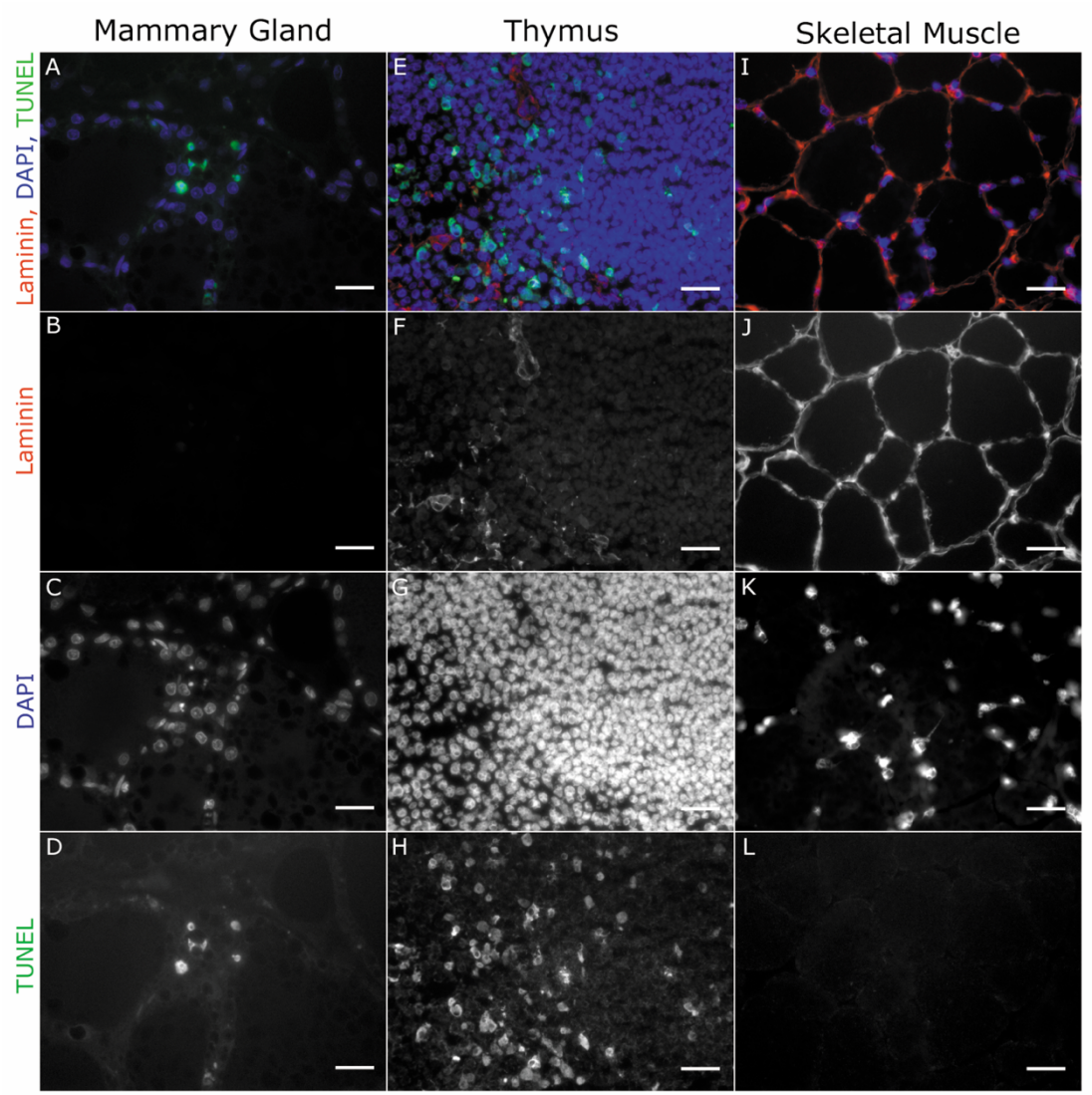

Figure 3.2: TUNEL staining of 2 control tissues (receding rat mammary gland and new born thymus) known to have high levels of apoptosis and non-dystrophic skeletal muscle as a negative control. A-D) TUNEL staining of receding rat mammary gland as a positive control for TUNEL staining, showing TUNEL positive nuclei (D); E-H) Mouse new born thymus with numerous TUNEL positive nuclei, used as a positive control (E and H); I-L) Mouse non-dystrophic (*3F-nLacZ-2E*) skeletal muscle stained for TUNEL and displaying no TUNEL positive nuclei (negative control). All scale bars = 50µm.

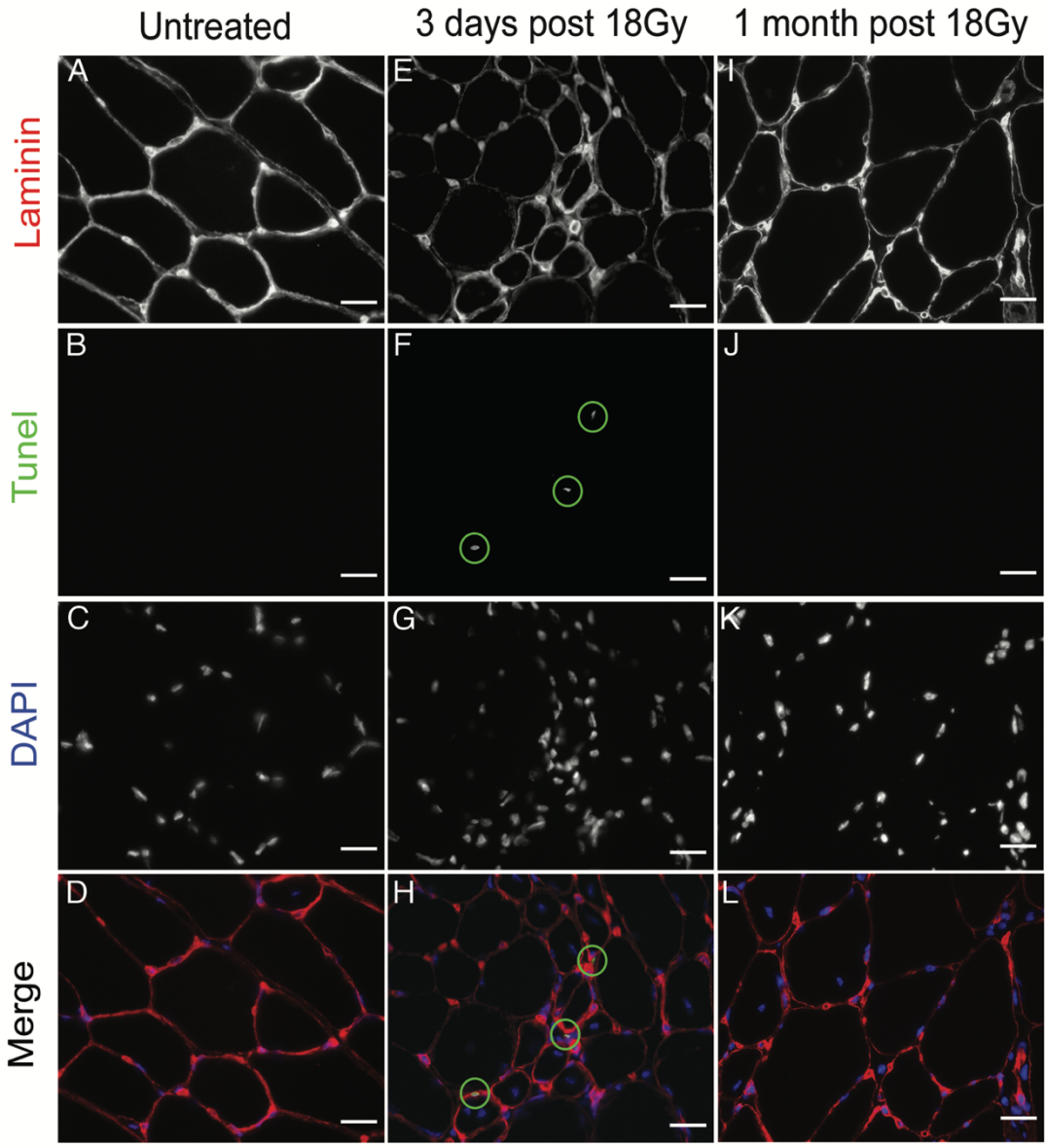

Figure 3.3: Representative images of TUNEL (green), laminin (red), DAPI (blue) staining of transverse sections of *mdx*$^{nu/nu}$ skeletal muscle, either untreated (A-D), 3 days after irradiation (E-F), or 1 month after irradiation (I-L). A-D) Non-irradiated *mdx*$^{nu/nu}$ skeletal muscle showing no TUNEL positive nuclei. E-H) Section of skeletal muscle irradiated with 18Gy 3 days previously, showing 3 TUNEL positive nuclei (within green circles) seen in figures F and H, none localised within the basal lamina. I-L) Representative image of *mdx*$^{nu/nu}$ skeletal muscle irradiated (18Gy) 1-month previously, showing no tunel positive nuclei (J and L). All scale bars = 50µm.

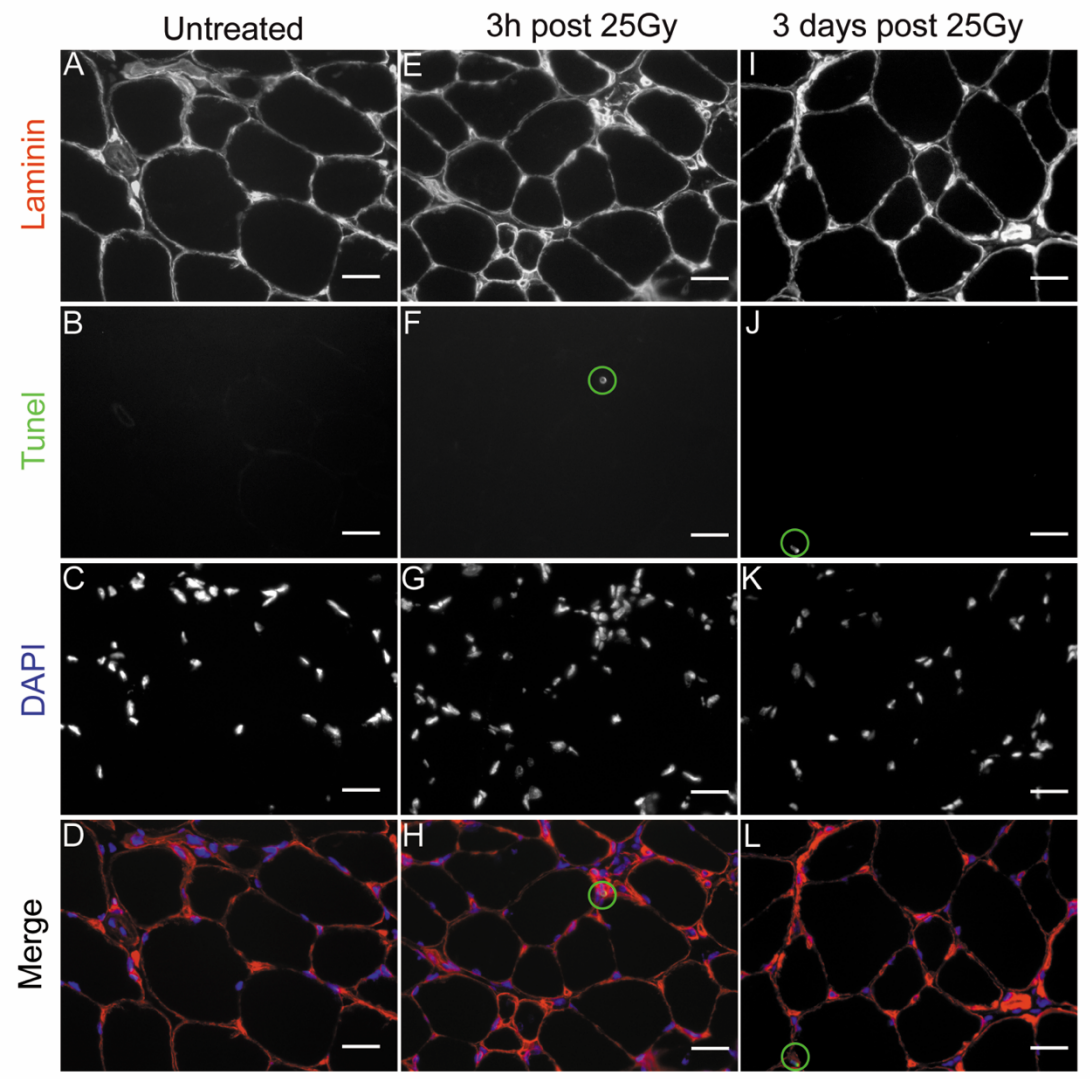

Figure 3.4: Representative images of transverse sedtions of *mdx*$^{nu/nu}$ skeletal muscle which has been either untreated (A-D), 3 hours after 25Gy irradiation (E-H), or 3 days after 25Gy irradiation (I-L). The sections were stained for laminin (red), TUNEL (green), and DAPI (blue). A-D) Untreated muscles showing no TUNEL positive staining. E-H) *mdx*$^{nu/nu}$ skeletal muscle 3 hours after 25Gy irradiation showing 1 TUNEL positive nucleus circled in green (F and H). I-L) Muscle 3 days after 25Gy irradiation displaying 1 TUNEL positive nucleus circled in green (J and L). All scale bars = 50µm.

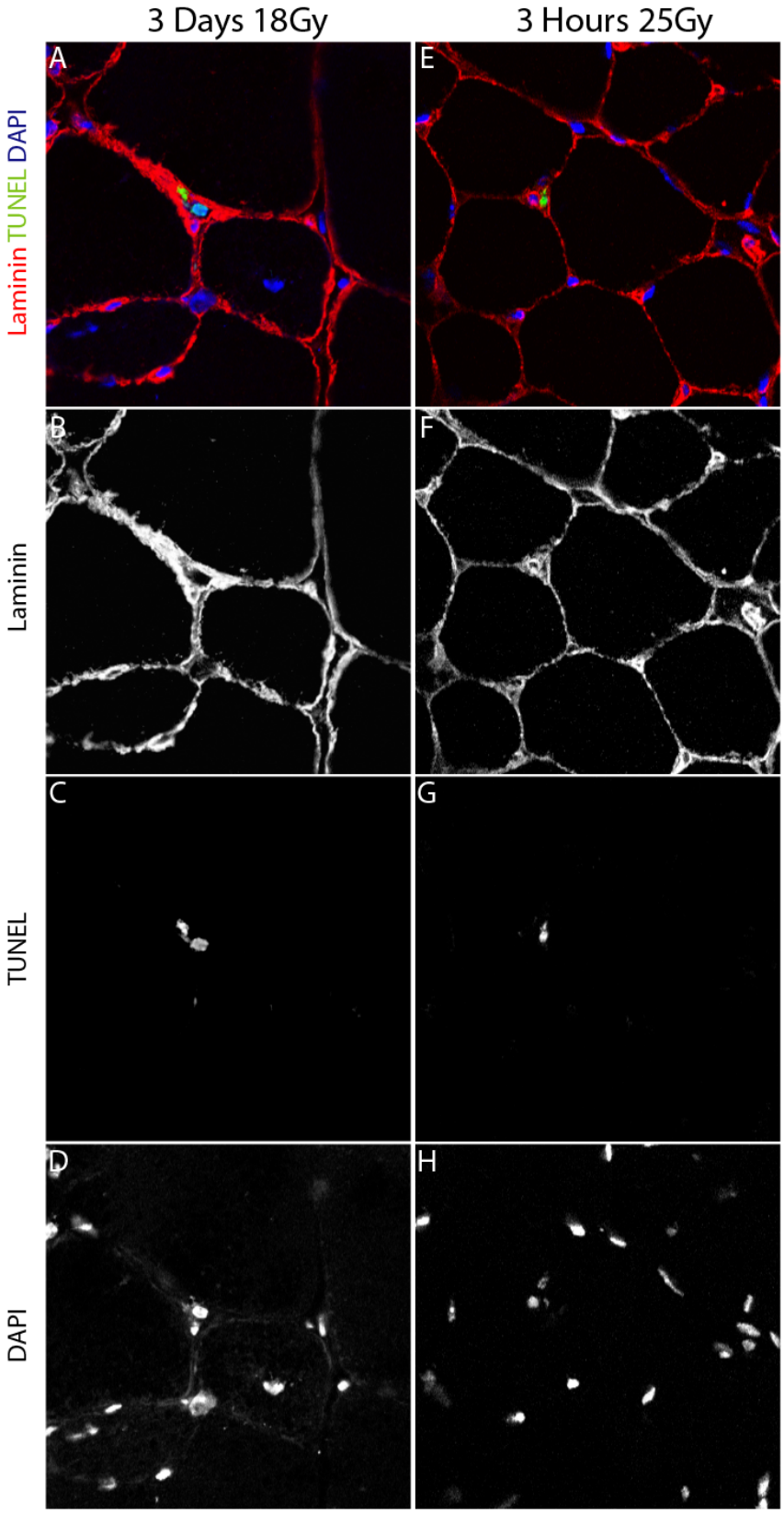

Figure 3.5: Representative confocal images of TUNEL positive cells 3 days after 18Gy (A-D) and 3 hours post-25Gy (E-H) showing that TUNEL positive cells localise outside the basal lamina.

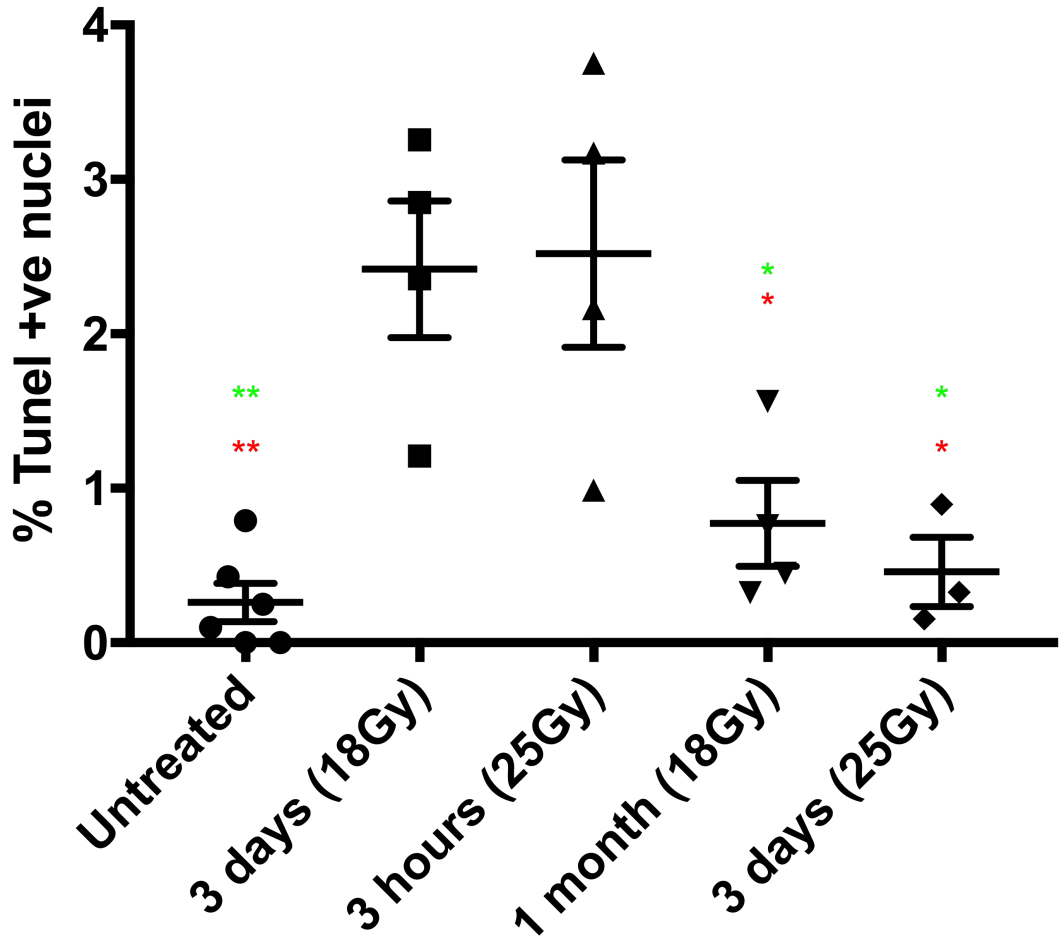

Figure 3.6: Comparison of the percentage of TUNEL positive nuclei under two different irradiation regimes. Asterisks in green shown significant difference compared to 3 hours after 25Gy group; those in red compare to the 3 days after 18Gy cohort. There was no statistically significant difference between muscles collected 3 days after 18Gy irradiation or 3 hours after 25Gy irradiation. There was no significant difference between those muscles collected 1 month after 18Gy compared to those collected 3 days after 25Gy. Neither of the latter groups had any statistically significant difference compared to the untreated control groups. The percentage of $TUNEL^{+}$ cells in untreated, 1 month after 18Gy, and 3 days after 25Gy groups were all significantly lower than either the muscles collected 3 days post-18Gy or 3 hours post-25Gy. ** $p<0.01$; * $p<0.05$; Line at mean; error bars = ±SEM.

3.4) Aim 3: Measuring the percentage of TUNEL positive cells in non-dystrophic mouse strains

Healthy adult muscles are stable post-mitotic tissues, and it has been established that differentiated or differentiating cells appear to be more radio-resistant than stem cells (Hendry 1979). The radio-sensitivity of parenchymal cells falls into 4 categories, and muscle falls into the last, 4th group, in which radiosensitivity is low and cells are highly differentiated (Jurdana 2008). Boldrin *et al.,* (2012) showed that satellite cell number per fibre in *mdx$^{nu/nu}$* mice is significantly reduced 3 days after 18Gy or 25Gy irradiation. In contrast, wild-type non-dystrophic mice show no such reduction in the number of satellite cells per fibre, although their regenerative capacity is obliterated by the high doses of radiation (Boldrin et al. 2012). It would be possible to explain these effects by assuming that in the *mdx$^{nu/nu}$* muscle, the constant cycles of degeneration and regeneration lead to a more mitotically active pool of cells formed of activated satellite cells and myoblasts, which would by definition be more susceptible to radiological damage than those in a quiescent state found in non-dystrophic muscles. Therefore, non-dystrophic mice should exhibit a greater level of radio-resistance than *mdx$^{nu/nu}$* mice. If the levels of apoptotic cells are relevant to the efficiency of donor satellite cell engraftment, this enhanced radio-resistance may affect the ability of γ-radiation to effectively modulate the host environment into a permissive niche for satellite cell transplantations. Therefore, the levels of TUNEL positive nuclei in *C5-/γ chain-/ Rag2-* (section 2.1.4) mouse muscles were quantified

in untreated controls, 3 days after 18Gy irradiation, and 1 month after 18Gy (figure 3.7).

The results showed that untreated *C5-/γ chain-/ Rag2*- mice had an average of 0.077% (SEM: ±0.077) TUNEL positive cells. After irradiation, the percentage of TUNEL positive cells was 0.152% (SEM: ± 0.152) and did not represent a significant increase compared to untreated controls (p=0.899). One month after irradiation, there was an average of 0.0677% (SEM: ±0.067) and it was not significantly different when compared to untreated controls (p=0.998) or 3 days after 18Gy (p=0.846).

It is likely that the lack of pathology, such as the presence of large amounts of fibrotic tissue seen in the $mdx^{nu/nu}$ muscles, allow for the increases in TUNEL positive cells, as none were observed beneath the basal lamina, indicating that they were interstitial cells (section 3.3). Conversely, in non-pathological mice such as non-dystrophic nude mice, there would be a significantly lower amounts of cells invading the muscle tissue. Therefore, it is likely that a similar response to *C5-/γ chain-/ Rag2*- would be observed in non-pathological mice.

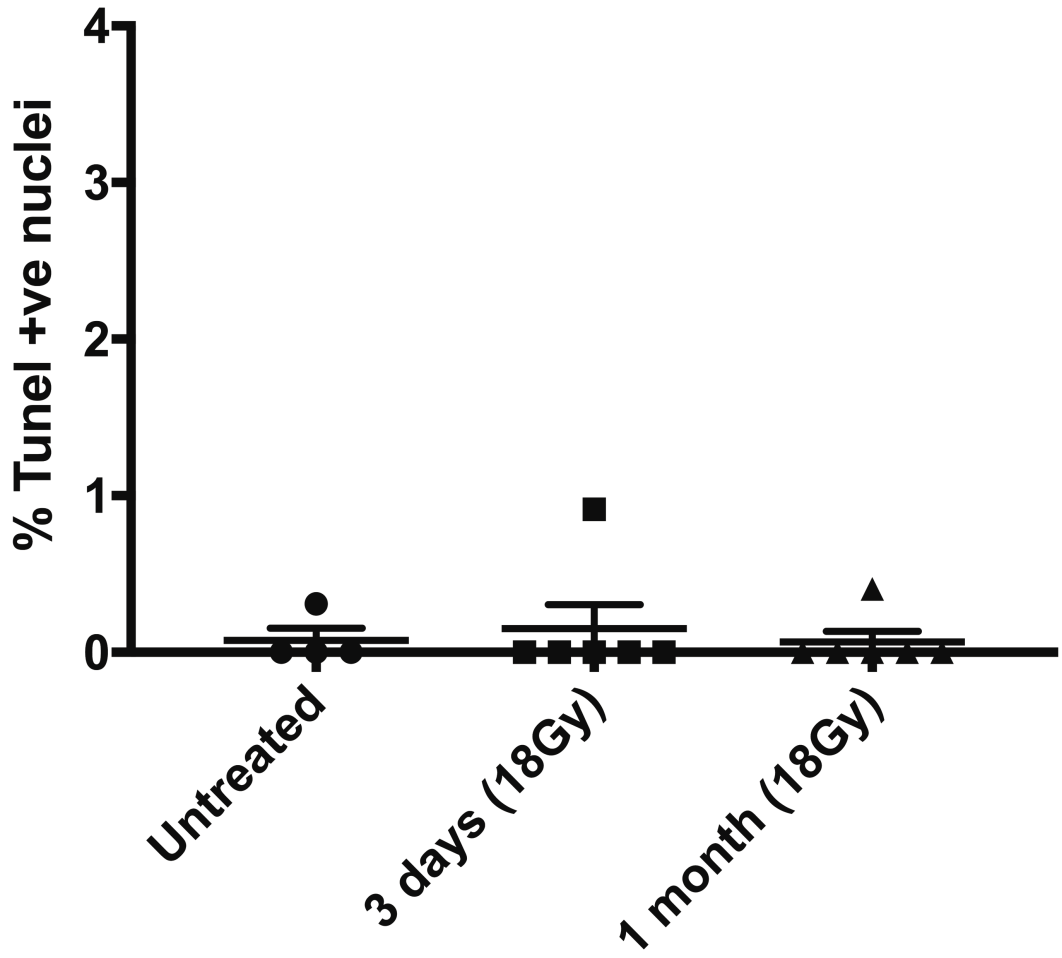

Figure 3.7: Quantification of the proportion of TUNEL positive nuclei in *C5^{-}/Rag2^{-}/Gamma Chain^{-}* mouse muscle 3 days after 18Gy irradiation and 1 month after 18Gy irradiation. At basal levels (untreated) there was a mean of 0.07725% (SEM: ±0.07725; n=4) TUNEL positive nuclei. 3 days after irradiation this remained unchanged with a mean of 0.1522% (SEM: ±0.1522; n=6) with no statistically significant difference compared to the control group (p=0.8995). 1 month after irradiation the proportion of TUNEL positive nuclei was 0.06767% (SEM: ±0.06767; n=6), with no statistically significant difference compared to the untreated group (p=0.9983) or to those measured 3 days after 18Gy irradiation (p=0.8457).

3.5) Aim 4: Determine whether the levels of apoptotic cells correlate with donor engraftment efficiency between mouse strains

Section 3.2 showed a significant (10-fold) increase in the number of TUNEL positive cells present in *mdx*$^{nu/nu}$ muscles at the time points where donor satellite cell engraftment is effective after 18Gy and 25Gy irradiation. In section 3.3, no significant increase in the number of TUNEL positive cells was observed after 18Gy irradiation in *C5-/γ chain-/ Rag2*- mouse muscles.

To determine if these strain differences impact on the ability of donor satellite cells to form muscle of donor origin, satellite cells from *B5EFGP* donors (section 2.1.4) were grafted (according to section 2.2.2) into the TAs of non-irradiated (n=12) and 3 day post-18Gy irradiated *C5-/γ chain-/ Rag2*- mice (n=12). As positive controls, *B5EGFP* satellite cells were also grafted into the TAs of 18Gy pre-irradiated *mdx*$^{nu/nu}$ hosts (n=12). The TAs were immersion fixed (section 2.4.2), stained for GFP (section 2.5.2), and the number of GFP positive donor muscle fibres was quantified (section 2.6.4.2).

In *mdx*$^{nu/nu}$ hosts, donor satellite cells engrafted and produced large amounts of muscle of donor origin, as shown in figure 3.8 (a-d), with a median of 229 (interquartile range (IQR): 317.8 – 113.3; n=12) fibres of donor origin (figure 3.9a). In contrast, cells grafted into pre-irradiated *C5-/γ chain-/ Rag2*- hosts produced few fibres of donor origin (figure 3.8, E-H) with a median of 7 (IQR: 22.25-0; n=12) fibres of donor origin (figure 3.9a-b), significantly lower than those grafted into *mdx*$^{nu/nu}$ mice (p=0.0019). In non-irradiated *C5-/γ chain-/ Rag2*- mice, there were no fibres of

donor origin (median: 0; IQR: 0-0; n=12), significantly lower ($p<0.0001$) than in pre-irradiated *mdx*$^{nu/nu}$ hosts (figure 3.9a).

However, the grafts performed in 3 day pre-irradiated *C5-/γ chain-/ Rag2-* do show a tendency towards a higher donor engraftment than grafts performed non-irradiated *C5-/γ chain-/ Rag2-* mice. To determine if this minor difference is significant, a Mann-Whitney test was performed for the data corresponding to these two groups, and is shown in figure 3.9b. This shows that although the formation of muscle of donor origin in pre-irradiated *C5-/γ chain-/ Rag2-* mice is negligible compared to pre-irradiated *mdx*$^{nu/nu}$ hosts, it is still significantly higher than in non-irradiated *C5-/γ chain-/ Rag2-* hosts ($p=0.0046$). This suggests that the engraftment enhancing effects of host muscle irradiation are not lost, but severely hampered in muscles that have lower levels of TUNEL positive cells after irradiation.

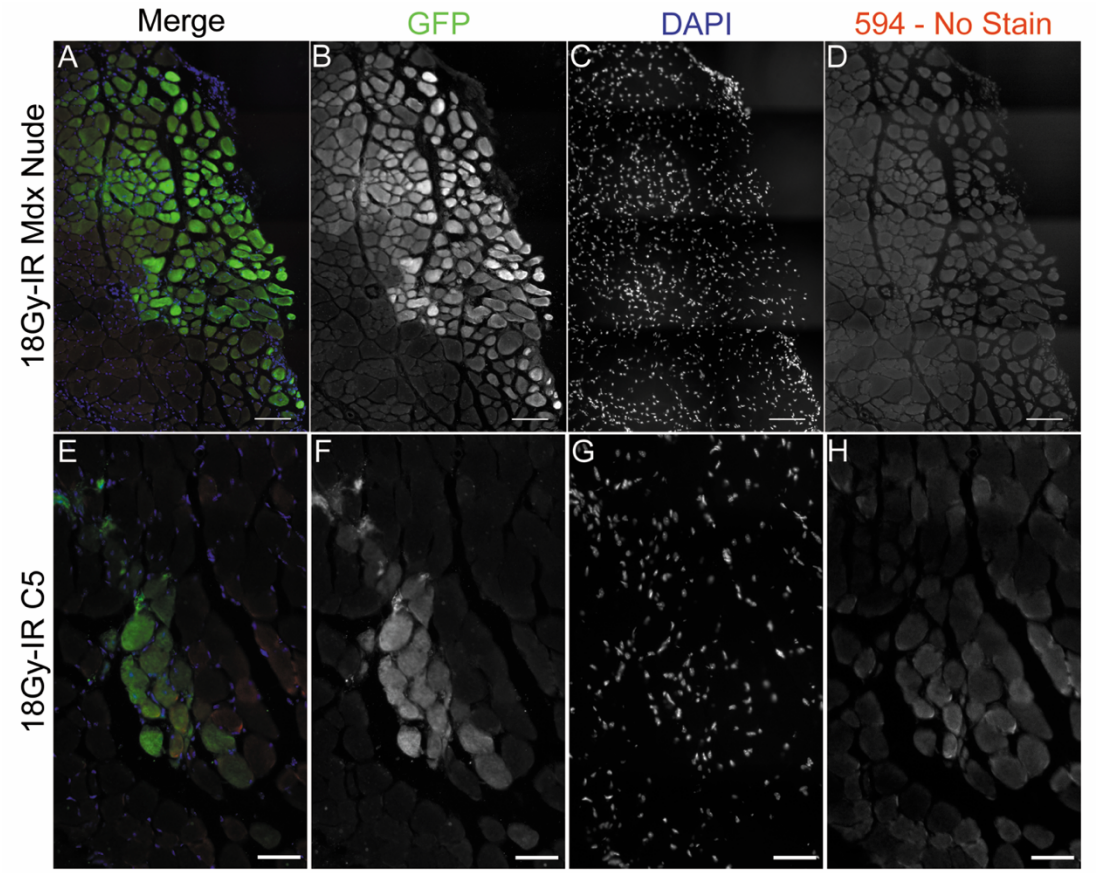

Figure 3.8: Representative images of the engraftment of *B5EGFP* satellite cells in 18Gy pre-irradiated *mdx*$^{nu/nu}$ (A-D) and *C5*$^{-}$*/Rag2*$^{-}$*/Gamma Chain* (E-H) mice, showing fibres of donor origin marked by GFP expression in representative transverse sections. GFP channels are displayed (B and F), with DAPI (C and G) and a non-stained 594nm filtered image (D and H) which was used to ensure that GFP positive areas were not a result of background fluorescence triggered by the paraformaldehyde immersion fixation protocol. Pre-irradiated *Mdx*$^{nu/nu}$ mouse muscles had better satellite cell engraftment (A and B) compared to pre-irradiated *C5*$^{-}$*/Rag2*$^{-}$*/Gamma Chain* mice (E and F). Non-irradiated *C5*$^{-}$*/Rag2*$^{-}$*/Gamma Chain* mice produced no fibres of donor origin, suggesting that, although less efficient than in the *mdx*$^{nu/nu}$ hosts, pre-irradiation enhances satellite cell engraftment in *C5*$^{-}$*/Rag2*$^{-}$*/Gamma Chain* hosts. Merge images show GFP - green, DAPI - blue, background - red. A-D scale bar = 100µm; E-H scale bar = 50µm.

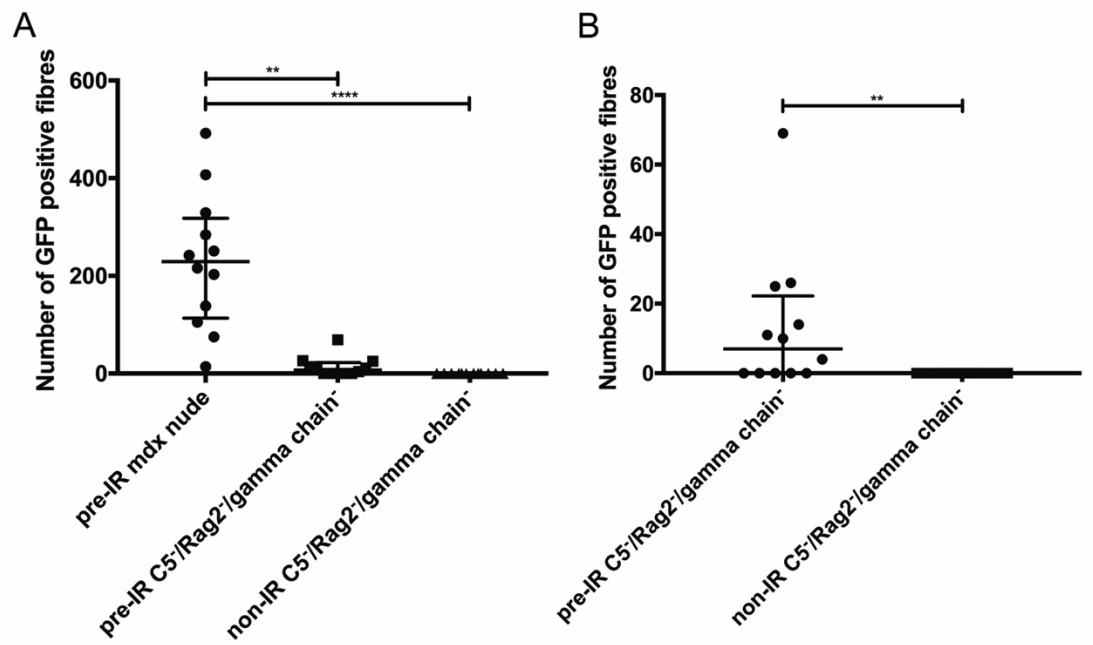

Figure 3.9: Quantification of GFP positive fibres of donor origin in 18Gy pre-irradiated *mdx*$^{nu/nu}$; 18Gy pre-irradiated *C5*$^{-}$*/Rag2*$^{-}$*/Gamma Chain*$^{-}$; and non-irradiated *C5*$^{-}$*/Rag2*$^{-}$*/Gamma Chain*$^{-}$ mouse muscles. A) Satellite cells grafted into pre-irradiated *mdx*$^{nu/nu}$ muscles (median: 229; IQR: 317.8-113-3; n=12) performed significantly better than in pre-irradiated *C5*$^{-}$*/Rag2*$^{-}$*/Gamma Chain*$^{-}$ muscles (median: 7; IQR: 22.25-0; n=12) (p=0.0019). Grafts into non-irradiated *C5*$^{-}$*/Rag2*$^{-}$*/Gamma Chain*$^{-}$ muscles produced no fibres of donor origin (median: 0; IQR: 0; n=12), which was significantly lower than grafts into *mdx*$^{nu/nu}$ muscles (p<0.0001). Using a Kruskall-Wallis test with all three groups, no statistically significant difference was reported between grafts in non-irradiated and pre-irradiated *C5*$^{-}$*/Rag2*$^{-}$*/Gamma Chain*$^{-}$ mice. B) Graph showing the median number of fibres of donor origin in *C5*$^{-}$*/Rag2*$^{-}$*/Gamma Chain*$^{-}$ muscles only. Using a Mann-Whitney test grafts in the pre-irradiated muscles perform significantly better than those in non-irradiated mice (p=0.0046). ** p<0.01; ****p>0.0001.

3.6) Aim 5: Determine if pre-irradiated satellite cells, single myofibres, or a monocytic cell suspension is able to enhance satellite cell engraftment.

3.6.1) Satellite Cell Co-transplants

Boldrin *et al.,* 2012 showed that 3 days after irradiation, most satellite cells in the *mdx*$^{nu/nu}$ muscle have died. If apoptosis induced proliferation plays a role in mediating the enhancement of satellite cell engraftment, the rapid death of satellite cells within the pre-irradiated host environment provides a candidate for investigation. Furthermore, the same author showed that complete ablation of the satellite cell pool prior to donor satellite cell engraftment lead to reduced formation of muscle of donor origin, therefore suggesting an important role for the remaining irradiated satellite cells in enhancing the efficiency of satellite cell transplantation.

To determine whether pre-irradiated satellite cells could be releasing the mitotic signals to enhance the engraftment of donor satellite cells a co-transplantation experiment was performed. Here satellite cells were isolated from *mdx*$^{nu/nu}$ muscles (as described in section 2.3.1) and irradiated according to section 2.3.1.5. Simultaneously, satellite cells were also isolated from *3F-nLacZ-2E* donors (section 2.3.1). The experiment was performed twice (table 3.1) and the results pooled (figure 3.11).

Table 3.1: Results for the satellite cell co-transplant experiments			
Experiment	Dystrophin positive fibres of donor origin		
	Irradiated	**Satellite Cell Co-Transplant**	**Non-Irradiated**
1	530	0	26
	168	0	46
	304	23	0
	212	0	0
	N/A	0	0
2	0	0	0
	453	0	12
	111	0	0
	47	11	19
	257	0	0
	21	N/A	N/A

Host mice were divided into two groups, pre-irradiated (according to section 2.2.1) and non-irradiated. Mice whose hindlimbs had been irradiated with 18 Gy 3 days previously (n=5, 10 muscles grafted) were employed as positive controls to test the ability of *3F-nLacZ-2E* satellite cells to form muscle of donor origin (figure 3.8). Non-irradiated hosts received *3F-nLacZ-2E* satellite cells in the left TA (n=10) as a negative control, and the contralateral limb was grafted with a mixture of 400 donor and 400 pre-irradiated satellite cells (n=10), as shown in figure 3.10.

Figure 3.17A-B shows a representative image of a successful graft (i.e. into pre-irradiated hosts), while 3.17C-D shows a satellite cell co-transplant with tissue of donor origin. First, muscle sections are stained for X-gal activity (section 2.5.3), and the serial sections of those samples containing fibres expressing ß-gal (figure 3.17 A, C, E, G) are then stained for dystrophin (section 2.5.2) (figure 3.17 B, D, F, H). The number of dystrophin positive fibres in the same region as the X-gal stain are considered fibres of donor origin and are quantified (section 2.6.4.1).

The results of the satellite cell co-transplant experiments are shown in figure 3.11. *3F-nLacZ-2E* satellite cells grafted into pre-irradiated muscles produced a median of

190 IQR: 390-40.5; n=10) fibres of donor origin. In contrast, non-irradiated muscles grafted with *3F-nLacZ-2E* satellite cells produced a median of 0 (IQR: 20.75-0; n=10) fibres of donor origin, significantly lower than those grafted into pre-irradiated hosts (p=0.0065). Non-irradiated muscles receiving a co-transplant of pre-irradiated *mdx*$^{nu/nu}$ satellite cells mixed with *3F-nLacZ-2E* donor satellite cells produced a median of 0 (IQR: 0-2.75; n=10) fibres of donor origin, which is significantly lower than those grafted into pre-irradiated muscles (p=0.0005) and shows no improvement over the negative controls (p>0.9999).

This indicates that pre-irradiated satellite cells from *mdx*$^{nu/nu}$ muscles grafted in combination with *3F-nLacZ-2E* donor satellite cells at a ratio of 1:1 failed to improve the production of muscle of donor origin in non-irradiated hosts. In contrast, pre-irradiation of host muscles shows a strong improvement in donor satellite cell engraftment compared to either co-transplants or *3F-nLacZ-2E* satellite cells grafted alone into non-irradiated host muscles. However, no co-transplantation experiments of pre-irradiated satellite cells with donor satellite cells were performed into pre-irradiated hosts. Therefore, the impact of pre-irradiated satellite cells on the donor satellite cells cannot be determined.

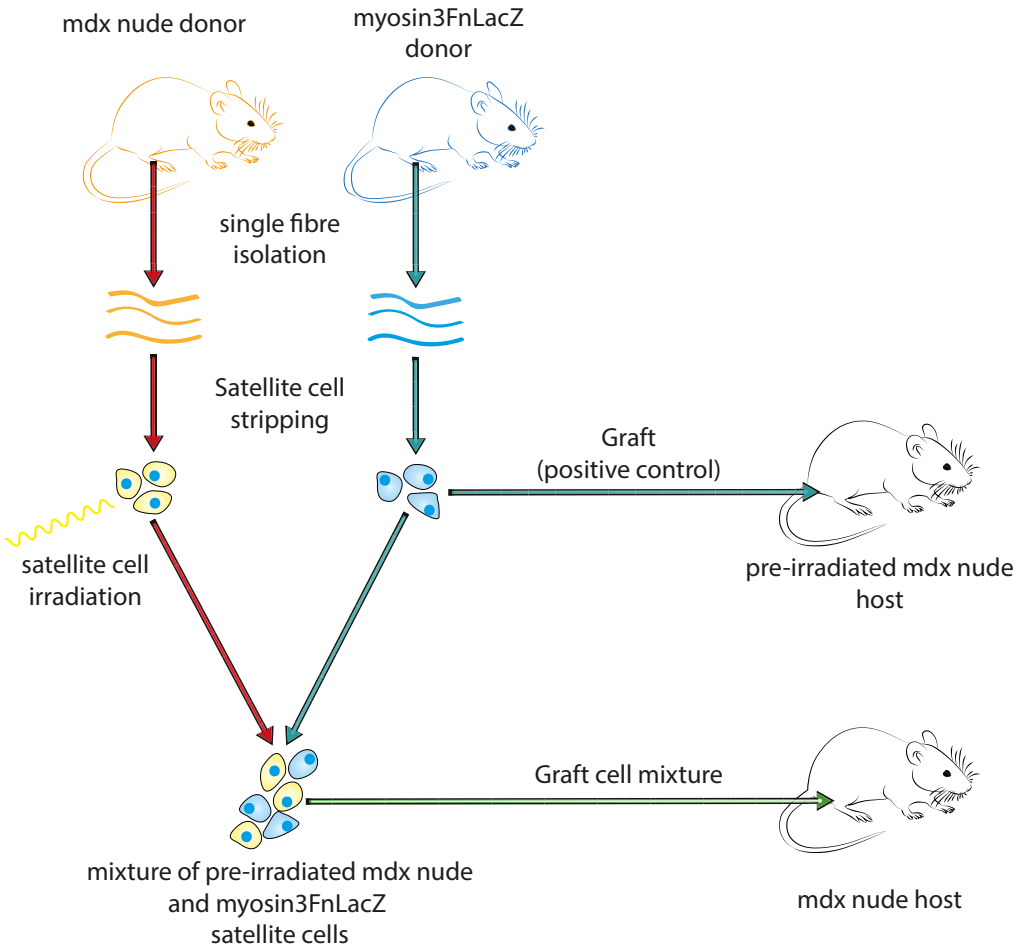

Figure 3.10: Schematic representation of satellite cell co-transplantation experiments. Briefly, donor *mdx*$^{nu/nu}$ mice were culled and single fibres were isolated from the EDL. Satellite cells were stripped from these fibres and the satellite cells underwent 18Gy irradiation on ice. Simultaneously, satellite cells from a *myosin3FnLacZ* donor were isolated, some were grafted into 18Gy pre-irradiated *mdx*$^{nu/nu}$ muscles as positive controls. As negative controls, *myosin3FnLacZ* satellite cells were grafted into the left non-irradiated TA of *mdx*$^{nu/nu}$ hosts. Finally, a mixture of pre-irradiated *mdx*$^{nu/nu}$ satellite cells with *myosin3FnLacZ* satellite cells was prepared and grafted into the non-irradiated right TA of *mdx*$^{nu/nu}$ hosts.

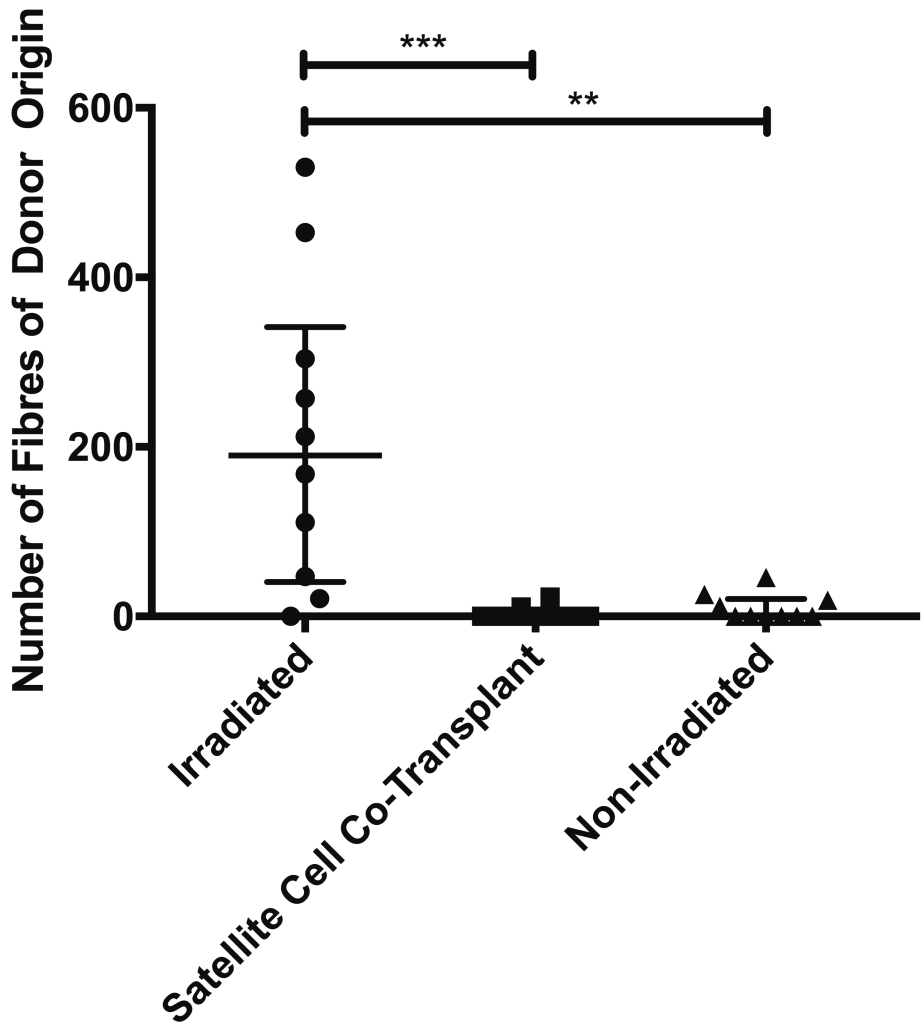

Figure 3.11: Results for satellite cell co-transplant experiments. Donor satellite cells grafted into mdx nude mouse muscles that had been irradiated with 18 Gy 3 days previously (controls) (median: 190; IQR: 390-40.5; n=10) performed significantly better than the satellite cell co-transplant into non-irradiated host muscles (median: 9; IQR: 2.75-0; n=10; p=0.0005) and the negative controls (donor satellite cells grafted into non-irradiated host muscles) (median: 0; IQR: 20.75-0; n=10; p=0.0065). There was no statistically significant difference between the satellite cell co-transplant group and the non-irradiated controls (p>0.9999). **p<0.01; ***p<0.001.

3.6.2) Single Fibre Co-Transplants

The results of section 3.5.1 showed that pre-irradiated satellite cells failed to enhance the formation of muscle of donor origin from *3F-nLacZ-2E* satellite cells. However, there is evidence that signals responsible for the modulation of muscle growth may be released from myofibres (Horsley et al. 2001; Jansen & Pavlath 2006). Boldrin and Morgan (2013) showed that the grafting of a single 3F-*nlacZ*-2E donor myofibre into non-irradiated *mdx*$^{nu/nu}$ muscles is able to cause a hypertrophic response. Their findings showed that *mdx*$^{nu/nu}$ muscles grafted with a single donor myofibre were significantly heavier, and the fibres had a larger cross-sectional area than muscles injected with DMEM alone. Furthermore, they demonstrated that there is no muscle formed from the satellite cells associated with the donor fibre, indicating that donor satellite cells are not contributing to the increased muscle weight and fibre size. Therefore, the grafted fibre must be triggering a true hypertrophic response instead of hyperplasia. This illustrates that single myofibres can have a significant modulatory effect in host muscles and raises the question of whether pre-irradiated myofibres are responsible for the modulation the behaviour of donor satellite cells within host *mdx*$^{nu/nu}$ muscles. To test this hypothesis, *mdx*$^{nu/nu}$ muscles were pre-irradiated with 18Gy (section 2.2.1). 3 days after irradiation single fibres were isolated from the irradiated EDL muscles (section 2.3.1.3). 2 pre-irradiated fibres were then grafted into non-irradiated *mdx*$^{nu/nu}$ hosts, together with 400 *3F-nLacZ-2E* donor satellite cells as shown in figure 3.12. Donor satellite cells were also grafted into pre-irradiated host mice as positive controls and into non-irradiated *mdx*$^{nu/nu}$ hosts as negative controls. The experiment was repeated twice (table 3.2) and the pooled results are displayed in figure 3.13.

Satellite cells grafted into pre-irradiated host muscles produced a median of 84.5 (IQR: 126.5-9.75; n=8) fibres of donor origin. Satellite cells grafted into non-irradiated hosts produced a median of 0 (IQR: 1-0; n=11) fibres of donor origin, that was significantly less than those grafted into pre-irradiated hosts (p=0.0102). Muscles that received both donor *3F-nLacZ-2E* satellite cells and pre-irradiated myofibres had a median of 4 (IQR: 36-0; n=11) fibres of donor origin, that was not significantly different to the negative controls (p=0.6422). However, due to the relatively low donor cell engraftment in the positive control muscles, there was also no significant difference between co-transplanted muscles and the irradiated positive controls (p=0.2202).

Table 3.2: Results for the single fibre co-transplant experiments

Experiment	Dystrophin positive fibres of donor origin		
	Irradiated	**Single Fibre Co-Transplant**	**Non-Irradiated**
1	119	12	38
	118	36	0
	N/A	0	0
	N/A	0	0
	N/A	0	0
	N/A	0	0
2	129	0	0
	0	68	10
	552	63	0
	39	31	1
	0	4	0
	51	N/A	N/A

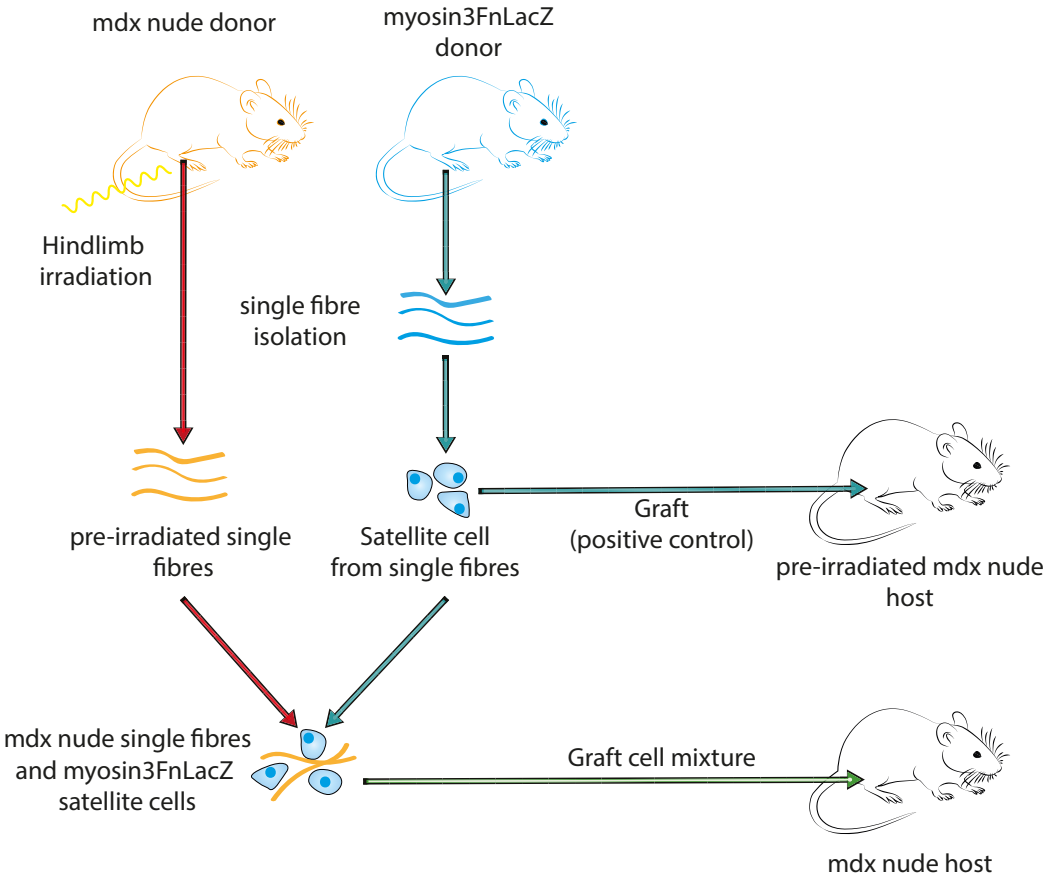

Figure 3.12: Diagram summarising the method for single fibre co-transplant experiments. Briefly, *mdx*$^{nu/nu}$ donors had their hindlimbs irradiated with 18Gy. Three days later the EDL was dissected and used to extract single muscle fibres. On the same day single fibres were prepared from *myosin3FnLacZ* donors. Satellite cells from *myosin3FnLacZ* donors were grafted into the TA of pre-irradiated *mdx*$^{nu/nu}$ hosts to serve as positive controls, these were also grafted into the left TA of non-irradiated *mdx*$^{nu/nu}$ hosts as negative controls. Finally, 2 single fibres derived from pre-irradiated *mdx*$^{nu/nu}$ donors were grafted together with *myosin3FnLacZ* satellite cells into the right TA of non-irradiated *mdx*$^{nu/nu}$ hosts.

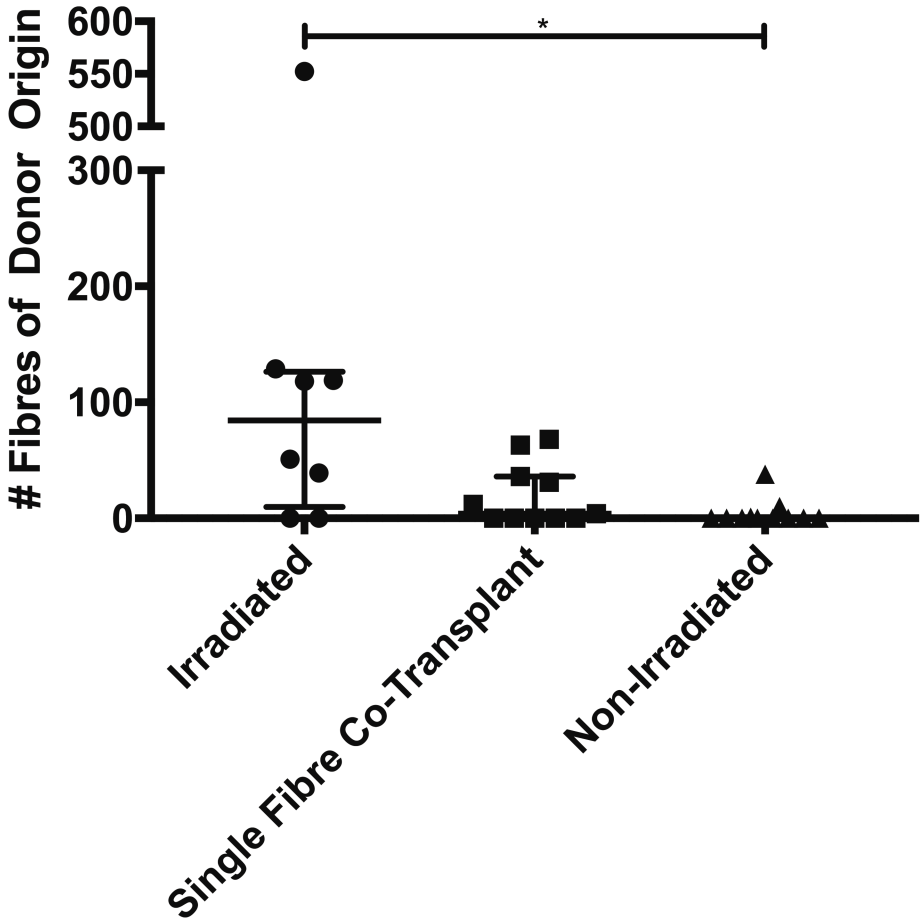

Figure 3.13: All single fibre co-transplantation experiments. As expected, satellite cell transplants into pre-irradiated controls (median: 84.5; IQR: 126.5-9.75; n=8) performed significantly better (p=0.0102) than non-irradiated controls (median: 0; IQR: 1-0; n=11). There was no significant difference between single fibre co-transplants (median: 4; IQR: 36-0; n=11) and non-irradiated negative controls (p=0.6422). Due to the relatively poor performance of positive irradiated controls there was also no significant difference between this group and the single fibre co-transplant (p=0.2202). * $p<0.05$

3.6.3) Monocytic Cell Suspension Co-Transplants

Sections 3.5.1 and 3.5.2 showed that grafting either pre-irradiated *mdx*$^{nu/nu}$ satellite cells or single fibres fails to improve the engraftment of donor *3F-nLacZ-2E* satellite cells. However, muscle is also composed of a variety of interstitial cells, including endothelial cells, macrophages, and fibroblasts that are also subject to radiation damage and may be mediating the enhancement of satellite cell engraftment. For example, there is evidence that M1 pro-inflammatory macrophages can improve skeletal muscle function after ischemia reperfusion injury (Rybalko et al. 2015). These macrophages have also been shown to enhance the *in vivo* regenerative capacity of human myoblasts grafted into *Raf2*$^{-/-}$ *γ-chain*$^{-/-}$ mice by extending the proliferation window, delaying differentiation, and increased migration (Bencze et al. 2012).

Interestingly it has also been shown that irradiation can modulate primary human macrophages towards an pro-inflammatory phenotype *in vitro,* leading to the activation of NFκB and significant increases in pro-inflammatory macrophage markers CD80, CD86, and HLA-DR (Teresa Pinto et al. 2016). They also displayed decreasing anti-inflammatory markers, along with morphological alterations, increases in their phagocytic rate, an increase of colorectal cancer cell invasion in-vitro, and increased angiogenesis in chick embryo chorioallantonic membrane. Whole body X-ray irradiation has also been shown to stimulate the secretion of pro-inflammatory cytokines in mouse peritoneal macrophages, increasing the secretion of TNFα, (IL)-1ß, IL-12 and IL-18, paralleled by the activation of NFκB as well as the up-regulated expression of CD14, TLR4-MD2, and MyD88 in a dose dependent manner (Shan et al. 2007).

Furthermore, pre-irradiated murine embryonic fibroblasts have been shown to trigger the non-autonomous proliferation of murine epidermal keratinocyte progenitor cells (in vivo and in vitro), neural stem cells (in vitro), and mesenchymal stem cells (in vitro) in a caspase 3 and 7 dependent manner (Li et al. 2010). Additionally, the exposure of human keratinocytes to UV light has also been shown to trigger the release of chemokines CXCL9 (interferon-γ (IFNγ) induced monokine 9), CXCL10 (IFNγ-inducible protein 10) and CXCL11 (IFNγ inducible T cell α chemoattractant) leading to the formation of an inflammatory infiltrate in skin biopsy specimens from locally UV irradiated patients of cutaneous lupus erythematosus, an autoimmune disease characterised by photosensitivity, apoptosis of keratinocytes, and an inflammatory infiltrate in the superficial and/or deep compartments of the skin (Meller et al. 2005).

Together, this suggests that other cell types within the pre-irradiated *mdx*$^{nu/nu}$ host muscles may be playing a crucial role in the modulation of the muscle environment after irradiation, and in turn the behaviour of donor satellite cells. To test whether the monocytic cell compartment (as opposed to myofibres) of pre-irradiated hosts is able to enhance the formation of muscle of donor origin, a single cell suspension was prepared from pre-irradiated *mdx*$^{nu/nu}$ donors (section 2.3.2), and 1.5x10^4 viable cells (as determined by trypan blue staining, section 2.3.2) were mixed with 400 *3F-nLacZ-2E* satellite cells, and grafted into the TAs of non-irradiated *mdx*$^{nu/nu}$ hosts as shown in figure 3.14. A group of positive control muscles were pre-irradiated (18Gy) and grafted with 400 *3F-nLacZ-2E* satellite cells, while negative controls consisted of satellite cells grafted into non-irradiated host muscles. The experiment was repeated 3 times (table 3.3) and the pooled results are shown in figure 3.15.

Table 3.3: Results for the single cell co-transplant experiments			
Experiment	Dystrophin positive fibres of donor origin		
	Irradiated	**Single Cell Co-Transplant**	**Non-Irradiated**
1	14	0	0
	45	19	0
	137	15	0
	182	30	14
	N/A	0	0
	N/A	0	0
2	538	28	45
	7	37	10
	44	228	4
	45	38	23
	5	21	46
	28	0	0
3	1	0	3
	104	90	21
	327	6	12
	487	2	0
	45	21	29
	597	19	25
	N/A	96	N/A

Grafts of donor satellite cells into pre-irradiated host muscles gave rise to a median of 45 (IQR: 290.8-17.5; n=16) fibres of donor origin, while negative controls produced significantly less (p=0.0010) muscle of donor origin (median: 7; IQR: 23.5-0; n=18). Muscles grafted with a mixture of the monocytic cell suspension and donor satellite cells had a median of 19 (IQR: 37-0; n=19) fibres of donor origin, with three outliers producing larger amounts of muscle of donor origin (238, 96 ,and 90 fibres of donor origin), however there was no statistically significant improvement in the formation of muscle of donor origin when compared to the negative controls (p=0.7773) and they formed significantly less muscle than the positive controls

(p=0.0336). The high variability in engraftment efficiency is likely due to local variations in muscle pathology and the response of the host to the radiation treatment, as discussed previously by Boldrin *et al.,* (2012). The variations in the radiation response are illustrated in Chapter 4, section 4.2, where the pre-irradiated sample BD1625 does not show the same pattern of gene expression as the other two pre-irradiated samples (figures 4.1, 4.10, 4.11, 4.12).

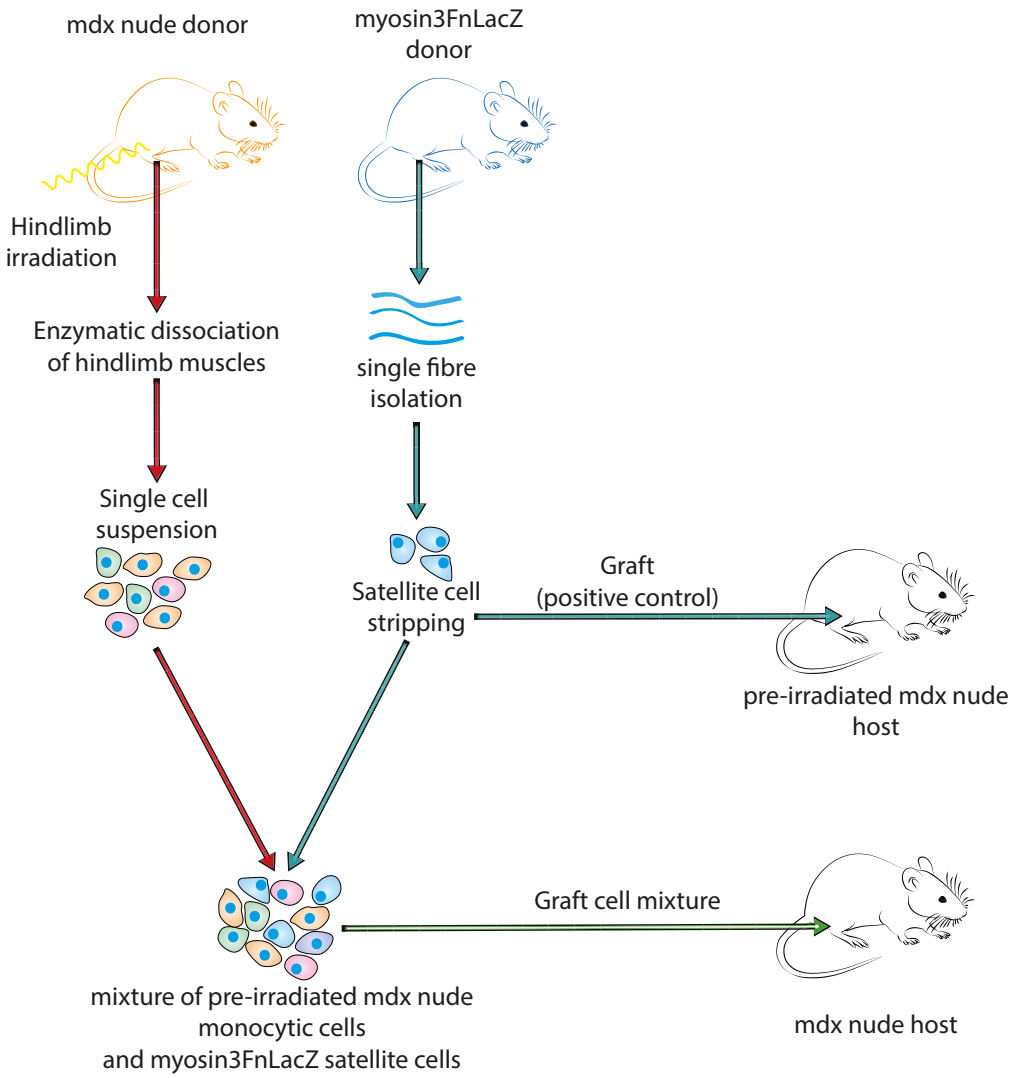

Figure: 3.14: Schematic representation of single cell co-transplant experiments. *Mdx*$^{nu/nu}$ donors were irradiated (18Gy) 3 days previously; on the day of grafting the pre-irradiated hind-limb muscles were dissected and enzymatically dissociated into a single cell suspension. *Myosin3FnLacZ* donors were used to prepare satellite cell donors; these satellite cells were grafted into the pre-irradiated TAs of *mdx*$^{nu/nu}$ hosts, and into the left non-irradiated TA of *mdx*$^{nu/nu}$ mice. The remainder were mixed with the single cell suspension derived from pre-irradiated *mdx*$^{nu/nu}$ donors and grafted into the right TA of non-irradiated *mdx*$^{nu/nu}$ hosts.

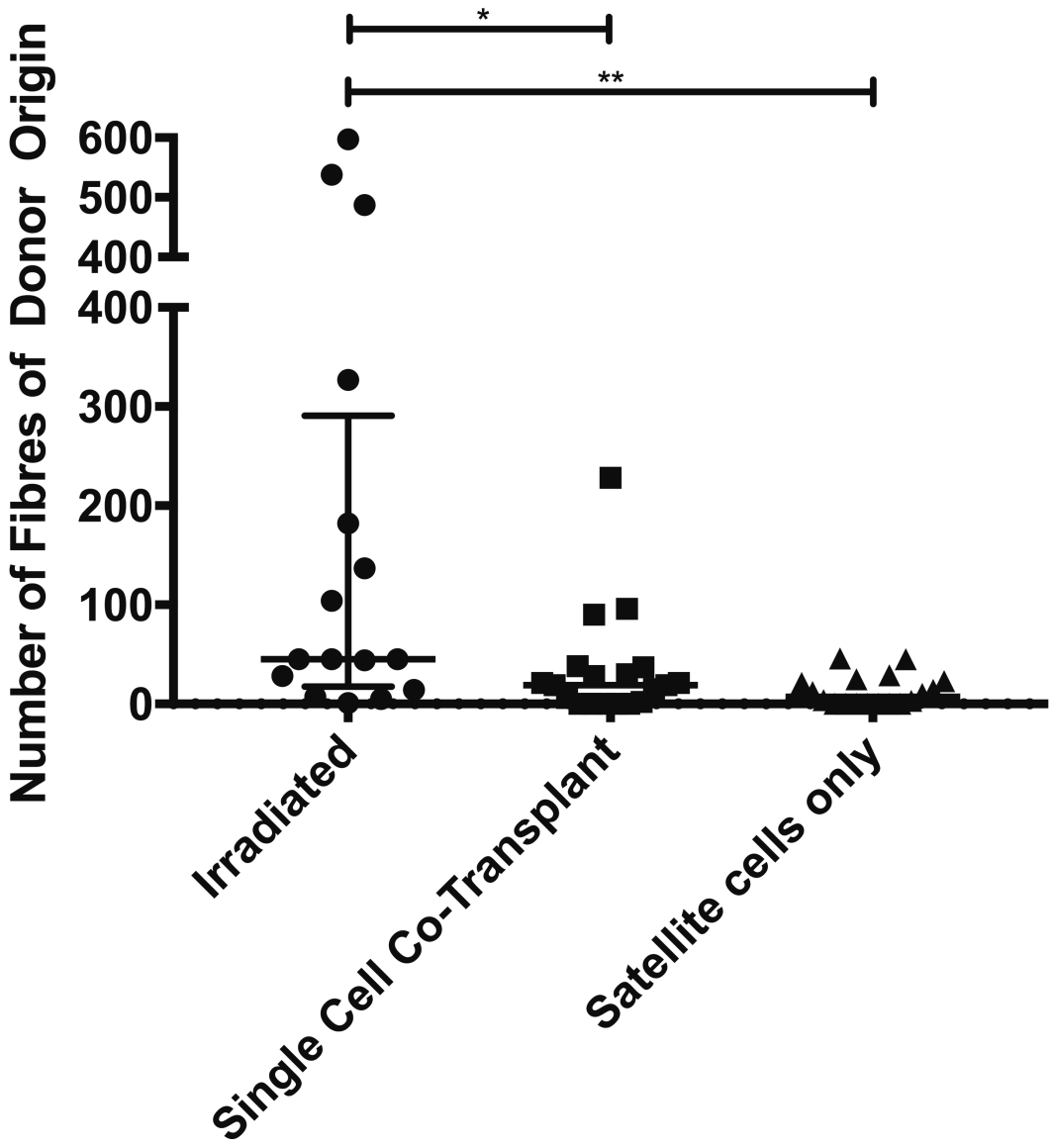

Figure 3.15: All single cell co-transplant experiments. Pre-irradiated controls (median: 45; IQR: 290.8-17.5; n=16) performed significantly better (p=0.0336) than the single cell co-transplantations (median: 19; IQR: 37-0; n=19) and the non-irradiated controls (median: 7; IQR: 23.5-0; n=18; p:0.0010). There was no statistically significant difference between the engraftment efficiency of single cell co-transplants and non-irradiated controls (p=0.7773).

3.6.4) Pooled Results

To determine if any particular co-transplant performed better than any of the others, the results were pooled (figure 3.16), additionally representative histological images are for each co-transplant are shown in figure 3.17. Irradiated positive controls produced a median of 77.5 (IQR: 292.3-22.75; n=32) fibres of donor origin, significantly more ($p<0.0001$) than non-irradiated negative controls (median: 0; IQR: 1-0; n=37).

Satellite cell co-transplants (median: 0; IQR: 2.75-0) produced significantly less muscle than positive controls ($p<0.0001$) and were not significantly different from the non-irradiated negative controls ($p>0.9999$). Additionally, satellite cell co-transplants were not significantly different from the single fibre co-transplants ($p=0.6808$) or co-transplants with a monocytic single cell suspension ($p= 0.1657$).

Single fibre co-transplants (median: 0; IQR: 19-0) had no statistically significant differences with the non-irradiated controls ($p>0.9999$) or the single cell co-transplant ($p>0.9999$) and performed significantly worse than the grafts into pre-irradiated positive controls ($p=0.0026$).

Finally, the amount of muscle of donor origin from donor satellite cells grafted with a single cell suspension derived from pre-irradiated *mdx*$^{nu/nu}$ donors (median: 19; IQR: 37-0) was not significantly different when compared to any of the other co-transplants, and did not significantly improve the amount of muscle of donor origin compared to non-irradiated negative controls ($p=0.9244$). They did however form significantly less muscle of donor origin than pre-irradiated positive controls ($p=0.0641$), albeit with a higher p value than any other comparison.

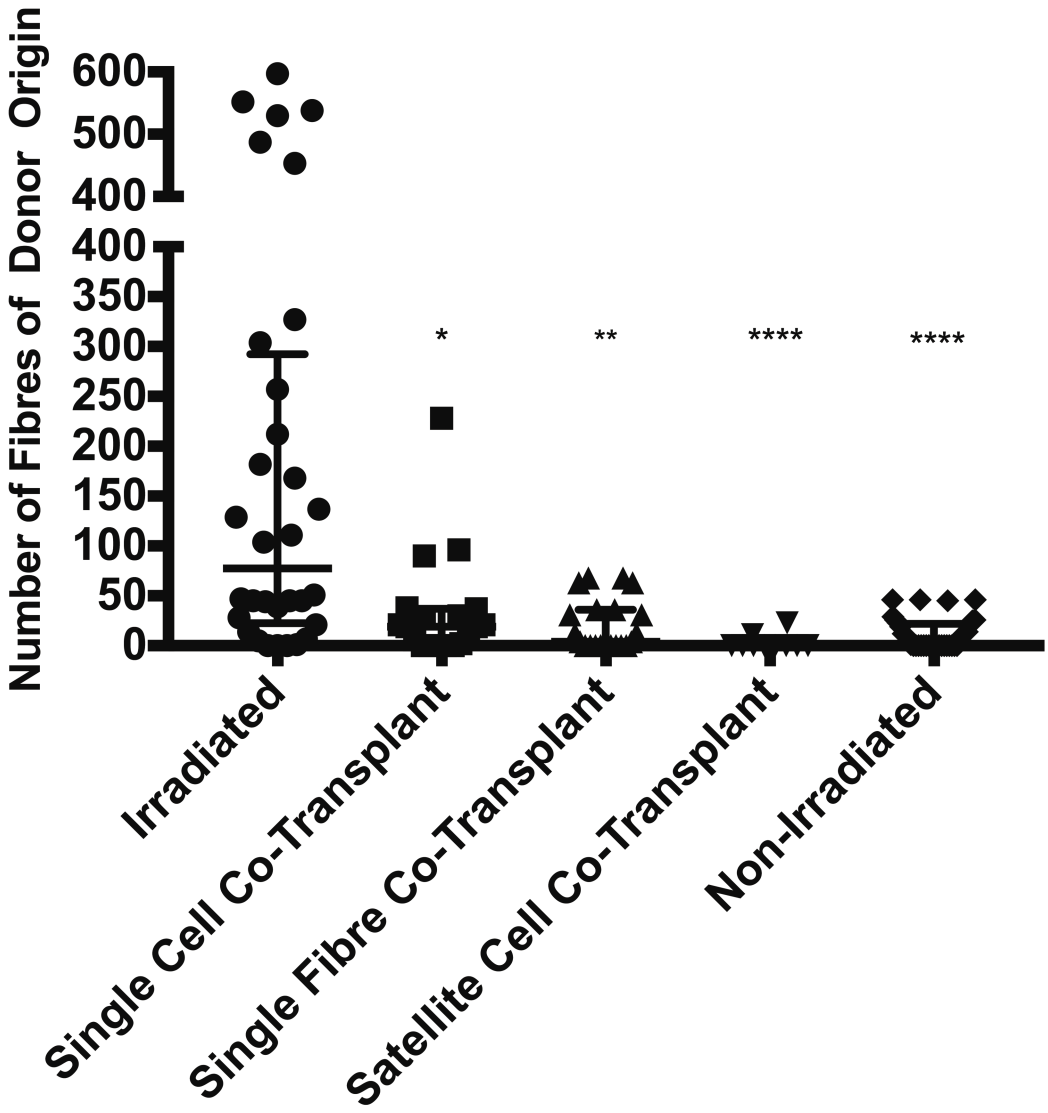

Figure 3.16: All co-transplantation experiments. Donor satellite cells grafted into pre-irradiated host muscles (positive controls) (median: 77.5; IQR: 292.3-22.75; n=32) performed significantly better than the single cell co-transplants (median: 19; IQR: 37-0; n=19; p=0.0641); single fibre co-transplants (median: 4; IQR: 36-0; n=11; p= 0.0026); satellite cell co-transplants (median: 0; IQR: 2.75-0; n=10 p<0.0001); and non-irradiated controls (median: 1; IQR: 22-0; n=37; p<0.0001). There were no statistically significant differences between any of the co-transplants, or between the co-transplants and the negative controls. * p<0.1; **p<0.01; **** p<0.0001.

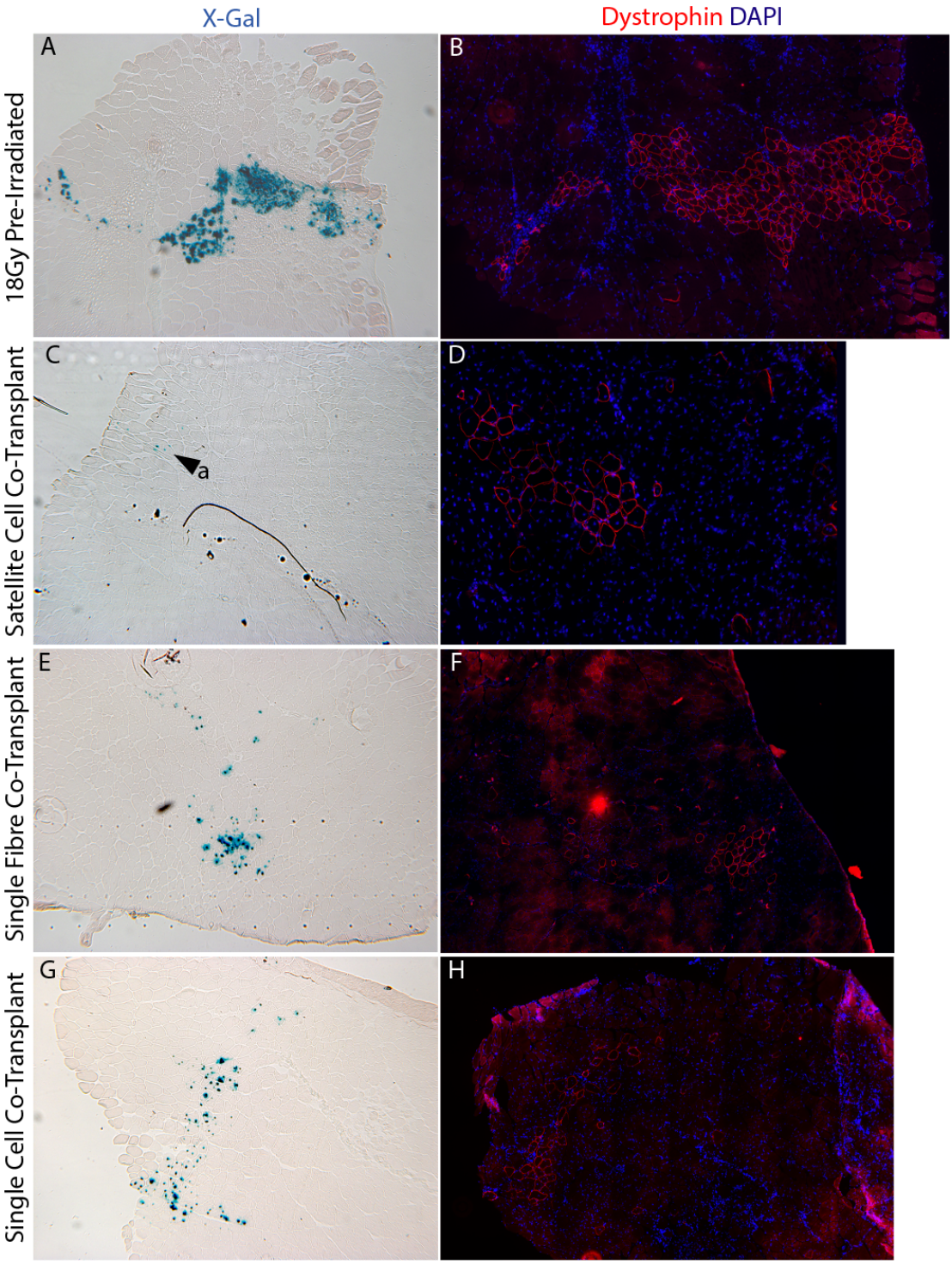

Figure 3.17: Representative images of all Co-Transplantation experiments. A-B) Positive control graft in pre-irradiated mdx$^{nu/nu}$ host showing X-gal (A) colocalising with dystrophin staining (B); C-D) Image of tissue of donor origin in a satellite cell co-transplant showing X-gal (C) and dystrophin (D); E-F) Tissue of donor origin in a single fibre co-transplant showing X-gal (E) and dystrophin (F); Tissue of donor origin in a single cell co-transplant showing X-gal (G) and dystrophin (H).

3.7) Discussion

A significant body of evidence suggests that cells that are undergoing apoptosis may have the ability to trigger non-autonomous proliferation in adjacent cells, with the effect being phylogenetically conserved from relatively primitive organisms such as the hydra (Galliot & Chera 2010), mammals such as mice (Li et al. 2010; Revesz 1956), and some human cancer cell lines (Kurtova et al. 2015; Huang et al. 2011; Donato et al. 2014). The consensus appears to be an executioner caspase dependent mechanism leading to the release of pro-mitotic signals, particularly PGE_2. Recent findings published by Ho et al., (2017) have suggested that PGE_2 is in fact an essential part of the innate inflammatory response in muscles, and can stimulate myoblast proliferation. Furthermore, when a bolus of PGE_2 is delivered 2 days after cardiotoxin injury, the number of Pax7 expressing cells beneath the basal lamina significantly increases 14 days after injury compared to medium only treated muscles (Ho et al. 2017). The ablation of the EP4 receptor in satellite cells, or the inhibition of prostaglandin synthesis using non-steroidal anti-inflammatory drugs (NSAIDs) hinders muscle regeneration and reduces muscle strength (Ho et al. 2017).

If PGE_2 is produced by dying cells in response to radiation damage, then the increase in TUNEL positive cells seen in skeletal muscle at the times of optimal engraftment (figure 3.4) should lead to increases in the levels of PGE_2 within the host environment that would potentially drive the proliferation of donor satellite cells within the host muscle. Furthermore, the fact that there was no significant increase in TUNEL positive cells in irradiated? *C5-/γ chain-/ Rag2*- mouse muscles (figure 3.5) combined with the very low donor cell engraftment efficiency in such muscles

(figures 3.6 and 3.7), gives further support to this hypothesis. Therefore, the engraftment of satellite cells should be augmented by the delivery of donor satellite cells with lethally pre-irradiated cells that are able to secrete this pro-inflammatory lipid, as shown by Li et al. (2010).

When grafting pre-irradiated mdx nude satellite cells, the cells were isolated, then irradiated on ice, and immediately grafted with donor *3F-nLacZ-2E* satellite cells, ensuring that although lethally damaged, the irradiated cells would not be all dead at the time of grafting, and should allow the enhancement of donor satellite cell engraftment. However, in figure 3.10 it is evident that pre-irradiated satellite cells fail to enhance the engraftment of donor *3F-nLacZ-2E* satellite cells.

No TUNEL positive nuclei were observed within single muscle fibres, confirming their predicted radio-resistance (Jurdana 2008), and suggesting that pre-irradiated myofibres are unlikely to be responsible for initiating the mechanisms related to apoptosis induced proliferation leading to the enhancement of donor satellite cells. However as shown by Boldrin & Morgan (2013) a single donor myofibre grafted into host *mdx*$^{nu/nu}$ muscles is able to trigger a hypertrophic response within the host muscle, highlighting the influence of myofibres in regulating the muscle environment. However, when pre-irradiated *mdx*$^{nu/nu}$ fibres were co-transplanted with donor satellite cells (n=11), no enhancement in donor cell engraftment were seen (figures 3.12 and 3.15). This indicates that irradiated muscle fibres are not triggering the enhancement of donor satellite cells after irradiation.

Finally, having excluded satellite cells and muscle fibres as the triggers for the effects leading to increases in satellite cell enhancement, cells from elsewhere in the host muscle was used for co-transplants by generating a single cell suspension from

pre-irradiated *mdx*$^{nu/nu}$ donors and grafting it with donor *3F-nLacZ-2E* satellite cells. The exact composition of this cell suspension prepared from pre-irradiated muscles remains undetermined, but it is likely to contain macrophages, endothelial cells, fibroblasts, haematopoietic stem cells (HSCs), and fibroadipogenic progenitor cells (FAPs) (Boldrin et al. 2017). This co-transplant experiment did not appreciably augment the engraftment of donor satellite cells, however, there are indications of a slight trend towards higher engraftment. The grafting efficiency was not significantly different from negative non-irradiated controls or pre-irradiated positive controls hosts (figure 3.14 and 3.15). However, the data does show some outliers in the single cell co-transplant group that perform relatively well compared to the remainder of co-transplants, with one sample producing 238 fibres of donor origin, and another two yielding 90 and 96 fibres of donor origin, suggesting that within this preparation there might be factors that may be able to enhance satellite cell engraftment. Finer control over the composition of this preparation would be beneficial, as different grafts may have received different ratios of different cell populations. It is possible, for example, that the outlier with 238 fibres of donor origin may have been grafted with an optimal number of pro-inflammatory macrophages, which have been shown to enhance myoblast engraftment (Bencze et al. 2012).

Taken together these data suggest that none of the co-transplants was able to significantly and robustly enhance satellite cell engraftment, which could mean that the desired cells were either lost during the isolation procedure due to the stress placed on them by radiation damage and enzymatic disaggregation or were not able to significantly enhance donor satellite cell engraftment.

However, the correlation between the increases of TUNEL positive cells at the optimal engraftment time are still highly relevant. In damaged tissues the release of intracellular molecules into the extracellular space by injured tissues, termed damage-associated molecular patterns (DAMPs), is able to elicit an inflammatory response within the damaged tissue and promote the regeneration process (reviewed by: Vénéreau et al. 2015). In terms of satellite cell function, pro-inflammatory cytokines (IL-1α, IL-13, TNF-α, and interferon gamma) have been shown to greatly enhance the proliferative capacity of cultured primary myoblasts (up to 20 passages), and greatly enhance their capacity to form muscle of donor origin upon grafting in-vivo. When grafted into cardiotoxin injured $Rag1^{-/-}$ muscles, these myoblasts were able to replenish the endogenous stem cell pool and repair the host muscle after multiple rounds of degeneration and regeneration (Fu et al. 2015). Furthermore, PGE_2 is an inflammatory cytokine that would be released in response to muscle injury as shown by Ho et al. (2017). It could therefore be hypothesised that the role of the TUNEL positive cells is not that they are directly signalling grafted donor cells, but that DAMPs released by their cellular debris is triggering a pro-inflammatory response within the host muscle that could be leading to the observed augmentation in satellite cell engraftment. To characterise changes in gene expression after irradiation that may point towards potential mechanisms as to how irradiation of host muscles augments donor satellite cell engraftment RNA-sequencing was used, the results are shown in the following chapter.

Chapter 4 - RNA-Sequencing Results, Network Centrality, and Pathway Analysis

4.1) Introduction and Aims

4.1.1) Introduction

The pre-irradiation of mouse skeletal muscle has been proven to enhance the engraftment of murine myoblasts (Morgan et al. 2002) and satellite cells (Boldrin et al. 2012) but not human derived cells (Meng et al. 2015). The simplest explanation, that is, niche depletion and repopulation by donor cells, is unable to explain the failure of human cell engraftment in pre-irradiated skeletal muscles compared to mouse donor cells. Furthermore, Boldrin (2012) demonstrated that complete ablation of the endogenous satellite cell niche hampers the engraftment efficiency of donor satellite cells. This observation excludes the possibility of simple niche ablation and replacement as a possible explanation for the augmentation of satellite cell engraftment in pre-irradiated muscles, and therefore indicates that the niche is actively modulated in response to irradiation. Therefore, it can be inferred that the modulation is not only active, but that the pathways modulating the enhanced engraftment are species specific.

Generally, it is assumed that radiation damage mainly causes cell death and detrimental bystander effects. However, in 1956 a report published by L. Revesz in the journal Nature titled “The effect of tumour cells killed by X-rays upon the growth of admixed viable cells” showed that lethally irradiated cells are able to enhance the proliferation of adjacent cells. Here the author grafted lethally irradiated (12000 rad or 120Gy) tumour cells from derived from either inbred mouse strains exposed to carcinogens, or a spontaneous

tumour cell line derived from a mouse of an unknown genetic background (Ehrlich ascites tumour), along with an aliquot of non-irradiated cells. Lethally irradiated cells failed to form a tumour in host mice. Controls grafted with only viable tumour cells produced tumours. However, when an aliquot of viable cells was grafted with a large population of lethally irradiated cells the latency period for tumour formation was reduced, as was the survival time of the animals compared to those grafted with only viable tumour cells.

These results were the first report of lethally irradiated cells actively promoting the proliferation of healthy adjacent cells. These proliferative effects from apoptotic cells have been shown in numerous organisms. Examples include the regeneration of the *Drosophila melanogaster* imaginal wing disc after irradiation (Haynie & Bryant 1977); the Hydra head regeneration by secretion of Wnt3 by apoptotic cells (Galliot & Chera 2010); the regeneration of *Xenopus* tadpole tails in a caspase 3 dependent manner (Tseng et al. 2007); and in mice this effect has been attributed to the release of prostaglandin E_2 from lethally irradiated cells in a caspase 3 dependent manner and its interactions with the Wnt-β catenin pathway (Li et al. 2010).

In Chapter 3 correlation between increases in TUNEL positive cells at the points of optimal engraftment was observed, but co-transplantation of donor satellite cells with different cell types from pre-irradiated muscles into non-irradiated hosts failed to enhance satellite cell engraftment. To further investigate which pathway(s) are involved in the augmentation of satellite cell engraftment in pre-irradiated muscles, RNA-sequencing (RNA-seq) was performed on the Tibialis Anterior (TAs) of 4 different groups (for all groups n=3) of mice, all $mdx^{nu/nu}$ males at 3 weeks of age. The groups consisted of:

- Non-irradiated controls
- Irradiated (dose: 18Gy) and collected 3 days after irradiation where satellite cell engraftment is possible and there is an increase of tunel positive cells

- Irradiated (18Gy), grafted with 400 donor satellite cells 3 days after irradiation and collected 2 days after surgery (grafted)
- Irradiated (18Gy), sham injected 3 days after irradiation with satellite cell medium only (section 2.3.1.4) and collected 2 days after irradiation (sham).

The two-day time-point after cell grafting or sham injection was selected as the kinetics of myoblast transplantation suggests that at this point is where the donor cells begin to proliferate within the host muscle (J R Beauchamp et al. 1999). By comparing the grafted group to the sham injected group we can identify if satellite cells are interacting with the host muscle to create a permissive niche. Comparing control tissues to 3 day irradiated muscles would yield a profile of how γ-radiation affects skeletal muscle. Additionally, by comparing grafted muscles to pre-irradiated muscles it would be possible to determine whether the grafted satellite cells are proliferating within the tissue, and comparing sham injected muscles to the 3 day irradiated tissues would highlight any changes in gene expression occurring 5 days after irradiation. By comparing both sham injected muscles to controls we can understand how the radiation injury evolves with time, while the grafted muscles compared to control will give insights into how irradiation and satellite cells injections modify the *mdx*$^{nu/nu}$ muscles.

4.1.2) Aims

The aim of these chapter is to determine which of the genes in the RNA-sequencing data play major regulatory roles in modulating the skeletal muscle environment, what are their likely functions, and what pathways are significantly enriched in these datasets. This is achieved by creating a network of protein-protein interactions and applying several network centrality algorithms to identify key members of these networks (section 2.7.5), performing Gene Ontology (GO) analysis on the core network regulators to identify their likely functions (section 2.7.5), and using Gene Set Enrichment Analysis (GSEA) to find over-represented pathways in the datasets (section 2.7.6). This will allow the characterisation of how skeletal

muscle responds to irradiation and satellite cell grafting, and the identification of potential pathways for future pharmacological intervention.

4.1) RNA preparation and quality control

RNA was extracted as described in section 2.7.2. After extraction, the concentration and quality of RNA was determined using spectrophotometry and Aligent TapeStation system. A summary of these results for the samples sent for sequencing is shown in table 4.1.

All samples met the required criteria, with at least a total of 2µg of RNA, a 260/280 absorbance ratio of approximately 2 and a RiN value equal to or larger than 8.0. A full report from the tape station system is in Appendix 4.1.

The average total number of reads was 74,016,340 with an average of 3,001,478 unmapped reads (or 4.06%). On average 74.40% of the mapped reads corresponded to protein coding RNAs, followed by an average of 22.40% of reads that did not have any known features. The other major feature was long non-coding RNAs with an average of 1.32% of all reads. The remainder of the groups (such as snRNAs, miRNAs, tRNAs) represented an extremely low fraction of the number of reads (<0.5%).

Principal Component Analysis (PCA) plots are shown in figure 4.1. Figure 4.1 A shows a good separation of control samples from 3 day irradiated samples (BD1618 and BD1626) along principal component 1 (PC1) showing that the treatment is the major source of variation between the samples (60.5% of the total variation, figure 4.1a) whilst BD1625 appears to have been unresponsive to irradiation as it clusters closely with control samples along PC1, it is important to note that this may skew the results of further analysis. In the comparison of grafted samples compared to sham injected samples there is a good separation of samples along PC1 (76.4% of the variance, figure 4.1b) according to treatment, although sample BD1612 does not cluster with the remaining grafted samples along PC1

(BD1613 and BD1611, figure 4.1b). 3-day irradiated samples compared to irradiated and grafted muscles show a good reparation along PC1 (accounting for 90.7% of the variance, figure 4.1c) except for sample BD1626. The grafted samples are clustered closely together along both PC1 and PC2. The comparison of 3-day irradiated samples and sham injected samples shows a similar separation as that seen on figure 4.1C. The remaining comparisons, which compare grafted (Figure 4.1E) and sham injected (Figure 4.1F) samples to controls, show a clear separation of control samples from either grafted or sham injected samples along PC1 (accounting for 89.1% and 88.1% of the variance respectively. There is no separation across PC2 in either of the samples, however this component represents a very small proportion of the total variance.

The lack poor clustering of 3-day 18Gy pre-irradiated sample BD1625 with the rest of the group indicates that this is likely to be an outlier that has not responded to the radiation treatment in the same way as the remainder of the samples. This is relevant as it may have affected both the significantly dysregulated genes and in turn GSEA and GO analysis. Ideally this sample should be removed, however as the raw data analysis for the RNA-seq experiments was performed at Ohio Children's hospital, it has not been possible to remove this sample from the group.

Table 4.1 Sample quality controls and details

A) Irradiated 18Gy, collected 72hrs

Mouse number	*RNA from Right Tibialis Anterior*			*Sample Details*				
	[C] ng/uL	$\frac{260}{280}$	*RiN*	*Sex*	*IR (18Gy)*	*Graft*	*Collection after IR*	*Collection after Grafting*
BD1618	171.10	2.12	9.4	male	yes	no	3 days	N/A
BD1625	202.70	2.08	9.1	male	yes	no	3 days	N/A
BD1626	315.80	2.07	9.1	male	yes	no	3 days	N/A

B) Non-Irradiated Controls

Mouse number	*RNA from Right Tibialis Anterior*			*Sample Details*				
	[C] ng/uL	$\frac{260}{280}$	*RiN*	*Sex*	*IR (18Gy)*	*Graft*	*Collection after IR*	*Collection after Grafting*
BD1621	138.40	2.09	9.7	male	no	no	N/A	N/A
BD1622	216.20	2.07	9.7	male	no	no	N/A	N/A
BD1623	229.20	2.00	9.4	male	no	no	N/A	N/A

C) 18Gy IR, Satellite Cell Grafted, collected 48hrs post-graft

Mouse number	*RNA from Right Tibialis Anterior*			*Sample Details*				
	[C] ng/uL	$\frac{260}{280}$	*RiN*	*Sex*	*IR (18Gy)*	*Graft*	*Collection after IR*	*Collection after Grafting*
BD1611	110.80	2.01	9.3	male	Yes	yes	5 days	2 days post graft
BD1612	154.00	2.10	9.4	male	Yes	yes	5 days	2 days post graft
BD1613	103.30	2.13	9.7	male	Yes	yes	5 days	2 days post graft
D) 18Gy IR, Sham injected, collected 48hrs post graft								
Mouse number	*RNA from Right Tibialis Anterior*			*Sample Details*				
	[C] ng/uL	$\frac{260}{280}$	*RiN*	*Sex*	*IR (18Gy)*	*Graft*	*Collection after IR*	*Collection after Grafting*
BD1629	162.90	2.10	9.7	male	yes	sham	5 days	2 days post graft
BD1630	293.50	2.08	9.2	male	yes	sham	5 days	2 days post graft
BD1632	283.9	2.09	9.2	male	yes	sham	5 days	2 days post graft

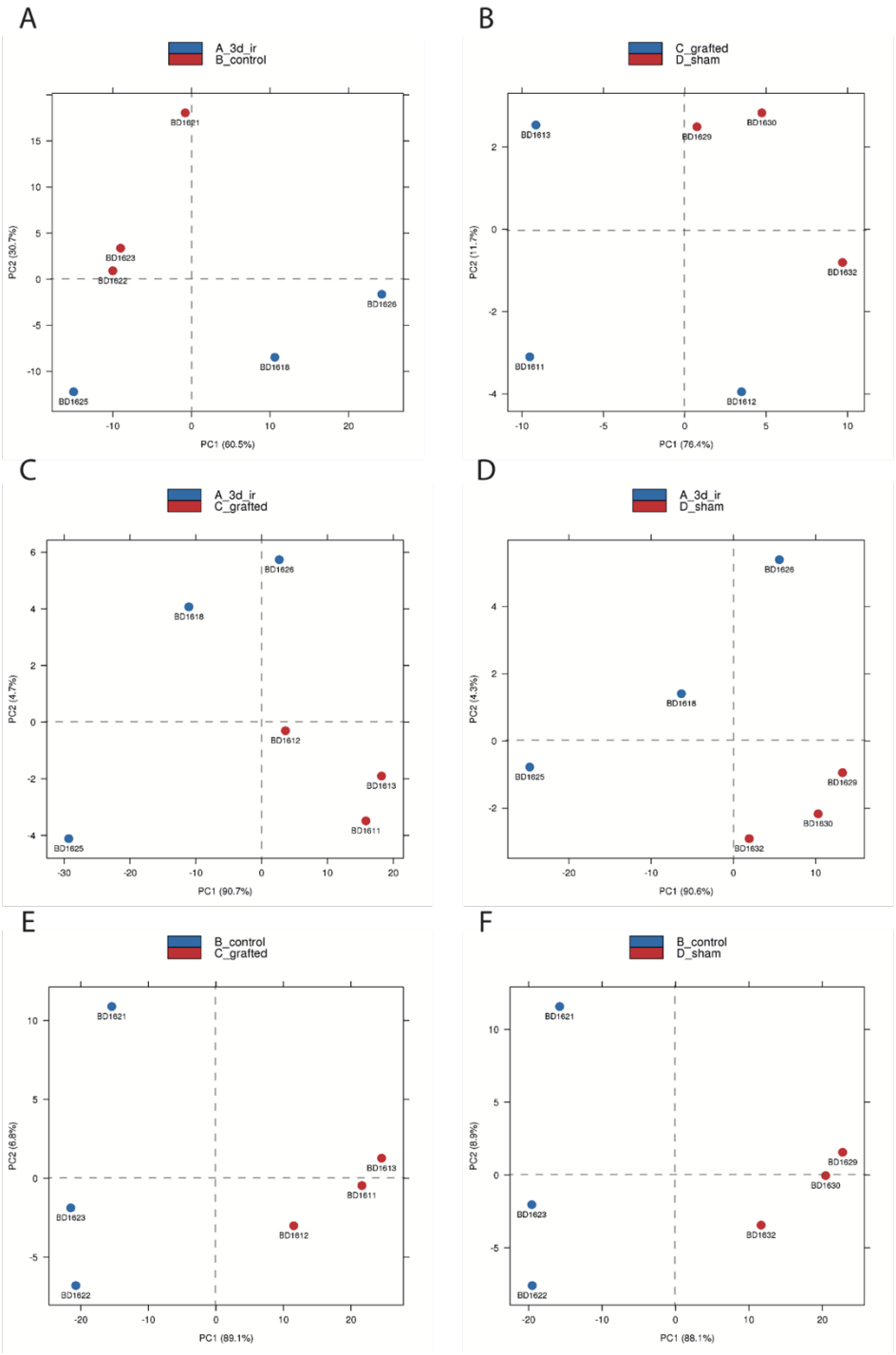

Figure 4.1: PCA plots for all comparisons made after RNA-seq showing: A) 3 days after 18Gy vs Control, here sample BD1625 does not cluster with the remainder of the pre-irradiated samples; B) Grafted vs Sham injected; C) 3 Days after 18Gy vs Grafted; D) 3 days after 18Gy vs Sham; E) Control vs Grafted; F) Control vs Sham. Raw data and PCA analysis was performed by Peter White's group at The Research Institute at Ohio Children's Hospital

4.2 Control vs 3 days post-18Gy

4.2.1) Network analysis

To determine which pathways may be dysregulated in pre-irradiated irradiated muscles non-irradiated and 3 days 18Gy irradiated muscle samples were compared after sequencing. Comparing these two samples returned 454 genes with an absolute 2-fold differential regulation. A protein-protein association network was created using the STRING database with the confidence interaction for protein interactions set at a value of 0.4 or above (medium confidence). In this network, there was a large group of 242 connected components, followed by an isolated group of 7 differentially regulated genes involved in the cytochrome P450 metabolism, and the remainder of the isolated nodes either had 1 or 2 interactions, or did not interact with any adjacent nodes, and were therefore excluded from further network analysis.

The largest group of 242 connected nodes was extracted into a new network, and the Eigenvector, Betweenness, Closeness, Stress, Eccentricity were calculated (section 2.7.5.2). The network parameters for each centrality (minimum, maximum, and average) are shown in table 4.2.

Table 4.2 – Centrality Values for Control Vs 3 Day Post-18Gy Network			
Centrality	Min	Avg	Max
Eccentricity	6.67E-02	9.91E-02	1.25E-01
Closeness	4.31E-04	1.05E-03	1.54E-03
Betweenness	0.00E+00	7.82E+02	8.63E+03
Stress	0.00E+00	1.29E+04	1.82E+05
Eigenvector	7.64E-14	1.85E-01	3.32E-02

The individual parameters for each gene can then be displayed on a scatterplot. Figure 4.2 shows the Eigenvector against Betweenness Centrality, Mapping Eigenvector to node size and Betweenness Centrality to the node colour allows an overlay of these data onto the network and is shown in figure 4.3**;** a larger image showing the main regulatory nodes is shown in figure 4.4. The nodes with the highest Eigenvector and Betweenness centrality were *Stat1*, *Oasl2*, *Rtp4*, *Oas2*, *Isg15*, *Oasl1*, and *Irf7*. These can be regarded as having a large number of interactions, together with interactions with other major nodes in the network (Eigenvector), and essential in maintaining communications between the nodes in network (Betweenness centrality). Therefore, they are can be considered as candidates for major regulatory nodes.

Plotting Closeness centrality against Eigenvector shows similar nodes as playing a critical part in the network (*Oasl2*, *Oas2*, *Isg15*, *Stat1*, *Oasl1*, and *Irf7*) which can be seen in figure 4.5. Their high Closeness centrality indicates that they are a short distance away from most other nodes, suggesting a major regulatory function. They are visualised on the network in figure 4.6 and a close up is provided in figure 4.7. With the exception of Rtp4, these are the same genes that were identified by

observing the Betweenness centrality. Combining both lists of genes we can conclude that *Oasl2*, *Oas2*, *Isg15*, *Stat1*, *Oasl1*, and *Irf7* are the core regulators of the network.

However, other centrality measures can further complement these selections, and Closeness centrality is best compared to eccentricity, whilst the measure of stress of a node can supplement information gathered by the Betweenness centrality measure. Applying network filters, only those nodes with a centrality value above the network average can be selected. Thus, for a node to be selected, it must contain values between the network mean and network maximum for all measures of centrality which are displayed in table 4.2. This indicates a role in holding together communications within the network (high Betweenness centrality and stress), an ability to easily reach the remaining nodes in the network, positioning the node at a central point (Closeness centrality and eccentricity), and factoring in that they must have a large number of interactions, or interact highly influential proteins (Eigenvector centrality).

This allows the selection of only central and top regulators in the network. From 242 nodes with 1472 interactions, we are able to select 14 nodes with 69 interactions between each other. The selected genes are *Tlr3*, *Oasl2*, *Oas1g*, *Oasl1*, *Oas1a*, *Ifitm3*, *Isg15, Irf7, Oas2*, *Stat1, Stat2, Gbp2, Rtp4,* and *Lgals3bp*. Their interactions are shown in figure 4.8 with the node Eigenvector (from the original network) mapped to node size, and the colour of the node from yellow to red indicating the fold change in expression.

Gene-Ontology (GO) analysis can be performed on these core regulators to determine their likely functions, and was set with a threshold p value lower than 0.001 to prevent the appearance of an excessive number of unspecific GO terms. A

hierarchical organisation of GO terms is shown in figure 4.9, and a table with enriched results is shown on table 4.3. The GO analysis shows that the probable function of these genes is an involvement in the immune response, in particular a response to exogenous dsRNA. It is worth noting that all mice used for sequencing were immunodeficient and bred under specific pathogen-free (SPF) conditions and no surgical procedure or grafting into the muscle has been performed on them, greatly reducing any possibility of a viral infection and indicating that the activation of the innate immune response is due to the irradiation procedure alone. Furthermore, these experiments are performed in immuno-compromised mice, and previous research has shown a lack of immune infiltrate in pre-irradiated muscles (C. N. Pagel & Partridge 1999), suggesting this is a tissue specific response, and not mediated by invading immune cells.

Table 4.3 GO-Analysis of top network regulators in Control Vs 3 Days post-18Gy

GO-ID	Description	Genes in test set	corr p-value
51707	response to other organism	*Stat1*, *Irf7*, Isg15, Tlr3	6.17E-04
9615	response to virus	*Irf7* , *Isg15*, *Tlr3*	6.17E-04
9607	response to biotic stimulus	*Stat1*, *Irf7*, Isg15, Tlr3	8.29E-04
43330	response to exogenous dsRNA	*Stat1, Tlr3*	8.29E-04
6955	immune response	*Irf7*, *Oas1a*, *Tlr3*, *Oasl2*	8.29E-04
51704	multi-organism process	*Stat1*, *Irf7*, *Isg15*, *Tlr3*	9.15E-04

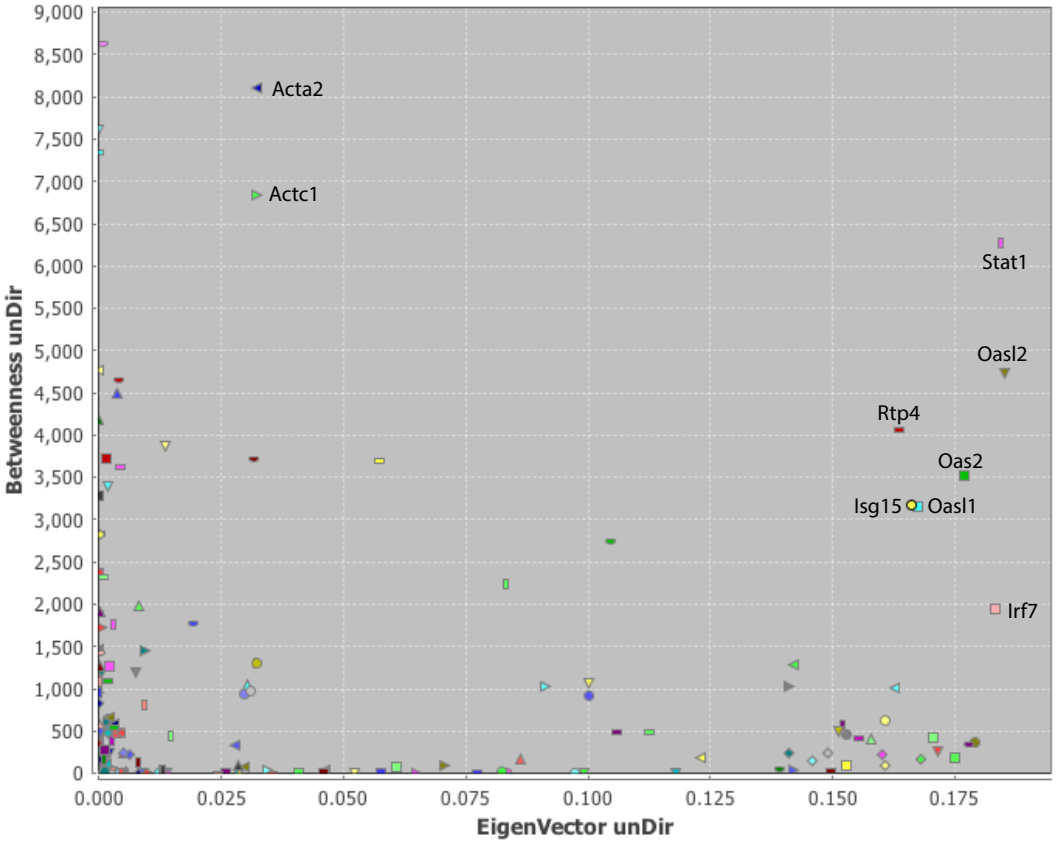

Figure 4.2: Eigenvector against Betweenness centrality plot. Nodes with a high Eigenvector compared to the network average can be considered proteins with a super-regulatory role or a critical target of a key regulatory pathway (Eigenvector) whilst those with a high Betweenness centrality are key in maintaining communications between other nodes in the network. Combining these two parameters we can see that Stat1, Oasl2, Rtp4, Oas2, Isg15, Oasl1, and Irf7 are key nodes in regulating and maintaining communications for the rest of network. Those with a high Betweenness Centrality but a low Eigenvector may be regarded as nodes that are acting as bridges between different groups of clusters of nodes, none of which are of major importance (Acta2 and Actc1).

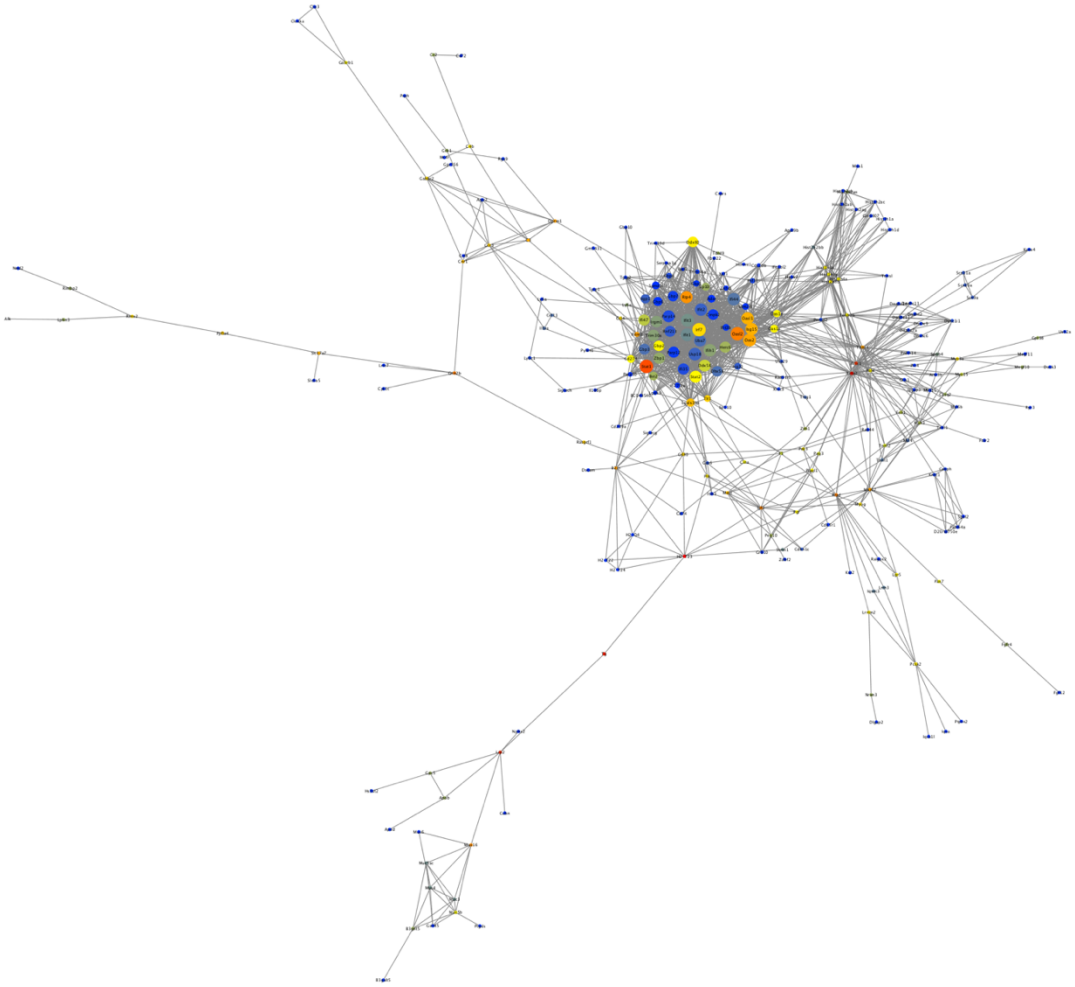

Figure 4.3: Full network view of results for genes that are differentially regulated by an absolute 2-fold change between non-treated and 3 days after 18Gy irradiation (3DIR). The Nodes remain of a constant size between the minimum and average network Eigenvector value, from the mean value to the maximum value the increase in size proportionally to their Eigenvector value. Betweenness centrality is represented as a colour gradient. Blue nodes denote low Betweenness centrality, yellow nodes denote a value close to the network average, and red nodes denote the largest values

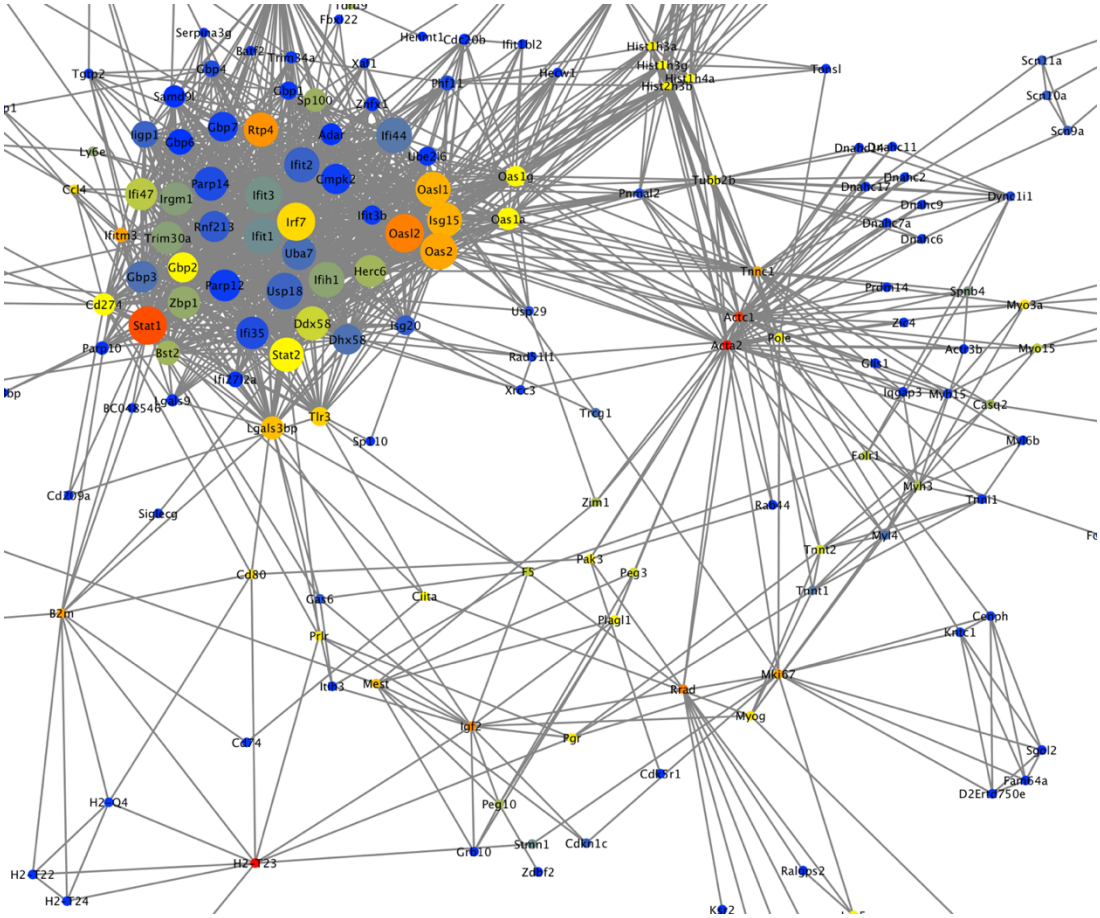

Figure 4.4: Close up view of the central network cluster. Here we can view our main hubs as defined by a large Eigenvector and high Betweenness Centrality (Stat1, Oasl2, Rtp4, Oas2, Isg15, Oasl1, and Irf7). It is also possible to view Acta2 and Actc1 in bright red but with a small node size. Here it becomes clear that these nodes are essential in connecting peripheral nodes to the main cluster of the network (high Betweenness Centrality) but do not connect to any major regulatory nodes, thus the low Eigenvector.

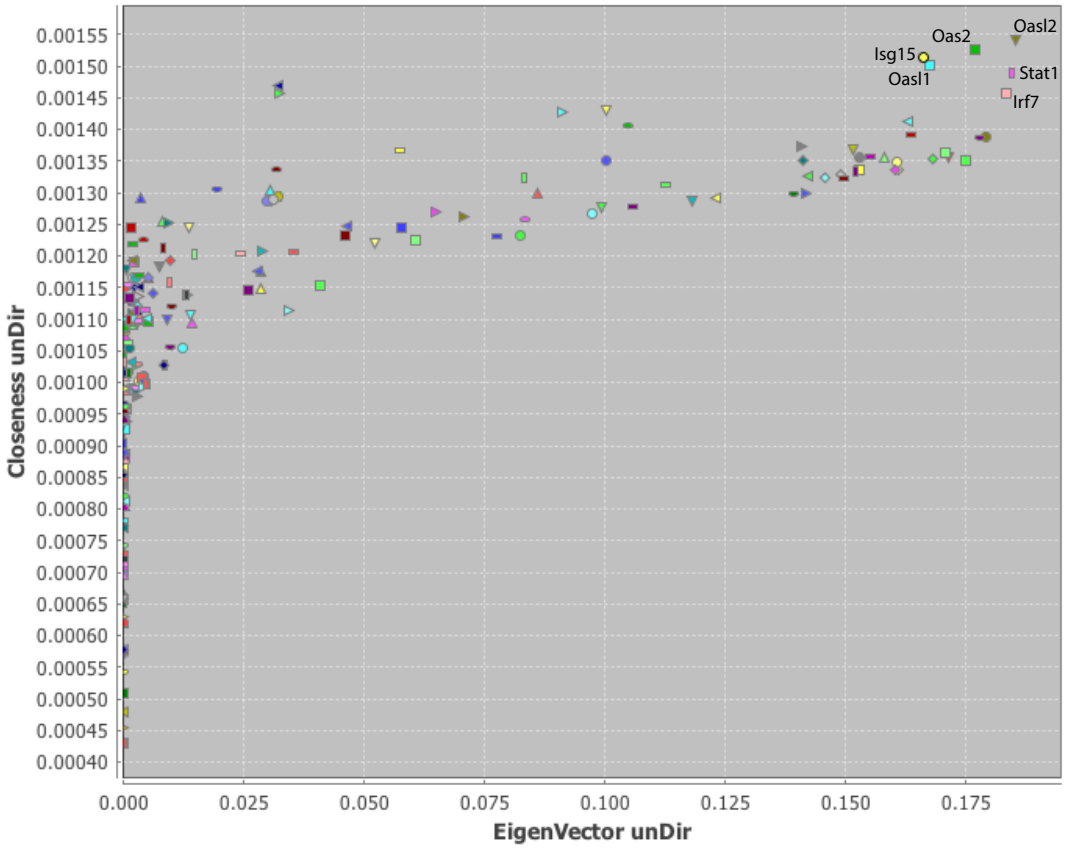

Figure 4.5: Eigenvector plotted against Closeness Centrality for Control vs 3DIR. Proteins with a high closeness centrality compared to the network average are likely to be close, either by directly interacting or a few steps away, to all other nodes in the network. Combined with a high eigenvector centrality we see that the proteins Oasl2, Oas2, Isg15, Stat1, Oasl1, and Irf7 are able to easily reach or are within reach of most other nodes in the network, along with having a large number of neighbours, some of which of high importance themselves.

Figure 4.6: Mapping Closeness centrality to node colour and the Eigenvector to node size central nodes in the network become easily identifiable by their large size and red colour, all appear to be concentrated in a central cluster within the core of the network.

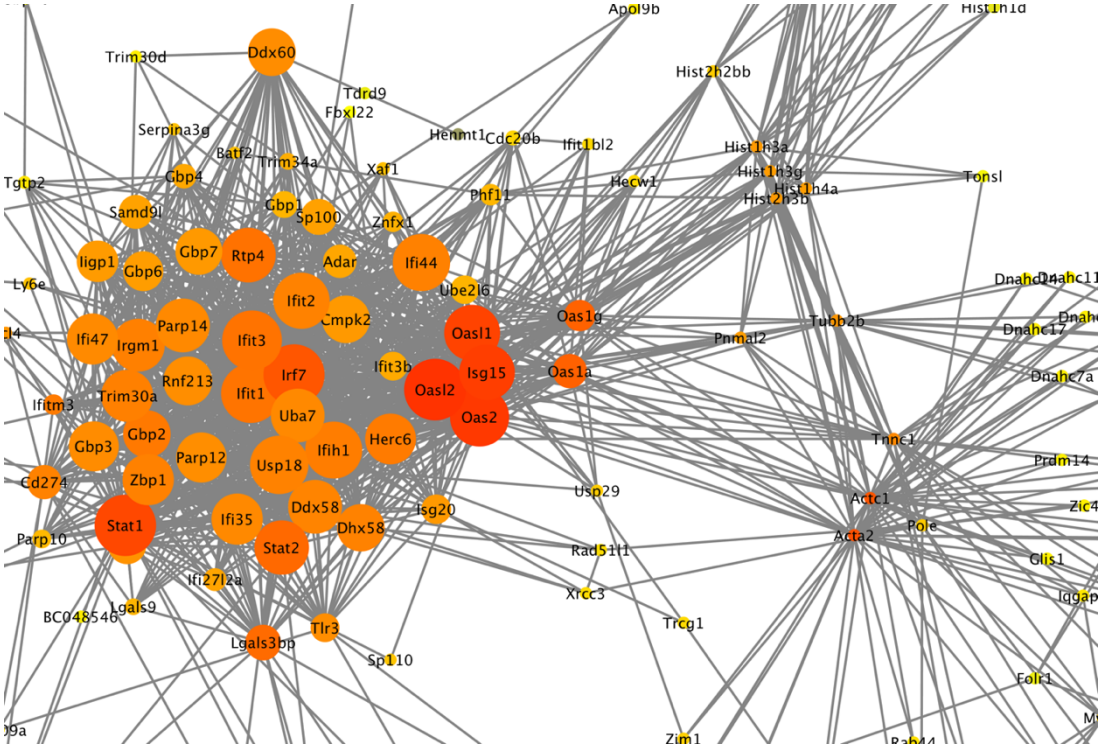

Figure 4.7: Close-up of central nodes as determined by eigenvector and closeness centrality. It can be observed that the main nodes (Oasl2, Oas2, Isg15, Oasl1, Stat1, and Irf7) appear as large red circles in the network.

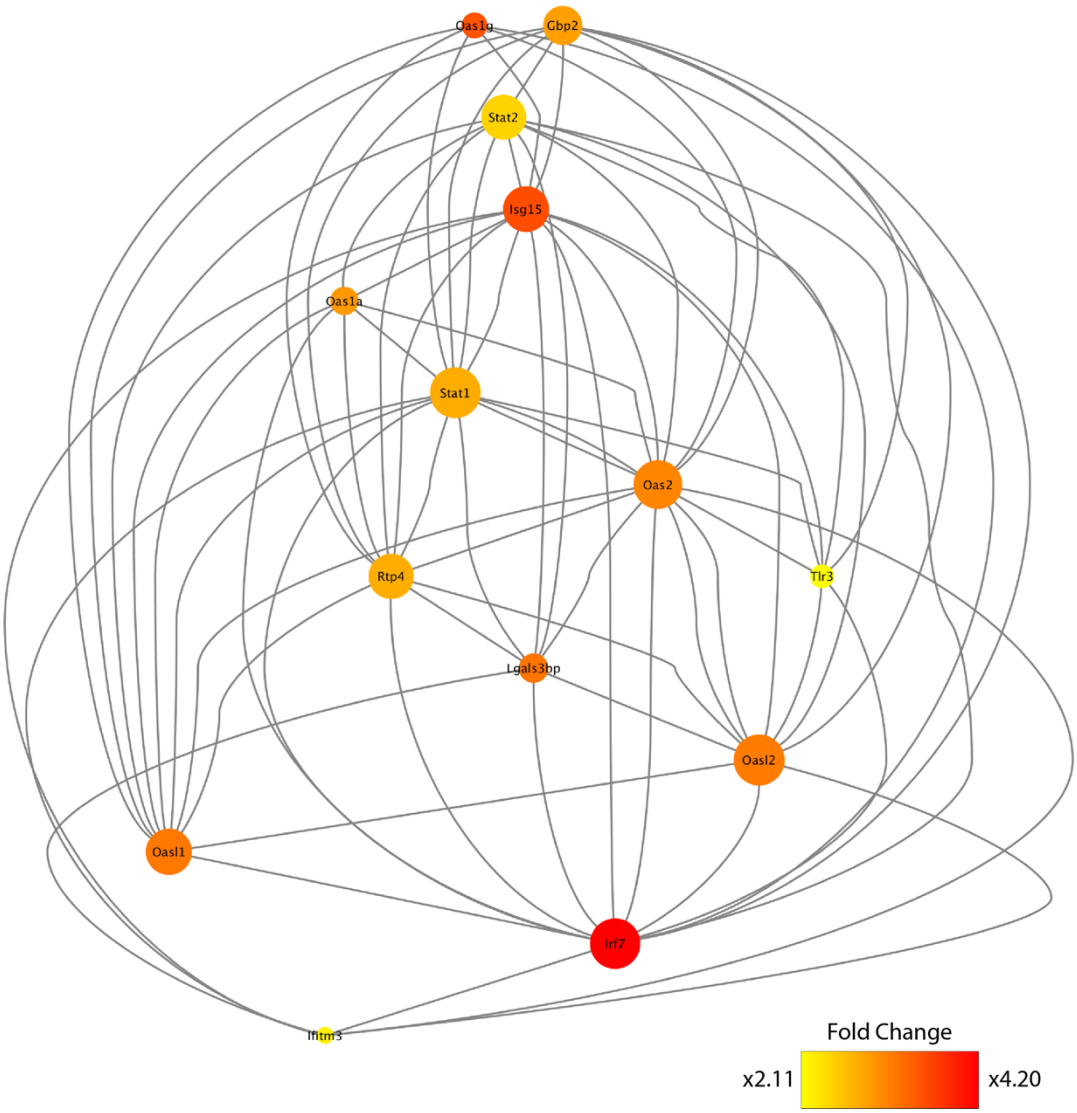

Figure 4.8: Top network regulators as defined by an above network average value for Eigenvector, Betweenness Centrality, Closeness Centrality, Eccentricity, and Stress. Node colour is mapped to the fold change in expression (2.11 fold to 4.20 upregulation) and their size is mapped to their original Eigenvector value.

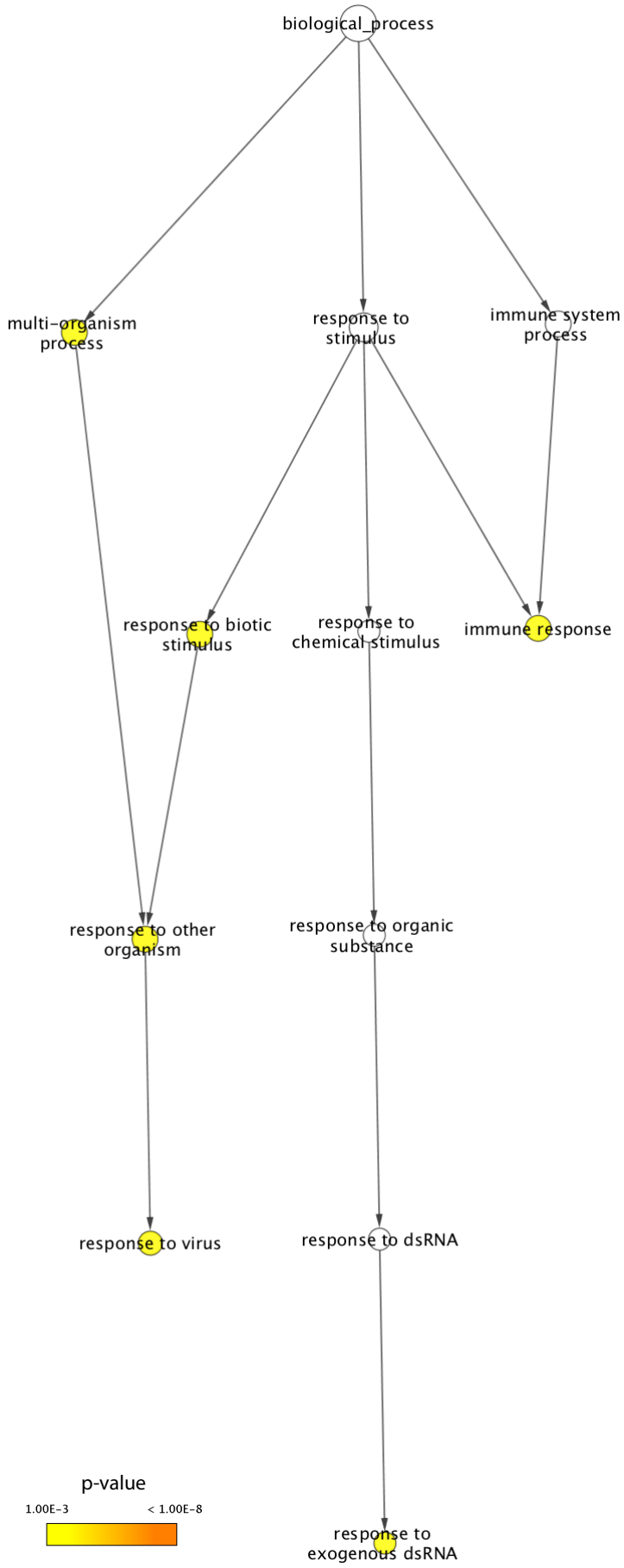

Figure 4.9: Results of gene-ontology analysis of the top network regulators between non-irradiated samples and those 3 days after 18Gy irradiation, indicating an immune response, in particular in response to exogenous dsRNA. Significance was determined using a Hypergeometric test with a Benjamini & Hochberg False Discovery Rate and the significance level was set at $p<0.001$. The categories visualised are those over-represented in the gene-set. The p-value is indicated by a colour gradient scale ranging from $p<0.001$ to $p<1x10^{-8}$

4.2.2) Gene Set Enrichment Analysis

To determine which pathways were over-represented in the network, Gene Set Enrichment Analysis (GSEA) was performed, using the molecular signatures database as a reference, on the full set of differentially expressed genes returned from RNA sequencing as described in section 2.7.6. Class A was the control samples and class B the 3DIR samples. No specific gene sets were significantly enriched in the control (non-irradiated) samples, while 3 gene sets were significantly enriched in the samples collected 3 days after irradiation (table 4.4). As predicted by the network analysis, the top 2 enriched pathways belong to the interferon response (gamma and alpha) which relate to the innate immune response. The last enriched gene-set is "Myogenesis".

Table 4.4: Gene-Sets significantly enriched in samples collected 3 days after 18Gy IR

NAME	Size	ES	NES	NOM p-val	FDR q-val	FWER p-val
HALLMARK INTERFERON GAMMA RESPONSE	36	-0.788	-5.356	0.000	0.000	0.000
HALLMARK INTERFERON ALPHA RESPONSE	28	-0.793	-4.297	0.000	0.000	0.000
HALLMARK MYOGENESIS	12	-0.599	-2.315	0.000	0.000	0.000

Heat-maps for each pathway are shown in figures 4.10 (interferon gamma response), 4.11 (interferon alpha response) and 4.12 (myogenesis). However, there is a significant overlap between the genes present in the interferon gamma response

and the interferon alpha response, with 24 genes being present in both sets. This leaves the interferon alpha response with two genes which are different from the interferon gamma response (*Gbp2* and *Trem140*), whilst the interferon gamma response has 9 unique genes not present in the interferon alpha response (*Gbp6*, *Cd274*, *Oas2*, *Il-18bp*, *Ifit1*, *Stat1*, *DDX58*, *Znfx1*, and *Ciita*).

Taken together, these results suggest that 3 days after 18Gy irradiation the innate immune response has been activated, leading to the activation of the interferon pathways. This shift in the inflammatory phenotype within the pre-irradiated mouse muscle might be responsible for the enhanced engraftment of donor satellite cells after host muscle irradiation.

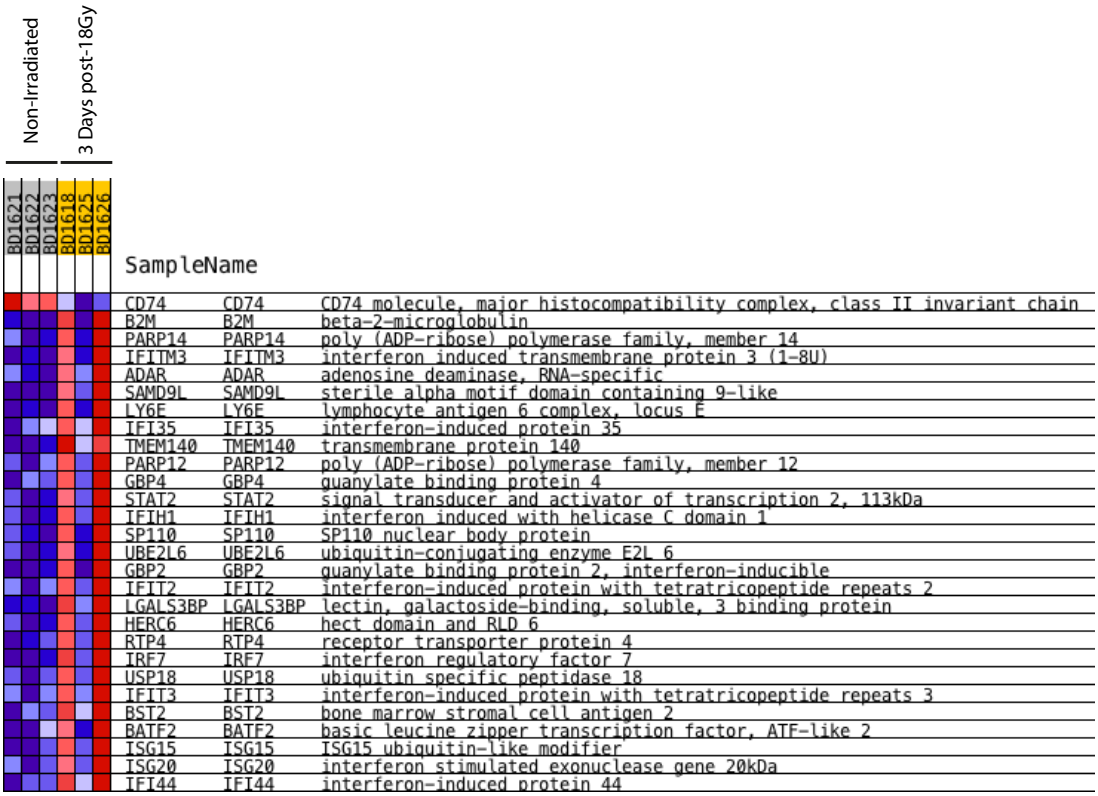

Figure 4.10: GSEA analysis results showing a gene-set enriched for an interferon alpha response. Two of the samples (BD1618 and BD1626) from the 3 days post-18Gy IR show a significant upregulation of the genes involved in interferon alpha signalling, whilst BD1625 shows no response. Non-irradiated samples show no significant enrichment. Additionally, two major network regulators are present in this gene-set (Irf7 and Isg15).

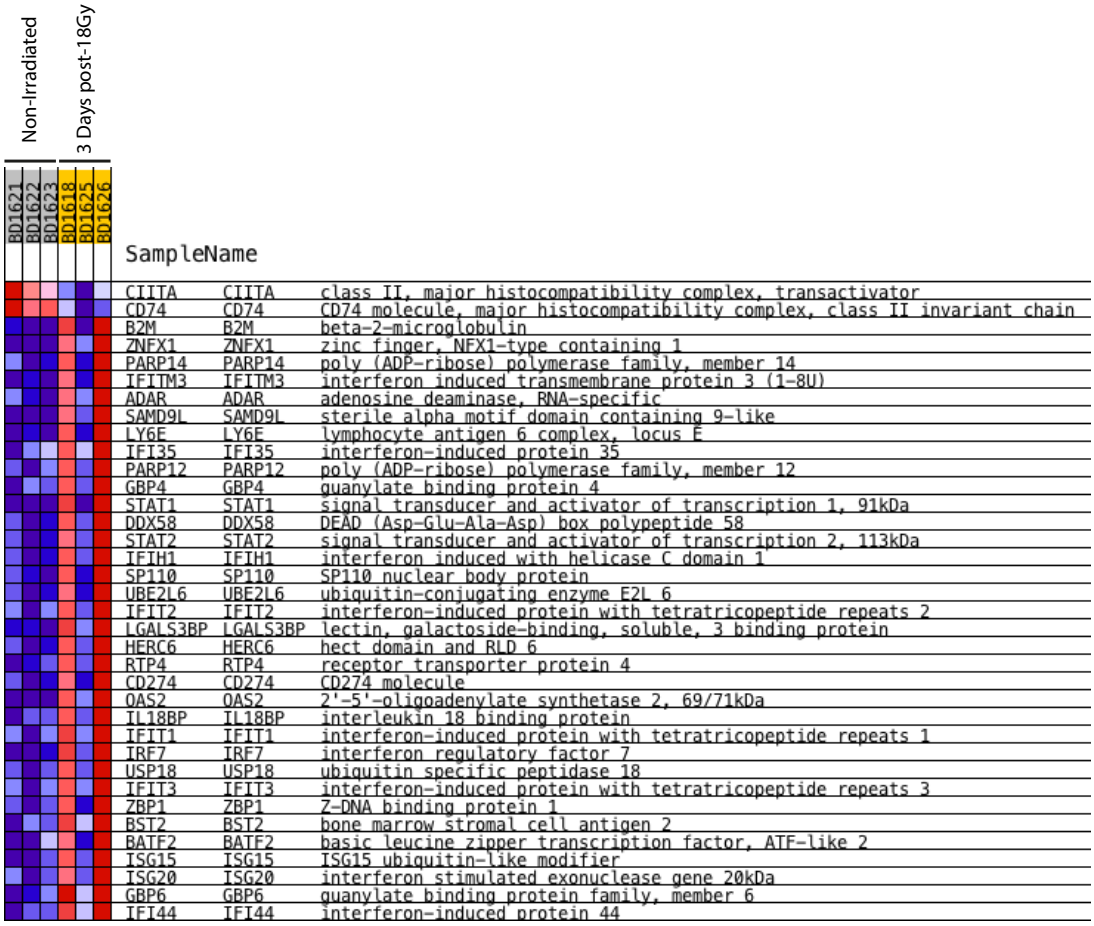

Figure 4.11: GSEA results for "Hallmark_Interferon Gamma Response" enriched 3 days after irradiation. Some of the major network regulators are present in this cohort, including Stat1, Isg15, Oas2, and Irf7. Sample BD1625 is again not responsive to the irradiation treatment.

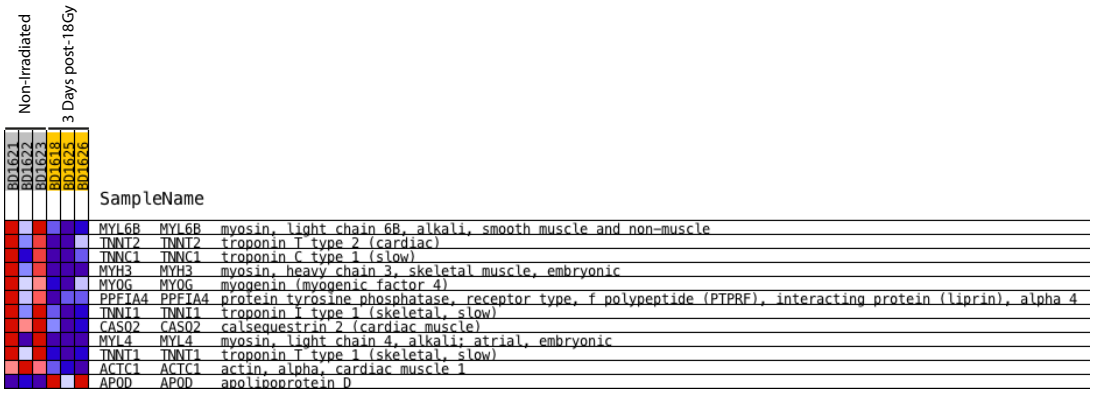

Figure 4.12: Enriched genes matching with the "Hallmark_Myogenesis" reference gene-set from the molecular signatures database. These genes are significantly downregulated in irradiated muscles compared to non-irradiated controls, indicating a reduction in the amount of myogenic differentiation after irradiation, as seen for example by a marked downregulation of the terminal differentiation marker MyoG (myogenin), consistent with the depletion of endogenous myoblasts after irradiation.

4.3) Sham vs Grafted

Comparisons of RNA-seq data between sham injected and grafted samples was performed to determine if the grafting procedure, or the interaction of donor satellite cells with the host muscle, led to any changes in gene expression that may enhance satellite cell engraftment. This comparison yielded 3 differentially dysregulated genes, suggesting that grafted satellite cells have little impact on the host muscle. This is in agreement with the poor separation of the samples in the PCA analysis (figure 4.1B). In samples from grafted tissues *Gbp10* (guanylate binding protein 10) was upregulated compared to the sham injected samples by a 2.19 fold increase in mRNA expression. Guanylate binding proteins are induced by interferon gamma and are essential for host-pathogen interactions and host defence (Kim et al. 2016). Additionally, grafted muscles had an upregulation (2.19-fold) of predicted gene 4841 (*Gm4841*) which is a predicted GTPase induced by interferon gamma.

Finally, *Mt2* (metallothionein 2) was downregulated in grafted compared to sham injected muscles. This family of proteins are involved in zinc ion binding. Their blockade has been associated with increases in muscle mass and strength (Summermatter et al. 2017) and their increase with a reduction in post-burn inflammation (Zhang et al. 2016), suggesting a role in mediating inflammatory responses.

No further analysis can be performed on these results as they do not form a network large enough for analysis or a gene set large enough for GSEA. I conclude that there are no differences between grafted and sham injected muscles that are detectable within the thresholds applied by RNA-seq analysis in this comparison.

4.4) 3 days post-18Gy irradiation Vs Sham

Sham injected muscles are 5 days post irradiation and can therefore be used to investigate how the muscle behaves 5 days after irradiation. 13 genes (shown in table 4.5) were differentially regulated between 3-day irradiated muscles and sham injected tissues. Only 2 of these proteins had any form of recorded interaction (*Cd40* and *Socs1*), and the gene list produces no significantly overrepresented gene ontology terms or match with any GSEA gene sets.

Table 4.5 Genes differentially expressed between 3-day irradiated muscles and Sham Injected muscles			
Gene Symbol	Full Name	Fold Change	padj
Cd40	CD40 antigen transcript variant 2	2.39	0.022
Aldh1b1	aldehyde dehydrogenase 1 family member B1	2.30	0.022
Gbp5	guanylate binding protein 5	2.21	0.059
Krt18	keratin 18	2.19	0.040
Socs1	suppressor of cytokine signaling 1 transcript variant 1	2.18	0.067
Pttg1	pituitary tumor-transforming gene 1 transcript variant X1	2.14	0.065
Igf2bp3	insulin-like growth factor 2 mRNA binding protein 3 transcript variant X3	2.10	0.014
Nmral1	NmrA-like family domain containing 1 transcript variant 4	2.01	0.014
Myh3	myosin heavy polypeptide 3 skeletal muscle embryonic	-2.06	0.000
Ddit4	DNA-damage-inducible transcript 4	-2.18	0.003
Arrdc2	arrestin domain containing 2	-2.24	0.014
Angptl7	angiopoietin-like 7	-2.44	0.002
Adamts8	a disintegrin-like and metallopeptidase (reprolysin type) with thrombospondin type 1 motif 8	-2.51	0.000

From this small gene set, we can conclude that there are no major differences between collected muscles at 3 and 5 days post irradiation, and that injection of medium alone caused no significant change to the muscle. But as the original analysis

excluded any genes that did not reach a threshold an absolute fold change of 2, smaller changes in gene expression between both samples are not represented.

4.5) 3 Days post-18Gy Irradiated Vs Grafted

4.5.1) Network Analysis

In the comparison of sham injected muscles to grafted muscles (section 4.3) no significant differences were found between the groups, while sham injected muscles compared to those irradiated 3 days prior also showed little changes in gene expression. To determine if satellite cell engraftment significantly alteres gene expression within the tissue, 3 days post-18Gy irradiated and grafted muscles were compared.

RNA-seq data returned 689 dysregulated genes for this comparison. The String database recognised 556 genes with known functions, and 540 of these formed a highly interconnected network, with 16 genes on the periphery that had no interactions. The large group of 540 interconnected genes was extracted for network analysis. A view of the network is shown in figure 4.13, and the network parameters for Eigenvector, Closeness centrality, Betweenness centrality, Stress, and Eccentricity are shown in table 4.6.

Table 4.6: Centrality Values for Control Vs Sham Network			
Centrality	Min	Avg	Max
Eccentricity	1.10E-01	1.60E-01	2.00E-01
Closeness	3.02E-04	6.80E-04	9.67E-04
Betweenness	0.00E+00	9.91E+02	2.92E+04
Stress	0.00E+00	2.29E+04	3.97E+05
Eigenvector	1.14E-10	2.37E-02	1.08E-01

By plotting the Eigenvector against Betweenness centrality for each node, one can identify key nodes in holding together network communications, as shown in figure 4.14. The most notable are Topoisomerase 2a (*Top2a*), Rac GTPase Activating Protein 1 (*Racgap1*), Cyclin Dependent Kinase 1 (*Cdk1*), Baculoviral IAP Repeat Containing 5 (*Birc5*), Marker of Proliferation Ki-67 (*Mki67*) and Proliferating Cell Nuclear Antigen (*Pcna*). All of these are major regulators of cell proliferation and some have a role in DNA damage repair (*Mki67 and Pcna*) whilst the remainder of the proteins are highly involved in orchestrating mitosis according to gene ontology analysis.

When looking at the Closeness centrality against Eigenvector (figure 4.15), similar proteins to those highlighted by a high Betweenness centrality and Eigenvector are seen - *Cdk1*, *Top2a*, and *Racgap1*. Additionally, we find Cyclin B1 (*Ccnb1*) which is essential in controlling the G2/M (mitosis) transition of the cell cycle (NCBI gene ID: 268697) and Aurora Kinase B (*Aurkb*) which participates in the

regulation of alignment and segregation of chromosomes during mitosis (NCBI gene ID: 20877).

Taken together, it can be inferred that a large number of cells are either undergoing cell division, or preparing to do so, within irradiated muscles that had been grafted with satellite cells 2 days previously.

Filtering the network to isolate only nodes with an above average value for Eigenvector, Closeness centrality, Betweenness Centrality, Stress, and Eccentricity, one can isolate the central nodes in the network. This yields a group of 45 genes with 881 interactions between them, which is shown in figure 4.16. Selecting only those with values within the 75^{th} percentile (Betweenness > 3662; Closeness > $8.91x10^{-4}$; Eigenvector > 0.1025) this core network can be reduced to 3 top interacting regulators (Top2a, Cdk1, and Aurkb) shown in figure 4.17a. Using BINGO to perform gene ontology analysis, we can determine the combined functions of this core of major regulatory genes. To avoid an excessive amount of redundant GO terms the p-value threshold is lowered from 0.05 to $1x10^{-3}$.

Four GO terms were significantly enriched and are shown in table 4.7 (figure 4.17b). These suggest that the major regulators in the network are implicated in the regulation of cell division and mitosis. It can be assumed that this is due to grafted satellite cells replicating within the host muscle 2 days after grafting

Table 4.7: GO-Analysis of top network regulators in 3 Days post-18Gy Vs Grafted			
GO-ID	Description	Genes in test set	corr p-value
30261	chromosome condensation	*Top2a*|*Cdk1*	8.34E-05
51301	cell division	*Top2a*|*Cdk1*|*Aurkb*	8.34E-05
6323	DNA packaging	*Top2a*|*Cdk1*	9.08E-04
71103	DNA conformation change	*Top2a*|*Cdk1*	9.08E-04

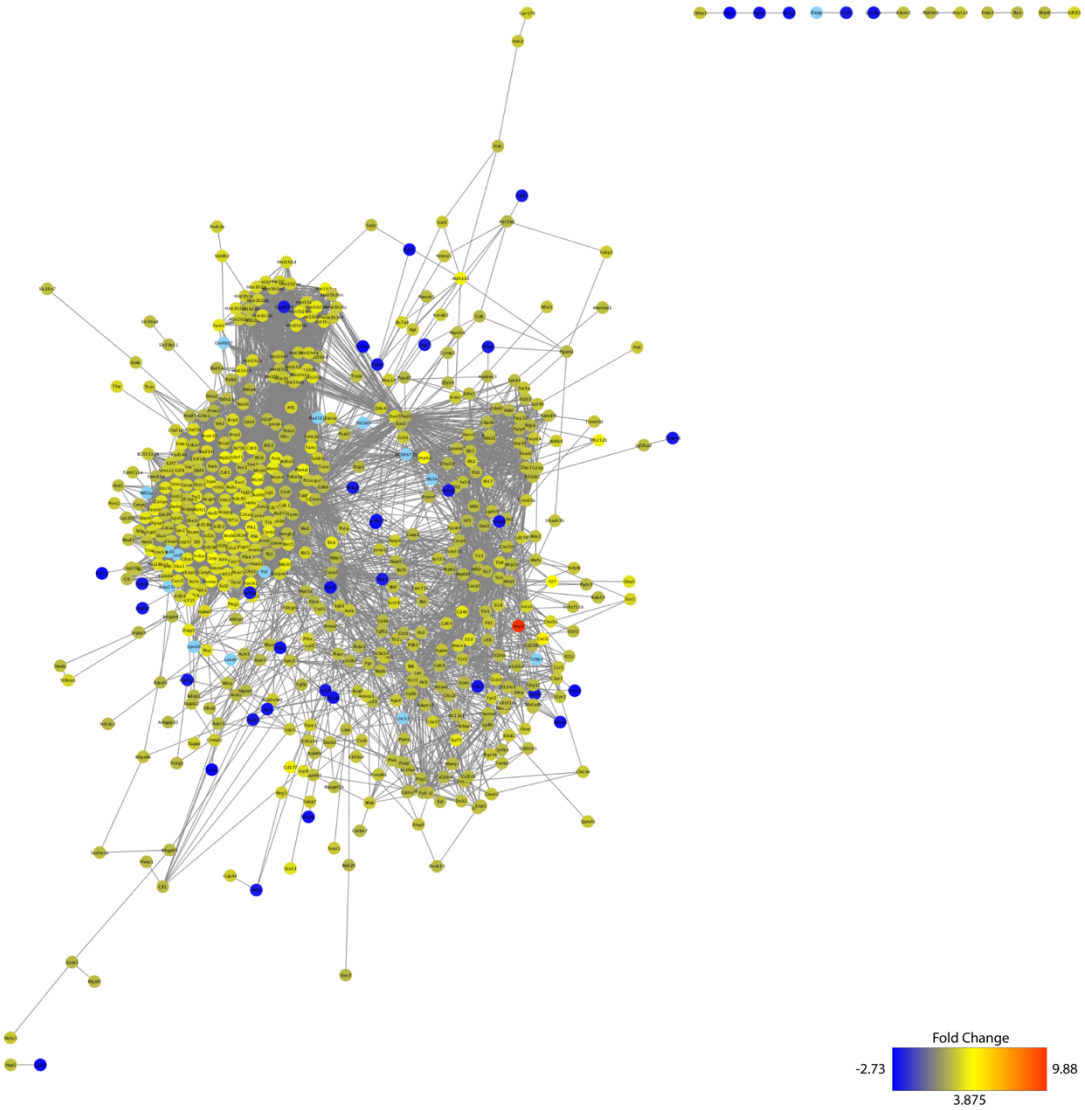

Figure 4.13: Network created by dysregulated genes between muscles collected 3 days after 18Gy irradiation and muscles that had been irradiated (18Gy), grafted with freshly isolated satellite cells 3 days later, and collected 2 days post-graft (grafted). Node colour is mapped on a blue-yellow-red gradient with blue marking downregulated genes and red marking an upregulation

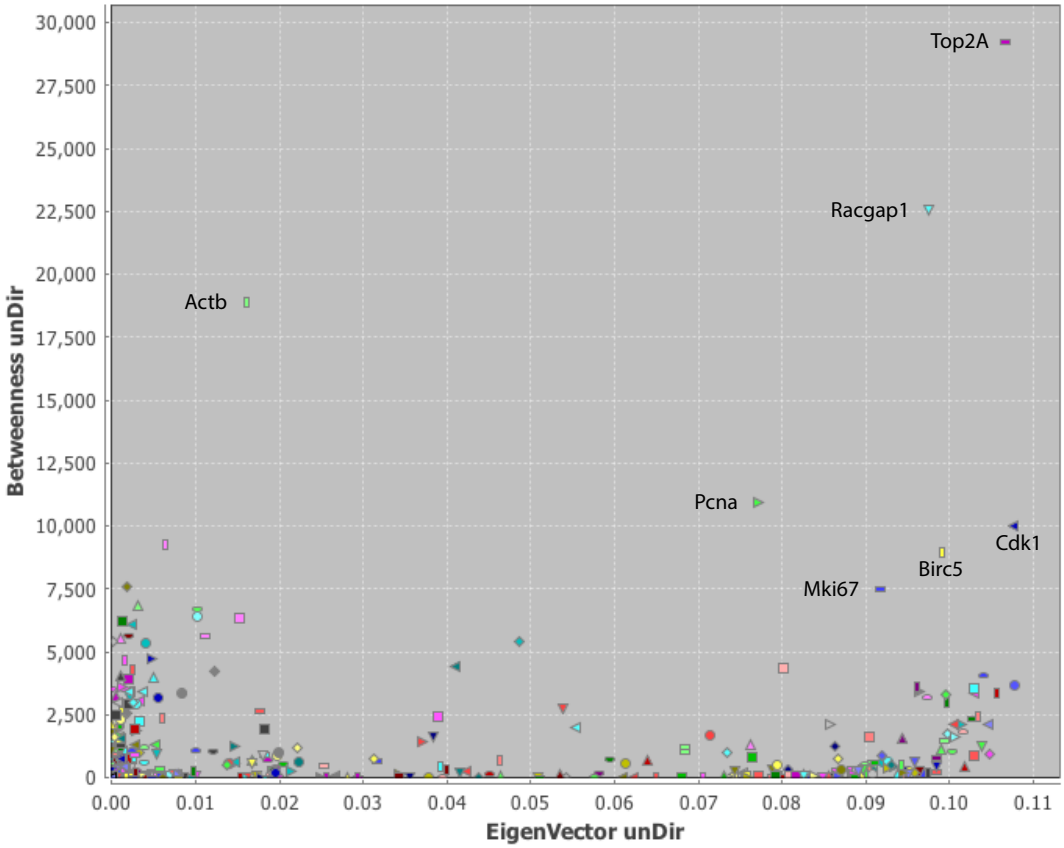

Figure 4.14: Eigenvector compared to Betweenness centrality for the network produced by the comparison of muscles collected 3 days post-18Gy irradiation and those which were pre-irradiated (18Gy), grafted with freshly isolated satellite cells, and collected 2 days post-graft. Two genes are highly noticeable as key hubs in the network essential in maintaining communication (*Top2a* and *Racgap1*) whilst 4 other genes show a higher eigenvector and Betweenness centrality than the rest of the network (*Cdk1*, *Birc5*, *Mki67*, *Pcna*). *Actb*, as seen previously (figure 4.2) is acting as a bridge between two major groups in the network, with a high Betweenness centrality but a low Eigenvector.

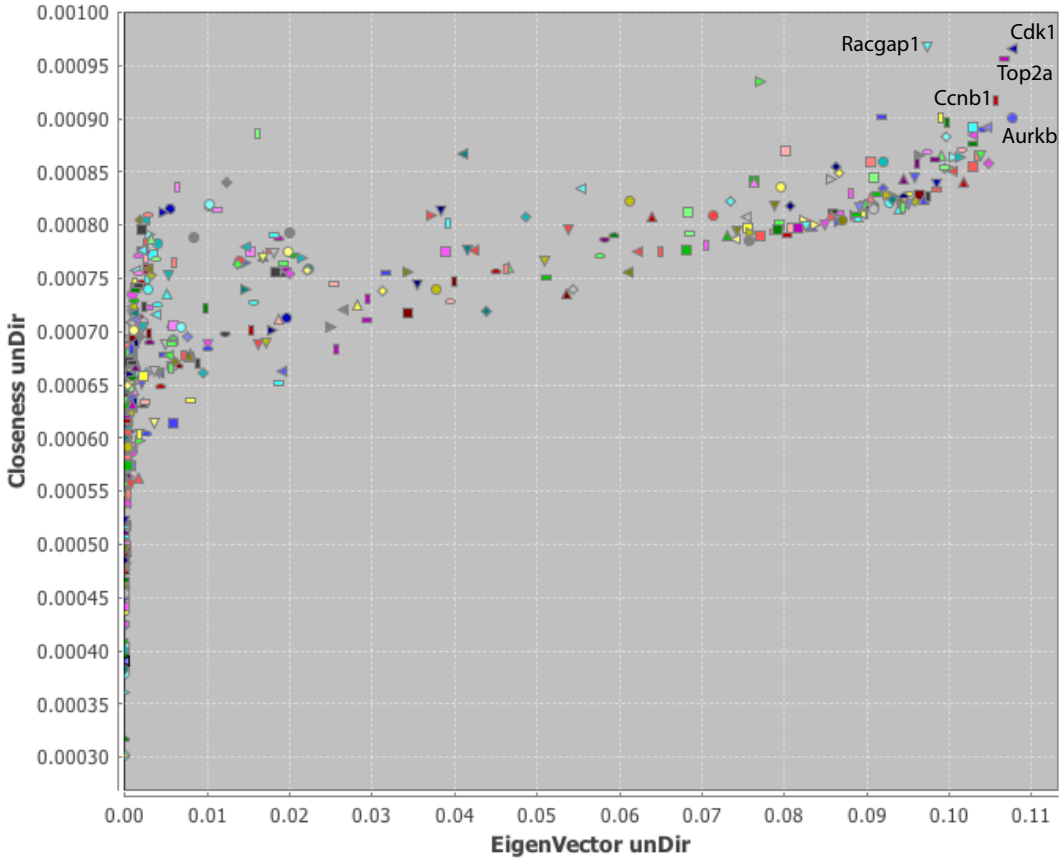

Figure 4.15: Eigenvector compared to Closeness centrality in the network created by comparing muscles collected 3 days after 18Gy irradiation and those which had been irradiated (18Gy), grafted with freshly isolated satellite cells 3 days post-IR, and collected 2 days after grafting. Central proteins in the network as indicated by a high closeness centrality become Cdk1, Top2a, Racgap1, Ccnb1, and Aurkb

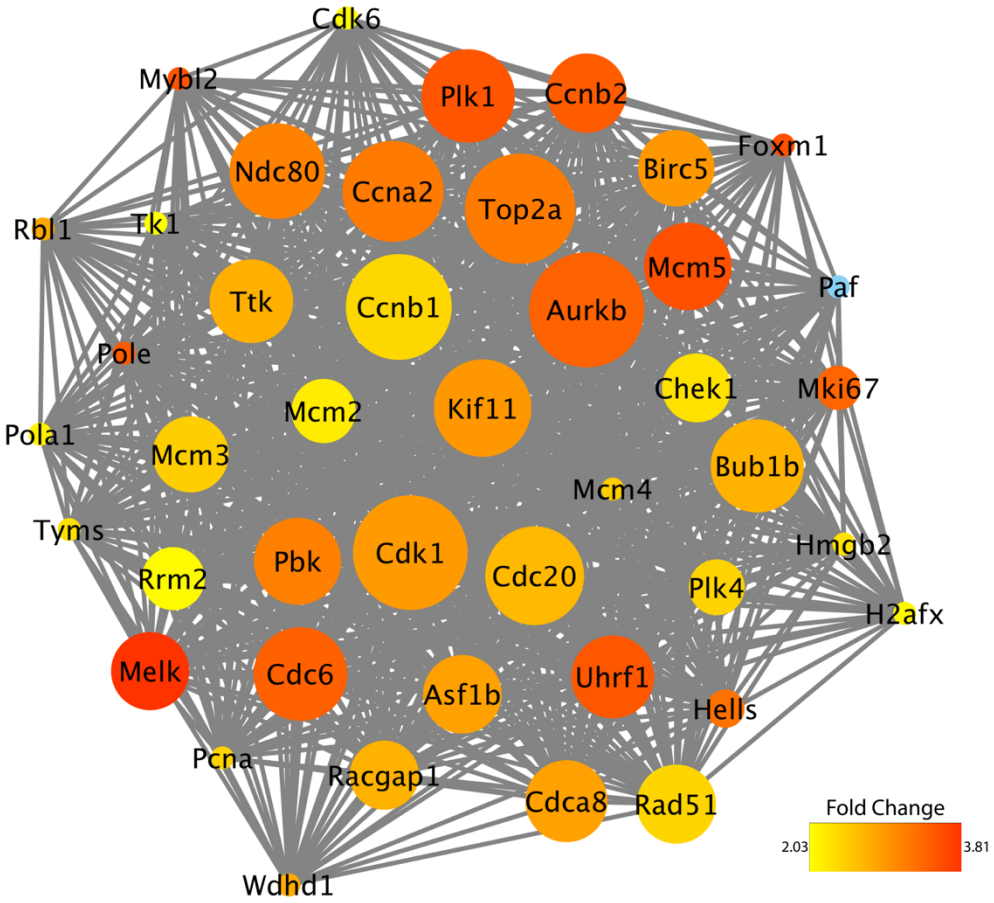

Figure 4.16: Top network regulators in the network created by comparing gene expression between muscles collected 3 days after 18Gy irradiation and those collected 2 days after satellite cell grafting in 3 day (18Gy) pre-irradiated muscles. Node size is matched to the original network Eigenvector value whilst node colour is matched to the fold change in gene expression, which for this group ranges from 2.03-fold to a 3.81-fold increase in expression.

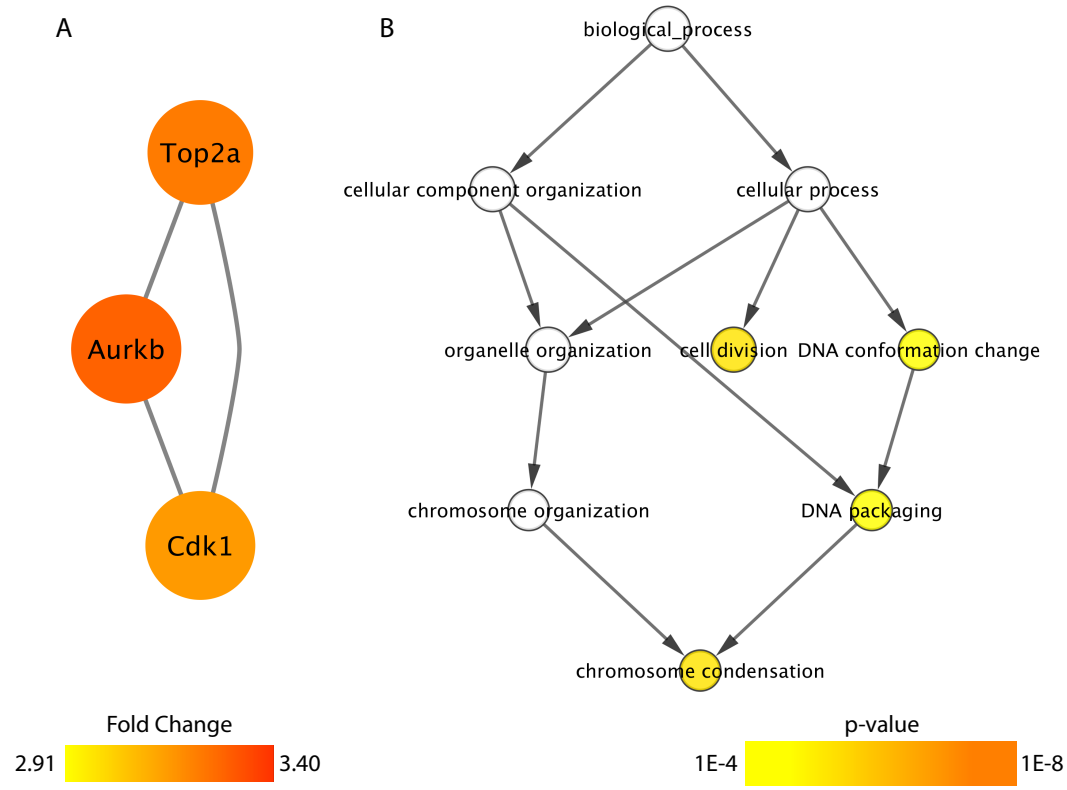

Figure 4.17: 3 days post-18Gy irradiated muscles vs muscles which were pre-irradiated (18Gy) muscles grafted with freshly satellite cells 3 days post-irradiation and collected 2 days post-graft. A) Top network regulators with centrality values in the 75th percentile, node size is mapped to Eigenvector and node colour to the fold change in grafted sample compared to 3 days post-18Gy irradiated samples. B) Gene-ontology analysis for the genes displayed in A, p-value is represented in a colour gradient from yellow to orange.

4.5.2) GSEA Analysis

GSEA analysis was performed, assigning Class A to 3-day irradiated samples and Class B to Grafted samples. 3-day irradiated samples displayed 5 gene sets significantly enriched to a FDR (false discovery rate) of 25% and a p value below 5% which are shown in table 4.8.

Table 4.8: Gene-Sets Enriched in 3-day irradiated samples compared to grafted

NAME	SIZE	ES	NES	NOM p-val	FDR q-val	FWER p-val
HALLMARK COMPLEMENT	15	0.481	2.324	0.000	0.005	0.002
HALLMARK EPITHELIAL MESENCHYMAL TRANSITION	11	0.481	1.979	0.011	0.029	0.015
HALLMARK HYPOXIA	10	0.480	1.846	0.019	0.034	0.025
HALLMARK INTERFERON GAMMA RESPONSE	41	0.204	1.627	0.000	0.058	0.067
HALLMARK INTERFERON ALPHA RESPONSE	23	0.267	1.587	0.041	0.057	0.086

As previously established by comparing 3-day irradiated to control muscles (section 4.2), most of the enriched gene sets are involved with the innate immune system. In this comparison, over-represented gene-sets involved in the innate immune response include the complement system, interferon gamma, and

interferon alpha responses. Additionally, a response to hypoxia and epithelial mesenchymal transition are over-represented with a positive enrichment score.

In contrast, grafted samples had 4 gene sets significantly enriched to an FDR of 25% and a nominal p-value of 5% and are shown in table 4.9.

Table 4.9: Gene-sets enriched in grafted samples compared to 3-day irradiated samples

NAME	SIZE	ES	NES	NOM p-val	FDR q-val	FWER p-val
HALLMARK G2M CHECKPOINT	64	-0.489	-2.367	0.000	0.000	0.000
HALLMARK MITOTIC SPINDLE	30	-0.502	-2.104	0.000	0.001	0.003
HALLMARK E2F TARGETS	52	-0.386	-1.814	0.003	0.020	0.080
HALLMARK SPERMATOGENESIS	10	-0.524	-1.609	0.029	0.092	0.402

The largest (64 genes) and most significantly enriched gene set are markers belonging to the G2/M Checkpoint (figure 4.18). This gene-set shares 22 genes with the top 45 major network regulators identified by network analysis on Cytoscape. The set with the second largest number of genes (52) is that referring to the targets of the E2F family of transcription factors which shares 26 genes with the top 45 network regulators (figure 4.19). After irradiation induced DNA damage cells will activate the DNA damage response, and E2F transcription factors are involved in DNA

damage repaid, DNA damaged induced induced apoptosis, and cellular proliferation(Stevens & La Thangue 2004). However, the enrichment of the mitotic spindle assembly pathway (figure 4.20) suggests that there are dividing cells within the tissue, confirming that at this stage, grafted satellite cells are already dividing 2 days after engraftment, similar to what Beauchamp et al. (1999) observed when grafting H2K-18 conditionally immortalised myoblasts into 18Gy pre-irradiated muscles.

The gene set representing spermatogenesis is extremely small (10 genes. Figure 4.21) and does not appear to contain any markers specific for germ-line development, with most of them being regulators of cell division and chromosome segregation. From these 10 genes, 5 overlap with the other more significantly upregulated pathways (*Kif2c*, *Nek2*, *Bub1*, *Ttk*, *Ccnb2*) and from the remaining 5 genes *(Nos1, Ncaph*, *Dbf4*, *Il12rb2*, and *Ddx4*) only *Ddx4* (DEAD box polypeptide 4/ Mouse Vasa homolog gene [Mvh]) is specifically involved in male germ line development, with mice deficient in this protein failing to produce sperm in the testis (Tanaka et al. 2000). Therefore, this set of genes can be disregarded as a false discovery.

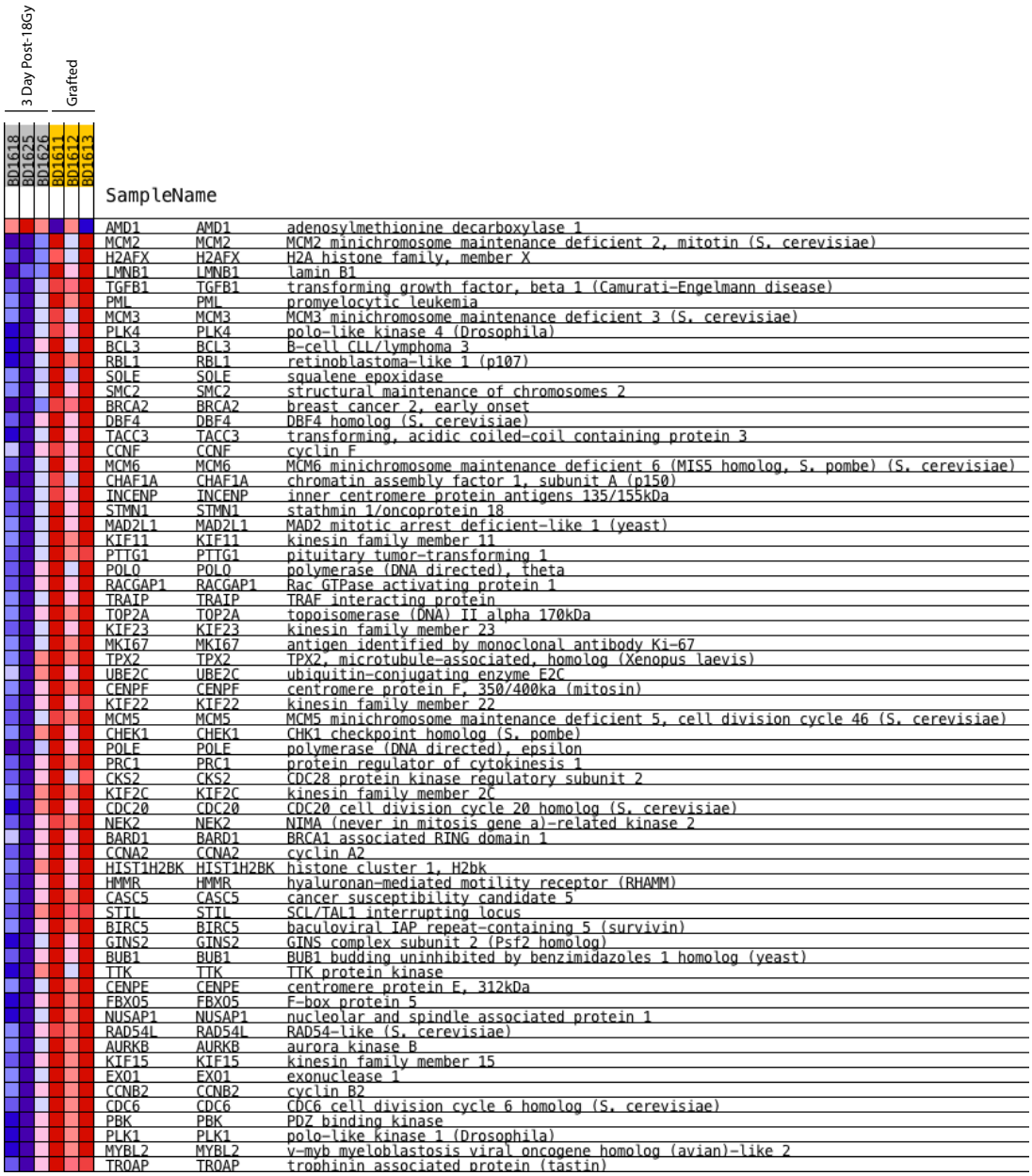

AMD1	AMD1	adenosylmethionine decarboxylase 1
MCM2	MCM2	MCM2 minichromosome maintenance deficient 2, mitotin (S. cerevisiae)
H2AFX	H2AFX	H2A histone family, member X
LMNB1	LMNB1	lamin B1
TGFB1	TGFB1	transforming growth factor, beta 1 (Camurati-Engelmann disease)
PML	PML	promyelocytic leukemia
MCM3	MCM3	MCM3 minichromosome maintenance deficient 3 (S. cerevisiae)
PLK4	PLK4	polo-like kinase 4 (Drosophila)
BCL3	BCL3	B-cell CLL/lymphoma 3
RBL1	RBL1	retinoblastoma-like 1 (p107)
SQLE	SQLE	squalene epoxidase
SMC2	SMC2	structural maintenance of chromosomes 2
BRCA2	BRCA2	breast cancer 2, early onset
DBF4	DBF4	DBF4 homolog (S. cerevisiae)
TACC3	TACC3	transforming, acidic coiled-coil containing protein 3
CCNF	CCNF	cyclin F
MCM6	MCM6	MCM6 minichromosome maintenance deficient 6 (MIS5 homolog, S. pombe) (S. cerevisiae)
CHAF1A	CHAF1A	chromatin assembly factor 1, subunit A (p150)
INCENP	INCENP	inner centromere protein antigens 135/155kDa
STMN1	STMN1	stathmin 1/oncoprotein 18
MAD2L1	MAD2L1	MAD2 mitotic arrest deficient-like 1 (yeast)
KIF11	KIF11	kinesin family member 11
PTTG1	PTTG1	pituitary tumor-transforming 1
POLQ	POLQ	polymerase (DNA directed), theta
RACGAP1	RACGAP1	Rac GTPase activating protein 1
TRAIP	TRAIP	TRAF interacting protein
TOP2A	TOP2A	topoisomerase (DNA) II alpha 170kDa
KIF23	KIF23	kinesin family member 23
MKI67	MKI67	antigen identified by monoclonal antibody Ki-67
TPX2	TPX2	TPX2, microtubule-associated, homolog (Xenopus laevis)
UBE2C	UBE2C	ubiquitin-conjugating enzyme E2C
CENPF	CENPF	centromere protein F, 350/400ka (mitosin)
KIF22	KIF22	kinesin family member 22
MCM5	MCM5	MCM5 minichromosome maintenance deficient 5, cell division cycle 46 (S. cerevisiae)
CHEK1	CHEK1	CHK1 checkpoint homolog (S. pombe)
POLE	POLE	polymerase (DNA directed), epsilon
PRC1	PRC1	protein regulator of cytokinesis 1
CKS2	CKS2	CDC28 protein kinase regulatory subunit 2
KIF2C	KIF2C	kinesin family member 2C
CDC20	CDC20	CDC20 cell division cycle 20 homolog (S. cerevisiae)
NEK2	NEK2	NIMA (never in mitosis gene a)-related kinase 2
BARD1	BARD1	BRCA1 associated RING domain 1
CCNA2	CCNA2	cyclin A2
HIST1H2BK	HIST1H2BK	histone cluster 1, H2bk
HMMR	HMMR	hyaluronan-mediated motility receptor (RHAMM)
CASC5	CASC5	cancer susceptibility candidate 5
STIL	STIL	SCL/TAL1 interrupting locus
BIRC5	BIRC5	baculoviral IAP repeat-containing 5 (survivin)
GINS2	GINS2	GINS complex subunit 2 (Psf2 homolog)
BUB1	BUB1	BUB1 budding uninhibited by benzimidazoles 1 homolog (yeast)
TTK	TTK	TTK protein kinase
CENPE	CENPE	centromere protein E, 312kDa
FBXO5	FBXO5	F-box protein 5
NUSAP1	NUSAP1	nucleolar and spindle associated protein 1
RAD54L	RAD54L	RAD54-like (S. cerevisiae)
AURKB	AURKB	aurora kinase B
KIF15	KIF15	kinesin family member 15
EXO1	EXO1	exonuclease 1
CCNB2	CCNB2	cyclin B2
CDC6	CDC6	CDC6 cell division cycle 6 homolog (S. cerevisiae)
PBK	PBK	PDZ binding kinase
PLK1	PLK1	polo-like kinase 1 (Drosophila)
MYBL2	MYBL2	v-myb myeloblastosis viral oncogene homolog (avian)-like 2
TROAP	TROAP	trophinin associated protein (tastin)

Figure 4.18: Heatmap showing an enrichment of the gene-set G2/M checkpoint in muscles irradiated (18Gy) grafted 3 days post-irradiation, and collected 2 days post-graft compared to muscles collected 3 days post-18Gy irradiation (FDR<1x10^{-4}; nominal p-value < 1x10^{-4}

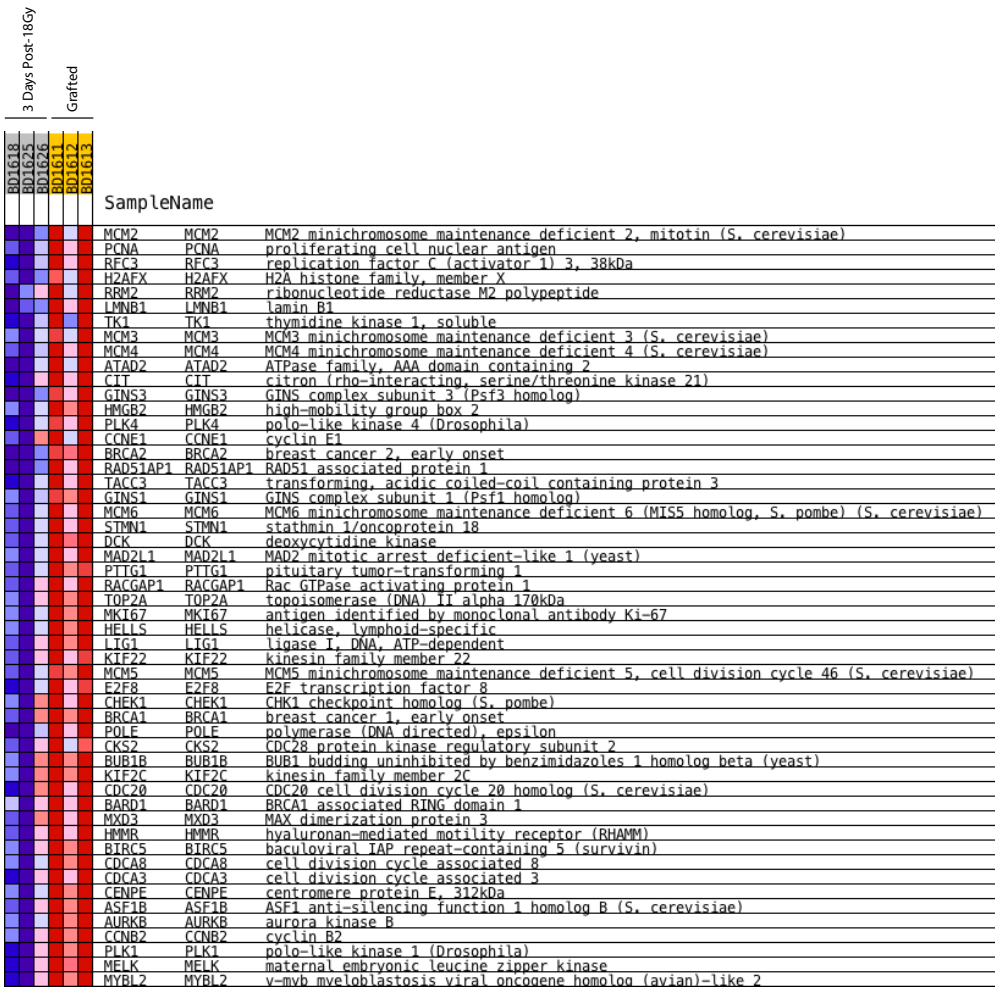

Figure 4.19: E2F targets in the molecular signatures database, all significantly upregulated in muscles irradiated (18Gy) grafted 3 days post-irradiation, and collected 2 days post-graft, compared to muscles collected 3 days post-18Gy irradiation (FDR: 0.02; nominal p-value = 0.003).

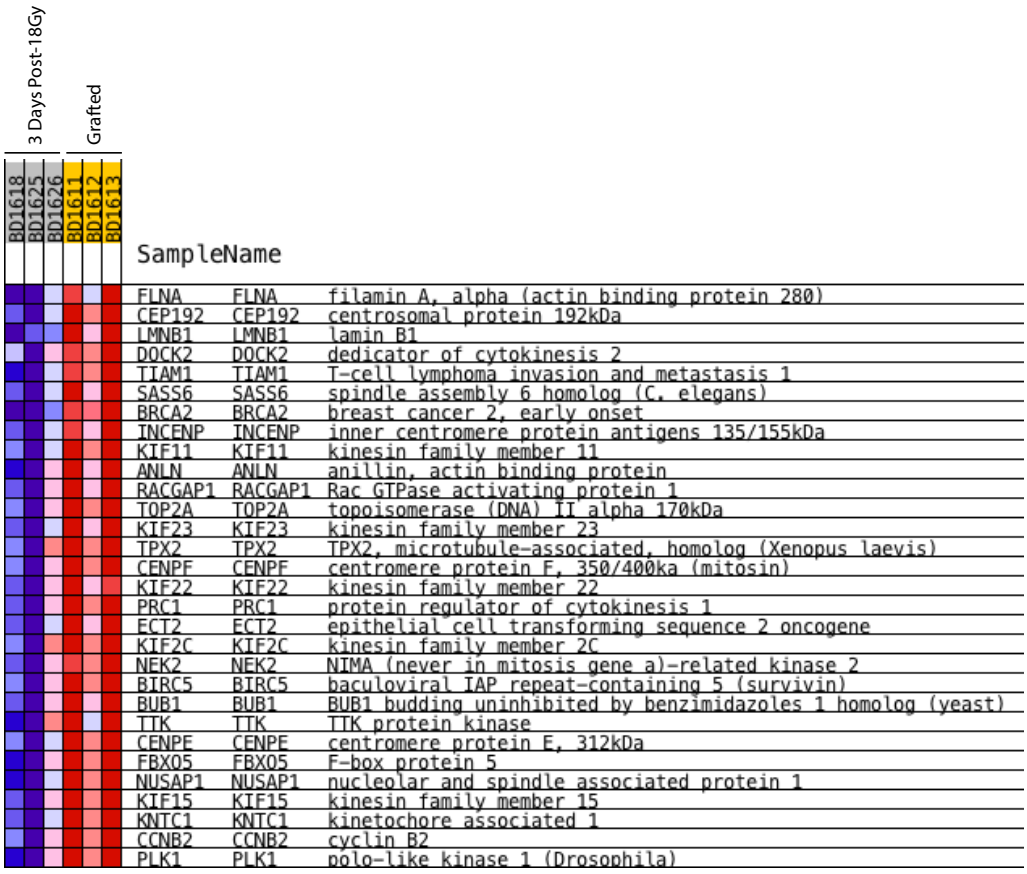

Figure 4.20: Heat-map displaying differentially regulated genes between 3 day irradiated and irradiated and grafted muscles which match the gene-set for mitotic spindle assembly in the molecular signatures database. All genes are upregulated in muscles irradiated (18Gy) grafted 3 days post-irradiation and collected 2 days post-graft compared to muscles collected 3 days post-18Gy irradiation (FDR: 0.001; nominal-value < $1x10^{-4}$).

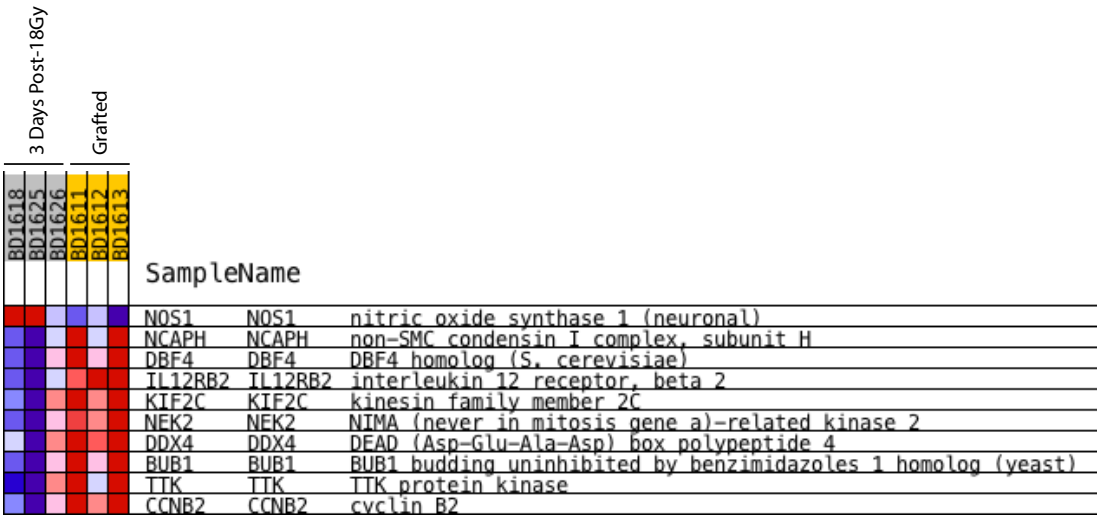

Figure 4.21: Enriched genes matching the Spermatogenesis gene-set in muscles irradiated (18Gy) grafted 3 days post-irradiation and collected 2 days post-graft compared to muscles collected 3 days post-18Gy irradiation (FDR:0.092; nominal value = 0.029). None of the enriched terms are exclusive for sperm cell development, and only *NOS1* is not directly involved in the regulation of the mitotic cell cycle.

4.6) Non-irradiated Vs Sham

4.6.1) Network Analysis

When comparing 3 days irradiated to sham injected muscles, few genes reached the absolute fold change (x2) required to be included in the results. To determine what pathways may have changed 5 days after 18Gy irradiation, control (non-irradiated) were compared to sham injected muscles.

This led to 1068 differentially regulated genes between non-irradiated and sham injected samples. 1028 protein coding genes were identified by the STRING database and imported into Cytoscape. One major group of connected components was seen, containing 728 nodes with 6465 interactions. The remaining genes formed 1 group of 3 interacting genes and 13 groups consisting of pairs of interacting genes. The remaining genes were not connected to any other parts of the network. These smaller clusters were discarded and the major group containing 728 nodes was used for network centrality analysis, this network is shown coloured according to fold change (blue = -7. 10; yellow= 0.00; red= 29.57) in figure 4.22. The minimum, average, and maximum centrality values for this network are shown in table 4.10.

Table 4.10: Centrality Values for Control Vs Sham Network

Centrality	Min	Avg	Max
Eccentricity	8.300E-02	1.22E-01	1.43E-01
Closeness	1.70E-04	4.200E-4	6.26E-04
Betweenness	0.000E+0	1754.912	59147.509
Stress	0.000E+0	31177.837	763318
Eigenvector	1.07E-11	0.0188	0.184

Plotting Eigenvector against Betweenness centrality (figure 4.23) shows which nodes are essential to maintaining network communications (nodes with the highest Eigenvector and Betweenness centrality) . *Il-6* with the highest Betweeness centrality is an inflammatory cytokine with a strong involvement in muscle development (Muñoz-Cánoves et al. 2013). Stat1, again the protein with the highest Eigenvector centrality indicating that it has a large number of interactions and affects a large number of other important proteins in the network, also has a high Betweenness centrality. Interferon gamma, *Ccl5*, *Cxcl10*, and *Irf7* are also identified as essential proteins in regulating and maintaining network communications.

Extracting all the nodes with an above network average Betweenness, Stress, Closeness, Eccentricity and Eigenvector, it yields a core network with 103 nodes and 1708 interactions which is represented in figure 4.25, with node size matched to the Eigenvector and colour matched to the fold change in expression. From these nodes, we can extract those with values above the 75th percentile for Eigenvector (>0.1043), Betweenness (>6588), and Closeness (>5.543x10^{-4}) to reduce the number of network regulators to the most significant ones. This yields a network with 7 genes, all upregulated, which are *Irf7*, *Il-6*, *Ccl5*, *Cxcl10*, *Ifnγ* , *Stat1*, *and Cxcl9* which are shown in figure 4.26.

Performing gene-ontology analysis (table 4.11) on this core network of regulators confirms their role in the mediation of an immune system process and inflammatory response, which leads to the release of cytokines that may create a favourable niche for satellite cell engraftment. For example, under the GO term "inflammatory response" *Cxcl10*, *Cxcl9*, *Il-6*, *Ccl5* are included, whilst under the term

"positive regulation of cell proliferation" *Il-6 and Cxcl10* are found, which are shared with the inflammatory response.

Table 4.11: Enriched GO-Terms for top network regulators for Control Vs Sham			
GO-ID	Description	Genes in test set	corr p-value
6955	immune response	*Cxcl10*|*Cxcl9*|*Il-6*|*Ifng*|*Ccl5*|*Irf7*	1.12E-08
2376	immune system process	*Cxcl10*|*Cxcl9*|*Il-6*|*Ifng*|*Ccl5*|*Irf7*	3.56E-07
6952	defense response	*Cxcl10*|*Cxcl9*|*Il-6*|*Ifng*|*Ccl5*|	2.87E-06
50896	response to stimulus	*Cxcl10*|*Cxcl9* |*Il-6*|*Ifng*|*Stat1* |*Ccl5* |*Irf7*	5.13E-06
1781	neutrophil apoptosis	*Il-6*|*Ifng*	5.32E-06
6954	inflammatory response	*Cxcl10*|*Cxcl9* |*Il-6* |*Ccl5*	1.08E-05
33028	myeloid cell apoptosis	*Il-6*|*Ifng*	1.14E-05
51707	response to other organism	*Il-6*| *Ifng* |*Stat1* |*Irf7*	1.40E-05
1780	neutrophil homeostasis	*Il-6*|*Ifng*	1.77E-05
9607	response to biotic stimulus	*Il-6*| *Ifng* | *Stat1*| *Irf7*	2.72E-05
9605	response to external stimulus	*Cxcl10*| *Ifng* | *Stat1*| *Ccl5*	3.25E-05
9611	response to wounding	*Cxcl10*| *Cxcl9*| *Il-6*| *Ccl5*	3.50E-05
2682	regulation of immune system process	*Cxcl10*| *Il-6*| *Ifng* | *Ccl5*	3.50E-05

51704	multi-organism process	*Il-6*| *Ifng* | *Stat1*|*Irf7*	3.50E-05
45073	regulation of chemokine biosynthetic process	*Il-6*| *Ifng*	3.50E-05
8284	positive regulation of cell proliferation	*Cxcl10*| *Il-6*| *Ifng* | *Stat1*	3.50E-05
42832	defense response to protozoan	*Il-6*| *Ifng*	4.38E-05
48583	regulation of response to stimulus	*Cxcl10*| *Il-6*| *Ifng* | *Ccl5*	4.87E-05
42330	taxis	*Cxcl10*|*Ifng*|*Ccl5*	4.90E-05
6935	chemotaxis	*Cxcl10*|*Ifng*|*Ccl5*	4.90E-05
2262	myeloid cell homeostasis	*Il-6*|*Ifng*	5.57E-05
7610	behavior	*Cxcl10*| *Il-6*| *Ifng* | *Ccl5*	5.57E-05
1562	response to protozoan	*Il-6*|*Ifng*	6.27E-05
6950	response to stress	*Cxcl10*|*Cxcl9* |*Il-6*|*Ifng*|*Ccl5*	6.27E-05

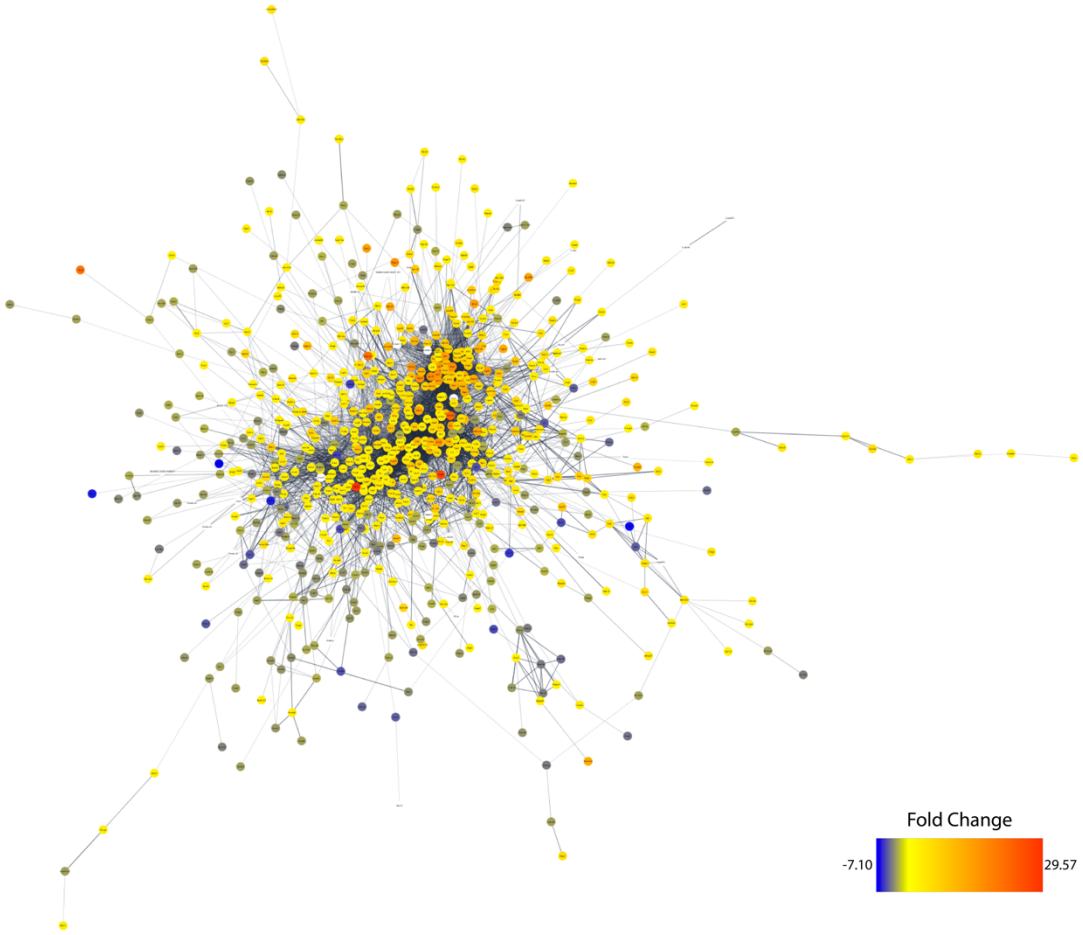

Figure 4.22: Major connected components of dysregulated genes for the comparison of non-irradiated vs sham injected muscles (irradiated 18Gy, sham injected 3 days later, collected 2 days post-injection). There are 728 nodes with 6465 interactions. The fold change in gene expression ranges from -7.10 to +29.57 compared to non-irradiated controls, nodes are colours in a colour gradient according to their fold change, with blue nodes representing downregulated genes and red nodes mark the highest fold change (x29.57).

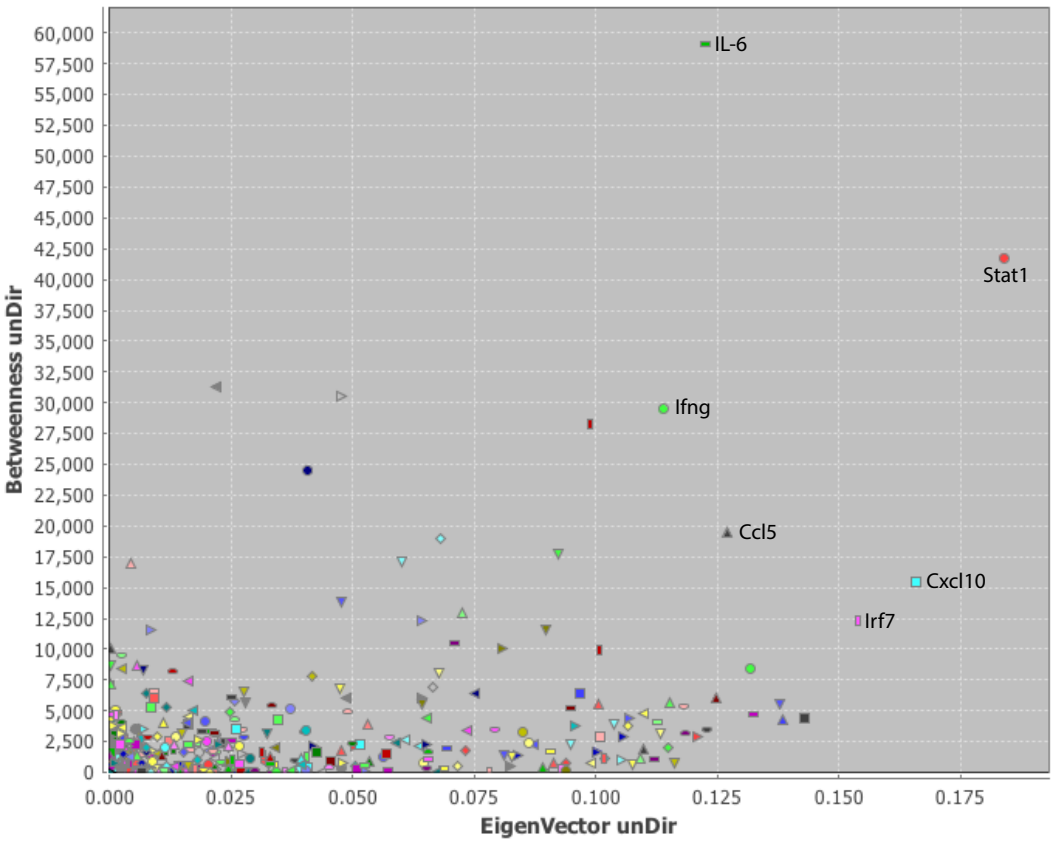

Figure 4.23: Eigenvector plotted against Betweeness Centrality for the network of controls compared to sham injected muscles (irradiated 18Gy, sham injected 3 days later, collected 2 days post-injection). *IL-6*, *Stat1*, *Ifng*, *Ccl5*, *Irf7*, and *Cxcl10* are seen to have a high Eigenvector and Betweeness centrality, showing that they have a central role in maintaining communication within the network and are highly influential.

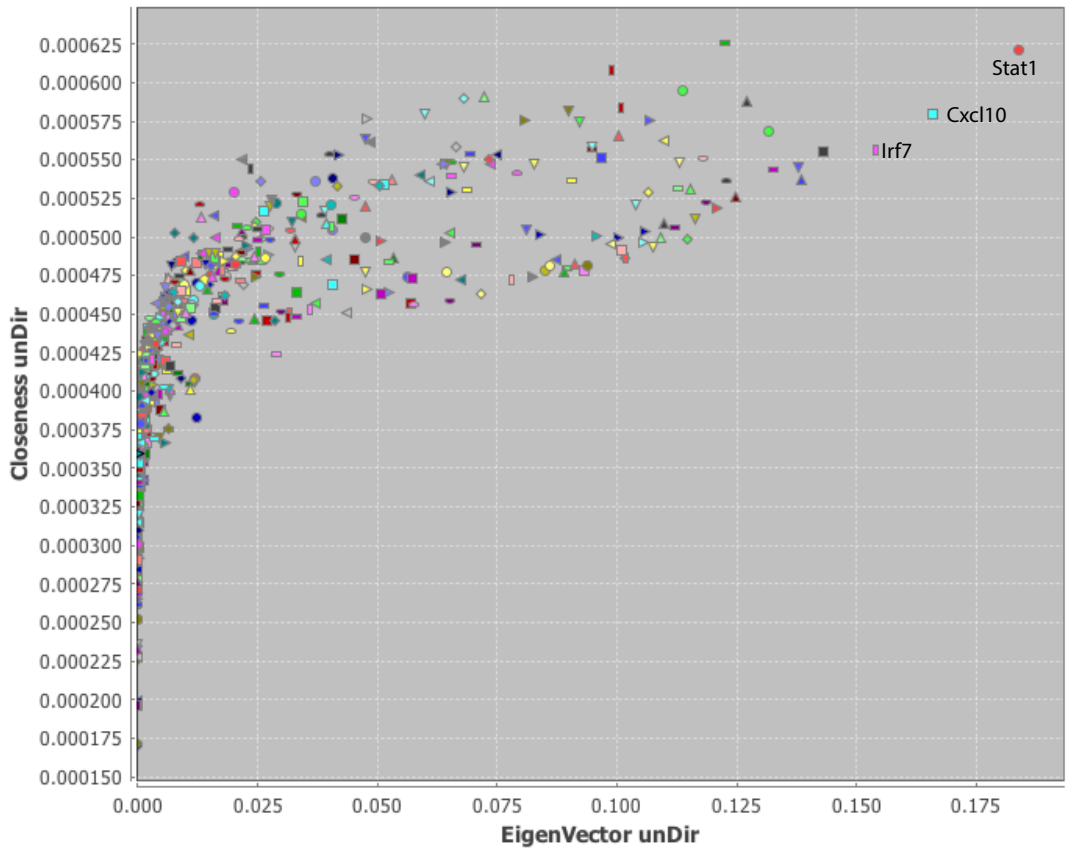

Figure 4.24: Eigenvector against Closeness centrality for the network created by the comparison of control vs irradiated 18Gy, sham injected 3 days later, collected 2 days post-injection. *Stat1*, *Cxcl10*, and *Irf7* are identified as being able to easily reach every other node in the network and they interact with many or some highly important nodes within the network. These 3 genes with very high values for both parameters can be identified as probably being central regulators of the network.

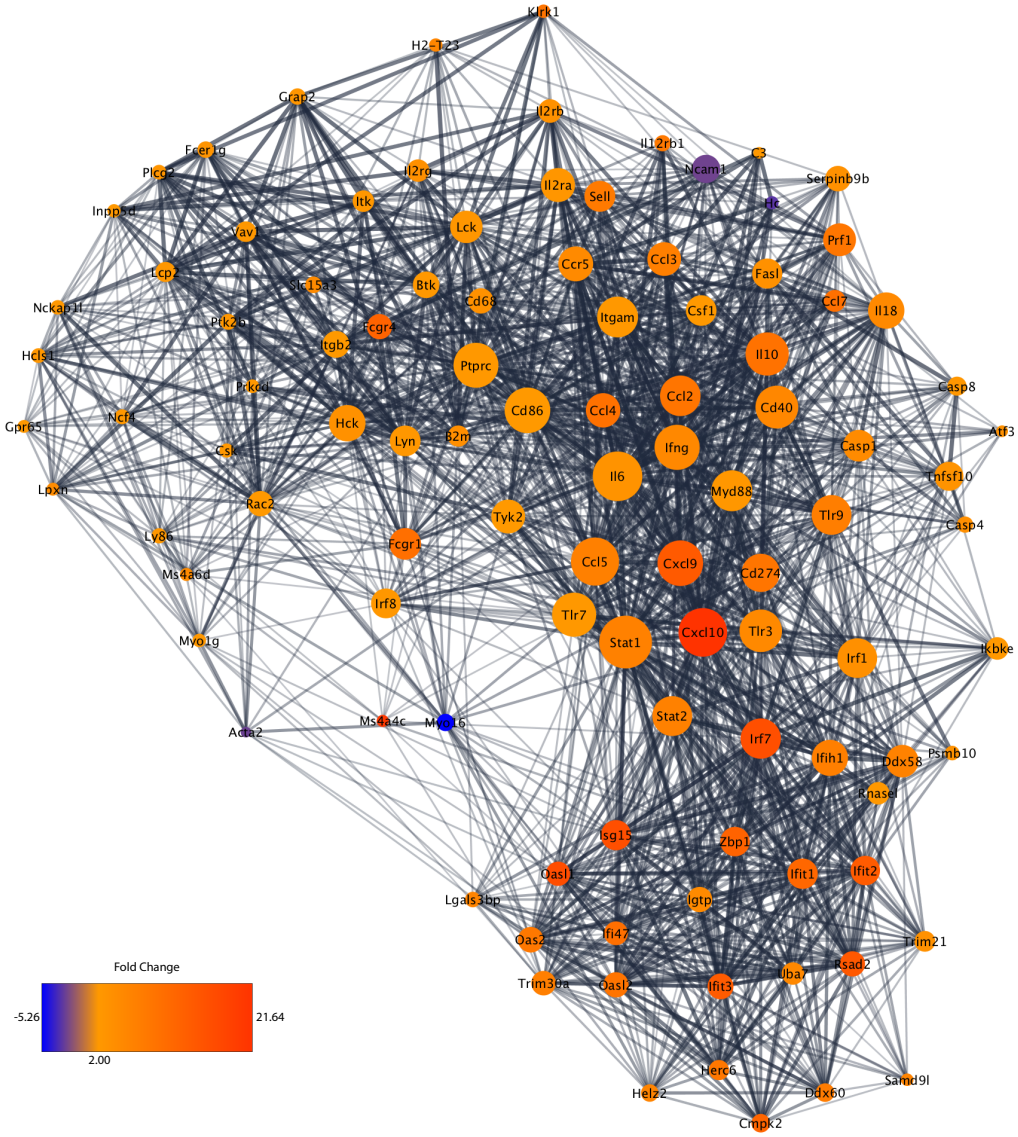

Figure 4.25: Top network regulators for the protein-protein interaction network comparing control (non-irradiated) with sham injected (irradiated 18Gy, sham injected 3 days later, collected 2 days post-injection) muscles. These are identified as having an above average value of Betweenness centrality, Closeness Centrality, Eigenvector, Stress, and Eccentricity. Node colour is mapped to fold change in expression and node size proportionally mapped to Eigenvector. The nodes with the highest Eigenvector within this network are clearly seen as *Stat1*, *Cxcl10* and *Irf7*. However, *Il-6* still possesses a high Eigenvector and the highest Betweenness and Closeness centrality, suggesting that this central to the network and key for maintaining network communication. On these two measures *Il-6* is closely followed by *Stat1*.

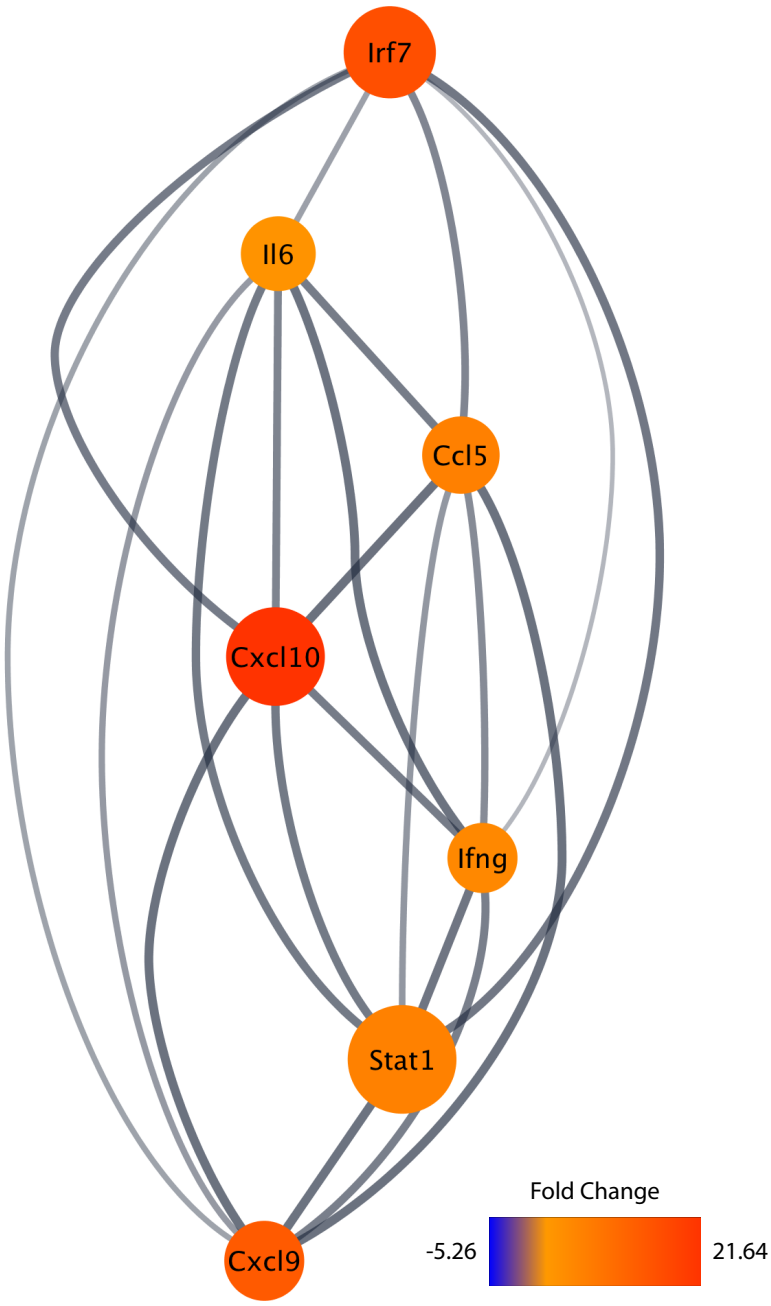

Figure 4.26: Top regulators for the network generated by control muscles compared to sham injected (irradiated 18Gy, sham injected 3 days later, collected 2 days post-injection) muscles made by selecting the nodes within the top 75th percentile for Closeness, Betweenness and Eigenvector centralities in the network shown in figure 4.23. Node colour has been mapped to fold change in expression and node size is directly proportional to their Eigenvector value.

4.6.2) GSEA Analysis

GSEA analysis was performed to identified over-represented pathways in the 1068 dysregulated genes. Control (non-irradiated samples) only had one significantly enriched pathway, represented by 15 genes present in our gene list. This was marked as “Hallmark Myogenesis” which is defined as genes involved in the development of skeletal muscle by the molecular signatures database (enrichment score: 0.59; normalised p: 0.009; FDR < 0.032). This showed higher levels of myogenesis in non-irradiated muscles compared to irradiated and sham injected muscles, which is consistent with either the destruction of proliferating cells (myoblasts) induced by irradiation, or the downregulation of terminal myogenic differentiation programs within the irradiated host muscle.

In contrast, sham injected muscles had 5 gene-sets upregulated with a FDR<25% and a p value below 5%, shown in table 4.12.

Table 4.12: Gene Sets Enriched in sham injected muscles compared to controls					
NAME	SIZE	ES	NES	NOM p-val	FDR q-val
HALLMARK INTERFERON GAMMA RESPONSE	79	-0.608	-3.335	0.000	0.000
HALLMARK ALLOGRAFT REJECTION	51	-0.534	-2.710	0.000	0.000
HALLMARK INTERFERON ALPHA RESPONSE	52	-0.525	-2.682	0.000	0.000
HALLMARK TNFA SIGNALING VIA NFKB	27	-0.502	-2.088	0.000	0.001
HALLMARK INFLAMMATORY RESPONSE	46	-0.434	-2.066	0.000	0.001

As predicted by network analysis, the pattern of gene expression shows an inflammatory response (figure 4.27), together with an interferon gamma (figure 4.28) and alpha response (figure 4.29). Furthermore, these 3 gene-sets have a significant overlap. All three gene-sets share 10 genes between them, while the interferon gamma and interferon alpha responses share 32 genes. Additionally, only sham injected muscles were analysed, so the appearance of an allograft rejection signature (figure 4.30) further suggests an inflammatory phenotype and the activation of the immune system as a consequence of irradiation. Finally, the tumour

necrosis factor alpha signalling via NFKB gene-set upregulation (figure 4.31) suggests the modulation of inflammation and muscle regeneration in sham injected muscles. Taken together, all these enriched gene-sets point towards a change in the inflammatory phenotype of the muscles.

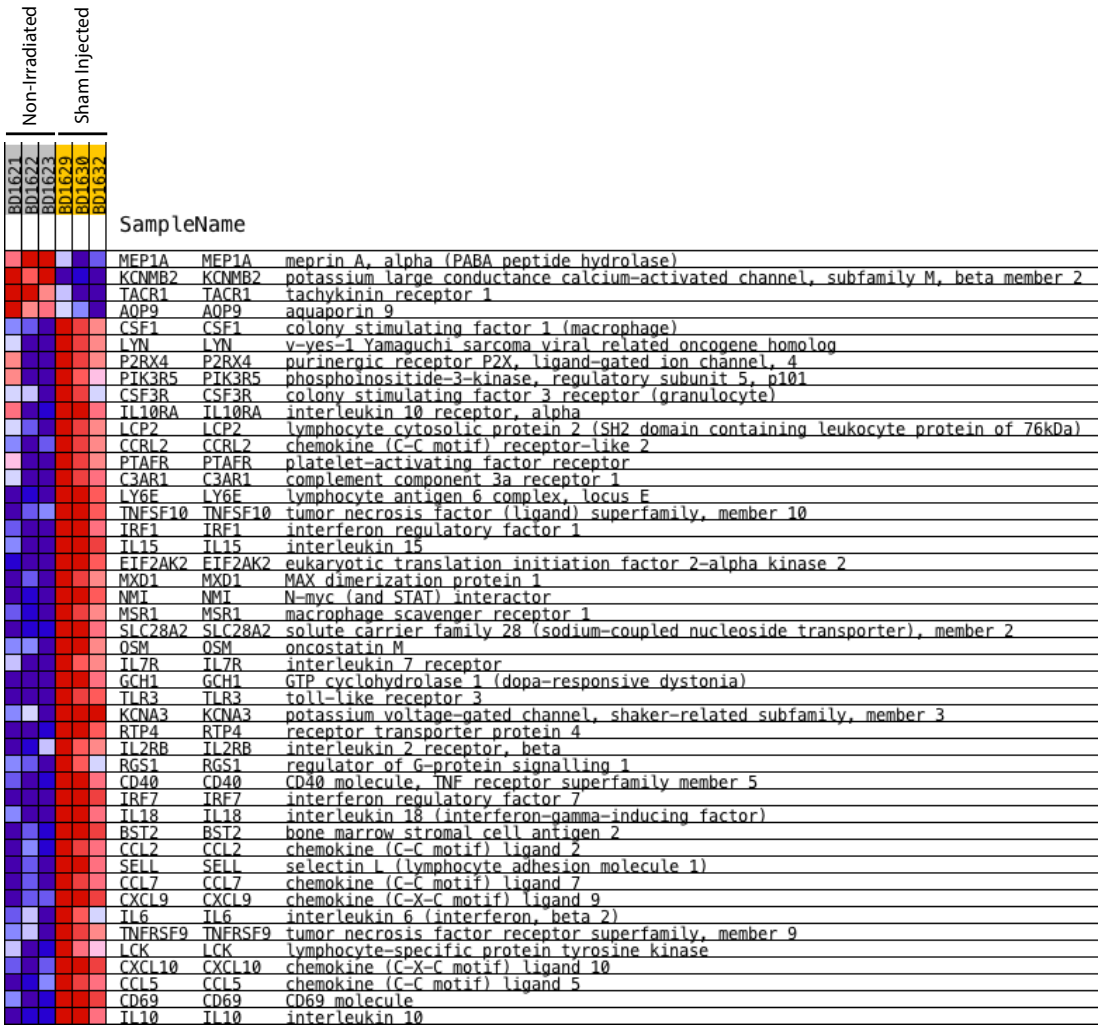

Figure 4.27: Inflammatory response gene-set enriched (FDR: 0.007; nominal p value <0.001) in sham injected (irradiated 18Gy, sham injected 3 days later, collected 2 days post-injection) muscles compared to non-irradiated controls.

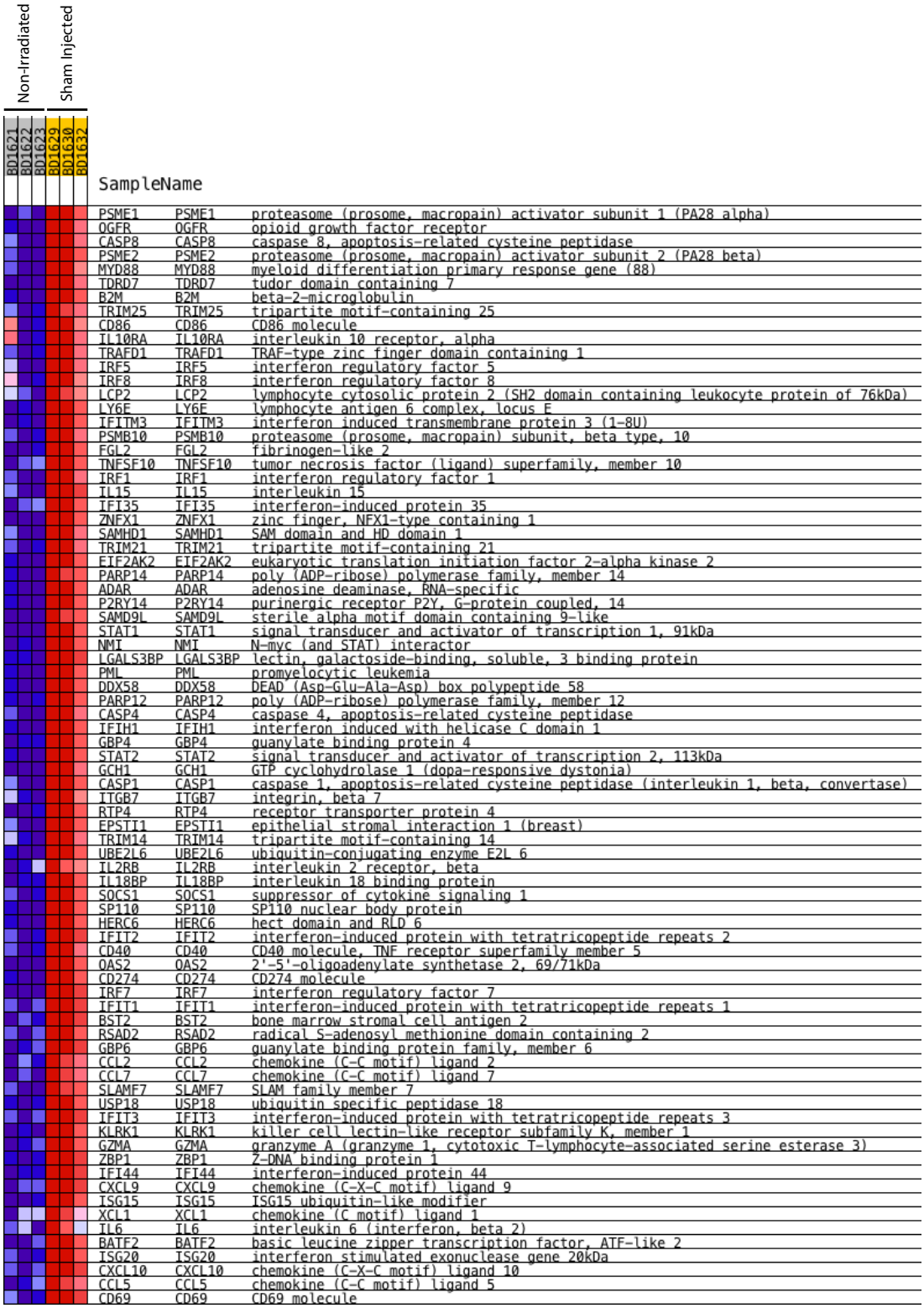

Figure 4.28: Genes marking an enrichment of an interferon gamma response in sham injected (irradiated 18Gy, sham injected 3 days later, collected 2 days post-injection) muscles compared to non-irradiated controls (FDR<0.000; p<0.000).

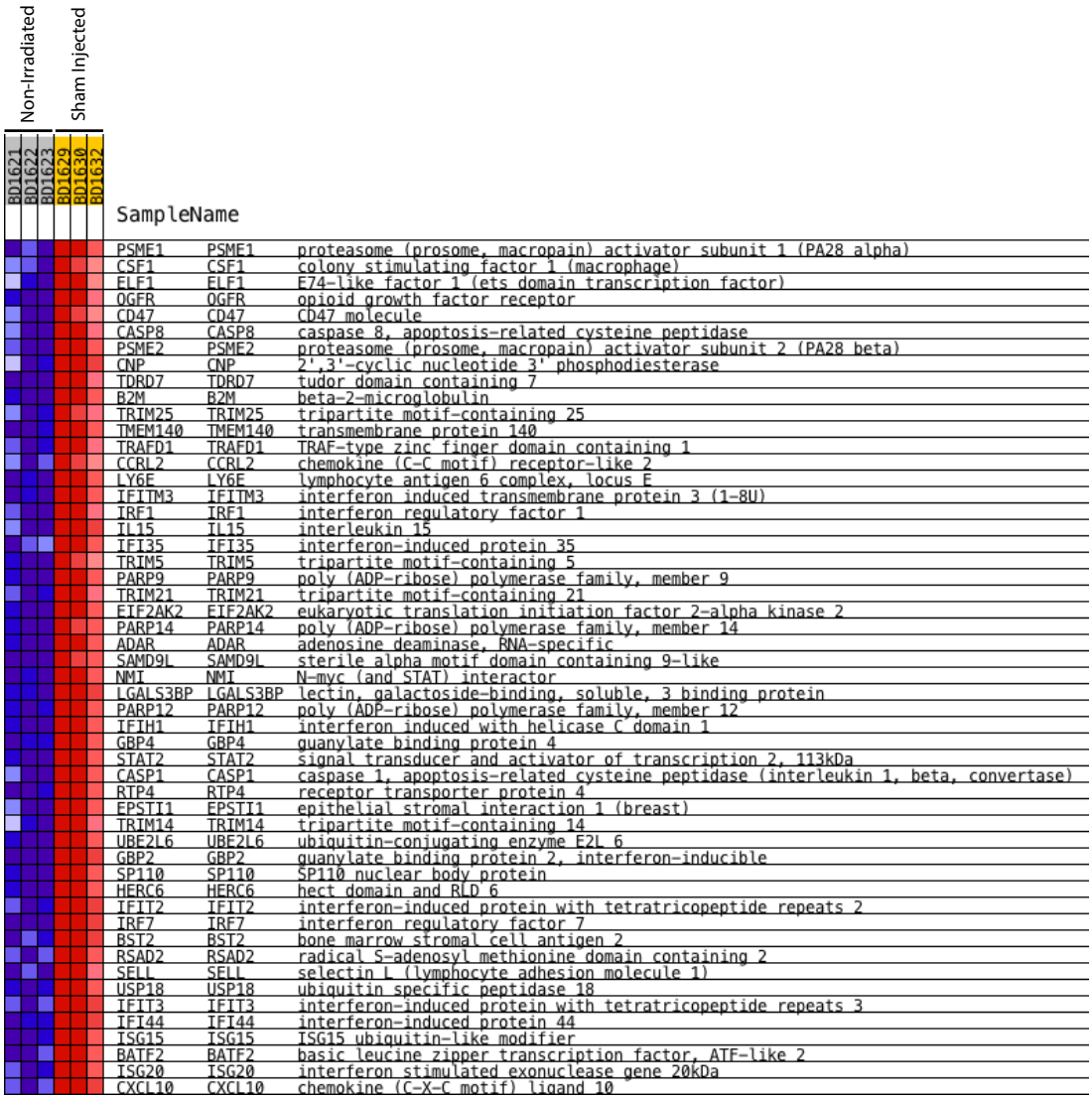

Figure 4.29: Genes upregulated in sham injected (irradiated 18Gy, sham injected 3 days later, collected 2 days post-injection) muscles compared to non-irradiated samples matching the gene-set corresponding to an interferon alpha response (FDR<0.000; p: 0.004).

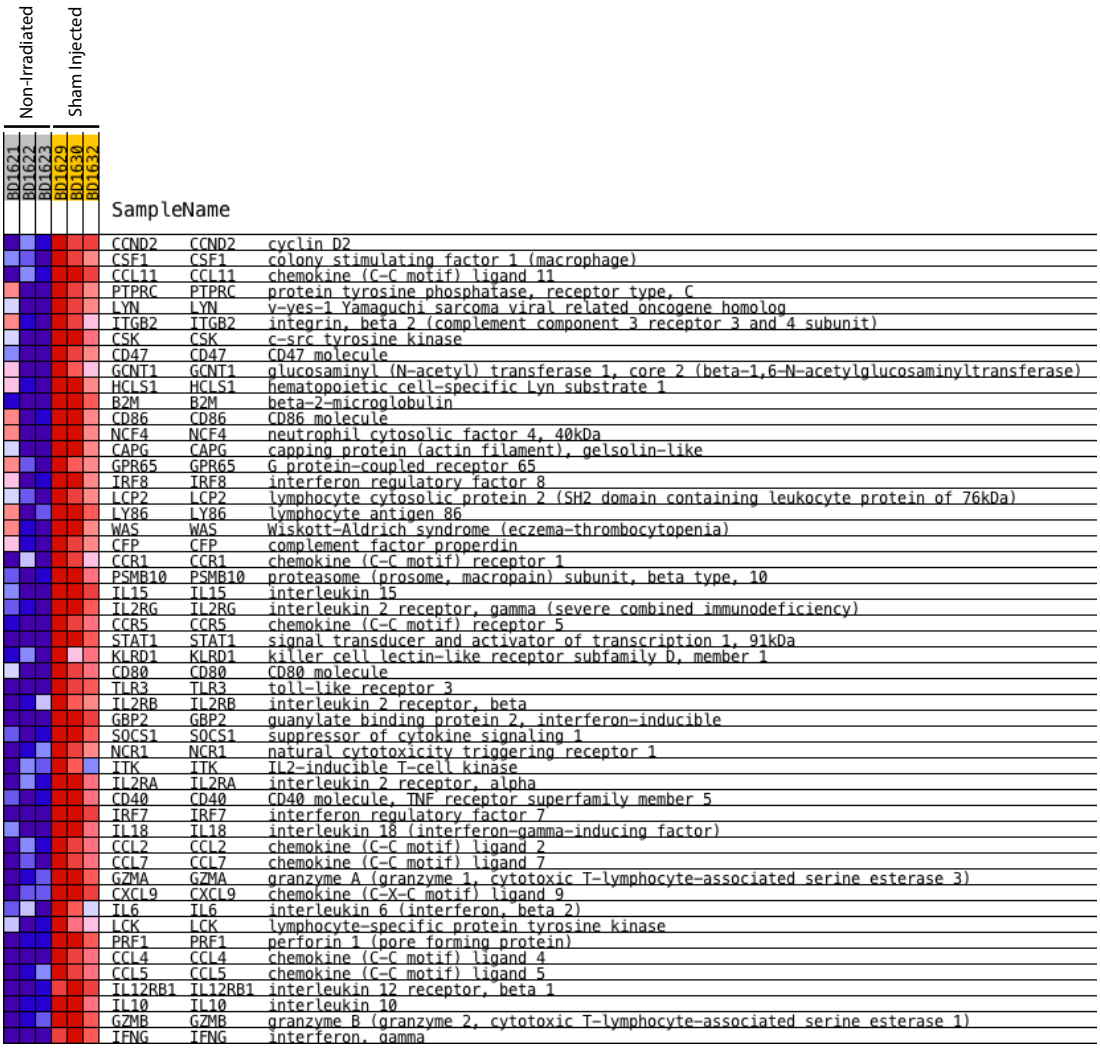

Figure 4.30: Genes indicating an up-regulated allograft rejection signature in sham injected (irradiated 18Gy, sham injected 3 days later, collected 2 days post-injection) muscles compared to controls (FDR: 0.035; nominal p-value: 0.001).

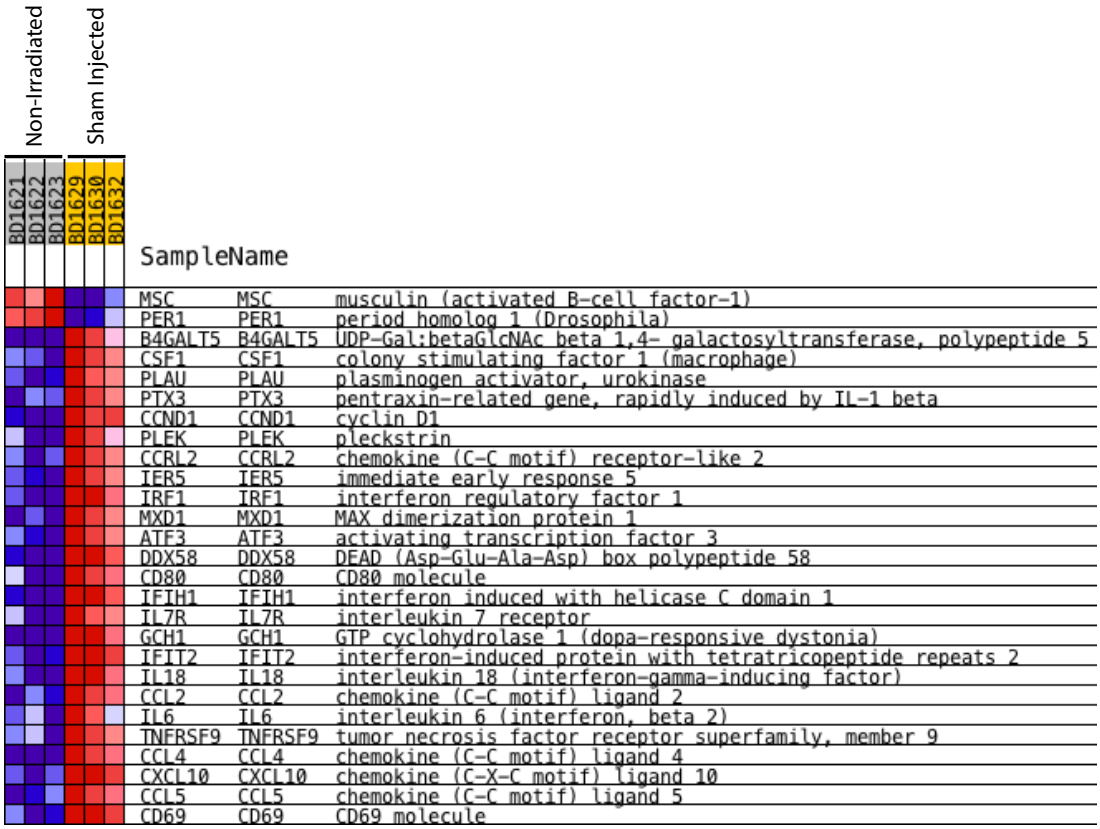

Figure 4.31: Enriched TNF alpha signalling via NFKB in sham injected (irradiated 18Gy, sham injected 3 days later, collected 2 days post-injection) muscles compared to controls (FDR: 0.055; nominal p-value: 0.008).

4.7) Control Vs Grafted

4.7.1) Network Analysis

To investigate how irradiation and grafting affect the host muscle, grafted samples were compared to control (non-irradiated) muscles. RNA-sequencing returned 1223 genes that were significantly dysregulated in grafted muscles compared to non-irradiated controls. From these, the STRING database returns 1027 recognised genes with 6280 interactions (figure 4.32). A major network of 836 connected components was created. One group of 3 interacting genes had no connection to the rest of the network, there were also 5 groups of 2 interacting genes isolated from the remainder of the network, and the remaining genes had no interactions with any of the other genes in the network. The largest group (836 nodes) was extracted on to a new network and used for analysis. Stress, Eccentricity, Eigenvector, Closeness, and Betweenness centralities were calculated. The minimum, average, and maximum values for each centrality measure are shown in table 4.13.

Table 4.13: Centrality Values for Control Vs Grafted Network

Centrality	Min	Avg	Max
Eccentricity	1.00E-01	1.44E-01	1.67E-01
Closeness	1.78E-04	3.68E-04	5.48E-04
Betweenness	0.00E+00	1.96E+03	5.98E+04
Stress	0.00E+00	2.66E+04	6.85E+05
Eigenvector	7.76E-09	1.69E-02	1.86E-01

Comparing Betweenness Centrality to the Eigenvector*, Il-6* stands out as a major regulator of this network, with a very high Betweenness centrality and the highest Eigenvector centrality. The next set of proteins with high scores for both fall s behind *Il-6* in terms of their relevance to maintaining network communication and are identified *as Tlr4* (toll-like receptor 4, indicating a role of the innate immune system), *Il-10* (an anti-inflammatory cytokine) and *Stat1. ActB* and *Lrkk2* also have a high Betweenness centrality but a low Eigenvector value and therefore likely to be essential for maintaining communication between a large number of nodes. A scatter-plot is shown in figure 4.33. Comparing Eigenvector to Closeness Centrality, *Il-6* is again the most central node in the network, together with *Tlr4*, *Il-10*, *Stat1*, and *Cxcl10* as shown in figure 4.34.

Isolating the nodes with above network average values for Closeness centrality, Betweenness, Eigenvector, Stress, and Eccentricity yields a network of 116 genes with 1799 interactions (figure 4.35), containing amongst them several interleukins, interferon regulatory factors and interferon inducible proteins with tetratricopeptide repeats, suggesting an inflammatory response and the activation of interferon signalling.

To further isolate the most relevant nodes, those within the 75^{th} percentile for Eigenvector (>0.103), Closeness ($>4.74 \times 10^{-4}$), and Betweenness (> 8749) were selected and exported onto a new regulatory network. From the core of 116 genes, 11 genes (with 52 interactions) matched these parameters and are shown in figure 4.36. Here interleukins 6 and 10 are represented. CCL2 and CCL5 have strong chemoattractant activities for monocytes, T-cells and dendritic cells. CXCL10 is another chemoattractant and is induced by interferon gamma, suggesting a role for

this signalling pathway in the gene regulatory network. Taken together, this suggests that this network is still mainly regulated by an inflammatory response.

Performing GO analysis on the top network regulators yields 168 enriched GO terms (appendix 4.1). Among them there is the term "positive regulation of cell proliferation" that includes *Cxcl10, Il-6*, *Ptprc, Stat1, Ccl2, and Tlr4* suggesting that an inflammatory response mediated by Toll-like receptors may be driving satellite cell expansion. To further investigate if this GO term is enriched in the full network, GO analysis was performed on the 836 connected components, and those genes associated with the positive regulation of cell proliferation were extracted. This returned 45 genes within the network, 40 of which were interconnected and are displayed on figure 4.36. Here notable myokines are seen to be upregulated, including leukaemia inhibitory factor and *Il-6*. Other interleukins are also present such as IL-15. Cyclins (*Ccnb1*) and oncogene *Lyn* (Thaper et al. 2017) are also present, which are linked to nodes associated with the innate immune response such as Toll-Like receptor 4 *(Tlr4)* and its adaptor Myeloid Differentiation Primary Response 88 *(Myd88).* Six (*Il-6. Stat1, Cxcl10, Tlr4, Ptprc,* and *Ccl2*) of the 11 top network regulators are also present in this network, suggesting that these are playing a crucial role in regulating the creation of a permissive nice for the engraftment of donor satellite cells within host skeletal muscle.

Additionally, multiple terms are enriched related to the regulation of the immune system, for example the terms "Immune system process" (p: 1.41×10^{-13}); "Defense response" (p: 4.23×10^{-13}); and "positive regulation of inflammatory response" (p: 1.40×10^{-4}) are all included. These suggest an inflammatory phenotype

that may be leading to the secretion of the appropriate cytokines that create a favourable environment for satellite cell proliferation within the host muscle.

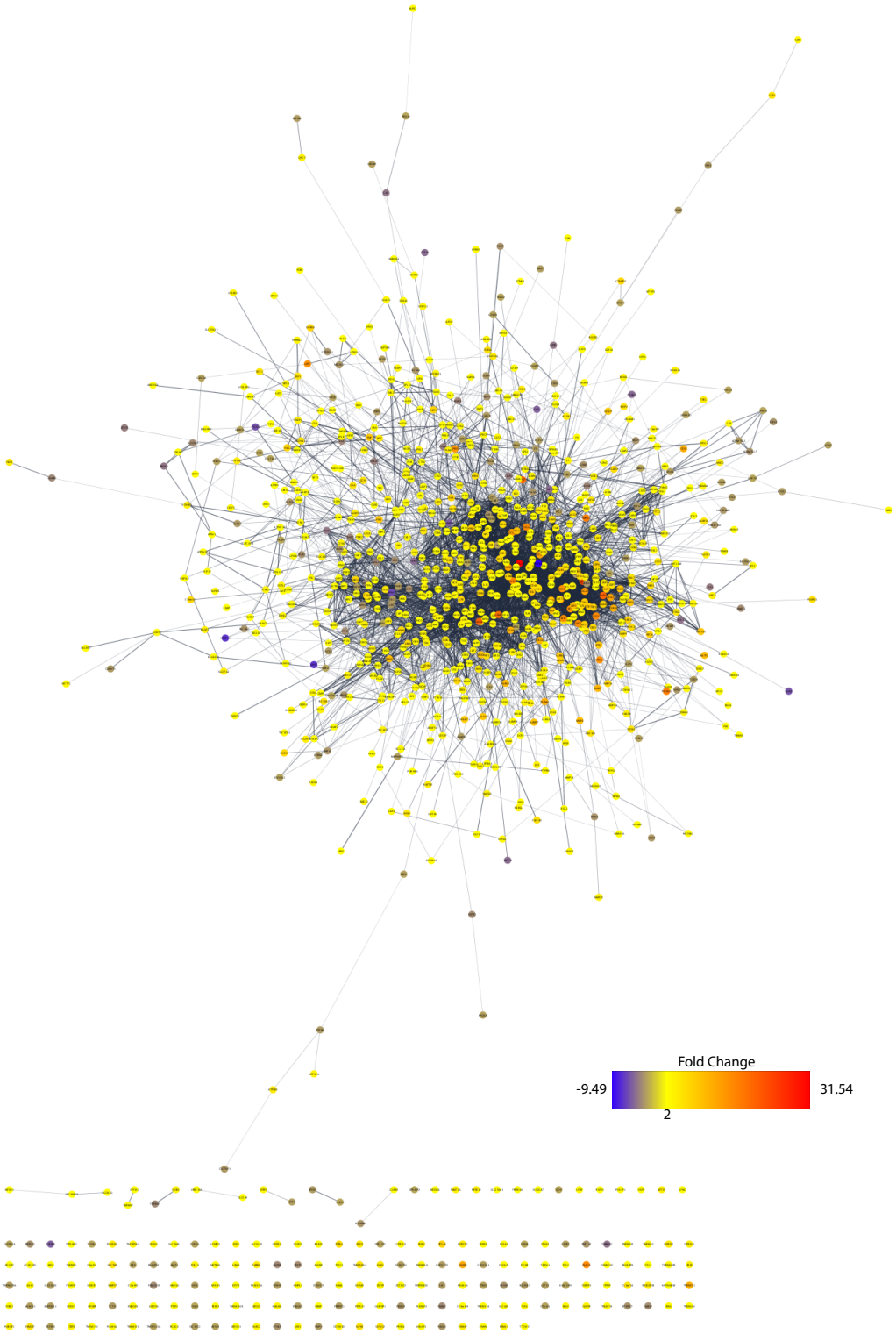

Figure 4.32: Full network created by the STRING database using differentially expressed genes between controls and grafted (18Gy irradiated, grafted with satellite cells 3 days post-IR, collected 2 days post graft) muscles with 1027 nodes and 6280 interactions.

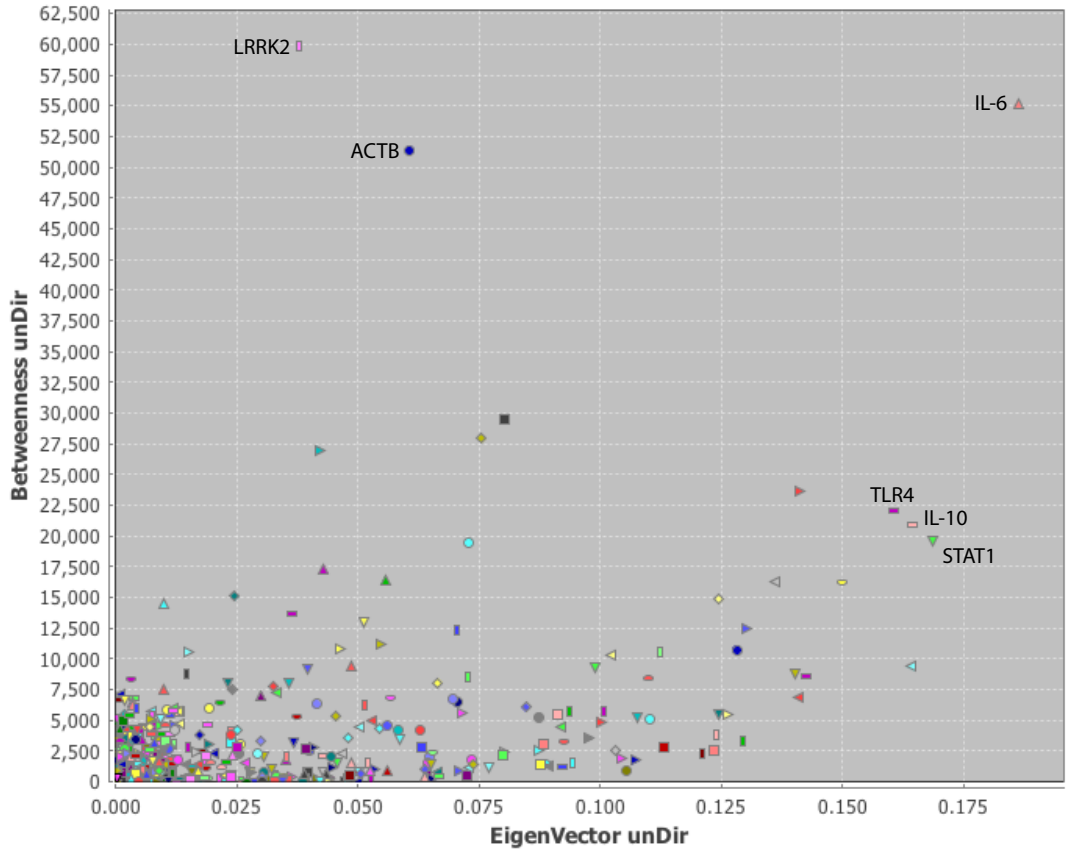

Figure 4.33: Eigenvector plotted against Betweenness Centrality for the major connected components in the control vs grafted (18Gy irradiated, grafted with satellite cells 3 days post-irradiation, collected 2 days post-satellite cell injection) network. *Il-6* stands out as a major network regulator which is both highly influential and close to most other nodes in the network.

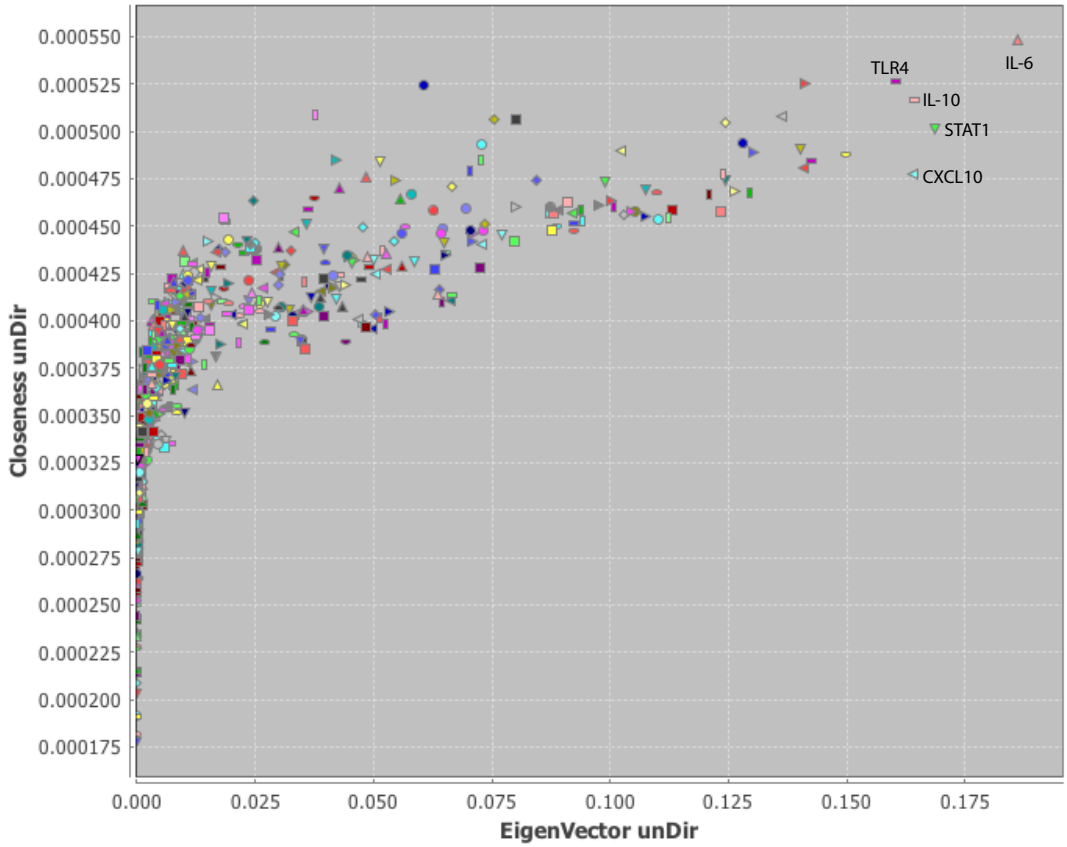

Figure 4.34: Scatterplot of Eigenvector plotted against Closeness Centrality for the major connected components in the control vs grafted (18Gy irradiated, grafted with satellite cells 3 days post-irradiation, collected 2 days post-satellite cell injection) network. *Il-6* stands out as a highly influential network regulator with the ability to reach most other nodes in the network. Other major regulators include *Tlr4, Il-10, Stat1,* and *Cxcl10.*

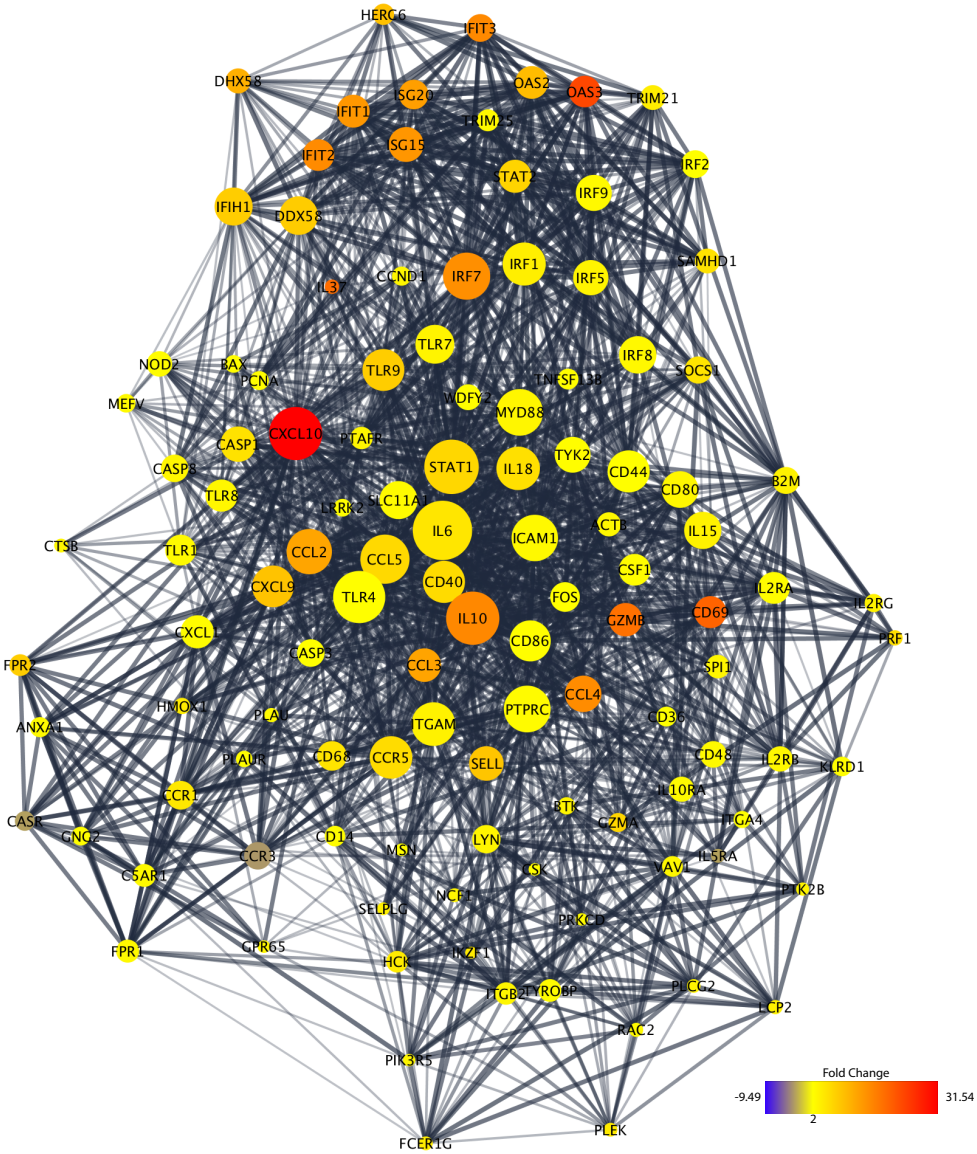

Figure 4.35: Nodes with above average values for all centrality measures in the network created by comparing control vs grafted (18Gy irradiated, grafted with satellite cells 3 days post-irradiation, collected 2 days post-satellite cell injection) muscles. This produces a regulatory network with 116 nodes and 1799 interactions. Node colour is mapped as a colour gradient according to fold change, and node size is directly proportional to the Eigenvector value.

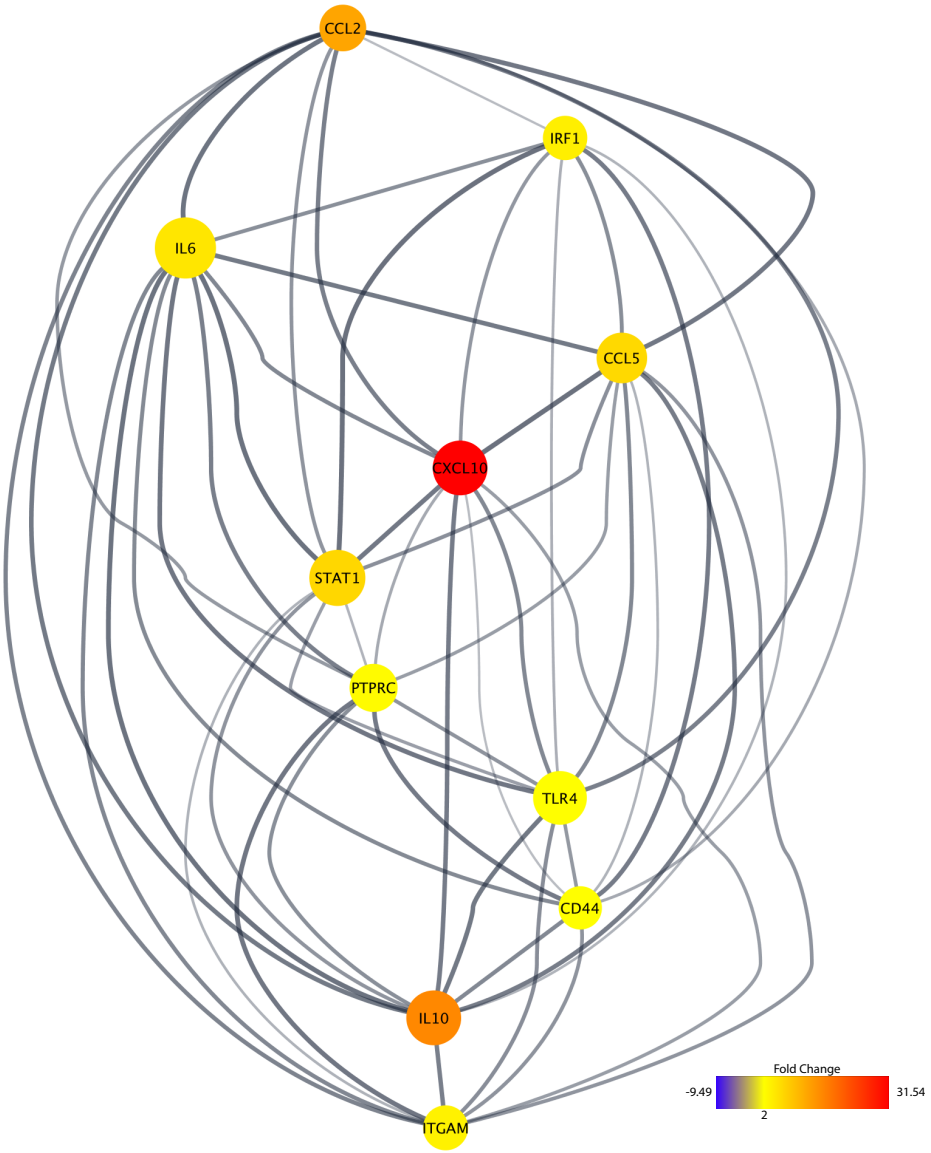

Figure 4.36: 11 genes with values for Eigenvector, Closeness, and Betweenness centrality within the 75th percentile in the network created from control vs grafted (18Gy irradiated, grafted with satellite cells 3 days post-irradiation, collected 2 days post-satellite cell injection) muscles. Node colour is matched to fold change and node size to Eigenvector.

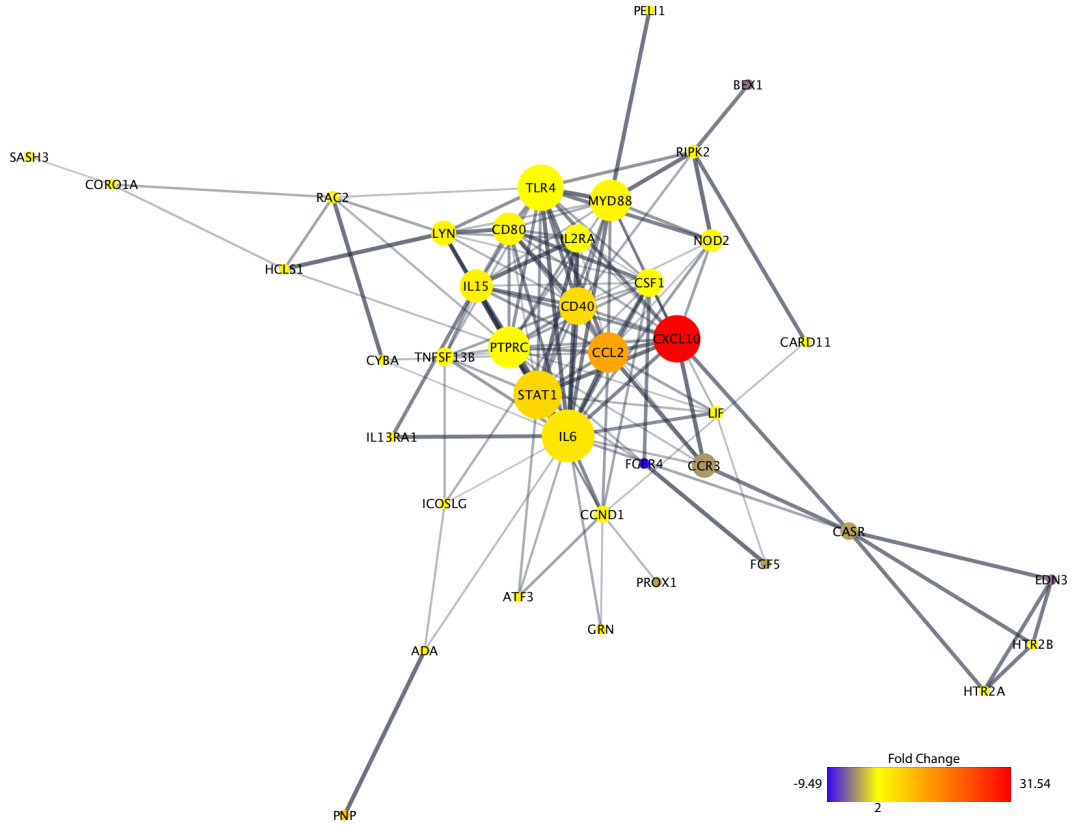

Figure 4.37: 40 interconnected genes represented in the GO-term "positive regulation of cell proliferation" in the comparison control vs grafted (18Gy irradiated, grafted with satellite cells 3 days post-irradiation, collected 2 days post-satellite cell injection). Six of the main network regulators are present in this sub-network. Additionally, it includes members of the innate immune system such as *Tlr4* and *Myd88*. Node size is directly proportional to Eigenvector and node colour is mapped to fold change.

4.7.2) GSEA Analysis

GSEA analysis was performed to identify over-represented signalling pathways within control and grafted muscles. Control non-irradiated muscles only had 1 significantly enriched gene-set (myogenesis; $p<0.001$; FDR < 25%) and the heatmap is shown in figure 4.38. Gene-sets enriched in grafted muscles are displayed in table 4.14.

Table 4.14: Gene-sets enriched in Grafted muscles

NAME	SIZE	ES	NES	NOM p-val	FDR q-val
HALLMARK INTERFERON GAMMA RESPONSE	86.000	-0.506	-2.416	0.000	0.000
HALLMARK INFLAMMATORY RESPONSE	60.000	-0.440	-1.995	0.000	0.007
HALLMARK INTERFERON ALPHA RESPONSE	55.000	-0.450	-1.992	0.000	0.004
HALLMARK ALLOGRAFT REJECTION	58.000	-0.392	-1.746	0.001	0.035
HALLMARK TNFA SIGNALING VIA NFKB	43.000	-0.400	-1.662	0.008	0.055

The enriched pathways are the same as those seen in sham injected muscles (section 4.6), indicating a shift in the inflammatory phenotype in skeletal muscle after irradiation. The largest gene-set is that of the signature corresponding to an

interferon gamma response (figure 4.39), followed by an inflammatory response (figure 4.40), interferon alpha (figure 4.41), allograft rejection (figure 4.42) and lastly TNFα via NFκβ (figure 4.43). The activation of type I interferons (interferon alpha response) suggests a role for the innate immune system, while TNFα and IFNγ are well stablished pathways involved in inflammation in the tumour microenvironment (Landskron et al. 2014). This shift in the inflammatory response may be responsible for the release of cytokines that may be enabling the engraftment and proliferation of satellite cells, for example by the release *of Il-6 or Lif* which are present in the gene sets of interferon gamma signalling, allograft rejection, and TNFα signalling via NFκβ.

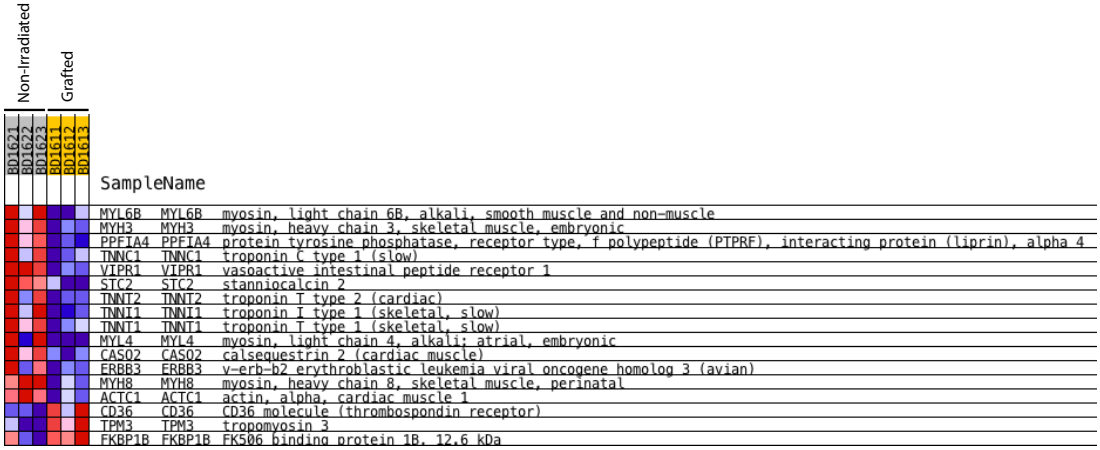

Figure 4.38: Genes matching the "myogenesis" gene-set are significantly enriched in control muscles compared to grafted (18Gy irradiated, grafted with satellite cells 3 days post-irradiation, collected 2 days post-satellite cell injection) ones (nominal p-value <0.001; FDR<0.001).

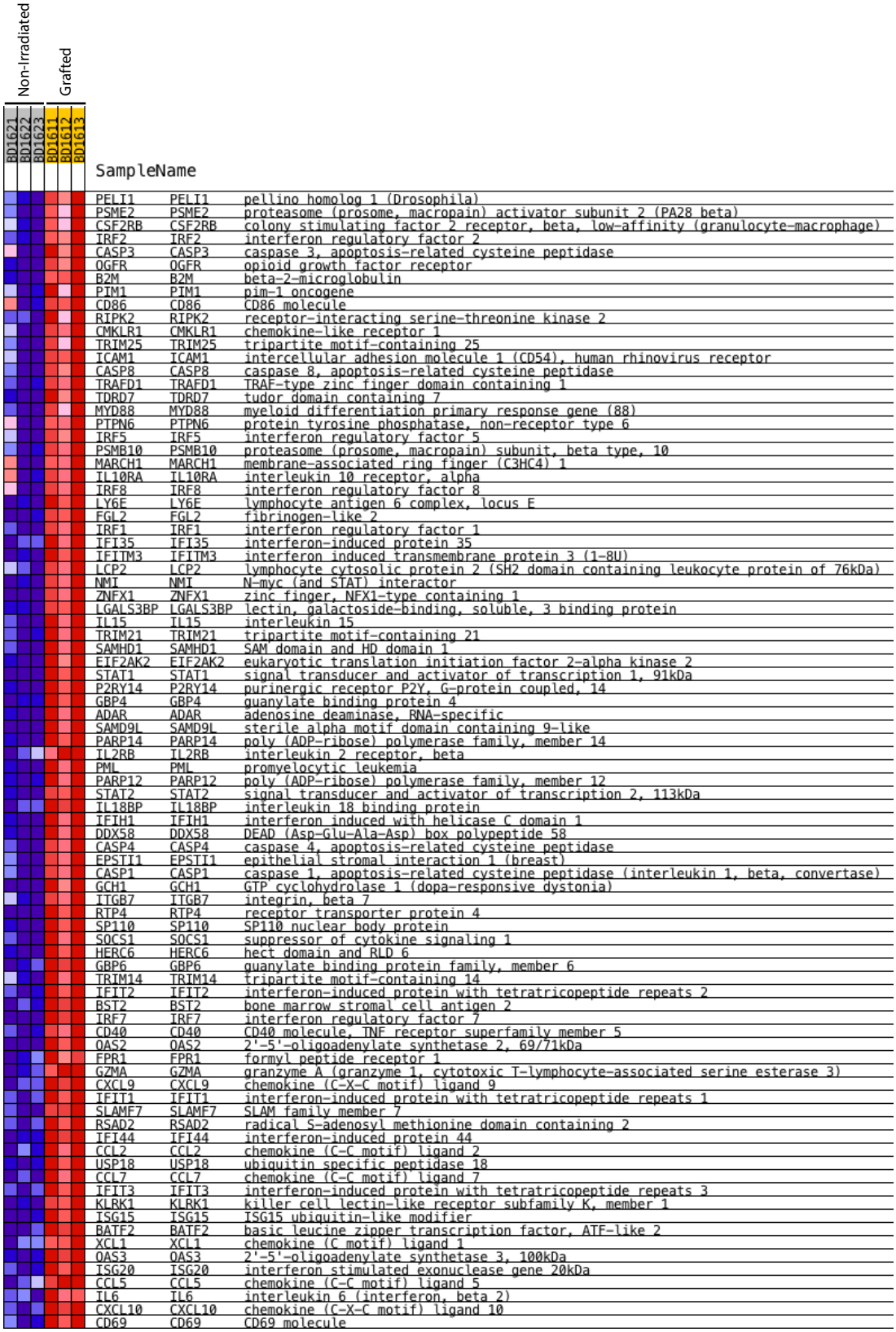

Figure 4.39: Genes matching the "interferon gamma response" gene-set in the molecular signatures data base are significantly enriched in grafted samples compared to non-irradiated controls (nominal p-value<0.001; FDR<0.001).

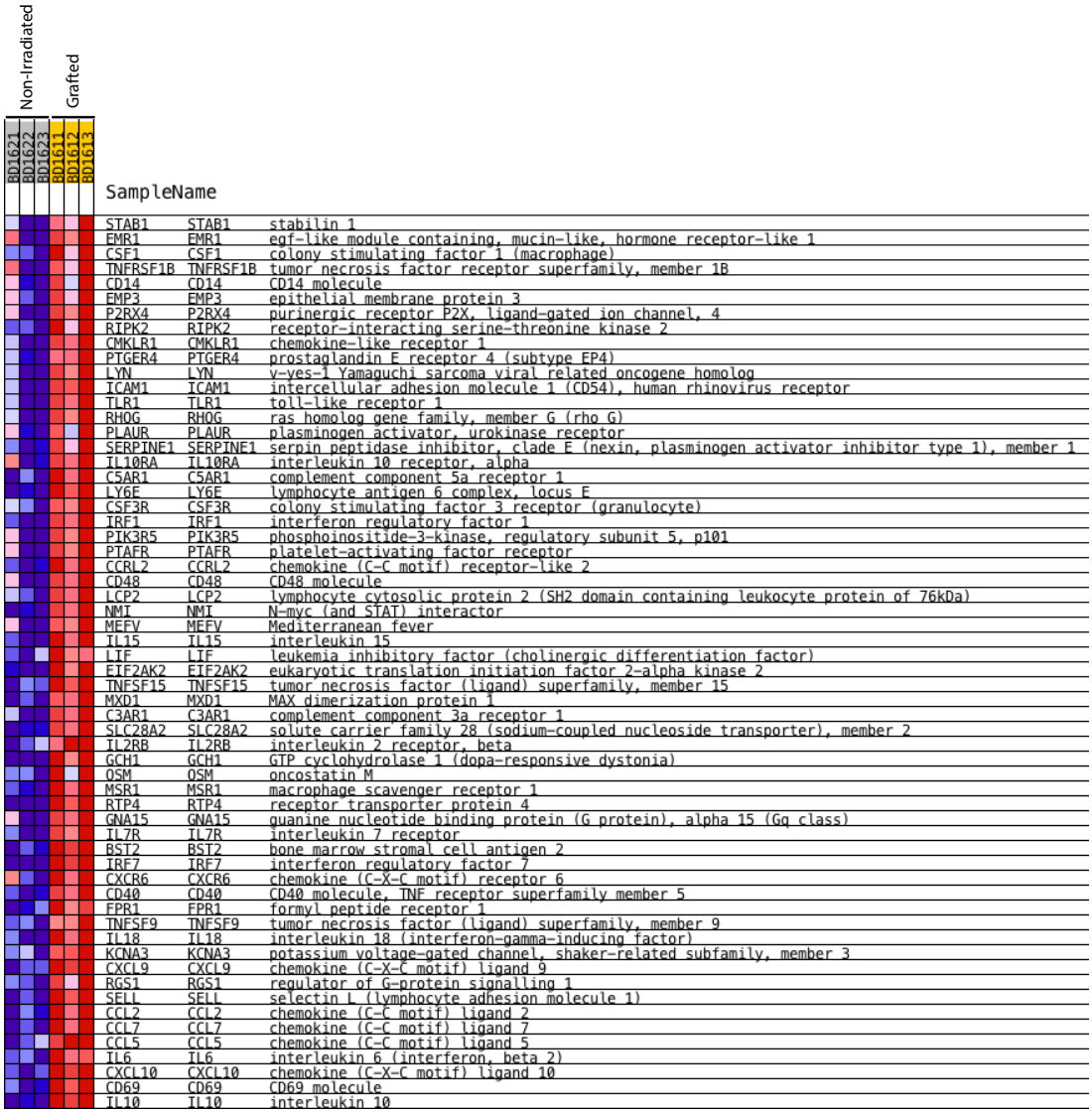

Figure 4.40: Genes matching the "inflammatory response" gene-set in the molecular signatures database are significantly enriched in grafted (18Gy irradiated, grafted with satellite cells 3 days post-irradiation, collected 2 days post-satellite cell injection) muscles compared to controls (nominal p-value <0.001; FDR<0.001).

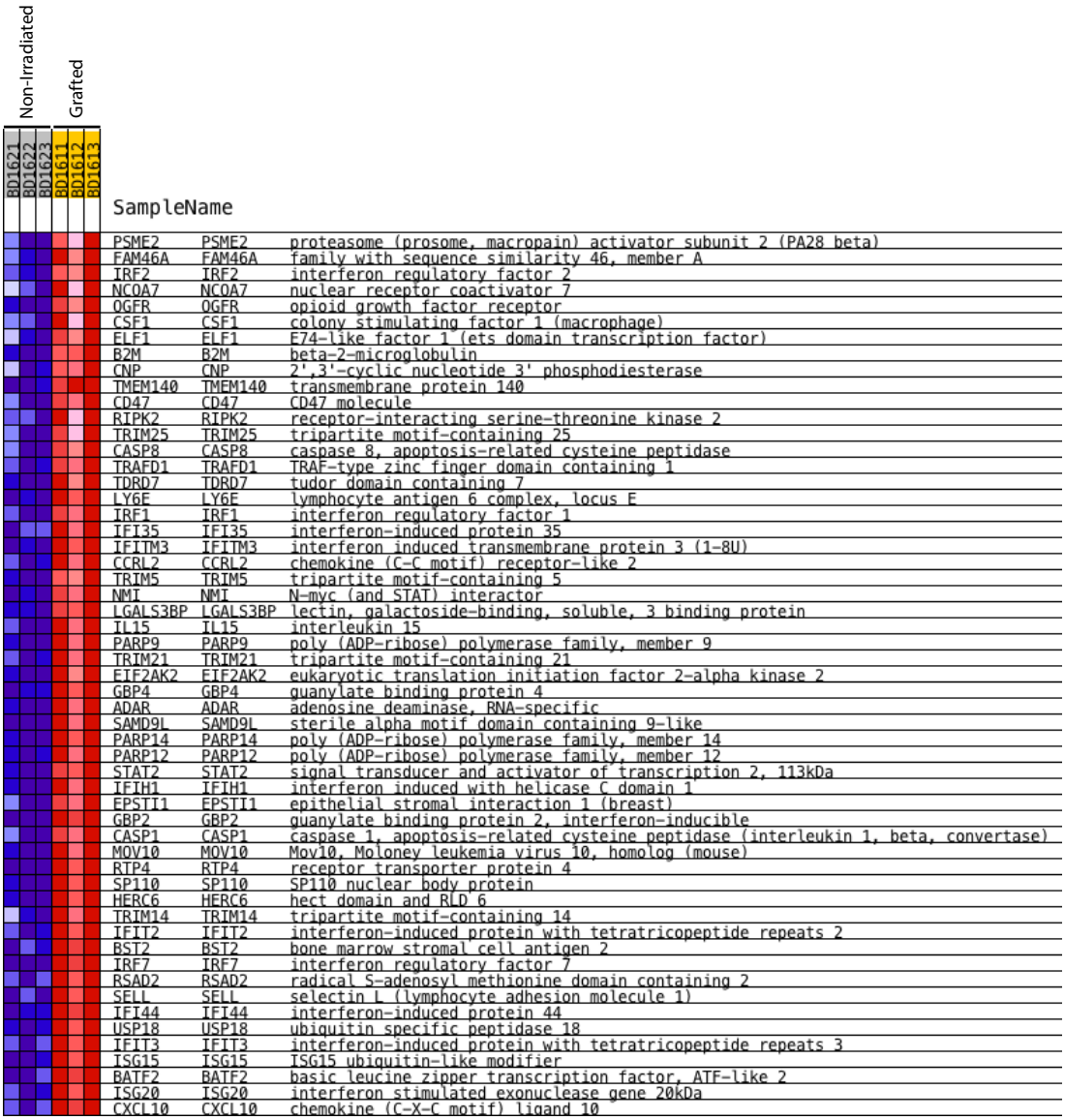

Figure 4.41: Genes matching a response to interferon alpha in the molecular signatures database are significantly enriched in grafted (18Gy irradiated, grafted with satellite cells 3 days post-irradiation, collected 2 days post-satellite cell injection) muscles compared to control muscles (nominal p-value <0.001; FDR: 0.004).

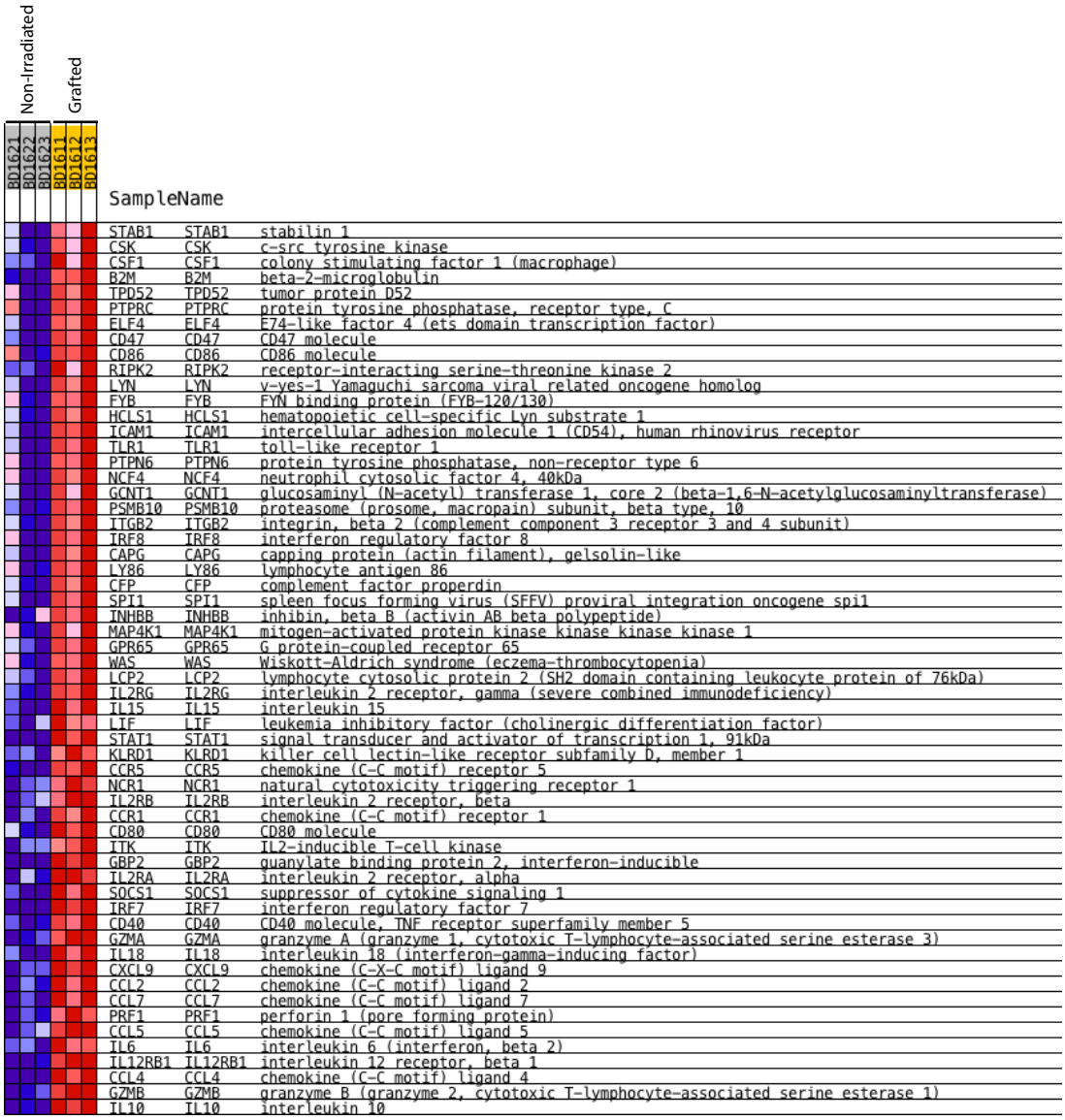

Figure 4.42: Genes significantly upregulated in grafted (18Gy irradiated, grafted with satellite cells 3 days post-irradiation, collected 2 days post-satellite cell injection) muscles compared to controls matching the gene-set for “Allograft Rejection” in the molecular signatures database (nominal p-value: 0.001; FDR: 0.0035).

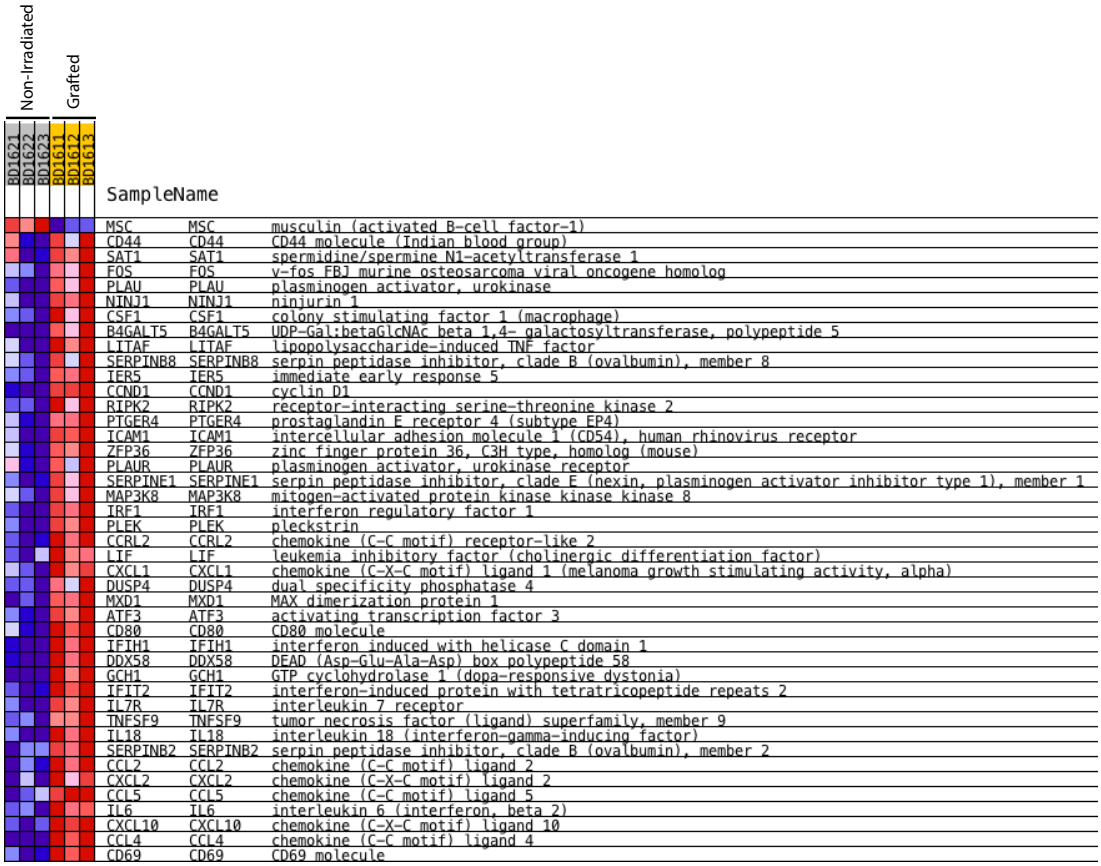

Figure 4.43: Genes enriched in grafted (18Gy irradiated, grafted with satellite cells 3 days post-irradiation, collected 2 days post-satellite cell injection) muscles compared to controls matching the gene-set for “TNFA Signalling via NFKB” from the molecular signatures database (nominal p-value: 0.008; FDR: 0.055).

4.8) Discussion

A consistent feature of these results is the constant appearance of patterns of gene expression which are linked to an innate immune response, both in the top network regulators and GSEA analysis, displaying genes matching gene-sets associated with allograft rejection signalling, activation patterns consistent with interferon signalling (alpha and gamma), and the complement response. This is seen in irradiated muscles compared to controls muscles, from mdx nude mice which were not subject to surgical interventions and would therefore not be facing any xenobiotic stimuli within their skeletal muscle as a result of surgery. Their maintenance within SPF conditions (necessary for immunodeficient mice) also minimises the possibility of viral infection. Furthermore, it has previously been noted that no immune infiltrate is seen within skeletal muscle after irradiation (C. N. Pagel & Partridge 1999) suggesting that this is a tissue specific response. This suggests a strong interplay between radiation damage and the immune system, which is crucial in regulating muscle regeneration after injury (Tidball 2017).

In the core regulatory network of muscles collected 3 days after 18Gy irradiation compared to controls, the toll-like receptor 3 *(Tlr3)* is up-regulated, and plays a central role in the gene regulatory network (figure 4.8*). TLR3* is a cell surface receptor traditionally associated with the detection of viral dsRNA (Alexopoulou et al. 2001). However, it has also been involved in the defence against infection of murine cytomegalovirus, a dsDNA virus, (Tabeta et al. 2004), as well as the parasites *Leishmania donovani* (Flandin et al. 2006) and *Schistosoma mansoni* (Aksoy et al. 2005) suggesting that TLR3 may be able to recognise other structures aside from

dsRNA, such as damage-associated molecular patterns (DAMPS) released by radiation damaged cells.

Mouse skeletal muscle (Boyd et al. 2006; Lang et al. 2003)and the C2C12 cell line (Frost et al. 2006) have been shown to express toll-like receptors, which have been shown to play an essential role in the regulation of muscle growth and repair. For example, TLR3 has been shown to be required for skeletal muscle regeneration after cardiotoxin injury (Mathes & Lafyatis 2011). In *Tlr3* deficient mice, the levels expression of pro-inflammatory cytokines *Il-6*, *Il-1ß*, and *Tnfα* were significantly reduced 2 days after cardiotoxin injury compared to wild type controls whose muscles were injured in the same way. Expression of myosin heavy chain 3 was also signficantly reduced 4 days after cardiotoxin injury indicating a potential delay in muscle repair (Mathes & Lafyatis 2011).

The core gene regulatory network of control vs grafted muscles also includes toll-like receptor, *Tlr4*. This receptor is traditionally stimulted by lipopolysaccharides (LPS) from bacterial cell walls, although there is also evidence that endogenous molecules, produced as a result of necrotic cells and the degradation of the extracellular matrix, can also lead to its activation (Yu et al. 2010). The presence of TLR4 in skeletal muscle has been also associated with the regulation of muscle regeneration in response to injuries caused by *Bothrops jararacussu* snake venom (Luiz Paiva-Oliveira et al. 2012). With *Tlr4* defficient mice showeing a 3-fold increase in the area of injury 10 days post-injury compared to the injured controls 10 days post-injury. The lession was characterised by intense inflammatory infliltrate and connective tissue deposition (Luiz Paiva-Oliveira et al. 2012).

Other TLR receptors are also present in the data collected from control vs grafted, including *Tlr*9, 13, 7, 8, 1, and 11. In control vs sham injected muscles, although TLR receptors are not represented in the core gene-regulatory network, the data include upregulation of *Tlr*9, *Tlr*3, *Tlr*13, and *Tlr*7. This contrasts with the upregulation of only *Tlr*3 in control tissues compared to 3 day irradiated muscles, showing an increase in the expression of several toll-like receptors between 3 and 5 days post irradiation. This, together with patterns of gene expression consistent with type I interferons suggests a priming of the innate immune sytem by increasing the expression of pattern recognition receptors like Toll-like receptors after radiation injury in skeletal muscle.

All Toll-like receptors contain an intracellular Toll-IL-1 receptor (TIR) domain, which transmits downstream signals recruiting TIR-containing adaptor proteins. These adaptors include MyD88 (myeloid differentiation primary response protein 88), TIRAP (TIR-domain-containing adaptor protein), TIRF (TIR-domain-conatining adaptor protein inducing IFNß, also TICAM1) and TRAM (TRIF-related adaptor molecule, also TICAM2). Signalling through TLRs can be broadly separated into two pathways, MyD88 dependent, and MyD88 independent pathways. All TLRs activate the MyD88-dependent pathways, while TLR3 and TLR4 activate the MyD88 indepentent pathway. However both pathways are linked through the NF-κß and the mitogen-activated protein kinase (MAPK) pathways (O'Neill & Bowie 2007). Additionally, there is mounting evidence that several interferon regulatory factor family members are also activated by the MyD88 dependent and Myd88-independent pathways (Akira et al. 2006). The core network regulators in figures 4.8,

4.26, and 4.36 all show either *Irf7* (figures 4.8 and 4.26) or *Irf1* (figure 4.36) as having essential roles in the regulation of the gene regulatory network.

Interferon regulatory factors IRF3 and IRF7 are thought to be responsible for TLR ligand-induced induction of type I interferon, with IRF3 preferentially regulating the induction of IFN-ß through the activation of TLR3 and TLR4 by dsRNA and LPS (Honda & Taniguchi 2006). In contrast IRF7 has a preferential ability to activate IFN-α promoters (Honda & Taniguchi 2006). It has been shown that the adaptor protein MyD88 interacts with an inhibitory domain of IRF7 resulting in the activation of the IFN-α dependent promoters, but does not interact with IRF3 (Kawai et al. 2004), further supporting the hypothesis of an activation of an IFNα response. Damage caused by ionising radiation has been shown to induce several Toll-like receptors, along with damage-associated molecular patterns (DAMPS) which are ligands to the TLR receptors (reviewed by: Ratikan et al. 2015). The significant upregulation of IRF7 after irradiation and the presence of gene expression patterns consistent with a response to interferon alpha in GSEA suggests that irradiation is inducing a type I interferon response, which could be caused by the activation of TLRs or other pattern recognition receptors detecting endogenous DAMPs after radiation damage.

Additonally, in the comparissons of 3 day post-18Gy, sham, and grafted to controls a response to IFNγ is recognised by GSEA analysis, which increases in size from 3 days irradiated (containing only 36 genes) to larger sets in sham injected muscles (79 genes matching the gene-set for IFNγ response) and grafted muscles (86 genes associated with the IFNγ response). Further support for the role of INFγ is also provided by the apperance of *Cxcl10* as a major regulator in control vs sham (figure 4.26) and in control vs grafted (figure 4.36). CXCL10 contains a Gamma Activating

Sequence (GAS) in its promoter region, so when IFNγ binds to its receptors it leads to the phosphorylation of STAT1 at Tyr701 and Ser727, This results in the formation of STAT1 homodimers known as Gamma-Activated Factor, which translocates to the nucleus and binds the GAS region of target genes, enhancing trascriptional activation by recruiting serveral transcriptional coactivators (Wen et al. 1995). This allows the regulation of well known IFNγ inducible genes such as IRF1 and CXCL10 (reviewed by Saha et al. 2010).

This suggests that the response to irradiation progresses from a IFNα response 3 days after irradiation and shifts to IFNγ 5 days after irradiation. Furthermore, a top regulator in controls vs 3DIR is ISG15, a protein induced by IFNα and IFNβ, that can be secreted to induce the synthesis of IFNγ in T-cells (not present in nude mice, section 2.1.2) and natural killer cells (that are present in nude mice) (Fan & Zhang 2013; Bogunovic et al. 2013) (figure 4.8). Therefore the activation of the interferon alpha response by the initial radiation damage could ultimately lead to the activation of an IFNγ response, spurred by the release of ISG15 as a consequence of the activation of an IFNα response.

This is very relevant, as interferon gamma has been shown to delay myoblast differentiation and induce myoblast proliferation through the major histocompatibility complex class II transactivator CIITA (Londhe & Davie 2011; Londhe & Davie 2013). To achieve this, IFNγ first increases the abundance Polycomb repressive complex 2 (PRC2) in skeletal muscle, where it is not normally present. CIITA then interacts with the Jumonji family protein JARID2, a non-catalytic subunit of PRC2, which causes RNA polymerase II (RNAPII) to pause at its target promoters. Aditional subunits of the PRC2 complex are then recruited in a JARID2 dependent

manner, concurrent with the loss of RNAPII and the methylation of Lys^{27} of histone H3 (H3K27), which is associated with gene repression. Via this mechanism IFNγ can block myogenesis by silencing the expression of muscle specific genes (Londhe & Davie 2011; Londhe & Davie 2013). In-vivo, uninjured IFNγ null mice showed no obvious differences in muscle morphology compared to wiltype counterparts. However, 5 days after intramuscular cardiotixin injury IFNγ deficient mice demonstrated a decreased number and area of regenerating fibres compared to injured wild-type mice. 10 days post-injury the number of regenerating fibres was still reduced in IFNγ null mice compared to wild-type mice, while trichrome staining showed increased fibrotic tissue staining which was not observed in the injured wildtype counterparts (Cheng et al. 2008). Furthermore, IFNγ has a high species specificity (Saha et al. 2010a), with human IFNγ being unable to bind the murine IFNγ receptor and vice-versa, suggesting a possible reason why irradiation does not enhance the engraftment of human stem cells into murine muscles (Meng et al. 2015).

Ionising radiation mainly causes cell death, as seen by the increases in tunel positive cells in irradiated mouse muscle that have already been described in Chapter 3. The release of debris and DAMPS from dying (tunel positive) cells into the surrounding tissue will lead to the activation of a type I interferon response within the tissue, and therefore to the activation of the interferon alpha and later gamma pathways, as well as TNFα via NFκB signalling from the activation of TLRs and IFNγ signalling.

The activation of TNF-alpha signalling (control vs sham, figure 4.31; and control vs grafted, figure 4.44) has also been shown to delay myogenic differentiation

of C2C12 myoblasts *in-vitro* (Langen et al. 2001) and of primary human myoblasts cultured *in-vitro* (Miller et al. 1988). Furthermore, TNFα can induce increaed expression of inflammatory cytokines such as *Il*-6 in C2C12 differnetiated myotubes. The release of pro-inflammatory cytokines such as IL-6, has been shown to be a powerful driver of human myoblast proliferation *in vitro* (Wang et al. 2008) and regulator of satellite-cell mediated hypertrophy *in vivo* (Serrano et al. 2008; Toth et al. 2011; reviewed by: Muñoz-Cánoves et al. 2013) that may explain the downregulation of myogenic differentiation markers such as MYH3 in irradiated muscles (figures 4.12 and 4.38, and table 4.4). Other members of the IL-6 family of cytokines are also upregulated, notably of leukaemia inhibitory factor (LIF) and Oncostatin M (OSM), for example in figure 4.40, under the MSigD term "Inflammatory Response". These members of the IL-6 family of cytokines are powerful myokines capable of further delaying myoblast differentiation and stimulate their proliferation (Xiao et al. 2011; Barnard et al. 1994; Mathieu et al. 2012). Both IL6 and LIF are visible in the network belongong to the GO term "positive regulation of cell proliferation" seen in grafted muscles and represented on figure 4.37.

The combination of TNFα, the IL-6 family of cytokines, and IFNγ would lead to a skeletal muscle enviroment where myogenic differentiation is severely hampered, while satellite cell and myoblast proliferation is encouraged. With the endogenous satellite cells killed or incapacitated by radiation (Boldrin et al. 2012), the grafted donor satellite cells are free to proliferate without competition from endogenous satellite cells, which would lead to enhanced donor satellite engraftment within irradiated host muscle.

Alternatively, the observed changes in gene expression could also correspond to a senescence associated secretory phenotype. The top network regulators show the presence of chemokines (figure 4.8, 4.26, 4.36) along with a central role for the inflammatory cytokine IL-6 (Chiche et al. 2017b) (figures 4.26, 4.36). While GSEA analysis shows enrichment for inflammatory pathway such as interferon gamma (figures 4.11, 4.28, 4.39) and inflammatory responses (figures 4.27, 4.40) which are characteristic of the senescence associated secretory phenotype (section 1.9) (Rodier et al. 2009; Coppé et al. 2010). Additionally, in grafted muscles GSEA analysis also reveals an Epithelial Mesenchymal transition (table 4.8) which has been shown to be induced by the SASP of senesecent fibroblasts on pre-malignant cells, aiding in the development of an invasive and metastatic phenotype (Coppé et al. 2008). suggesting that the SASP may aid the dispersion of grafted donor satellite cells. Furthermore, it has been shown that senescent cells play a role tissue regeneration (Demaria et al. 2014), and they appear in a transitory manner after muscle injury (Le Roux et al. 2015), indicating that they may play a role in muscle regeneration. Together, with the observation of TUNEL positive cells are located outside the basal lamina (Chapter 3, figure 3.5), indicates that non-muscle senscent cells may be aiding in the engraftment of donor satellite cells.

Evidence suggesting the proliferation of donor satellite cells comes from the comparison of grafted muscles (irradiated, transplanted with donor satellite cells 3 days later and analysed 2 days after cell transplantation) to muscles collected 3 days after irradiation, where the top network regulators all relate to GO terms to mitosis, DNA packaging and chromosome condensation (figure 4.17). Using GSEA analysis to consider all the dysregulated genes indicates the enrichment of pathways related to

the regulation of the cell cycle (E2F Targets (figure 4.19); G2/M checkpoint (figure 4.18); and mitotic spindle assembly (figure 4.20).

Once the inflammatory response caused by the radiation injury is lost, or shifts to a less favourable state, the ability of the host muscle to receive grafted satellite cells may be lost, which would explain why donor satellite cells contribute to very little muscle regeneration when grafted into host muscles 4 weeks after they were irradiated with 18 Gy (Boldrin et al. 2012).

In conclusion, RNA-sequencing data suggests the activation of an innate immune response via Toll-like receptor activation caused by DAMPS released from dying cells within the muscle and initially focused on an interferon alpha response mediated by IRF7. Over 2 days this response shifts towards an interferon gamma response, triggered by the release of ISG15 and mediated by IRF1, which would be expected to delay myoblast differentiation. TNFα signalling via NFκB triggered by the Toll-Like receptors further enhances the release of inflammatory cytokines of the IL-6 family. Alternatively, this inflammatory response may be mediated by senescent cells within the pre-irradiated host muscle, leading to the release of a SASP that could aid satellite cell proliferation and their invasion of the host tissue. However, regardless of the source, the combination of these inflammatory signalling molecules would then create an environment which inhibits myoblast or satellite cell differentiation, and promotes their proliferation, allowing the succcesful engraftment of satellite cells at certain points after irradiation where the inflammatory response has created an optimally permissive environment.

Chapter 5 - Characterisation of the Irradiation Induced Interferon Response

5.1 Background

In chapter 4 RNA sequencing revealed a central role for genes involved in the type I and type II interferon responses in the regulation of the alterations in gene expression after irradiation. Of particular interest is the response to interferon-gamma (IFNγ), as it has been previously shown to delay myogenic differentiation and promote myoblast proliferation through the class II transactivator (CIITA), which interacts with the Jumonji family protein JARID2, a member of the polycomb repressive complex 2 (PRC2), which causes RNA polymerase II to pause at its target promoters. Additionally PRC2 causes the methylation of lysine 27 in histone H3, leading to the repression of myogenic gene expression in primary myoblasts and *in vivo* (Londhe & Davie 2013).

Furthermore, Fu et al. (2015) showed that a cocktail of four inflammatory cytokines, IL-1α, IL-13, TNF-α, and IFNγ, could increase the long term expansion of primary myoblasts *in vitro* while minimising the loss of their myogenic potential when grafting *in vivo* into cardiotoxin injured muscles of $Rag1^{-/-}$ immunodeficient mice. However, if IFNγ is withdrawn from *in vitro* culture, the proliferation abilities of primary myoblasts is decreased dramatically, the formation of myotubes is increased, and myogenin expression levels increased significantly, showing that IFNγ

is essential to regulate myoblast proliferation and maintain their myogenic potential (Fu et al. 2015).

To further characterise the interferon response after radiation injury in skeletal muscle, I performed RT-qPCR arrays (SAB Bioscience: PAMM-064Z - mouse interferons and receptors) specific for mouse interferon signalling pathways on RNA extracted from muscles that were either permissive to satellite cell grafting (3 days after 18Gy, 3 hours after 25Gy) or non-permissive (non-irradiated, 3 days after 25Gy). Genes of interest were then further characterised by qPCR using both RNA from the micro-array samples and those used for next-generation sequencing. The aim was to obtain interferon related gene expression patterns that might be predictive of a permissive environment for satellite cell engraftment and a target for pharmacological modulation.

5.2) RT-qPCR Arrays

5.2.1) Results

Twelve mouse interferons and receptors RT-qPCR arrays were purchased and divided into 4 groups with 3 biological repeats within each group. These consisted of:

- Non-treated controls – This group provides a non-permissive niche where satellite cell engraftment fails
- 3 days post-18Gy – These muscles should possess a permissive niche where satellite cell engraftment is augmented
- 3 hours post-25Gy – This group should be permissive to satellite cell engraftment

- 3 days post-25Gy – These muscles should no longer provide a permissive niche for satellite cell engraftment.

All groups were normalised to the non-treated controls, manually selecting Actin and *Gusb* Glucuronidase Beta) from the 5 housekeeping gene candidates included in the array. The threshold for fold change in expression was set at x1.5 fold, and the p value was set to $p<0.05$. The plates contained 84 genes related to interferon signalling and its receptors, plus 5 housekeeping genes, a mouse genomic DNA contamination control, 3 RT reaction controls, and 3 positive PCR controls. The 84-interferon signalling related genes and 5 candidate housekeeping genes are shown with their fold regulation compared to controls, along with their p-values. Significant p-values (<0.05) are highlighted in red, and those with an absolute fold regulation larger or equal to 2 are highlighted in green in table 5.1.

Table 5.1: Fold Regulation and p value of all the PCR arrays compared to controls						
Gene Symbol	3 Days Post-18Gy		3 Hours post-25Gy		3 Days post-25Gy	
	Fold Regulation	p-value	Fold Regulation	p value	Fold Regulation	p value
Adar	1.2528	0.395871	1.0629	0.83768	1.6533	0.12058
Crlf2	1.0241	0.861089	1.3948	0.16815	1.075	0.622899
Csf2	-7.5395	0.040094	-2.2986	0.5661	-11.4475	0.007471
Csf3	-2.7423	0.106935	1.1415	0.635438	-13.9876	0.058031
Csf3r	1.1982	0.599067	2.3366	0.069123	2.748	0.153032
Ctf2	-1.4236	0.251903	-1.2311	0.674391	-3.7076	0.132644
Cxcl10	3.5166	0.182075	-1.0639	0.8016	17.8103	0.000752
Ebi3	1.4318	0.201398	-1.8829	0.158611	1.5933	0.178639
Epor	1.2168	0.228789	-2.016	0.127578	-1.6862	0.287681
F3	-1.0086	0.971257	1.0225	0.775867	-2.2373	0.097451
Ghr	-1.5154	0.262029	-1.3244	0.400753	-4.6298	0.081644
Ifi204	1.4646	0.256414	1.6694	0.182962	3.1195	0.009904
Ifi27	1.0006	0.938586	-1.33	0.080281	-1.413	0.039676
Ifi27l2a	1.8834	0.100891	-1.2963	0.249272	3.4344	0.000263
Ifi30	-1.2723	0.277787	-1.0597	0.81432	1.2187	0.272147
Ifi35	-1.1651	0.068413	1.185	0.230411	-1.37	0.298471
Ifi44	3.1183	0.158425	1.0651	0.762846	9.647	0.000181
Ifih1	1.3187	0.290379	-1.3063	0.282786	3.2018	0.004974
Ifit1	3.0354	0.145689	-1.5229	0.350794	8.3579	0.000008
Ifit2	1.8758	0.197923	-1.6956	0.227013	5.4431	0.005917
Ifit3	2.3862	0.216022	-2.4368	0.034986	9.802	0.001647
Ifitm1	-2.1627	0.080769	1.8743	0.097699	-3.5651	0.041888
Ifitm2	1.031	0.811043	1.2564	0.383411	-1.4743	0.346793
Ifna11	-2.0829	0.392811	-1.9005	0.310173	-5.7467	0.186344
Ifna12	-1.4307	0.601097	1.1805	0.542072	-3.1662	0.058574

Ifna14	-1.4307	0.601097	-1.4838	0.270368	-4.1971	0.050982
Ifna2	-1.3731	0.24947	-3.8608	0.396046	-9.3028	0.006785
Ifna4	-1.8635	0.16105	-1.4256	0.505667	-3.9799	0.013974
Ifna9	-1.4307	0.601097	-1.4838	0.270368	-2.3561	0.946981
Ifnab	-2.5242	0.10648	-4.3622	0.215104	-9.4799	0.054931
Ifnar1	-1.3493	0.074815	1.0884	0.617964	-1.5432	0.113282
Ifnar2	-1.2428	0.057697	-1.0845	0.375767	-1.238	0.038197
Ifnb1	-1.8193	0.264588	-1.0957	0.721886	1.2662	0.649923
Ifne	-2.6139	0.281462	-2.7109	0.239076	-7.6683	0.160354
Ifng	1.5836	0.567795	-1.931	0.297295	6.0438	0.075548
Ifngr1	-1.4496	0.007934	-1.1373	0.219664	-2.5499	0.009528
Ifngr2	-1.4058	0.091778	-1.1119	0.56281	-2.3026	0.13588
Ifnk	1.1693	0.902867	-1.1803	0.76206	-1.3228	0.401322
Ifnz	1.153	0.519274	-1.0415	0.982258	-1.6429	0.864029
Il10rb	-1.0616	0.412587	-1.1252	0.317888	1.0565	0.636876
Il12b	-8.4755	0.248152	-4.5329	0.300225	-2.1881	0.362793
Il12rb1	1.146	0.870605	-1.5566	0.401272	1.6943	0.296285
Il12rb2	1.4424	0.3449	-1.2138	0.640262	1.5539	0.31116
Il13	1.1862	0.475742	1.1588	0.575118	-4.0143	0.005009
Il13ra1	-1.3836	0.041239	2.5084	0.224666	-1.395	0.043972
Il15	-1.8151	0.124709	-2.5781	0.077268	-3.2798	0.039828
Il20ra	-1.4647	0.439369	-1.4879	0.767612	-2.0273	0.333
Il21	-1.4743	0.508523	-1.6927	0.127654	-4.7882	0.024428
Il21r	1.855	0.379827	2.321	0.316422	4.438	0.019986
Il22ra2	-1.6502	0.483327	-1.7572	0.312057	-4.9705	0.139372
Ifnl3	-1.4307	0.601097	-1.4838	0.270368	-2.4899	0.924913
Ifnlr1	-3.2816	0.169102	-1.0787	0.727233	-3.3349	0.243932
Il2rb	-1.5096	0.872218	-2.0606	0.218961	2.5301	0.221409
Il2rg	1.3941	0.222896	1.6737	0.020897	2.5796	0.025619

Il3ra	-1.2761	0.606931	-2.2615	0.069032	-1.9787	0.060603
Il4	-1.0083	0.561669	-1.4883	0.919383	-1.3007	0.638964
Il4ra	-1.115	0.367714	2.6997	0.214094	1.0537	0.596548
Il6	1.0324	0.566358	7.5664	0.329244	1.8305	0.88011
Il6ra	-1.1746	0.443539	1.3513	0.105378	1.0671	0.76661
Il6st	-1.7832	0.015192	1.114	0.564256	-3.3661	0.01438
Il7	-1.2311	0.545135	-1.3443	0.546544	-1.198	0.749636
Il7r	-2.1378	0.613204	1.093	0.845179	1.3988	0.361921
Il9	-1.4842	0.54568	1.3783	0.466617	-2.61	0.132684
Il9r	-5.7216	0.027756	-2.1129	0.15826	-15.8904	0.018701
Irf1	-1.1983	0.10514	-1.1277	0.475309	1.0047	0.955141
Irf2	-1.7217	0.029328	1.0888	0.62202	-2.4922	0.016132
Irf2bp1	-1.7889	0.035605	-1.2922	0.277195	-3.458	0.046537
Irf3	-1.4389	0.093857	-1.2138	0.272565	-3.4618	0.015679
Irf4	-1.6745	0.054051	-2.432	0.052864	-3.228	0.009487
Irf5	-1.0424	0.790543	-1.1443	0.545029	1.0754	0.675091
Irf6	-1.1366	0.653773	-1.2779	0.407622	-1.8287	0.399183
Irf7	3.003	0.21981	-1.1154	0.816043	10.0128	0.010115
Irf8	-1.1882	0.750446	1.0552	0.526889	1.3127	0.326878
Irgm1	1.1873	0.482043	-1.0906	0.586056	2.1675	0.022583
Isg15	2.7779	0.121158	-1.0251	0.9838	8.1424	0.000058
Lepr	-1.471	0.148676	-1.8731	0.047988	-3.0484	0.105858
Lif	7.5183	0.013052	10.4251	0.011918	5.6587	0.151296
Lifr	-1.5273	0.056794	-1.759	0.006961	-3.3104	0.043923
Mpl	-2.1626	0.105059	-2.9124	0.533721	-7.1444	0.021202
Mx1	5.2702	0.151212	1.6756	0.212884	14.1704	0.009443
Oas1a	2.0097	0.227859	-1.1298	0.596968	4.599	0.028526
Osm	2.0176	0.34207	2.6898	0.173838	1.5518	0.672147
Osmr	-1.2777	0.05788	2.6181	0.139881	-1.974	0.02821

Prlr	8.0975	0.057905	1.3304	0.952304	2.7402	0.444028
House Keeping Candidates						
Actb	1.0009	0.951261	-1.0775	0.569114	-1.1545	0.314441
B2m	1.0952	0.622838	-1.0783	0.524799	1.7418	0.055227
Gapdh	-1.8064	0.019376	-1.3133	0.492064	-4.9324	0.009077
Gusb	-1.0009	0.936988	1.0775	0.569838	1.1545	0.30886
Hsp90ab1	-1.5487	0.026402	-1.0885	0.655441	-3.0413	0.02614

5.1.2) 3 days post-18Gy Vs Control

Three days after 18 Gy irradiation, the niche is permissive for satellite cell transplantation (Boldrin et al. 2012). When 3-day irradiated samples were sequenced and compared to controls, gene ontology analysis of the core network regulators suggested an innate immune response in response to double stranded RNA (section 4.2.1). This was then confirmed by GSEA analysis (section 4.2.2) which showed significant enrichments for interferon alpha and gamma signalling, which mediate innate immunity. To characterise the interferon response after irradiation, 3 muscles from mice which had their hindlimbs irradiated with 18Gy 3 days previously were used for the interferon and receptors RT^2 RT-pPCR microarray. For analysis of the RT-qPCR arrays, the threshold for fold change was set to a minimum x2 absolute fold change, with a p-value <= 0.05. The data are represented in a volcano plot (figure 5.1) with the vertical dotted lines showing the 2-fold change mark, and the horizontal line representing the Log(p-value) corresponding to p=0.05.

The only significantly upregulated gene was leukaemia inhibitory factor (*Lif*) (fold regulation: 7.52; p=0.013052). Two genes were significantly downregulated compared to non-irradiated controls: colony stimulating factor 2 (*Csf2*) (fold regulation: -7.54; p-value: 0.040094,) and the IL-9 receptor (*Il9r*) (fold regulation: -5.72; p-value: 0.027756).

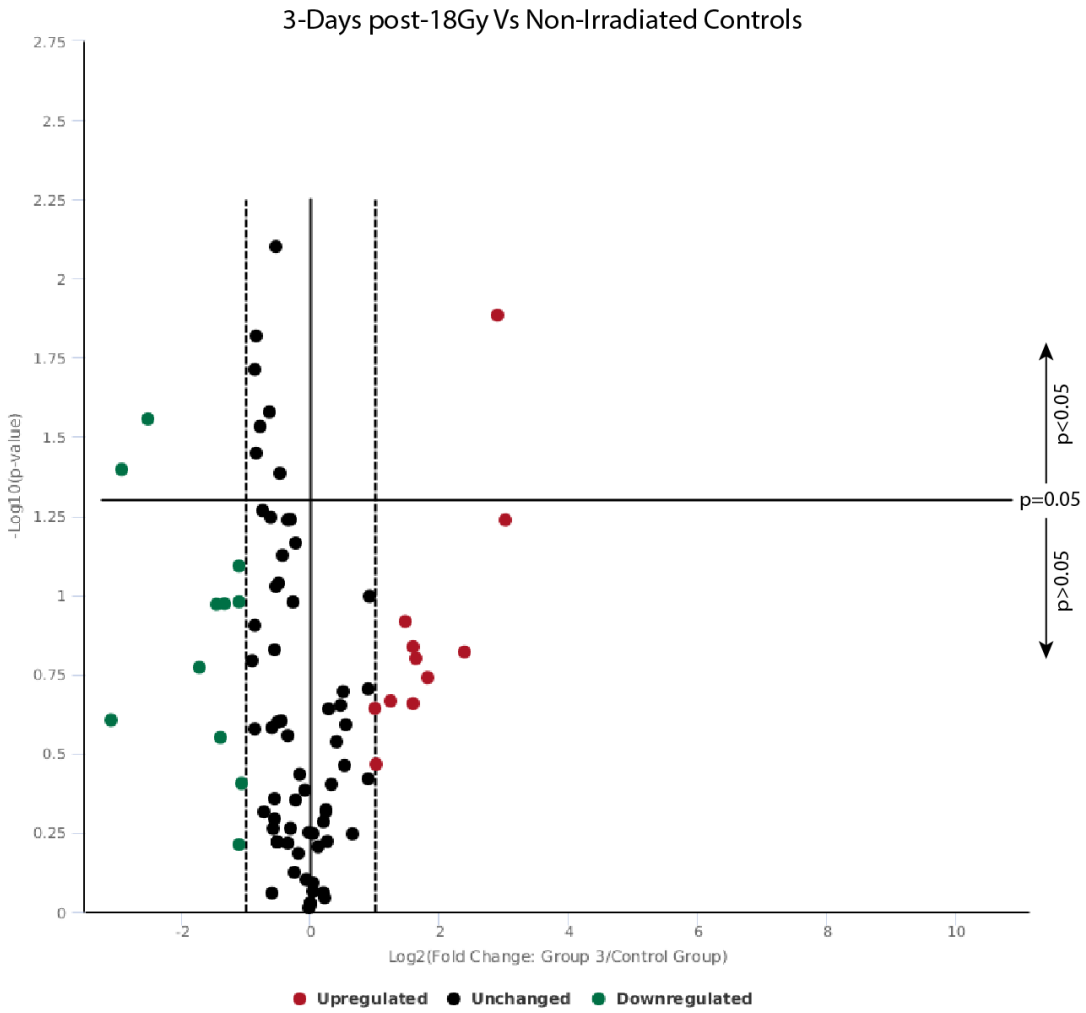

Figure 5.1: Volcano plot showing significantly dysregulated genes 3 days after 18Gy compared to non-irradiated controls. The only significantly dysregulated genes are *Lif* (fold regulation = 7.52; p = 0.013052), *Csf2* (fold regulation = -7.54; p = 0.040094), and *Il-9r* (fold regulation = -5.72; p = 0.027756). The dotted vertical lines denote the threshold for a 2-fold change, while the horizontal line marks the threshold for a p value of 0.05. Anything outside the dotted lines and above the horizontal line is considered a significant change in gene expression.

5.1.3) 3 hours post-25Gy Vs Control

Three hours after 25Gy, the muscle niche is permissive to satellite cell transplantation (Boldrin et al. 2012) and should therefore display similar gene expression patterns as muscles collected 3 days after 18Gy. When 25Gy irradiated samples are compared to non-irradiated controls (figure 5.2) 2 genes are significantly dysregulated (minimum 2-fold-change, p-value< 0.05). Under these conditions, there was a 10.43-fold upregulation of *Lif* (p-value: 0.011918) and Ifit3 with a -2.44 downregulation (p-value: 0.034986). The only significantly dysregulated gene in both permissive environments (3 days after 18Gy and 3 hours after 25Gy) was *Lif.*

5.1.3) 3 Hours post-25Gy vs 3 Days post-18Gy

To determine if there are any significant differences between both permissive environments (3 days after 18Gy and 3 hours after 25Gy) these two groups were compared (figure 5.3). These two groups showed little difference between one and other with only 2 genes being differentially expressed. *Ifitm1* (interferon induced transmembrane protein 1) was significantly upregulated (fold regulation: 4.05; p-value: 0.012160) and *Ifi27l*α was significantly downregulated (fold regulation: -2.44; p-value: 0.040942) in the samples collected 3 hours after 25Gy compared to the 3-day post-18Gy irradiated samples.

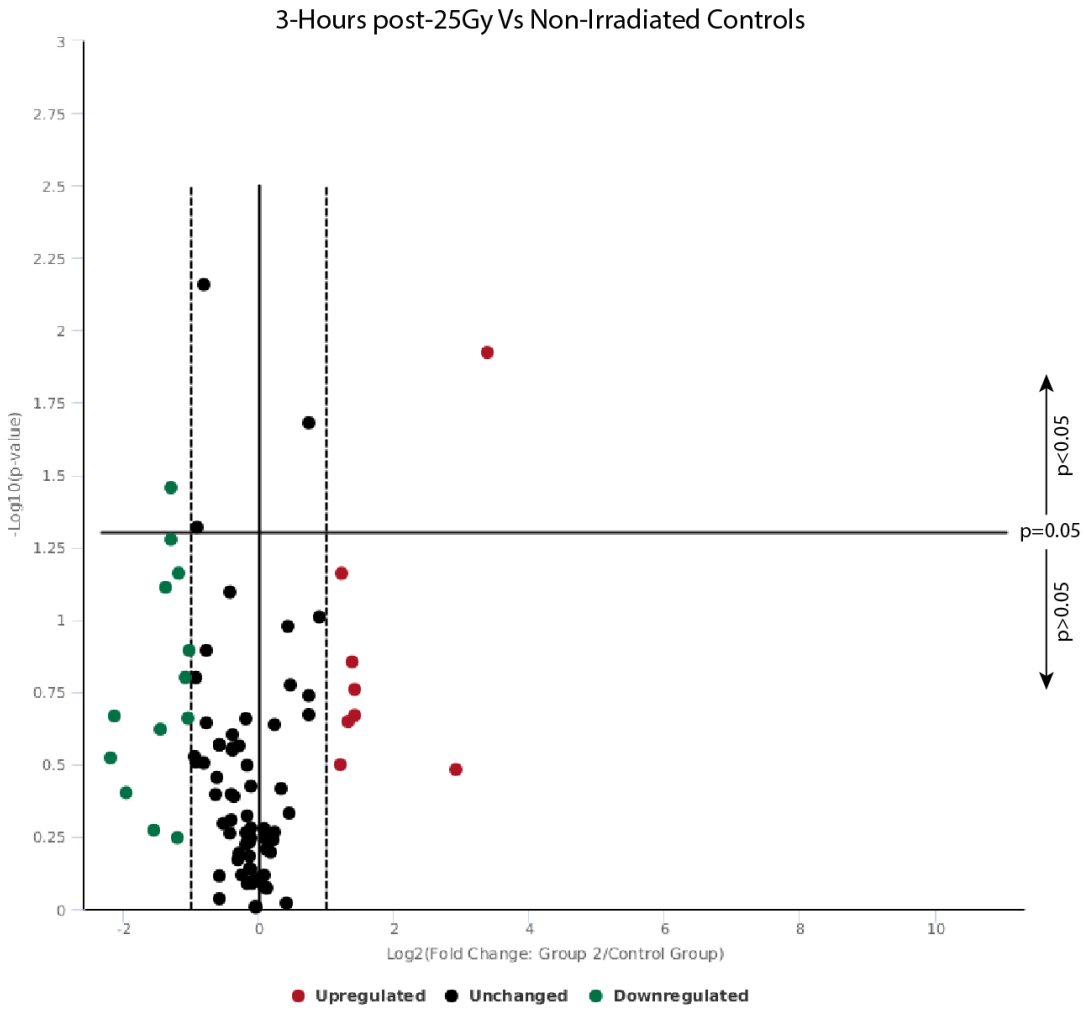

Figure 5.2: Volcano plot showing significantly dysregulated genes 3 hours after 25Gy compared to non-irradiated controls. The only significantly dysregulated genes are *Lif* (fold regulation = 10.43; p = 0.01198) and *Ifit3* (fold regulation = -2.44; p = 0.034986). The dotted vertical lines denote the threshold for a 2-fold change, while the horizontal line marks the threshold for a p value of 0.05. Anything outside the dotted lines and above the horizontal line is considered a significant change in gene expression.

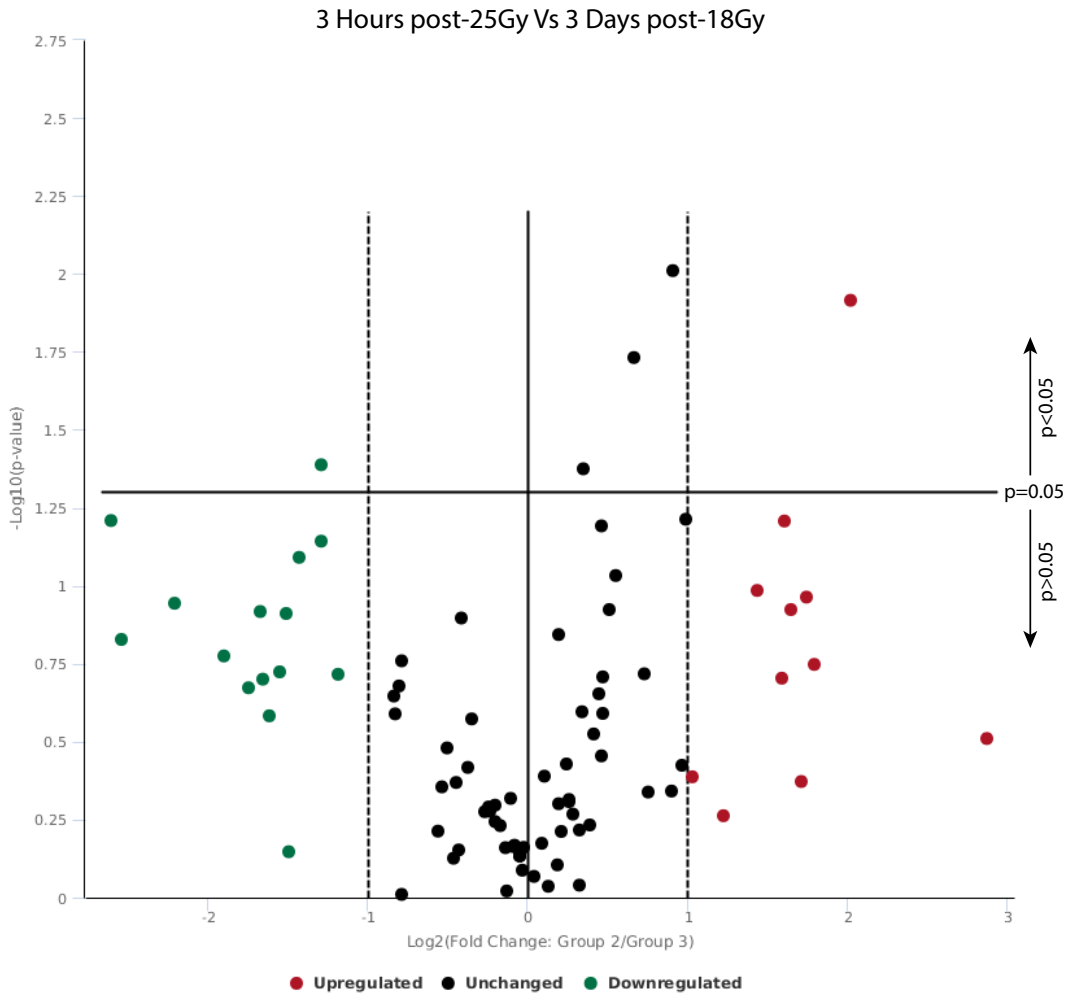

Figure 5.3: Volcano plot showing significantly dysregulated genes 3 hours after 25Gy compared to samples collected 3 days after 18Gy irradiation. The only significantly dysregulated genes are *Ifitm1* (fold regulation = 4.05; p = 0.012169) and *Ifit27l2*α (fold regulation = -2.44; p = 0.040942). The dotted vertical lines denote the threshold for a 2-fold change, while the horizontal line marks the threshold for a p value of 0.05. Anything outside the dotted lines and above the horizontal line is considered a significant change in gene expression.

5.1.5) 3 days post-25Gy vs Control

Three days after 25Gy, the TA of mdx$^{nu/nu}$ mice is restored to a non-permissive environment for satellite cell grafting. The RT-qPCR arrays returned a list of 33 differentially regulated genes compared to non-irradiated controls (absolute fold change > 2; p-value < 0.05) with 15 genes upregulated and 18 downregulated genes, shown in table 5.2 and figure 5.4.

To determine the potential functions of the significantly upregulated and downregulated genes, the BINGO app was used (Materials and Methods, section 2.7.5.4). The GO analysis of upregulated genes is shown in table 5.3, and that for downregulated genes is shown in table 5.4.

Table 5.2: Differentially regulated genes in samples collected 3 days after 25Gy compared to controls		
Gene	Fold Regulation	P-value
Cxcl10	17.8103	0.000752
Mx1	14.1704	0.009443
Irf7	10.0128	0.010115
Ifit3	9.802	0.001647
Ifi44	9.647	0.000181
Ifit1	8.3579	0.000008
Isg15	8.1424	0.000058
Ifit2	5.4431	0.005917
Oas1a	4.599	0.028526
Il21r	4.438	0.019986
Ifi27l2a	3.4344	0.000263
Ifih1	3.2018	0.004974
Ifi204	3.1195	0.009904
Il2rg	2.5796	0.025619
Irgm1	2.1675	0.022583
Irf2	-2.4922	0.016132
Ifngr1	-2.5499	0.009528
Hsp90ab1	-3.0413	0.02614
Irf4	-3.228	0.009487
Il15	-3.2798	0.039828
Lifr	-3.3104	0.043923
Il6st	-3.3661	0.01438
Irf2bp1	-3.458	0.046537
Irf3	-3.4618	0.015679
Ifitm1	-3.5651	0.041888
Ifna4	-3.9799	0.013974
Il13	-4.0143	0.005009
Il21	-4.7882	0.024428
Gapdh	-4.9324	0.009077
Mpl	-7.1444	0.021202
Ifna2	-9.3028	0.006785
Csf2	-11.4475	0.007471
Il9r	-15.8904	0.018701

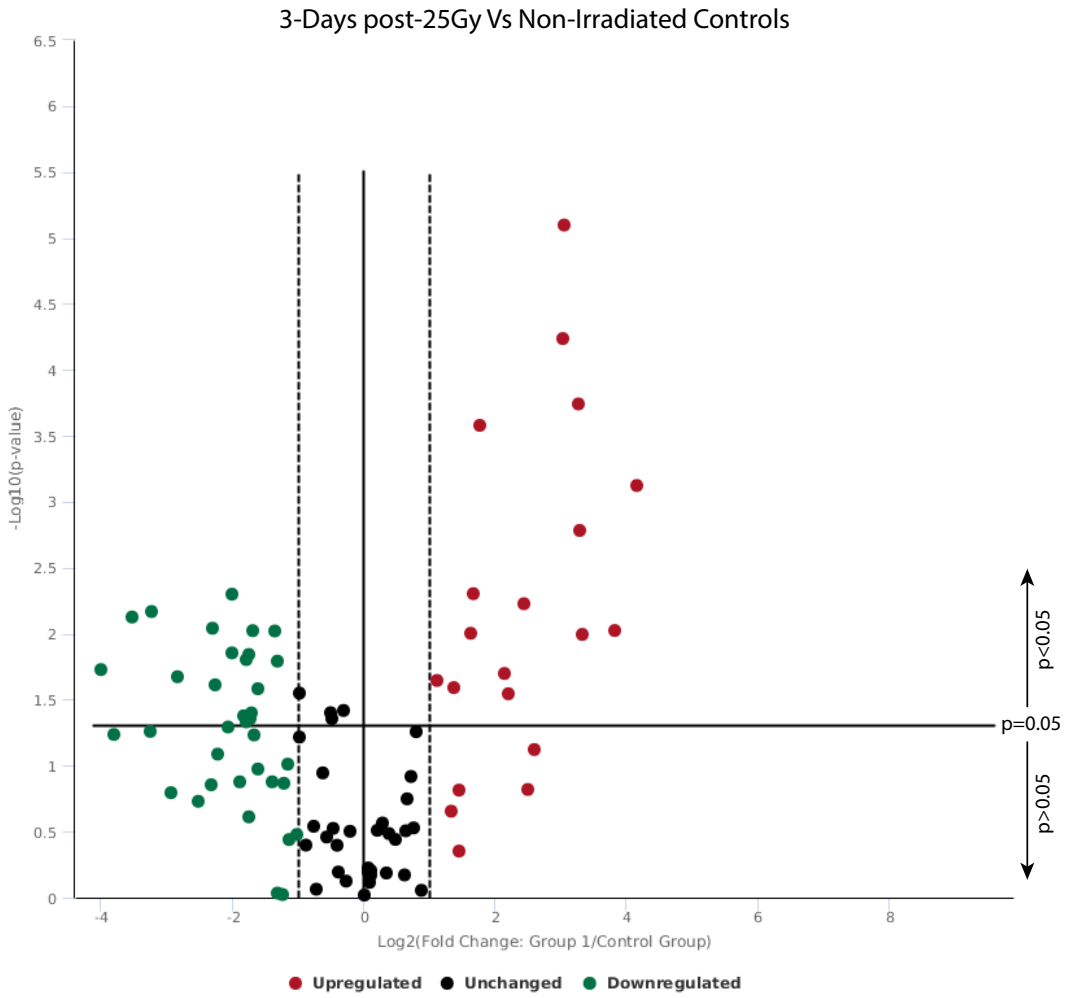

Figure 5.4: Volcano plot showing significantly dysregulated genes 3 hours after 25Gy compared to non-irradiated controls. There are 15 significantly upregulated genes and 18 significantly downregulated genes, shown in table 5.2. The dotted vertical lines denote the threshold for a 2-fold change, while the horizontal line marks the threshold for a p value of 0.05. Anything outside the dotted lines and above the horizontal line is considered a significant change in gene expression.

Table 5.3: GO analysis of upregulated genes in samples collected 3 days after 25Gy irradiation			
GO-ID	Description	Genes in test set	corr p-value
9615	response to virus	IFIH1|MX1|IRF7|ISG15|IFI27L2A	3.67E-08
50896	response to stimulus	IFIH1|CXCL10|IFI204|MX1|IRF7|OAS1A|IRGM1|ISG15|IFIT1|IFI27L2A|IFIT2	7.15E-08
6955	immune response	IFIH1|CXCL10|MX1|IRF7|OAS1A|IRGM1	6.33E-07
51707	response to other organism	IFIH1|MX1|IRF7|ISG15|IFI27L2A	5.72E-06
35455	response to interferon-alpha	IFIT1|IFIT2	8.18E-06
35457	cellular response to interferon-alpha	IFIT1|IFIT2	8.18E-06
9607	response to biotic stimulus	IFIH1|MX1|IRF7|ISG15|IFI27L2A	9.81E-06
2376	immune system process	IFIH1|CXCL10|MX1|IRF7|OAS1A|IRGM1	1.40E-05
51704	multi-organism process	IFIH1|MX1|IRF7|ISG15|IFI27L2A	1.66E-05
71345	cellular response to cytokine stimulus	IFIT1|IFIT2	2.94E-05
45087	innate immune response	IFIH1|MX1|IRGM1	5.02E-04
6952	defense response	IFIH1|CXCL10|MX1|IRGM1	8.78E-04

Table 5.4: GO analysis of significantly downregulated genes in samples collected 3 days after a 25Gy radiation dose			
GO-ID	Description	Genes in test set	corr p-value
48522	positive regulation of cellular process	IL21|CSF2|IL15|IRF4|IL13|LIFR|IL6ST|IL9R	3.88E-04
8284	positive regulation of cell proliferation	CSF2|IL15|IL13|LIFR|IL6ST	3.88E-04
50896	response to stimulus	IL21|IFNA4|HSP90AB1|CSF2|IRF3|IFNGR1|IL15|IL13|IFNA2	3.88E-04
48518	positive regulation of biological process	IL21|CSF2|IL15|IRF4|IL13|LIFR|IL6ST|IL9R	3.88E-04
9615	response to virus	IFNA4|IRF3|IFNA2	6.08E-04
43011	myeloid dendritic cell differentiation	CSF2|IRF4	6.08E-04
1773	myeloid dendritic cell activation	CSF2|IRF4	6.08E-04
23036	initiation of signal transduction	LIFR|IL6ST|IL9R	6.08E-04
23038	signal initiation by diffusible mediator	LIFR|IL6ST|IL9R	6.08E-04
23049	signal initiation by protein/peptide mediator	LIFR|IL6ST|IL9R	6.08E-04
19221	cytokine-mediated signaling pathway	LIFR|IL6ST|IL9R	6.08E-04
2702	positive regulation of production of molecular mediator of immune response	IL21|IL13	8.56E-04
51251	positive regulation of lymphocyte activation	IL21|IL15|IL13	8.56E-04

42127	regulation of cell proliferation	CSF2|IL15|IL13|LIFR|IL6ST	8.56E-04
2697	regulation of immune effector process	IL21|IL15|IL13	8.90E-04
2696	positive regulation of leukocyte activation	IL21|IL15|IL13	8.90E-04
2376	immune system process	IL21|CSF2|IL15|IRF4|IL13	9.00E-04
50867	positive regulation of cell activation	IL21|IL15|IL13	9.02E-04
6955	immune response	IL21|CSF2|IL15|IL13	9.08E-04

Upregulated genes in this sample group associated with GO terms consistent with the activation of the innate immune system. It additionally includes genes which were highlighted as core network regulators in chapter 4, including *Irf7*, *Cxcl10*, and *Isg15*. Downregulated genes also associated with immune system processes. However, *Csf2*, *Il-15*, *Il-13*, *Lifr* (LIF receptor), and *Il-6st* (IL-6 signal transducer) are all associated with the positive regulation of cell proliferation (GO_ID: 8284) and are downregulated compared to control samples. However, these can be ruled out as potential candidates as it has already been shown that when grafted into non-irradiated hosts (where these molecules would be upregulated compared to the non-permissive niche) satellite cells fail to engraft (see Chapter 3 and Boldrin et al. 2012).

5.1.6) 3 Hours post-25Gy vs 3 Days post-25Gy

To determine if there are any significantly dysregulated genes between muscles that have been irradiated and are a permissive point for engraftment (3 hours post-25Gy) and those which are no longer permissive (3 days post-25Gy) their

gene expression data were compared. This yielded 19 differentially regulated genes in the muscles collected 3 hours after 25Gy compared to those 3 days post-25Gy, shown in table 5.5 and figure 5.5.

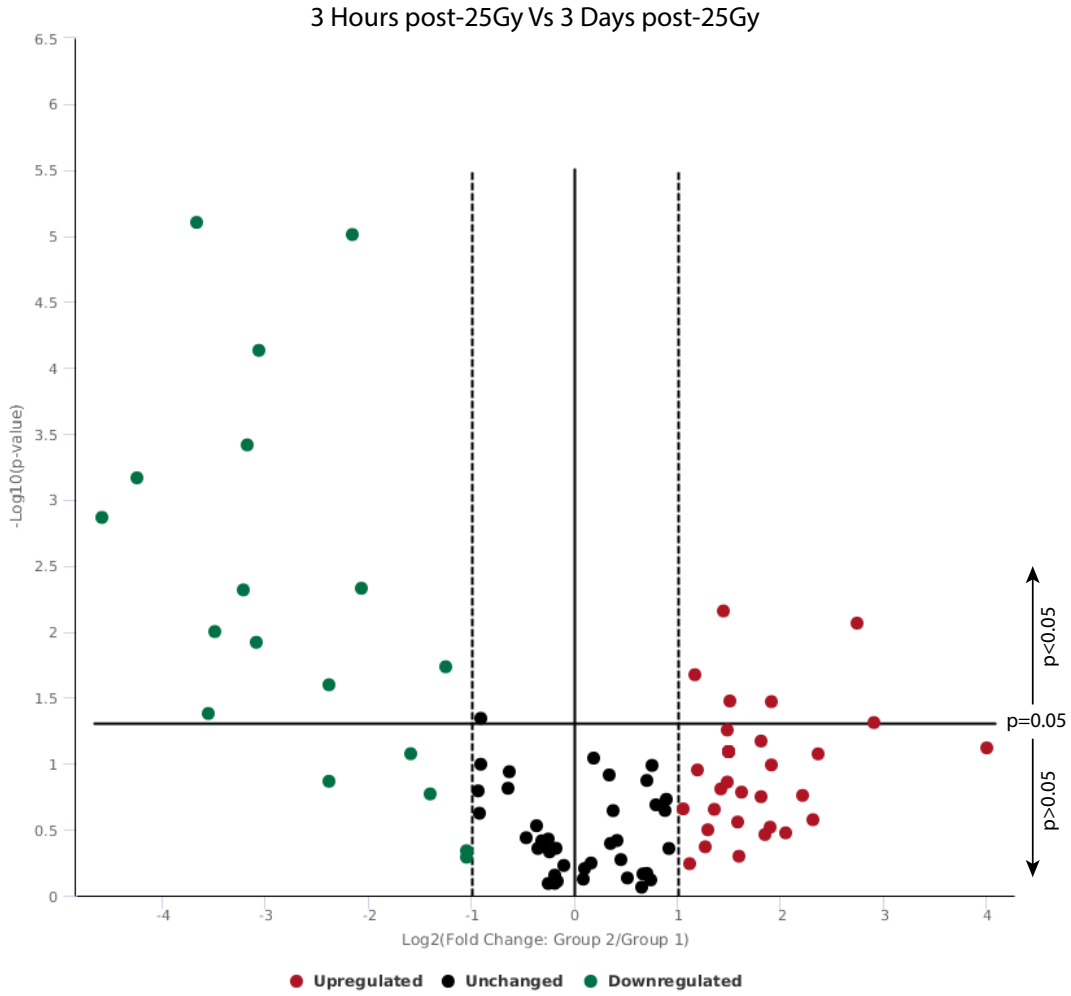

Figure 5.5: Volcano plot showing significantly dysregulated genes 3 hours after 25Gy compared to samples collected 3 days after 25Gy. There are 15 significantly upregulated genes and 18 significantly downregulated genes, shown in table 5.5. The dotted vertical lines denote the threshold for a 2-fold change, while the horizontal line marks the threshold for a p value of 0.05. Anything outside the dotted lines and above the horizontal line is considered a significant change in gene expression.

Upregulated genes (table 5.5) show no significant GO enrichments, however the 6 significantly upregulated genes contain the IL-9 receptor*, Il6-st*, and interferon gamma receptor ligand binding chain (alpha) (*Ifngr1*). These are pro-inflammatory cytokine receptors (*Ifngr1* and *IL-6st*) and anti-inflammatory cytokine receptors (*Il-9r*) which have been shown to be upregulated in response to TNFα stimulation (100ng/ml) of C2C12 derived myotubes (Alvarez et al. 2002), and is consistent with the finding of TNFα signalling via NFκB seen in sham injected muscles and grafted muscles in the RNA-sequencing data (Chapter 4, sections 4.6.2 and 4.7.2).

Table 5.5 Differentially regulated genes in muscles collected 3 hours post-25Gy compared to those collected 3 days post-25Gy		
Gene	Fold Regulation	p-value
IL9r	7.52	0.048866
Ifit1m	6.68	0.008606
IL6st	3.75	0.033889
Irf3	2.85	0.033485
Irf2	2.71	0.006963
Ifngr1	2.24	0.021156
Irgm1	-2.36	0.018416
Ifih1	-4.18	0.004683
Ifi27l2α	-4.45	0.000100
Oas1α	-5.2	0.025225
Isg15	-8.35	0.000074
Mx1	-8.46	0.012030
Ifi44	-9.06	0.000384
Ifit2	-9.23	0.004815
Irf7	-11.17	0.009965
Ifng	-11.67	0.041670
Ifit1	-12.73	0.000008
Cxcl10	-18.95	0.000682
Ifit3	-23.89	0.001359

Significantly downregulated genes in muscles collected 3 hours after 25Gy irradiation compared to those collected 3 days after 25Gy do return enriched GO terms, seen in table 5.6. These consistently associate with an innate immune

response, suggesting that the inflammatory response initiated by irradiation steadily increases over time after irradiation.

Table 5.6: GO analysis of downregulated genes in muscles collected 3 days after 25Gy compared to those collected 3 days after 25Gy			
GO-ID	Description	Genes in test set	corr p-value
9615	response to virus	IFIH1|IFNG|MX1|IRF7|ISG15	7.97E-09
6955	immune response	IFIH1|CXCL10|IFNG|MX1|IRF7|IRGM1	1.19E-07
50896	response to stimulus	IFIH1|CXCL10|IFNG|MX1|IRF7|IRGM1|ISG15|IFIT1|IFIT2	3.49E-07
51707	response to other organism	IFIH1|IFNG|MX1|IRF7|ISG15	1.27E-06
2376	immune system process	IFIH1|CXCL10|IFNG|MX1|IRF7|IRGM1	2.56E-06
9607	response to biotic stimulus	IFIH1|IFNG|MX1|IRF7|ISG15	2.56E-06
51704	multi-organism process	IFIH1|IFNG|MX1|IRF7|ISG15	4.61E-06
35455	response to interferon-alpha	IFIT1|IFIT2	4.61E-06
35457	cellular response to interferon-alpha	IFIT1|IFIT2	4.61E-06
6952	defence response	IFIH1|CXCL10|IFNG|MX1|IRGM1	7.25E-06
71345	cellular response to cytokine stimulus	IFIT1|IFIT2	2.26E-05
45087	innate immune response	IFIH1|MX1|IRGM1	2.63E-04
71310	cellular response to organic substance	IFNG|IFIT1|IFIT2	6.19E-04
6950	response to stress	IFIH1|CXCL10|IFNG|MX1|IRGM1	8.44E-04

5.2.7) Non-supervised Hierarchical Clustering

The very small number of differentially regulated genes between the permissive and non-permissive environments led me to assess how the gene expression patterns within each sample group would cluster (Hierarchical clustering), to determine if the all genes represented in this array present patterns of gene expression in different samples that allow differentiation of a permissive niche from a non-permissive niche. This was achieved using the manufacturer's web analysis tools (section 2.8, Materials and Methods). The result is shown as a heatmap, with dendograms indicating co-regulated genes across groups and individual samples, as well as clustering closely those samples that present similar overall patterns of gene expression in figure 5.6.

Focusing on the clustering of the samples, we can see that the baseline control for the normalisation of the qPCR data, the non-irradiated muscles, do not cluster together. One sample clusters with a permissive sample (3 days after 18Gy) and the other two non-irradiated samples cluster closely together with a group of permissive and non-permissive samples. This indicates a high variation in the gene expression patterns related to interferon signalling in the control groups, which probably explains the lack of significantly dysregulated genes. Only 2 out of 3 samples collected 3 days after 25Gy cluster in a coherent manner, displaying a similar pattern of gene expression different from the remaining groups. The remainder seem stochastic, with no clear distinction between sample groups. This contradicts the next generation sequencing data, whose principal component analysis showed a relatively good separation when comparing irradiated, grafted, or sham injected samples to the non-irradiated control group (section 4.1).

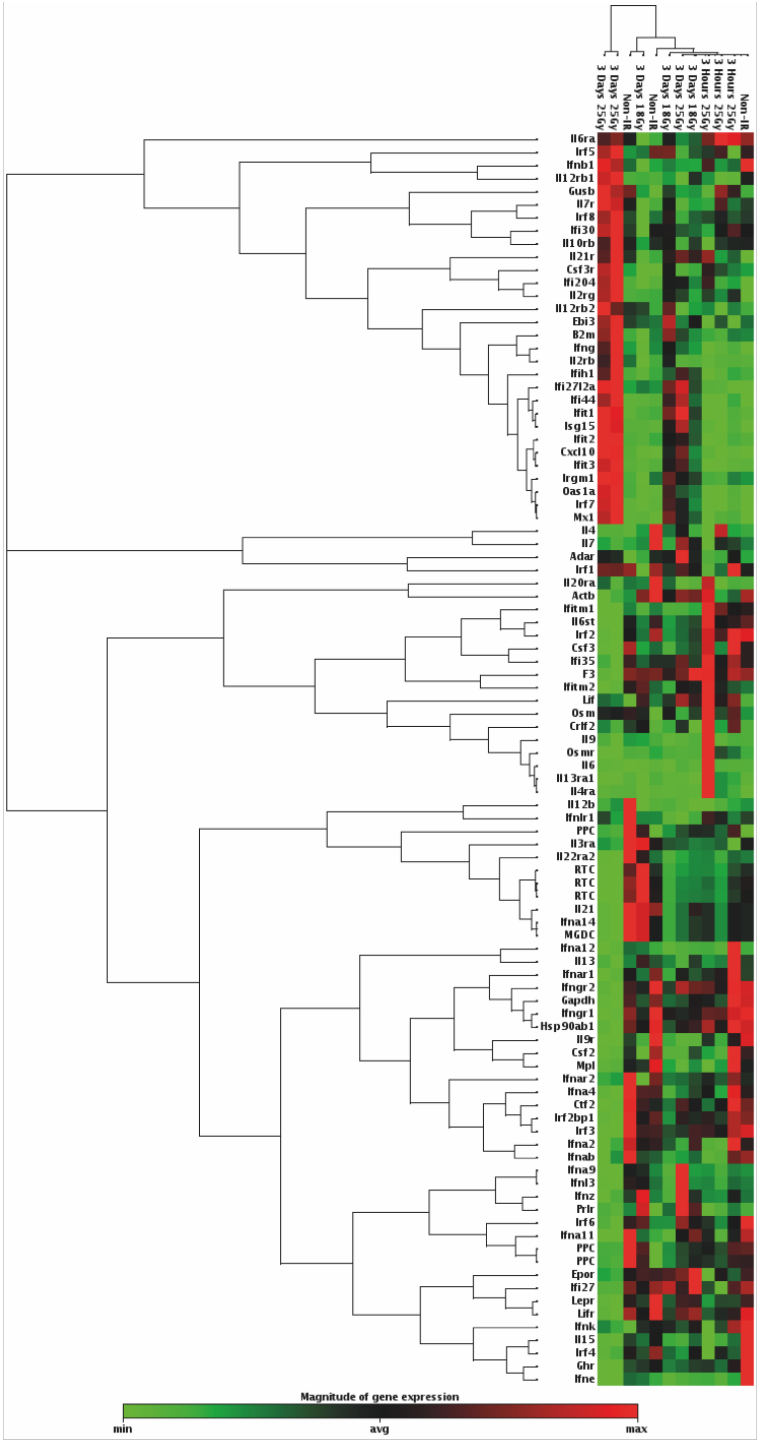

Figure 5.6: Unsupervised hierarchical clustering of the entire dataset displayed as a heatmap, with dendograms indicating co-regulated genes across groups or individual samples. There is no clear separation between non-irradiated control samples and irradiated samples.

5.3) RT-qPCR comparison of genes of interest between RNA-sequencing and Micro-array samples

The RT^2-profiler arrays showed little evidence of a strong interferon response when compared to the RNA-sequencing data. However, in these arrays there are no technical repeats for each sample, relying only on one RT-qPCR per gene per sample. To test whether the data between the sequencing and micro-array data was consistent, RT-qPCRs were done with 3 technical repeats per sample. The genes tested included Interferon Gamma, due to its potential role in delaying satellite cell differentiation and the constant appearance of the pathway in the RNA-sequencing data; Irf7 which was identified as a major network regulator in samples collected 3 days after 18Gy (permissive niche); and leukaemia inhibitory factor, which according to the RT^2 profiler arrays was significantly upregulated at the time points where engraftment was viable, but not significantly upregulated in the non-permissive niche, and therefore provides a potential candidate marker of a permissive niche.

5.3.1) Interferon Gamma

Gene expression patterns consistent with Interferon Gamma (IFNγ) signalling were up-regulated in irradiated muscles, although interferon gamma itself was seldom detected. Additionally, IFNγ was not significantly upregulated in any of the samples used for the micro-arrays. To compare if there are any significant differences of IFNγ at the mRNA level between those samples used for sequencing and those used on the microarrays, their mRNA was used for an RT-qPCR.

In samples used for RNA sequencing, IFNγ was significantly upregulated in sham injected muscles (mean fold change: 8.219; SEM: ±0.033733; n=3; p: 0.0011),

and was upregulated but not statistically significant to a p-value below 0.05 in samples collected 3 days after 18Gy (mean fold change: 4.197; SEM: ±1.484; n= 3; p: 0.0870) and grafted samples (mean fold change: 4.558; SEM: ±0.9689; n=3; p: 0.0570). The results are shown in figure 5.7a.

However, these results are not replicated in the samples employed for the micro-arrays (figure 5.7b). Here there was a high variability in the expression of IFNγ. Samples collected 3 days after 18Gy showed a mean fold change in expression of 2.042 (SEM: ±0.5046; p: 0.8855) compared to controls. 3 hours after 25Gy, the mean fold change was 1.189 (SEM: ±0.5073; p: 0.7028), and 3 days after 25Gy there was a mean fold change of 7.144 (SEM: ±3.11; p: 0.4469).

To compare levels of expression between both sample groups, the 3-day post-18Gy irradiated samples (n=6) from the micro-array and Next-generation sequencing experiments were run on the same plate together with all the non-irradiated controls (n=6). This is illustrated in figure 5.7c and shows an extremely high variability in the levels of IFNγ expression in both control tissues and muscles collected 3 days after 18Gy.

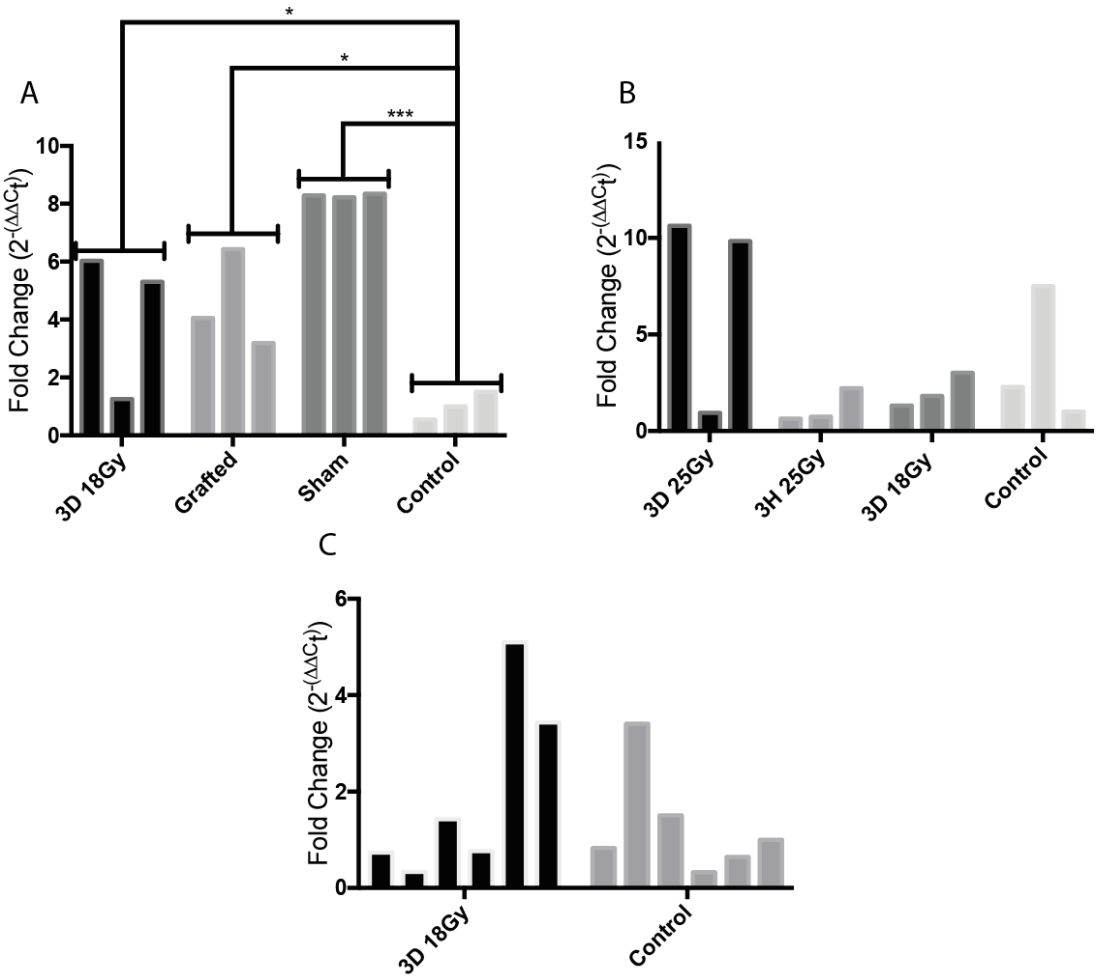

Figure 5.7: RT-qPCR for Interferon Gamma mRNA A) Samples (n=3 for each group) used for RNA-sequencing, showing an upregulation compared to non-irradiated control in all sample groups. Samples 3 days after 18Gy irradiation (3D 18Gy; p = 0.0365); samples irradiated (18Gy), grafted with satellite cells 3 days later, collected 2 days later (Grafted; p = 0.0235); and sham injected samples, irradiated (18Gy), injected with medium 3 days after irradiation, and collected 2 days later (Sham; p= 0.0004). B) Samples employed for PCR arrays include samples irradiated 25Gy and collected 3 days later (3D 25Gy); 25Gy irradiated and collected 3 hours later (3H 25Gy); 18Gy irradiated and collected 3 days later (3D 18Gy) and non-irradiated controls: no significant changes in expression are observed. C) Comparison between all 18Gy IR samples and controls: no significant change in interferon gamma expression.

5.3.2) Interferon Regulatory Factor 7

Interferon regulatory factor 7 (IRF7) was identified as a major network regulator in the networks produced comparing 3 day irradiated samples to non-irradiated controls, and was significantly upregulated (section 4.2). However, it was not significantly upregulated when comparing 3 day 18Gy irradiated samples to controls in the micro-arrays.

RT-qPCRs for Irf7 on the mRNA used for RNA-sequencing was consistent with the results seen in the RNA-seq data (figure 5.8a) with muscles collected 3 days after 18Gy irradiation showing a mean fold change of 19.29 (SEM: ±7.4; n: 3; p: 0.0421) compared to controls, grafted muscles had an increase in Irf7 expression of 18.88 fold (SEM: ±1.91; n=3; p: 0.0466) and sham injected muscles showing a mean fold change of 26.65 (SEM: ±2.9; n:3; p: 0.0070). However, in the samples used for the micro-array (figure 5.8b) only those samples collected 3 days after 25Gy had a significantly higher level of Irf7 expression (mean fold change: 13.4; SEM: ±4.004; n=3) compared to those collected 3 hours after 25Gy (mean fold change: 1.742; SEM: ±0.4987; n=3; p: 0.0398) and 3 days after 18Gy (mean fold change: 0.9016; SEM: ±0.3409; n=3 p: 0.0332). These data suggest that the up-regulation of Irf7 after irradiation is not consistent between both experimental groups.

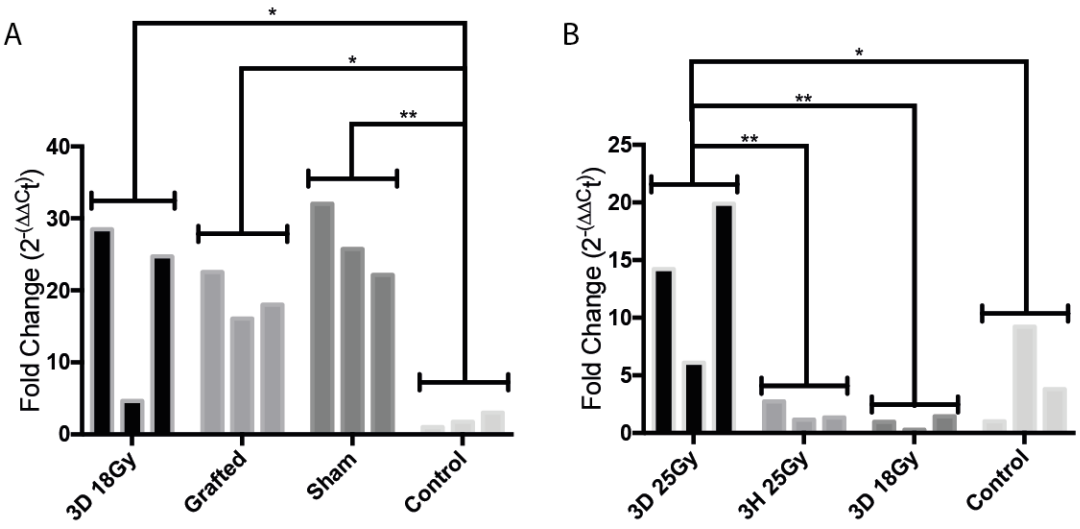

Figure 5.8: RT-qPCR for *Irf7* in samples used for RNA-sequencing (A) and the qPCR arrays (B). A) *Irf7* expression is significantly higher compared to non-irradiated controls in all the samples used for RNA-seq: 3 days post-18Gy (3D 18Gy; p = 0.0172); irradiated (18Gy) grafted 3 days later and collected 2 days post-graft (Grafted; p= 0.0191); irradiated (18Gy), sham injected 3 days later and collected 2 days post-injection (Sham; p = 0.0027). B) The results are not reproduced in the samples used for the qPCR arrays, with only samples collected 3 days after 25Gy (3D 25Gy) showing a significant increase in expression compared to: samples collected 3 hours post-25Gy (3H 25Gy; p = 0.0081); 3 days post-18Gy (3D 18Gy; p = 0.0056); and non-irradiated controls (control: p = 0.0307).

5.3.3) Leukaemia Inhibitory Factor

Leukaemia inhibitory factor (Lif) was significantly upregulated both in muscles collected 3 hours after 25Gy and 3 days after 18Gy (both time points are permissive for engraftment) when compared to controls. Additionally, it is also seen as an up-regulated gene (fold change: 2.06; p: 0.03) in the comparison of grafted samples to non-irradiated controls, and GO analysis classes it as a positive regulator of cell proliferation (Chapter 4, figure 4.37). Performing an RT-qPCR for Lif on the samples used for the microarrays shows the same pattern of expression (figure 5.9a), with Lif showing a significant fold change of 2.384 (SEM: ±0.01164; n=3; p: 0.0323) in samples collected 3 hours after 25Gy compared to controls; and a mean fold change of 2.464 (SEM: ±0.2688; n=3; p: 0.0323) in samples collected 3 days after 18Gy compared to controls. In contrast, in the non-permissive niche (3 days after 25Gy) the mRNA levels of Lif had returned to levels comparable to the non-irradiated tissues, with no significant difference between the two (mean fold change: 1.822; SEM: ±0.653; n=3; p: 0.0810).

Similarly, in the samples employed for sequencing, Lif was significantly upregulated 3 days after 18Gy irradiation compared to controls (mean fold change: 2.175; SEM: ±0.2809; n: 3; p: 0.0115). 5 days after 18Gy irradiation, in sham injected (mean fold change: 0.943; SEM: ±0.1143; n: 3; p: 0.5618) and grafted (mean fold change: 0.6862; SEM: 0.1532; n: 3; p: 0.3468) samples, the levels of Lif mRNA decreased and were not statistically significant when compared to controls. The levels of Lif in the samples collected 3 days after 18Gy irradiation were also

significantly higher when compared to grafted samples (p: 0.0022) and sham injected samples (p: 0.0061) (figure 5.9b).

Together, this indicates that Lif may be a significant factor in enhancing satellite cell engraftment after irradiation, as it is upregulated in the permissive host muscle compared to those which are not permissive for grafting (3 days after 25Gy and non-irradiated), and this is consistent between both sample groups (those used for sequencing and those used for the arrays). However, it is not known whether 5 days after 18Gy, when the levels of Lif return to control levels (sham injected and grafted), the niche is still permissible for satellite cell grafting.

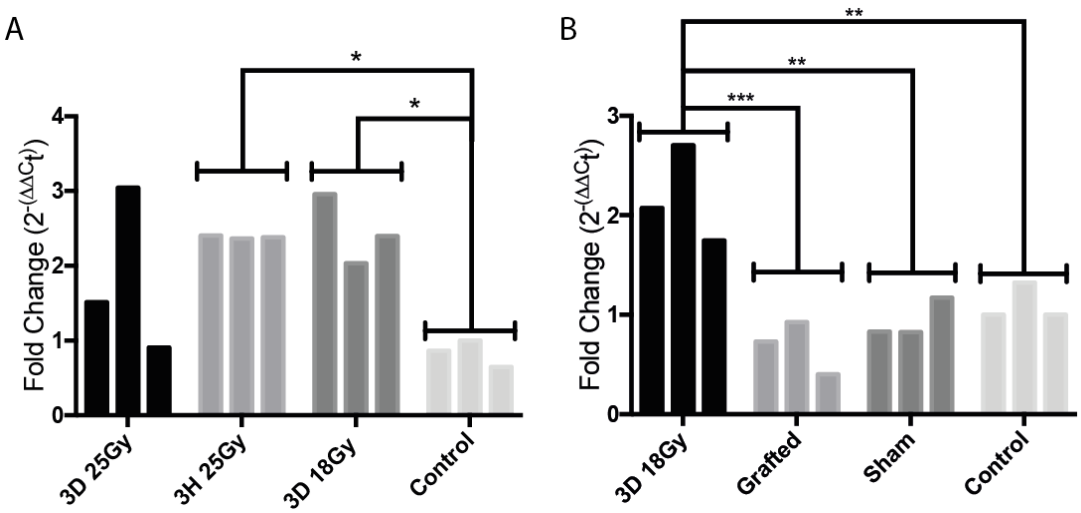

Figure 5.9: *Lif* mRNA expression in the samples used for the qPCR arrays (A) and for RNA-sequencing (B) measured by RT-qPCR. A) Both muscles collected at the points where they are permissive for satellite cell grafting, show a significant upregulation in the expression of *Lif* compared to controls. 3 hours post-25Gy (3H 25Gy) *Lif* increased by 2.334 fold which was significantly higher than non-irradiated controls ($p = 0.0139$), similarly 3 days after 18Gy Lif expression increased on average by 2.464 fold compared to non-irradiated controls ($p = 0.0109$). B) In the samples that were sent for RNA-sequencing only the group that is known to be permissive to satellite cell engraftment, 3 days after 18Gy (3D 18Gy) shows a significant increase in *Lif* expression compared to grafted ($p = 0.0004$), to sham injected ($p = 0.0012$) and non-irradiated controls ($p = 0.0029$).

5.3.4) Interferon Inducible Gene 204

Analysis of the RNA-sequencing data, in particular in those samples collected 3 days after 18Gy (section 4.2.1, figure 4.9), GO analysis showed the activation of an innate immune response, in particular the recognition of dsRNA, which I postulated could be present due to either the leaking of DNA into the cytoplasm of cells, or to the sensing of cell debris from dying cells, that are able to trigger an innate immune response. This was further supported by the priming of the anti-microbial immunity interferons alpha and gamma pathways. The interferon inducible gene 204 (Ifi204) and its human analogue interferon gamma inducible gene 16 (Ifi16) both perform the same function as sensors of cytosolic DNA, in particular dsDNA, and is essential in the activation of the type I interferon system activation in response to bacterial (Storek et al. 2015) and retroviral (Lee et al. 2012) infections, as well as priming the type I interferon response to promote anti-microbial innate immunity in response to DNA damage (such as radiological insults), where damaged DNA accumulates in the cytoplasm and is sensed by ifi204 (IFI16 in humans) to activate a type I interferon response (Härtlova et al. 2015).

To determine whether the radiation induced DNA damage could potentially be triggering the observed innate immune response, the levels of expression of this gene after irradiation was tested in both sample groups. The samples employed for RNA sequencing were consistent with the known role of ifi204 in priming the innate immune after DNA damage, as in all irradiated samples ifi204 was significantly upregulated compared to non-irradiated controls (figure 5.10a). 3 days post-18Gy, ifi204 showed a significant increase in fold change compared to non-irradiated controls (mean fold change: 4.475; SEM: $\pm$1.301; p: 0.0381); grafted samples similarly

showed a significant (p: 0.0115) increase in ifi204 expression compared to controls (mean fold change: 5.507; SEM: ±0.6116) as did sham injected samples (mean fold change: 6.254; SEM: ±1.16; p: 0.0050). There were no significant differences in ifi204 expression between any of the irradiated samples.

In stark contrast, the samples used for the micro-array (figure 5.10b) did not give results consistent with the above experiment. Here, only the samples collected 3 days after 25Gy showed a significant increase in ifi204 expression compared to controls (mean fold change: 4.159; SEM: ±0.7712; p: 0.0114). The remaining samples showed no significant increase in ifi204 expression. In those samples collected 3 days after 18Gy, there was a mean fold change of 2.314 (SEM: ±0.6715) which was not significantly higher than in non-irradiated tissues (p: 0.2058); those collected 3 hours post-25Gy irradiation showed a mean fold change of 2.561 (SEM: ±0.9234) which was not significant compared to non-irradiated controls (p: 0.1418). This suggests a significant difference in the response to radiation induced DNA damage between those mice used for RNA-sequencing and those used for the micro-arrays.

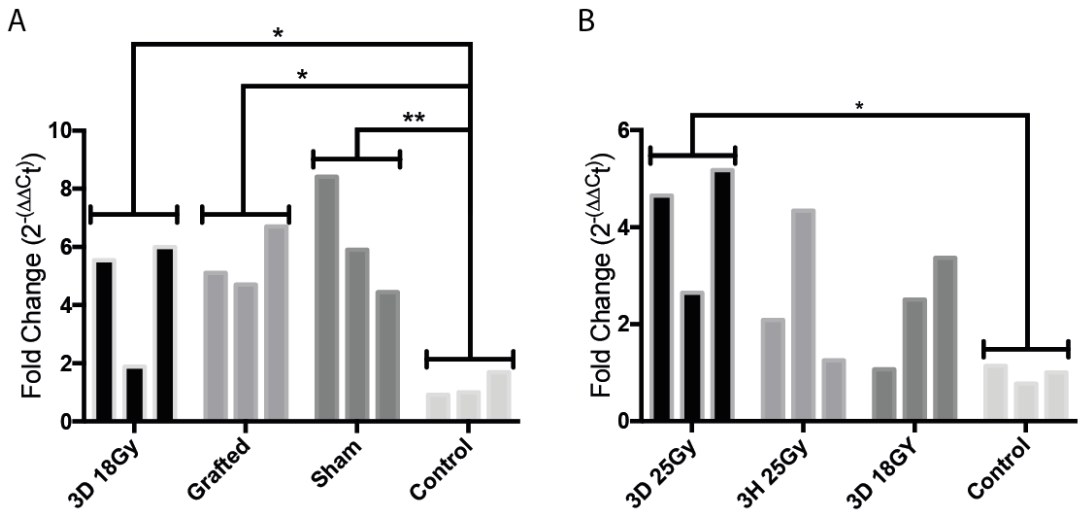

Figure 5.10: Changes in *Ifi204* mRNA expression in samples from the RNA-sequencing experiment (A) and the samples used for the qPCR arrays (B). A) I*fi204* is significantly upregulated compared to non-irradiated controls in samples collected 3 days after 18Gy irradiation (mean fold change: 4.475; SEM: ±1.301; p: 0.0381); in samples grafted 3 days after 18Gy irradiation and collected 2 days post-graft (mean fold change: p: 5.507; SEM: ±0.6116; p: 0.0115); and in sham injected samples (mean fold change: 6.254; SEM: ±1.16; p:0.0050). There is no significant difference in expression between any of the pre-irradiated groups. B) In the group employed for the PCR arrays, only those samples collected 3 days after a 25Gy dose of gamma radiation show a significant increase in *ifi204* expression compared to control samples (mean fold change: 5.159; SEM: ± 0.7712; p: 0.0114). None of the other comparisons show a statistically significant difference between any groups.

5.4) In-vivo testing of Leukaemia Inhibitory Factor (LIF) as a predictor of a permissive environment for satellite cell grafting

To determine whether the levels of Lif correlate with a permissive environment for satellite cell grafting, and if Lif alone is able to enhance satellite cell engraftment in non-irradiated hosts, a series of transplantation experiments were performed.

3FTGnLacZ satellite cells were grafted into 18Gy pre-irradiated muscles of *mdx*$^{nu/nu}$ hosts 3 days after irradiation (positive controls, n:6) and 5 days after irradiation (n:5), where Lif expression is restored to the same levels as non-irradiated muscles according to the micro-arrays and RT-qPCRs. As a negative control, donor satellite cells were grafted into non-irradiated *mdx*$^{nu/nu}$ hosts (n:6). A final set of grafts was performed where satellite cells were incubated with murine Lif (Lif: 10ng/ml in 0.1% bovine serum albumin carrier), on ice, for 1 hour before grafting them in medium containing Lif (10ng/ml in 0.1% bovine serum albumin carrier) into non-irradiated mdx$^{nu/nu}$ hosts muscles (n:6).

Representative images of each graft are shown in figure 5.11, and the results are displayed in figure 5.12. Satellite cells grafted into 18Gy pre-irradiated hosts 3 days previously produced a median of 161.5 (IQR: 233.5-13; n:6) fibres of donor origin, which was significantly larger (p: 0.0172) than the amount of muscle produced in non-irradiated muscles grafted with satellite cells alone (median: 12; IQR: 23.25-0; n:6), as expected.

When the satellite cells were grafted into muscles that had been irradiated 5 days previously, they produced a median of 148 (IQR: 215-44.5; n:6) fibres of donor origin, which was significantly more than those produced by the negative controls (p: 0.0419) and not significantly different from the positive controls (p>0.9999), indicating that 5 days after 18Gy irradiation the niche is still permissive. Therefore, the spike in Lif expression at the time points after irradiation where satellite cell engraftment is permissive, does not correlate with the efficiency of satellite cell engraftment.

Finally, muscles grafted with satellite cells incubated in Lif and grafted in Lif containing medium only produced a median of 43.5 (IQR: 54.75-12.25; n: 6) fibres of donor origin, which was not significantly different when compared to non-irradiated controls (p>0.9999) or grafts performed 3 days after 18Gy irradiation (p: 0.4413) or 5 days after 18Gy irradiation (p: 0.7127). Together, this indicates that lif may have the potential to enhance satellite cell engraftment, but it is not responsible for the augmentation of satellite cell engraftment after host muscle irradiation.

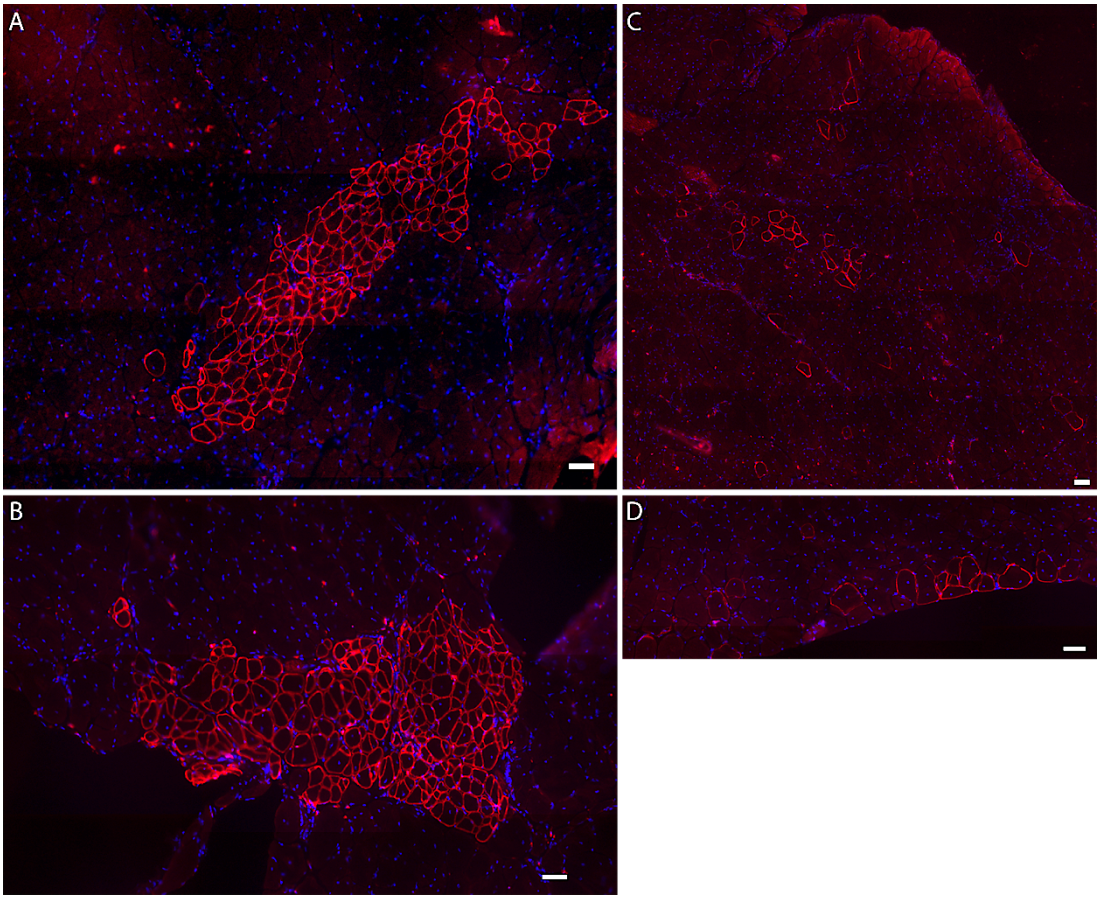

Figure 5.11: Representative images of dystrophin positive fibres of donor origin in *mdx*$^{nu/nu}$ host TA muscles grafted with *3FTGnLacZ*. A) Graft performed 5 days after 18Gy irradiation; B) Cells grafted 3 days after 18Gy irradiation; C) Cells incubated in 10ng/ml of LIF and grafted into a non-irradiated host with LIF; D) Satellite cells grafted into a non-irradiated host. Red = Dystrophin; Blue = DAPI; All Scale bars = 50µm.

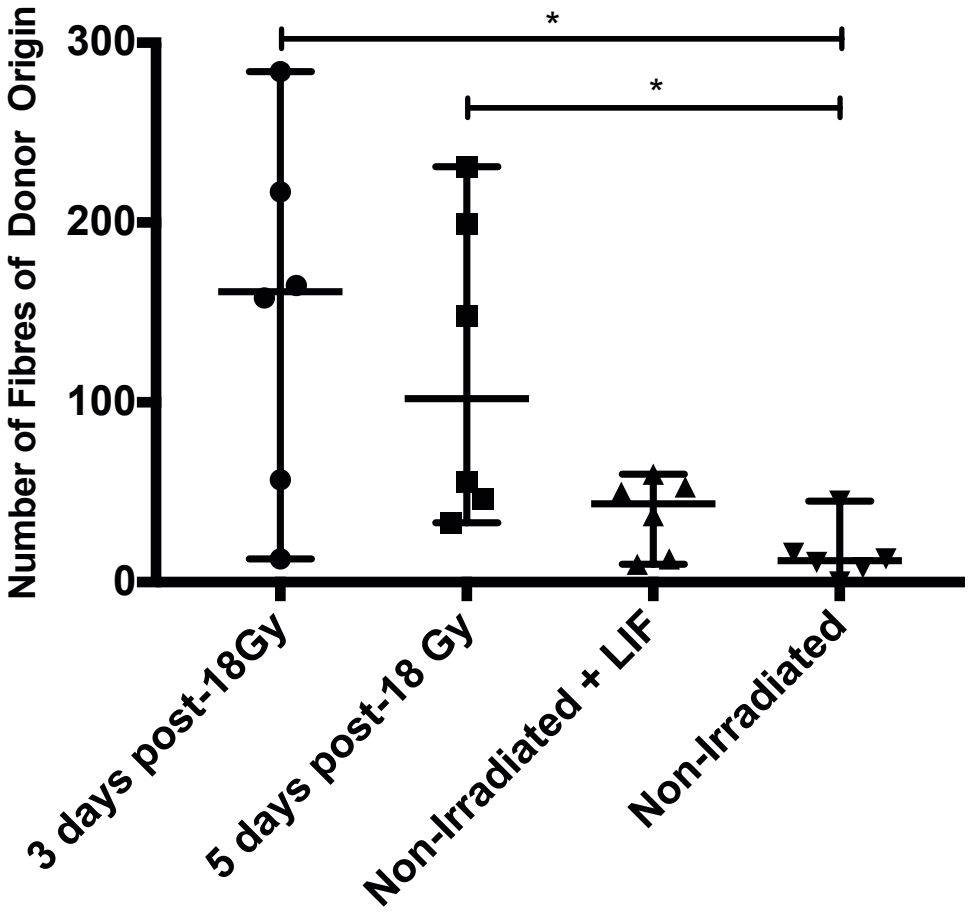

Figure 5.12: Quantification of the number of fibres of donor origin in *mdx*$^{nu/nu}$ host muscles grafted with *3FTGnLacZ* donor satellite cells either 3 days post-18Gy irradiation, 5 days post-18Gy, non-irradiated controls (Non-Irradiated) or into Non-irradiated hosts with leukaemia inhibitory factor (LIF). Grafts performed into muscles irradiated 3 days previously had a median of 161.5 (IQR: 233.8-46; n=6) fibres of donor origin, which is significantly higher than those grafted into non-irradiated hosts (median: 12; IQR: 23.25-6; n=6 p: 0.0131) but not significantly different from any other group. Muscles grafted 5 days after 18Gy irradiation had a median of 102 (IQR: 207-42.75; n=6) fibres of donor origin, significantly higher than non-irradiated controls (p: 0.0420) but was not significantly different to any other group. Satellite cells grafted into non-irradiated hosts with the addition of LIF produced a median of 43.5 (IQR: 54.75-12.25; n=6) fibres of donor origin, which was not significantly different to the grafts performed into non-irradiated or pre-irradiated hosts.

5.5 Discussion

The interpretation of the results from this chapter is challenging, as we observe two independent groups of *mdx*$^{nu/nu}$ mice experiencing the same sterile radiation injury but reacting differently to the same stimulus. The mice used for RNA sequencing experiments displayed a strong signal corresponding to an innate immune response mediated by type I and type II interferons. This inflammatory response is expected, as there is a well-established link between the DNA damage response and the priming of the innate immune system. This is mediated by damaged DNA leaks into the cytosol detected as a foreign biotic stimulus, or DAMPs released by apoptosing cells leading to the activation of anti-microbial defence mechanisms, such as the activation of type I and type II interferons and the increased expression of Toll-like receptors (reviewed by: Candéias & Testard 2015; Chatzinikolaou et al. 2014; Ratikan et al. 2015). The creation of this pro-inflammatory environment after irradiation by a cross talk between the DNA damage response and the innate immune system could explain the augmentation of satellite cell engraftment after irradiation.

However, when using another cohort of mdx$^{nu/nu}$ mice to characterise the interferon response using the RT^2-profiler arrays the results were inconsistent with the findings of the previous experiment. This could have been caused by the skewing of RNA-seq data by the unresponsive sample DB1625 (figure 4.1). It has already been established in previous chapters that the response to radiation that enables the augmentation of satellite cell engraftment is highly variable, as when performing transplantation experiments (chapter 2 or figure 5.11) some donor satellite cells transplanted into host muscles that had been irradiated with 18 Gy 3 days previously

(positive control grafts) failed to give rise to many fibres of donor origin. For example, in figure 5.11 some of the grafts performed 3 days after 18Gy irradiation produce between 165 to 284 fibres of donor origin, but two out of 6 grafts underperformed, giving rise to only 13 and 57 fibres of donor origin, which is similar to the levels of engraftment seen in negative controls (donor satellite cells grafted into non-irradiated host muscles). Furthermore, when RNA-sequencing was performed, this lack of responsiveness can be observed in the heatmaps produced by GSEA (figures 4.10, 4.11, and 4.12) where sample BD1625 shows patterns of gene expression that closely relate to the non-irradiated controls, and not matching to the response of the other two samples. This variability may have affected the results from the PCR arrays, especially as there was a low number of biological repeats employed (n=3), and that each array does not include technical replicates of the same sample.

Furthermore, the control samples do not appear to be reliable in the experimental cohort used for the PCR arrays. For example, gene expression levels of Irf7 determined by RT-qPCR shows that in this cohort, one sample has a 9-fold upregulation in Irf7 (figure 5.8b), which could easily skew statistically analysis and mask any changes in gene expression in the treated samples. Interferon gamma appears to behave in a similar pattern, with one control group sample showing a 7.5-fold increase in expression.

In the irradiated samples this variability is also apparent. In the samples used for RNA-sequencing, 3 days after a dose of 18Gy two of the samples display a 6-fold and 5-fold increase in the expression of interferon gamma, but one had only a 1.25-fold upregulation. Similarly, in the array group of samples, two of the three-day irradiated samples show a 1.3 and 1.8-fold upregulation, while the remaining sample

had a 3-fold upregulation. The same is seen in samples collected 3 days after 25Gy, where two of the samples show an almost 10-fold upregulation of interferon gamma, but one sample is down-regulated compared to controls (0.94-fold change).

The variability in the inflammatory phenotype of non-irradiated mice suggests that a higher number of samples may be needed to obtain statistically significant results using the RT^2 profiler arrays. However, this variability, combined with the knowledge that irradiation does not greatly enhance satellite cell engraftment in non-dystrophic mice (chapter 3, figure 3.8), and the variability in gene expression patterns in response to ionising radiation (for example the un-responsive sample (BD1625) discussed previously) suggests that the level to which gamma radiation is able to enhance satellite cell engraftment is dependent on either the underlying inflammatory phenotype, or the pathology of the muscle being irradiated. If a pool of mitotically active cells (i.e. a pool of cells highly sensitive to radiation damage) is required to enhance engraftment as suggested by the TUNEL assays in chapter 3, then it would be reasonable to hypothesise that those *mdx*$^{nu/nu}$ mice with a milder pathology at the time of irradiation might not be sufficiently susceptible to radiation damage, therefore failing to raise the required inflammatory response to a level that might enhance satellite cell engraftment.

Furthermore, underlying differences in the response to ionising radiation are highlighted by the expression Ifi204. This protein and its human homologue (IFI16) have been associated as a sensors for DNA damage (Härtlova et al. 2015; Ouchi & Ouchi 2008), in particular detecting damaged DNA that leaks into the cytosol. Upon detection it triggers a type I interferon response. Ifi204 is consistently upregulated in all the irradiated (3 days post-18Gy, grafted, and sham injected) samples from the

cohort of mice used for the RNA-sequencing (figure 5.10a) experiments, which is expected after hind limb muscle irradiation. Furthermore, it shows consistency with RNA sequencing data, with sample BD1625 (which seemed unresponsive to treatment in RNA-seq data) having non-elevated levels of ifi204 compared to the remaining samples in the 3-day post-18Gy irradiated group.

On the other hand, ifi204 was not significantly upregulated in 2 of the 3 irradiated samples used in the micro-arrays (3 days post-18Gy and 3 hours post-25Gy), suggesting that the TA muscles of these mice were less susceptible to radiation injury than the previous cohort (figure 5.10b). This would explain the high variability in gene expression patterns, as well as the variability in the number of fibres of donor origin after transplantation.

From the information extracted from the micro-arrays, it is clear that Lif was significantly upregulated at the time points where satellite cell engraftment was possible, and this was further confirmed by individual RT-qPCRs. Three days after 25Gy, when the niche is no longer permissive, the levels of Lif drop to levels that are not significantly higher than those in non-irradiated controls, whereas Lif is elevated 3 days after 18Gy (figures 5.9b). In the samples used for sequencing, the permissive muscles (3 days post-18Gy) also shows a significant increase in Lif expression, which is restored to control levels in sham injected and grafted samples (figure 5.9a), which can be interpreted as a decrease in Lif expression 5 days after irradiation.

Interestingly, Lif has been shown to promote the survival of cultured male C57BL10/ScSn myoblasts upon transplantation into female C57Bl10/mdx mice (Hunt et al. 2011). Alginate rods carrying Lif (delivering 5ng/lif per day) implanted subcutaneously have also been shown to enhance myoblast proliferation, survival,

and muscle regeneration after crush injury in-vivo (White et al. 2001). These rods also enhanced the incorporation of C57BL10/ScSn myoblasts into the muscle of *mdx* mice (White et al. 2001). Therefore, the observed increases in Lif expression at the time of satellite cell engraftment (average approximately 2-fold) may be facilitating the survival of myoblasts of donor origin upon transplantation. To determine if this was the case, a series of transplantations were performed. From these we can conclude that Lif does not need to be elevated within host muscle to make them a permissive environment for grafting, as 5 days after 18Gy irradiation, where Lif levels decline, donor satellite cells engraft as efficiently as they do into host muscles at 3 days after 18Gy irradiation (figure 5.12). Grafting freshly isolated satellite cells with Lif (10ng/ml) into non-irradiated host muscles does not significantly augment engraftment, although it does show a tendency towards enhanced engraftment, as it is not significantly different either from grafts into non-irradiated controls or from 3 day pre-irradiated grafts. This suggests that, as previously described in the literature, Lif could be used to enhance engraftment if it were delivered by a vehicle that would allow steady release over a prolonged period of time, such as alginate carriers, as shown by White et al 2001.

Alternatively, the observation that satellite cells engraft 5 days post 18Gy irradiation could suggest the present of senescent cells releasing an SASP that enables satellite cell engraftment. This is supported by the observations of Le Roux et al. (2015) who showed a transitory increase in the number of senescent cells within skeletal muscle after cardiotoxin injury which remained up to 10 days post injury (DPI), and significantly decreased by 21DPI. This suggests that these cells may play a role in muscle regeneration after injury. Therefore, the enhanced engraftment

at 5 days post irradiation suggests that the augmentation of satellite cell engraftment may be mediated by the appearance of a transient population of senescent cells and their associated secretory phenotype, in accordance to the findings by Le Roux et al. However, further research is needed to ascertain if at 5 days post irradiation a population of senescent cells is still present in irradiated muscles.

Taken together, these data suggest that high Lif expression is not predictive of a niche that is permissive for satellite cell engraftment. However, data from RNA-sequencing combined with the results from the satellite cell graft 5 days after irradiation, suggest that an inflammatory response is triggered that steadily increases up to 5 days after 18Gy irradiation. A combination of pro-inflammatory cytokines such as TNFα, Interferon gamma, the IL-6 family of cytokines, triggered by host muscle irradiation, combined with loss of host satellite cells, are likely to be mediating the augmentation of donor satellite cell engraftment after irradiation. However, further research will be required to ascertain which pathways are essential to trigger this effect.

Chapter 6 - General Discussion

6.1) Background

The potential of myoblast or cell therapies for the treatment of muscular dystrophies is severely limited by the hostility of skeletal muscle to accept grafted cells unless the host has been modulated prior to the injection of donor cells (Morgan et al. 2002; Boldrin et al. 2012; Meng et al. 2015). Furthermore, the type of modulation required for enhancing engraftment is dependent of the cell type to be grafted. Meng et al 2015 showed that human skeletal muscle-derived pericytes or CD133+ cells used for intramuscular transplantation into the *Tibialis Anterior* (TA) *Rag2-/γ chain-/C5-* mice or *mdx*$^{nu/nu}$ produce significantly more nuclei and muscle fibres of donor origin in host muscles that had been modulated by cryoinjury or irradiation and cryoinjury, than by irradiation alone, and irradiation had no additive effects on transplantation efficiency than cryodamage alone (Meng et al. 2015). Furthermore, there is also an influence of the host strain on the efficiency of donor myoblast engraftment, with both CD133+ cells and pericytes giving rise to significantly more muscle of donor origin in the more highly immunodeficient *Rag2*$^{-}$*/γ chain*$^{-}$*/C5*$^{-}$ mice than in *mdx*$^{nu/nu}$ mice (Meng et al. 2015).

Conversely, conditionally-immortal mouse H2K-18 myoblasts (Morgan et al. 1994) produce more muscle of donor origin in pre-irradiated *Rag2*$^{-}$*/γ chain*$^{-}$*/C5*$^{-}$ and *mdx*$^{nu/nu}$ mice (Morgan et al. 2002) than in non-irradiated muscles of the same mouse strain. If immortalized C2C12 myoblasts (Yaffe & Saxel 1977) were grafted into *mdx*$^{nu/nu}$ pre-irradiated muscles, they formed macroscopic tumours, but not when

grafted into non-irradiated muscles. Similarly to human donor cells, there was a host strain specific effect, with pre-irradiation failing to enhance the engraftment of H2K-18 conditionally immortalised myoblasts in the beige/nu/Xid mouse (Morgan et al. 2002).

Boldrin et al. 2012 performed a rigorous and systematic study on *mdx*$^{nu/nu}$ mice to determine the effect of the host muscle environment on donor satellite cell engraftment. They used five different regimes to modulate host muscle: barium chloride, cardiotixin, notexin, cryoinjury, and irradiation, to test their effects on donor satellite cell engraftment. Myotoxins (notexin, cardiotoxin, and barium chloride) destroy muscle fibres but preserve the muscle fibre basal lamina, nerves, blood vessels, and satellite cells (Harris 2003). Cryoinjury destroys local cells at the injury site but preserves the basal lamina of muscle fibres (Grounds & Yablonka-Reuveni 1993). However, following cryoinjury, skeletal muscle is capable of regeneration, indicating that at least some satellite cells survive the injury, or that they move into damaged areas from either non-damaged areas of the same muscle, or neighbouring muscles. High doses of radiation applied locally to skeletal muscle preserves the post-mitotic muscle fibres, but reduces the growth of the muscle and other surrounding tissues such as bones. The majority of satellite cells are radiation sensitive and die shortly after irradiation (Boldrin et al. 2012) but a minority survives and can be recruited to muscle regeneration. However, these cells are rare within the skeletal muscle of *mdx* mice (Gross & Morgan 1999; Heslop et al. 2000).

Boldrin's experiments concluded that cardiotoxin, notexin, or cryoinjury did not allow grafted donor satellite cells to produce significantly more muscle of donor origin than the very small amount found in non-injured host muscles (Boldrin et al.

2012). In contrast, when the host muscle had been irradiated with 18Gy of gamma radiation, donor satellite cells contributed efficiently to muscle regeneration when grafted either immediately after irradiation, or up to 3 days after irradiation. At higher doses (25Gy) engraftment was effective immediately, but not 3 days later when the host's satellite cells are completely ablated (Boldrin et al. 2012) indicating a dose and time dependent effect. In addition, they found no change in the area of inflammation either immediately or 3 days after irradiation, and a cytokine expression array showed no changes in cytokines that might be responsible for satellite cell engraftment.

This thesis aimed to expand on the work performed by Boldrin et al 2012, by determining if the host muscle pre-irradiation was able to effectively enhance satellite cell engraftment when applied to normal (non-dystrophic) hosts compared to *mdx*$^{nu/nu}$ hosts; which cellular component within the pre-irradiated host muscle is critical to mediate this effect, and determine which pathway(s) may be altered that enable the augmentation in receptivity of the host muscle to donor cells.

Taking into account that Boldrin et al. found no significant changes in the inflammatory area of pre-irradiated mdx$^{nu/nu}$ muscles, and that cytokine arrays revealed no significant changes in cytokine expression, I sought an explanation that would be independent from an inflammatory response. Since severe radiological insults, such as 18Gy and 25Gy, mainly results in cell death, I hypothesised that dying cells within the tissue could be releasing signals that may promote the proliferation of adjacent cells, as observed in several organisms, including mice (see: Revesz 1956; Li et al. 2010; and discussed in section 1.7.1) and might therefore promote the proliferation of grafted satellite cells. This is termed apoptosis induced proliferation,

and in mammals it has been associated with a caspase dependent release of prostaglandin E_2 and a subsequent cross talk with the Wnt signalling pathways (section 1.7.2; Li et al. 2010). Alternatively, these cells may not be apoptotic, but instead be entering a state of cellular senescence due to extensive DNA damage after irradiation (section 1.9, figure 1.13).

In this chapter the results will be consolidated, placed in the context of current knowledge, and their contribution to the field of cell therapies for muscular dystrophies will be discussed.

6.2) Satellite Cell Engraftment Efficiency is Modestly Augmented in Non-Dystrophic Mice

In chapter 3, satellite cells derived from *ßactinGFP* donors were grafted into non-irradiated *C5$^-$/γ chain$^-$/Rag2$^-$* hosts, and pre-irradiated *mdx$^{nu/nu}$* and *C5$^-$/γ chain$^-$/Rag2$^-$* hosts (figures 3.8 and 3.9). Grafting satellite cells into 18Gy pre-irradiated *C5$^-$/γ chain$^-$/Rag2$^-$* host muscles led to an extremely modest increase in the number of fibres of donor origin produced compared to non-irradiated controls (figure 3.9b). As expected, transplantation into pre-irradiated mdx$^{nu/nu}$ hosts produced large areas of muscle of donor origin, producing a significantly higher number of fibres of donor origin than satellite cells grafted into either pre-irradiated or non-irradiated *C5$^-$/γ chain$^-$/Rag2$^-$* (figure 3.9a).

In contrast to the findings described chapter 3, where satellite cell engraftment into pre-irradiated non-myopathic host muscles was negligible (median = 7 fibres of donor origin), Morgan et al 2012 found that H2K-18 myoblasts grafted into 18Gy pre-irradiated *C5$^-$/γ chain$^-$/Rag2$^-$* formed significantly more muscle of

donor origin than those grafted into non-irradiated hosts. These same myoblasts grafted into pre-irradiated non-myopathic beige/nu/Xid mice (Zietman et al. 1991) led to no significant increases in the formation of muscle of donor origin compared to their non-irradiated controls, highlighting the impact of the host strain on the ability of radiation to enhance cell grafting into the tissue. Beauchamp et al. 1999 used $5x10^5$ radio-labelled H2K-18 myoblasts derived from male mice, and grafted them into 18Gy pre-irradiated female *mdx*$^{nu/nu}$ mouse muscles to characterise the dynamics of myoblast transplantation. They showed that, 1 hour after injection of the donor myoblasts, only 30% of the grafted myoblasts remained, as measured by the levels of the radiolabel and Y chromosome content. 8-12 hours after transplantation, a second phase of donor cell death occurred, reducing the total number of donor myoblasts present in the tissue to 1%. The remaining cells then started proliferating 48 hours after their transplantation, as measured by Y chromosome content. They then further demonstrated that host muscle pre-irradiation does not enhance myoblast survival, as in both pre-irradiated and non-irradiated muscles there was a rapid and equivalent loss of Y chromosome and radiolabel. Instead they found that host pre-irradiation was able to enhance the proliferation of grafted myoblasts 24 hours after grafting.

The drastic changes in the efficiency of both myoblasts and freshly isolated satellite cells to engraft between pre-irradiated muscles of different host strains suggests that the mechanism that enhances cell proliferation is activated (or inhibited) to a different extent between mice of differing genetic backgrounds, immunodeficient status and pathologies, and different cell types might be more sensitive than others to this stimulus. For example, the mitogenic signals received by

H2K-18 cells within pre-irradiated *mdx*$^{nu/nu}$ hosts and *C5*$^{-}$/γ *chain*$^{-}$/*Rag2*$^{-}$ might be sufficient to encourage their proliferation, but the levels of this mitogen present in the beige/nu/Xid might not be sufficient to trigger the wave of proliferation required for enhanced engraftment. Similarly, freshly isolated satellite cells, of which only a very small amount are grafted (400, Boldrin et al. 2012) compared to myoblast transfer experiments (5x10^5 cells , Morgan et al. 2002; Beauchamp et al. 1999), would require a significant mitotic stimulus to populate the host muscle. I hypothesise that the mechanism that is responsible for satellite cell engraftment varies in its intensity depending on the radiosensitivity of the host strain. Therefore, although it might be activated within *C5*$^{-}$/γ *chain*$^{-}$/*Rag2*$^{-}$ pre-irradiated muscles, the level to which this activation occurs might not be sufficient to encourage donor satellite cells to proliferate to the same extent as observed within the *mdx*$^{nu/nu}$ host, thus leading to only a modest enhancement in the production of muscle of donor origin when compared to non-irradiated *C5*$^{-}$/γ *chain*$^{-}$/*Rag2*$^{-}$ mice.

This variability in the response of different mouse strains to the same dose of ionising radiation is supported by existing literature, as there are known differences in radiosensitivity of different mouse strains. These differences have been observed in terms of lethality, genomic instability, DNA repair, and epigenetic aberrations. For example, Grahn & Hamilton (1957) compared the $LD_{50/30}$ (the dose expected to kill 50% of the animals in 30 days) of four different mouse strains (BALB/c, A/Jax, A/He, $C3H_f$/He, and C57BL/6 mice) and found that the dosage required to achieve the $LD_{50/30}$ after whole body irradiation varied by as much as 130 rad, equivalent to 1.3Gy. Roderick (1963) compared the radiosensitivity of 27 different mouse strains, which at 120 days of age were subjected to daily doses of 100r (1Gy) of X-irradiation

until they died. This experiment also showed significant differences in radiation resistance, allowing the author to rank all different mouse strains in accordance to their sensitivity to radiation exposure.

However, these differences are not only noticeable in lethality studies. There are also genetic differences in the resistance of mouse strains to the induction of genetic abnormalities. For example, cultured primary mammary epithelial cell cultures from the radiosensitive BALB/c mouse and the radioresistant C57BL/6 mouse that had been irradiated by a Cs-137 source to induce genetic aberrations display a rapid decline in the number of genetic abnormalities after irradiation. However, after 16 population doublings, cells from the BALB/c mouse displayed an increased frequency of chromatid-type breaks that remained for up to 28 population doublings. In contrast, cells from C57BL/6 mice showed no increases in the number of genetic aberrations after they were cleared in the initial a phase (Ponnaiya et al. 1997). The transcriptional prolife of irradiated mice also show significant variation. C57BL/6 and BALB/c mice exposed to weekly exposure to low doses of radiation (7.5cGy weekly for 4 weeks) showed opposing transcriptional signatures relating to proliferation, senescence, and microenvironment functions one month after exposure (Snijders et al. 2012). Changes in DNA methylation after 1Gy X-ray whole body irradiation over time between C57BL/6 and BALB and CBA mice have also been shown to be dependent on genetic background, as well as gender (Newman et al. 2014). S*cid* mice have been shown to have a hypersensitivity to ionising radiation due to significant deficiency in their ability to carry out repairs on chemically and radiation induced DNA double strand breaks (Biedermann et al. 1991).

Together, this supports the observed differences in the ability of ionising radiation to produce a produce a permissive niche for donor cell engraftment between different host strains and mouse cell types, as they will likely show differing responses to the radiation treatment, not only in intensity, but could even show opposing responses, as observed by Snijders et al. (1997).

6.3) The Percentage of TUNEL Positive Cells Correlates with Engraftment Efficiency

To test whether there might be a potential role for apoptosis induced proliferation in the augmentation of engraftment efficiency in skeletal muscle, the percentage of TUNEL positive cells (figure 3.3, 3.4, and 3.5) was quantified in $mdx^{nu/nu}$ and *C5*$^{-}$*/γ chain*$^{-}$*/Rag2*$^{-}$ mouse TA muscle under different irradiation regimes at different time points (figure 3.5). This showed that in the $mdx^{nu/nu}$ hosts there is a significant 10-fold increase in the percentage of TUNEL positive cells (TUNEL+ nuclei/total number of DAPI positive nuclei) at the time points after irradiation where the host muscle environment is considered permissive for satellite cell grafting (3 days post-18Gy and 3 hours post-25Gy). However, in the *C5*$^{-}$*/γ chain*$^{-}$*/Rag2*$^{-}$ mice, the percentage of TUNEL positive cells did not significantly increase 3 days after 18Gy irradiation compared to either non-irradiated controls or 1 month after an 18Gy dose of radiation. This correlates with the modest augmentation in engraftment efficiency seen in the pre-irradiated *C5*$^{-}$*/γ chain*$^{-}$*/Rag2*$^{-}$ muscles and suggests a role for dying cells in the augmentation of engraftment efficiency, as discussed in section 1.7 and demonstrated by studies on apoptosis induced proliferation (Li et al. 2010; Castellone et al. 2005; Donato et al. 2014). Interestingly, no TUNEL positive cells were

within the muscle fibres. If apoptosis or dying cells play a role in the augmentation of satellite cell engraftment, it is likely to be provided by the mononuclear cellular compartment of skeletal muscle, rather than by satellite cells or muscle fibres.

An important limitation is the determination of whether these cells are truly apoptotic. For this reason, in this thesis they have been referred to as dying rather than apoptotic cells. The TUNEL assay is based on the detection of double strand breaks in DNA (dsDNA) which are triggered by the degeneration of the nucleus during apoptosis. However, these breaks also occur in necrotic cells, while radiation damage is notable for being able to induce dsDNA breaks both through direct energy deposition by photons or by the nucleophilic attacks of OH radicals to the phosphate backbone and nucleobases of DNA, as illustrated in section 1.6.3.1 and figures 1.1, 1.2, and 1.3. Depending on the extend of DNA damage cellular senescence may also occur, and senescent cells would still show positive TUNEL staining. These problems could potentially be overcome by using staining for the executioner Caspase 3, and using markers of cellular senescence (such as $p16^{INK4a}$, acidic ß-galactosidase, and foci of H2AXγ) to differentiate these cells from being either apoptotic or senescent. However, Caspase 3 is required for muscle differentiation (Fernando et al. 2002) and within the *mdx*$^{nu/nu}$ mouse e there are constant rounds of degeneration and regeneration (which requires myogenic differentiation). Therefore, staining for Caspase 3 yields a high background that makes the identification of cells positive for nuclear caspase 3 impossible to objectively differentiate from those undergoing differentiation.

6.4) The Monocytic Cellular Fraction of *mdx*$^{nu/nu}$ Pre-Irradiated Muscles, and not the Myofibres, is Responsible for the Enhancement of Satellite Cell Engraftment

TUNEL assay experiments showed that only cells outside the basal lamina were TUNEL+. Boldrin et al (2012) also demonstrated that 3 days after 18Gy irradiation, most of the endogenous satellite cells have been cleared from the host muscle. Together, this indicates that if dying cells play a role in enhancing satellite cell engraftment, they are interstitial cells, not satellite cells.

The series of co-transplantation experiments performed in chapter 3 (figures 3.9 -3.16) sought to determine whether satellite cells alone (figures 3.9 and 3.11), single fibres (figures 3.12 and 3.13), or single cell suspensions from pre-irradiated *mdx*$^{nu/nu}$ muscles (figures 3.14 and 3.15), grafted in conjunction with donor *3F-nLacZ-2E* satellite cells, would enhance the production of muscle of donor origin within non-irradiated *mdx*$^{nu/nu}$ hosts. Both the satellite cell and single fibre co-transplants completely failed to enhance the production of muscle of donor origin when compared to non-irradiated controls, and the numbers of muscle fibres of donor origin were significantly lower than in the pre-irradiated controls. Together, this suggests that neither pre-irradiated satellite cells or single muscle fibres are able to enhance satellite cell engraftment.

However, single cell co-transplants, although giving no significant improvement, do show a trend towards an enhanced engraftment of satellite cells. Using the median of the positive controls (median: 77.5, IQR: 292.3-22.75) as a threshold for the definition of a successful graft, and taking into account that

maximum number of donor fibres observed in the 37 negative control grafts was only 46 fibres of donor origin, then 3 grafts in this co-transplant performed better than expected when compared to non-irradiated controls, forming 228, 96, and 90 fibres of donor origin. This suggests that on 3 occasions, the grafting of a single cell suspension from a pre-irradiated *mdx*$^{nu/nu}$ donor was able to enhance satellite cell engraftment. The largest increase was observed in the second replicate experiment (228 fibres of donor origin), and the remaining 2 were observed in the third experiment (96 and 90 fibres of donor origin), excluding the variability in response to ionising radiation as a factor as to why some of these grafts might have no increased satellite cell engraftment. It possible that in these 3 grafts, an optimal ratio of the cells mediating the enhanced engraftment were transferred together with the donor satellite cells into the non-irradiated host muscle. This could occur if, for example, a large pool of pro-inflammatory macrophages were grafted with the satellite cells, which have been shown to enhance human myoblast engraftment in immunodefcient host mice (Bencze et al. 2012). However, the composition of this single cell suspension derived from skeletal muscle is likely to be highly variable, and I did not characterise its composition.

The single cells preparation is a mixed cell population that may be separated into its component parts by techniques such as Fluorescent Activated Cell Sorting (FACS) or Magnetic-Activated Cell Sorting (MACS), which would allow the isolation of specific cell types for co-transplants. There are two reasons as to why neither of these techniques were deployed. The first matter is one of logistics. The preparation of freshly isolated satellite cells from single muscle fibres, in sufficient numbers for the experiments performed in this thesis, is a labour-intensive procedure that

requires near constant attention throughout the day. For example, each muscle fibre from the extensor digitorus muscle has on average 3-4 associated satellite cells (Collins et al. 2005). If 6 host mice are to be grafted in one experiment, which is equivalent to 12 grafts requiring 400 satellite cells each, this requires a minimum of 4800 satellite cells. Assuming 3.5 satellite cells per fibre, this means the manual isolation, counting, and stripping of 1372 single muscle fibres over the course of one day, to enable the transplants to be performed in the evening. This workload prevents a single experimenter from performing labour intensive methods in parallel for the isolation of pre-irradiated cell populations by FACS or MACS.

To overcome this, attempts were performed to isolate stromal cells from pre-irradiated *mdx*$^{nu/nu}$ mouse muscles and subsequently freeze them to be defrosted and used when required for transplantation. Here problems were encountered, as only a very small number of live cells could be isolated, and after thawing, no live cells remained. This was not surprising as the cells being isolated have been subjected to the stress of lethal doses of radiation (18Gy), enzymatic disaggregation, passage through a FACS machine, and the freezing and thawing procedure.

Since the cell type, or interacting cell types, responsible for the augmentation of engraftment efficiency are not known, I decided to begin experiments with a single cell suspension derived from pre-irradiated *mdx*$^{nu/nu}$ skeletal muscle. If significant improvements in the formation of muscle of donor origin were observed, then a more refined approach would be deployed. However, no significant increases in engraftment were observed, and due to logistical and technical limitations, the subdivision of this preparation into more refined fractions was not pursued.

In conclusion, the set of co-transplantation experiments is able to exclude both the single muscle fibre or endogenous irradiated satellite cells as playing a major role in the augmentation of donor satellite cell engraftment. The results from the single cell co-transplant did not significantly enhance donor satellite engraftment, but there are signs that under certain conditions, the mononuclear cellular fraction of pre-irradiated *mdx*$^{nu/nu}$ host muscles can enhance donor satellite cell engraftment. Additionally, this is consistent with the localisation of TUNEL+ cells described in chapter 3 sections 3.3, 3.4 and 3.5, suggesting that these damaged cells are responsible for enhancing donor satellite cell engraftment.

6.5) A Cross-Talk Between the DNA Damage Response and the Innate Immune System Is the Likely Mediator of the Augmentation of Donor Satellite Cell Engraftment

The results obtained from RNA sequencing experiments shows that pre-irradiated *mdx*$^{nu/nu}$ muscles are displaying the activation of the innate immune system and presenting an inflammatory response. When comparing muscles collected 3 days after 18Gy irradiation to non-treated controls (Chapter 4, section 4.2) the core network regulators of this network (figure 4.8) associate with the GO terms matching a response to virus, response to dsRNA, and an immune response (figure 4.9). Furthermore, GSEA reveals the activation of patterns of gene expression corresponding to both interferon alpha and interferon gamma. The core network regulators of sham injected muscles compared to non-treated controls (section 4.6) are also associated with the innate immune response and an inflammatory response (table 4.2). GSEA analysis shows that large groups of genes associate with the

interferon gamma and alpha response, along with the activation of TNFα signalling via NFκβ (table 4.13, figures 4.28, 4.29, and 4.31). When comparing grafted muscles to non-irradiated controls, the same expression profile is observed, with a core regulatory network (figure 4.36) associating with an immune response (appendix 4.1) while GSEA shows a gene expression profile that matches the response to interferons gamma (figure 4.39) and alpha (figure 4.41), together with TNFα signalling via NFκβ (figure 4.43). These patterns of gene expression are consistent with the activation of the innate immune system by crosstalk with the DNA damage response, as previously described in the literature (reviewed by: Pateras et al. 2015; Chatzinikolaou et al. 2014; Ratikan et al. 2015).

Traditionally, DNA damage, including the formation of dsDNA strand breaks, in the host genomic DNA triggers the DDR machinery by recruiting the MRE11-RAD50-NSB11 (MRN) complex together with the kinase ATM (section 1.6.3.1, reviewed by: Lavin et al. 2015; D'Amours & Jackson 2002; van den Bosch et al. 2003).The persistence of a DNA damage response encourages the presence of cytosolic sDNA and dsDNA. When DNA from the "immune-privileged" nucleus leaks into the cytoplasm it is detected by sensors of cytoplasmic DNA, such as Ifi204 (Härtlova et al. 2015) (IFI16 in humans) or Mre11, which traditionally belongs to the DNA repair MRN complex (Wu & Chen 2014). The accumulation and detection of cytoplasmic DNA then sets in motion the activation of type I interferons via the STING (stimulator of interferon genes) pathway, mediated by TBK1 and IRF3 (Härtlova et al. 2015; Wu & Chen 2014). This can be observed by the detection of patterns of expression matching "response to interferon alpha" in the gene set enrichment analysis (figures 4.10, 4.29, and 4.41) which belongs to the innate immune system.

The increased expression and release of type I interferons then primes the innate immune system of adjacent cells for an amplified response upon stimulation, in particular pattern recognition receptors such as Toll-Like receptors (Härtlova et al. 2015; Pateras et al. 2015). This priming of the innate immune system is clearly seen in the RNA sequencing data, where 3-day 18Gy irradiated samples show a significant upregulation of TLR3. 2 days later, in grafted and sham injected muscles, the number of significantly upregulated Toll-like receptors increases. Grafted muscles show significant increases in expression of TLR9, 13, 7, 8, 1 and 11 while sham injected muscles display the increased expression of TLR 9, 13, 7, and 3. These toll-like receptors will in turn be able to respond to Damage Associated Molecular Patterns (DAMPS) released by damaged cells within the host tissue and produce an inflammatory response. For example, activated TLR9 transmits its signal through MyD88 which activates the transcription factors NFκβ and Irf7 which are involved in the induction of inflammatory genes such as tumour necrosis factor (TNF), interleukin 6, and type I interferons (Chatzinikolaou et al. 2014). Furthermore, in accordance with these findings, satellite cells grafted 5 days after 18Gy irradiation engraft to a similar extent as do those grafted 3 days after irradiation (figures 5.11 and 5.12). This confirms that the inflammatory response seen 5 days after irradiation in sham injected and grafted muscles still provides a viable environment for donor satellite cell engraftment.

Additionally, this mechanism might explain the association of prostaglandin E_2 in apoptosis induced proliferation observed in previous reports (section 1.7.2). This is supported by previous reports indicating an important role for the TLR/MyD88 pathway in the generation of the tumour inflammatory environment (reviewed by:

(Pradere et al. 2014). Moreover, the disruption of the TLR adaptor protein MyD88 gene (*Myd88)* in mouse models has been show to suppress the sporadic appearance of intestinal tumors (Rakoff-Nahoum & Medzhitov 2007; Lee et al. 2010), colitis associated colon cancer (Uronis et al. 2009; Schiechl et al. 2011), gastric cancer (Kennedy et al. 2014), liver cancer (Naugler et al. 2007), and sarcomas (Swann et al. 2008). Notably, in the Apc^{Min} mouse, which develops spontaneous intestinal tumours in a COX1/COX2 and PGE_2 dependent manner (Chulada et al. 2000; Oshima et al. 1996), disruption of **MyD188** has been associated with supressed expression of COX2 and other cytokines crucial for the development of tumorigenesis (Rakoff-Nahoum & Medzhitov 2007). This suggests that the interplay of the DNA damage response with the innate immune system could lead to increased levels of PGE_2 expression via the increased expression and subsequent activation of Toll-Like Receptors, allowing the creation of the tumorigenic environment described by Morgan et al. 2002, and support the proliferation of grafted myoblasts (J R Beauchamp et al. 1999) and satellite cells (Collins et al. 2005; Boldrin et al. 2012). However, further work will be needed to confirm this.

In summary, radiological insult leads to a DNA damage response that cross talks with the innate immune system, priming pattern recognition receptors for an amplified response upon stimulation. This, in conjunction with DAMPs released by damaged cells within the pre-irradiated host, such as the TUNEL positive cells observed in chapter 3, leads to an inflammatory response that would enhance the proliferation, and delay the differentiation, of grafted satellite cells, therefore augmenting engraftment efficiency. This can be seen in figure 3.47, which is a network extracted from the comparison of grafted muscles to non-irradiated

controls, which matches the GO term for “positive regulation of cell proliferation”. Here, we see the presence of TLR4, with the TLR mediator MyD88 and several inflammatory cytokines such as IL-6 and IL-15. However, the possibility that a cross talk between the DNA damage response and the establishment of cellular senescence has not been excluded and further research would be required to determine whether senescence or DAMPs are mediating the inflammatory responses driving satellite cell engraftment.

6.6) Challenges in Validating RNA-sequencing Results

To validate the results from the RNA-sequencing experiments, a series of PCR arrays were performed on samples that were known to be permissive for satellite cell engraftment (3 hours after 25Gy and 3 days after 18Gy) and non-permissive (3 days after 25Gy and non-irradiated), with the expectation of seeing a strong interferon response in both permissive muscle environments that may indicate an upregulation of the innate immune system. However, the results from these were disappointing, yielding only a small number of significantly regulated genes between samples (section 5.2). This is further illustrated by the lack of separation of samples in different treatment groups according to their patterns of gene expression when unsupervised hierarchical clustering was performed. These findings suggest that the response to radiation might be highly variable depending on the underlying muscle pathology.

RT-qPCRs on selected genes in the samples that were employed for RNA sequencing showed that this cohort of mice was internally consistent with the sequencing results. However, the response of the second group of mice employed

for the micro-arrays did not match the expected results from sequencing. This is likely due to the large amount of variation in gene expression seen within samples of the same treatment group, suggesting that a larger number of samples may be required to validate the previous results.

In spite of these inconsistencies, the expression of leukaemia inhibitory factor was increased in both cohorts of muscles collected at the stage after irradiation where the niche is permissive for satellite cell engraftment, and downregulated in the samples that were non-permissive (figure 5.9a). Similarly, in the muscle samples employed for RNA-sequencing, a similar pattern of expression was observed, with LIF being upregulated 3 days after 18Gy compared to non-irradiated controls (figure 5.9b). Since the levels of LIF expression were downregulated in both grafted and sham injected muscles the hypothesis was made that 5 days after irradiation, the environment might no longer be permissive for satellite cell grafting.

However, when satellite cells were grafted into 5-day irradiated muscles, the grafting efficiency was comparable to the 3 day 18Gy irradiated hosts, and significantly improved compared to both non-irradiated controls and satellite cells grafted with LIF (figure 5.11 and 5.12). This experiment therefore supports the evolution of gene expression patterns in the RNA sequencing data, where 5 days after irradiation there appears to be an inflammatory response that should encourage satellite cell engraftment. Therefore, the levels of LIF expression do not predict the permissiveness of the host muscle environment for satellite cell engraftment.

6.7) Conclusions

The main aims of this thesis were to determine the cell type and pathway that are responsible for the augmentation of satellite cell engraftment after irradiation. The experiments described here suggest a role for damaged or dying cells in enhancing engraftment, however the specific cell type responsible for this has not been determined. RNA-sequencing allowed us to develop a working hypothesis as to how host-muscle pre-irradiation may enhance donor satellite cell engraftment. Unfortunately, the validation experiments that followed were disappointing and, although the pathway has support in the literature, its role in the augmentation of satellite cell engraftment remains to be confirmed.

The data presented in this thesis suggests a two-stage mechanism, where DNA damage caused by irradiation leads to the release of DNA from the immunoprivileged nucleus and is detected by cytosolic DNA sensors. These sensors act via the STING pathway which leads to the activation of a type I interferon response. The secretion of type I interferons into the extracellular environment then primes the innate immune system in adjacent cells. The pattern recognition receptors, such as Toll-Like receptors, of these primed cells are then stimulated by the debris of the IR damaged tissue (for example, from dying cell or fragments from IR damaged extracellular matrix). The TLR receptors then signal through their interferon regulatory factors (IRFs) to promote the expression of inflammatory cytokines. This inflammatory environment then delays satellite cell differentiation and encourages their proliferation. The extent of this priming also appears to depend on the radiosensitivity of the host muscle, which is determined by the genetic

background of the host, and the underlying pathology within the host muscle at the time of irradiation. From the released cytokines, LIF does not appear to play a major role in enhancing satellite cell engraftment, and the effect is likely to be mediated by a multitude of inflammatory factors acting together, as shown by Fu et. al (2015). However, future work will be required to isolate the required pathways and signalling molecules.

6.8) Future Work

Determining which specific pathway leads to the augmentation of satellite cell requires significant work beyond the time, scope, and resources of this thesis. Although significant further work is required to determine the precise mechanism by which radiation enhances satellite cell engraftment, this section will provide some suggestions as to how future work may evolve.

6.8.1) Validating RNA-Sequencing Data at the Protein Level

6.8.1.1) Concentration of Type I and Type II Interferons in Pre-Irradiated Hosts

A series of ELISAs should be performed to measure the concentration of type I interferons (alpha and beta) and type II interferon (IFN gamma) after *mdx*$^{nu/nu}$ host muscle irradiation to determine if their concentration is indeed increased. This should also help determine optimal concentrations that may be used to enhance donor satellite cell engraftment by grafting them with a cocktail of pro-inflammatory cytokines as done with primary myoblasts by (Fu et al. 2015). The levels of interferon release should be determined in pre-irradiated host muscles at the optimal time points for engraftment, as well as those time points after irradiation where engraftment is no longer viable and in non-irradiated controls. It is predicted, based

on RNA-sequencing data, that after irradiation there should be increases in the intramuscular concentrations of type I and II interferons.

Additionally, it would also be interesting to compared the increases in intramuscular interferon concentrations between different strains of non-myopathic immunodeficient mice, such as *C5$^-$/γ chain$^-$/Rag2$^-$* and beige/nu/Xid, to determine if the levels of interferon release are affected by genetic background, muscle pathology or immunodeficient status and if this correlate with the number of TUNEL+ cells in the tissue.

6.8.1.2) Assessing the Activation of the STING Pathway

To determine the activation of the STING pathway, a series of western bolts could be performed on samples from non-irradiated, 3-day 18Gy pre-irradiated mice and 1-month pre-irradiated *mdx$^{nu/nu}$* mouse muscles. These should include quantification of TBK1 and pTBK1 Ser^{172} as well as IRF3 and pIRF3 Ser^{396}, and also comparing the levels of dimerized IRF3. These are key mediators in the activation of type I interferon release upon detection of cytosolic DNA (Tanaka & Chen 2012).

6.8.1.2) Assessing the Role of TUNEL+ Cells

The measurements of the level of TUNEL positive cells in Chapter 3 suggested a correlation between the percentage of dying or damaged cells in the host tissue and the efficiency of satellite cell transplantation. In chapter 5 (figure 5.12) it was demonstrated that satellite cell engraftment is still viable 5 days after irradiation. Therefore, I believe that a determination of the percentage of TUNEL positive cells in the host tissue 5 days after 18Gy irradiation would be very informative. Furthermore, I suggest this should be performed by flow cytometry to provide more accurate measurements at all the time points tested and in the *C5$^-$/γ chain$^-$/Rag2* mouse, to

determine if they do truly play a role in the augmentation of the formation of muscle of donor origin.

Furthermore, it would be important to determine whether these TUNEL positive cells are apoptotic or senescent cells. To assess senescence staining for biomarkers of cellular senescence should be carried out. These could include the $p16^{INK4a}$ tumor suppressor protein, which is activated during cellular senescence and is one of the most specific markers of senescence *in vivo* (Krishnamurthy et al. 2004). However, this marker has its limitations, for example $p16^{INK4a}$ independent senesnce can occur *in vitro*, and can be expressed in non-senescent cells (such as cancer cells) (Sharpless & Sherr 2015). Therefore, this marker should be used in conjunction with other biomarkers of cellular senescence such as *acidic **ß**-galactosidase* and nuclear foci of H2AXγ. Further *in vivo* testing of the relevance of senescent cells to the augmentation of satellite cell engraftment could also be determined by the treatment of mice with senolytic compounds such as ABT263 (Chang et al. 2016) as used by Chiche et al. (2017) to determine the role of senescent cells in allowing *in vivo* reprogramming within skeletal muscle. This could be delivered prior and after host muscle pre-irradiation and satellite cell engraftment. This would allow the confirmation of the role of senescent cells in enhancing satellite cell engraftment, as if the efficiency of engraftment is reduced in hosts muscles treated with ABT263 is reduced, a clear correlation would be established between the presence of senescent cells after irradiation and the engraftment efficiency of satellite cells.

6.8.2) Determining the Relevance of the DNA Damage Response and the Innate Immune System in Augmenting Satellite Cell Engraftment

Based on the results of this thesis and published literature, a sequence of molecular events that lead to an inflammatory response as a consequence of DNA damage has been suggested. Key to the initiation of this mechanism is the detection of leaked cytosolic DNA within the cytoplasm, which can be detected by a multitude of cytosolic DNA sensors. Key to the translation of cytosolic DNA detection in the cytoplasm to changes in gene expression is the protein STING (encoded by the transmembrane protein 173 (Tmem173), also known as Mita, MPYS, or ERIS) which enabled TBK1 to phosphorylate IRF3 and translocate to the nucleus to induce type I interferon production upon detection of cytosolic DNA.

To determine the relevance of this mechanism in inducing the inflammatory response that may enhance satellite cell engraftment, I propose the elimination of STING in the m*dx*$^{nu/nu}$. This could be achieved by cross breeding with homozygous STING knockout mice, such as the Goldenticket (Gt) mutant mouse, which harbours a variant of STING that functions as a null allele and fails to produce detectable protein (Sauer et al. 2011), with *mdx*$^{nu/nu}$ mice. This will be a lengthy process, that will be further hampered by the fact that nude females are not successful mothers female infertility caused by the nude mutation. Alternatively, iPSCs derived from *mdx*$^{nu/nu}$ mice could be generated, and STING directly removed via CRISPR/Cas9. These iPSCs can then be employed to generate chimeric mdx$^{nu/nu}$ Tmem173^{gt} mice which can be crossed until the triple mutant is obtained. The triple mutant mice can then be irradiated and employed for satellite cell transplantation experiments. If a

reduction in engraftment efficiency after irradiation is observed, this will confirm the crucial requirement of a cross talk between the DDR and the innate immune system in enhancing satellite cell engraftment. However, this methodology will be a lengthy and expensive process.

6.8.3) Determining the Role of Interferon Gamma in the Augmentation of Satellite Cell Engraftment

One of the major pathways detected in the sequencing data was a response to interferon gamma, although Interferon gamma itself was not consistently increased at the mRNA level after irradiation. However, if its concentration is found to be increased in pre-irradiated host muscles at the protein level by the use of ELISAs, I suggest transplanting donor satellite cells deficient in the interferon gamma receptor, such as those isolated from the *Ifngr1*^{tm1Agt}*,* into pre-irradiated *mdx*$^{nu/nu}$ hosts. This would allow us to determine the importance of interferon gamma in modulating the host muscle niche to enhance satellite cell engraftment.

6.8.4) Determining a Role for PGE_2 in Augmenting Satellite Cell Engraftment

My initial hypothesis relied on PGE_2 production, however, this idea was not supported by RNA sequencing data and was not investigated. However, since RNA-sequencing appears to point towards an inflammatory response, and taking into account recent findings by Ho et al. (2017) that indicate that PGE_2 is essential for efficacious muscle regeneration, I hypothesise that this molecule may still play a role in augmenting satellite cell engraftment. To determine this, the changes in the concentration of PGE_2 could be measured in pre-irradiated host muscles compared

to non-irradiated controls. If elevated after irradiation, this would suggest that the inflammatory response seen in the RNA-sequencing data may also be activating, among other things, the synthesis of PGE_2. Confirmation of its role in augmenting satellite cell engraftment could be determined by the treatment of $mdx^{nu/nu}$ hosts with a COX2 inhibitor prior to, and in the days following, host muscle irradiation and satellite cell transplantation. If the contribution of donor satellite cells to the host muscle is reduced, it would provide strong evidence of its involvement in mediating the irradiation induced augmentation of engraftment efficiency.

Bibliography

Aartsma-Rus, A. et al., 2009. Theoretic applicability of antisense-mediated exon skipping for Duchenne muscular dystrophy mutations. *Human Mutation*, 30(3), pp.293–299.

Abad, M. et al., 2013. Reprogramming in vivo produces teratomas and iPS cells with totipotency features. *Nature*, 502(7471), pp.340–345.

Abou-Khalil, R. et al., 2009. Autocrine and Paracrine Angiopoietin 1/Tie-2 Signaling Promotes Muscle Satellite Cell Self-Renewal. *Cell Stem Cell*, 5(3), pp.298–309.

Akira, S., Uematsu, S. & Takeuchi, O., 2006. Pathogen recognition and innate immunity. *Cell*, 124(4), pp.783–801.

Aksoy, E. et al., 2005. Double-stranded RNAs from the Helminth Parasite *Schistosoma* Activate TLR3 in Dendritic Cells. *Journal of Biological Chemistry*, 280(1), pp.277–283.

Al-Zaidy, S.A. et al., 2015. Follistatin Gene Therapy Improves Ambulation in Becker Muscular Dystrophy. *Journal of Neuromuscular Diseases*, 2(3), pp.185–192.

Alexopoulou, L. et al., 2001. Recognition of double-stranded RNA and activation of NF-kappaB by Toll-like receptor 3. *Nature*, 413(6857), pp.732–8.

Allen, R.E. et al., 1985. A serum-free medium that supports the growth of cultured skeletal muscle satellite cells. *In Vitro Cellular & Developmental Biology*, 21(11), pp.636–640.

Alvarez, B. et al., 2002. TNF-α modulates cytokine and cytokine receptors in C2C12

myotubes. *Cancer Letters*, 175(2), pp.181–185.

Amantana, A. et al., 2007. Pharmacokinetics, biodistribution, stability and toxicity of a cell-penetrating peptide-morpholino oligomer conjugate. *Bioconjugate chemistry*, 18(4), pp.1325–31.

Anders, S., Pyl, P.T. & Huber, W., 2015. HTSeq--a Python framework to work with high-throughput sequencing data. *Bioinformatics*, 31(2), pp.166–169.

Anderson, J.L. et al., 2002. Brain function in Duchenne muscular dystrophy. *Brain : a journal of neurology*, 125(Pt 1), pp.4–13.

Arechavala-Gomeza, V. et al., 2012. Antisense oligonucleotide-mediated exon skipping for Duchenne muscular dystrophy: progress and challenges. *Current gene therapy*, 12(3), pp.152–60.

Ayene, I.S., Koch, C.J. & Krisch, R.E., 2007. DNA strand breakage by bivalent metal ions and ionizing radiation. *International journal of radiation biology*, 83(3), pp.195–210.

Aykin-Burns, N. et al., 2011. Sensitivity to low-dose/low-LET ionizing radiation in mammalian cells harboring mutations in succinate dehydrogenase subunit C is governed by mitochondria-derived reactive oxygen species. *Radiation research*, 175(2), pp.150–8.

Azuaje, F.J., 2014. Selecting biologically informative genes in co-expression networks with a centrality score. *Biology direct*, 9, p.12.

Azzam, E.I., Jay-Gerin, J.P. & Pain, D., 2012. Ionizing radiation-induced metabolic oxidative stress and prolonged cell injury. *Cancer Letters*, 327(1–2), pp.48–60.

Bachrach, E. et al., 2004. Systemic delivery of human microdystrophin to regenerating mouse dystrophic muscle by muscle progenitor cells. *Proceedings*

of the National Academy of Sciences, 101(10), pp.3581–3586.

Barabási, A.-L., Gulbahce, N. & Loscalzo, J., 2011. Network medicine: a network-based approach to human disease. *Nature Reviews Genetics*, 12(1), pp.56–68.

Barnard, W. et al., 1994. Leukemia inhibitory factor (LIF) infusion stimulates skeletal muscle regeneration after injury: injured muscle expresses lif mRNA. *Journal of the Neurological Sciences*, 123, pp.108–113.

Beard, B.C. et al., 2007. Unique Integration Profiles in a Canine Model of Long-Term Repopulating Cells Transduced with Gammaretrovirus, Lentivirus, or Foamy Virus. *Human Gene Therapy*, 18(5), pp.423–434.

Beauchamp, J.R. et al., 1999. Dynamics of myoblast transplantation reveal a discrete minority of precursors with stem cell-like properties as the myogenic source. *The Journal of cell biology*, 144(6), pp.1113–22.

Beauchamp, J.R. et al., 1999. Dynamics of Myoblast Transplantation Reveal a Discrete Minority of Precursors with Stem Cell–like Properties as the Myogenic Source. *The Journal of Cell Biology Differentiation. J . Cell Sci*, 144(60), pp.1113–112147.

Beauchamp, J.R. et al., 2000. Expression of CD34 and Myf5 defines the majority of quiescent adult skeletal muscle satellite cells. *The Journal of cell biology*, 151(6), pp.1221–34.

Beckman, J.S. et al., 1990. Apparent hydroxyl radical production by peroxynitrite: Implications for endothelial injury from nitric oxide and superoxide (endothelium-derived relaxing factor/desferrioxamine/ischemia/superoxide dismutase). *Medical Sciences*, 87, pp.1620–1624.

Beckman, J.S. & Koppenol, W.H., 1996. Nitric oxide, superoxide, and peroxynitrite: the good, the bad, and ugly. *The American journal of physiology*, 271(5 Pt 1),

pp.C1424-37.

Benabdallah, B.F. et al., 2009. Overexpression of Follistatin in Human Myoblasts Increases Their Proliferation and Differentiation, and Improves the Graft Success in SCID Mice. *Cell Transplantation*, 18(7), pp.709–718.

Benchaouir, R. et al., 2007. Restoration of Human Dystrophin Following Transplantation of Exon-Skipping-Engineered DMD Patient Stem Cells into Dystrophic Mice. *Cell Stem Cell*, 1(6), pp.646–657.

Bencze, M. et al., 2012. Proinflammatory Macrophages Enhance the Regenerative Capacity of Human Myoblasts by Modifying Their Kinetics of Proliferation and Differentiation. *Molecular Therapy*, 20(11), pp.2168–2179.

Bentzinger, C.F. et al., 2013. Fibronectin regulates Wnt7a signaling and satellite cell expansion. *Cell Stem Cell*, 12(1), pp.75–87.

Bentzinger, C.F. et al., 2014a. Wnt7a stimulates myogenic stem cell motility and engraftment resulting in improved muscle strength. *The Journal of cell biology*, 205(1), pp.97–111.

Bentzinger, C.F. et al., 2014b. Wnt7a stimulates myogenic stem cell motility and engraftment resulting in improved muscle strength. *The Journal of cell biology*, 205(1), pp.97–111.

Biedermann, K.A. et al., 1991. scid mutation in mice confers hypersensitivity to ionizing radiation and a deficiency in DNA double-strand break repair. *Proceedings of the National Academy of Sciences of the United States of America*, 88(4), pp.1394–7.

Bischoff, R., 1986. Proliferation of muscle satellite cells on intact myofibers in culture. *Developmental biology*, 115(1), pp.129–39.

Bischoff, R., 1975. Regeneration of single skeletal muscle fibers in vitro. *The Anatomical Record*, 182(2), pp.215–235.

Bizzozero, O.A. et al., 2005. Elevated protein carbonylation in the brain white matter and gray matter of patients with multiple sclerosis. *Journal of Neuroscience Research*, 81(5), pp.687–695.

Blanco-Bose, W.E. et al., 2001. Purification of mouse primary myoblasts based on alpha 7 integrin expression. *Experimental Cell Research*, 265(2), pp.212–220.

Blau, H.M., Chiu, C.P. & Webster, C., 1983. Cytoplasmic activation of human nuclear genes in stable heterocaryons. *Cell*, 32(4), pp.1171–80.

Bogunovic, D., Boisson-Dupuis, S. & Casanova, J.-L., 2013. ISG15: leading a double life as a secreted molecule. *Experimental & Molecular Medicine*, 45(4), p.e18.

Boldrin, L. et al., 2012. Donor Satellite Cell Engraftment Is SignificantlyAugmented When the Host Niche Is Preserved and Endogenous Satellite Cells Are Incapacitated. *STEM CELLS*, 30(9), pp.1971–1984.

Boldrin, L. et al., 2017. The effect of calorie restriction on mouse skeletal muscle is sex, strain and time-dependent. *Scientific Reports*, 7(1).

Boldrin, L. & Morgan, J.E., 2013. Grafting of a Single Donor Myofibre Promotes Hypertrophy in Dystrophic Mouse Muscle A. Musaro, ed. *PLoS ONE*, 8(1), p.e54599.

Boldrin, L. & Morgan, J.E., 2013. Stem Cell Niche. , 1035, pp.179–190.

Bollinger, C.R., Teichgräber, V. & Gulbins, E., 2005. Ceramide-enriched membrane domains. *Biochimica et Biophysica Acta - Molecular Cell Research*, 1746(3), pp.284–294.

Bonacich, P., 1987. Power and Centrality: A Family of Measures. *American Journal of*

Sociology, 92(5), pp.1170–1182.

van den Bosch, M., Bree, R.T. & Lowndes, N.F., 2003. The MRN complex: coordinating and mediating the response to broken chromosomes. *EMBO reports*, 4(9), pp.844–849.

Bouchentouf, M., Benabdallah, B.F. & Tremblay, J.P., 2004. Myoblast survival enhancement and transplantation success improvement by heat-shock treatment in mdx mice. *Transplantation*, 77(9), pp.1349–56.

Boukamp, P. et al., 1988. Normal keratinization in a spontaneously immortalized aneuploid human keratinocyte cell line. *The Journal of cell biology*, 106(3), pp.761–71.

Boyd, J.H. et al., 2006. Toll-like receptors differentially regulate CC and CXC chemokines in skeletal muscle via NF-κB and calcineurin. *Infection and Immunity*, 74(12), pp.6829–6838.

Brunetti-Pierri, N. et al., 2004. Acute Toxicity After High-Dose Systemic Injection of Helper-Dependent Adenoviral Vectors into Nonhuman Primates. *Human Gene Therapy*, 15(1), pp.35–46.

Buchanan, F.G. & DuBois, R.N., 2006. Connecting COX-2 and Wnt in cancer. *Cancer Cell*, 9(1), pp.6–8.

Bulfield, G. et al., 1984. X chromosome-linked muscular dystrophy (mdx) in the mouse. *Proceedings of the National Academy of Sciences of the United States of America*, 81(4), pp.1189–92.

Buono, R. et al., 2012. Nitric Oxide Sustains Long-Term Skeletal Muscle Regeneration by Regulating Fate of Satellite Cells Via Signaling Pathways Requiring Vangl2 and Cyclic GMP. *STEM CELLS*, 30(2), pp.197–209.

Bushby, K. et al., 2014. Ataluren treatment of patients with nonsense mutation dystrophinopathy. *Muscle & Nerve*, 50(4), pp.477–487.

Cailleau, R., Olivé, M. & Cruciger, Q. V, 1978. Long-term human breast carcinoma cell lines of metastatic origin: preliminary characterization. *In vitro*, 14(11), pp.911–5.

Canaday, D. et al., 1994. Membrane Permeability Changes in Gamma-irradiated Muscle Cells. *Annals of the New York Academy of Sciences*, 720(1), pp.153–159.

Candéias, S.M. & Testard, I., 2015. The many interactions between the innate immune system and the response to radiation. *Cancer Letters*, 368(2), pp.173–178.

Cardasis, C.A. & Cooper, G.W., 1975. An analysis of nuclear numbers in individual muscle fibers during differentiation and growth: A satellite cell-muscle fiber growth unit. *Journal of Experimental Zoology*, 191(3), pp.347–357.

Castellone, M.D. et al., 2005. Prostaglandin E2 promotes colon cancer cell growth through a Gs-axin-beta-catenin signaling axis. *Science (New York, N.Y.)*, 310(5753), pp.1504–10.

Cerletti, M. et al., 2008. Highly Efficient, Functional Engraftment of Skeletal Muscle Stem Cells in Dystrophic Muscles. *Cell*, 134(1), pp.37–47.

Chang, J. et al., 2016. Clearance of senescent cells by ABT263 rejuvenates aged hematopoietic stem cells in mice. *Nature Medicine*, 22(1), pp.78–83.

Charrasse, S. et al., 2007. M-Cadherin Activates Rac1 GTPase through the Rho-GEF Trio during Myoblast Fusion. *Molecular Biology of the Cell*, 18(5), pp.1734–1743.

Chatzinikolaou, G., Karakasilioti, I. & Garinis, G.A., 2014. DNA damage and innate immunity: links and trade-offs. *Trends in Immunology*, 35(9), pp.429–435.

Chavali, S. et al., 2010. Network properties of human disease genes with pleiotropic effects. *BMC Systems Biology*, 4(1), p.78.

Cheng, M. et al., 2008. Endogenous interferon- is required for efficient skeletal muscle regeneration. *AJP: Cell Physiology*, 294(5), pp.C1183–C1191.

Chiche, A. et al., 2017a. Injury-Induced Senescence Enables In Vivo Reprogramming in Skeletal Muscle. *Cell Stem Cell*, 20(3), p.407–414.e4.

Chiche, A. et al., 2017b. Injury-Induced Senescence Enables In Vivo Reprogramming in Skeletal Muscle. *Cell Stem Cell*, 20(3), p.407–414.e4.

Choi, K.-M. et al., 2007. Ionizing radiation-induced micronucleus formation is mediated by reactive oxygen species that are produced in a manner dependent on mitochondria, Nox1, and JNK. *Oncology reports*, 17(5), pp.1183–8.

Choudhry, Z. et al., 2014. Sonic hedgehog signalling pathway: a complex network. *Annals of neurosciences*, 21(1), pp.28–31.

Chulada, P.C. et al., 2000. Genetic disruption of Ptgs-1, as well as Ptgs-2, reduces intestinal tumorigenesis in Min mice. *Cancer research*, 60(17), pp.4705–8.

Collins-Underwood, J.R. et al., 2008. NADPH oxidase mediates radiation-induced oxidative stress in rat brain microvascular endothelial cells. *Free Radical Biology and Medicine*, 45(6), pp.929–938.

Collins, C.A. et al., 2005. Stem Cell Function, Self-Renewal, and Behavioral Heterogeneity of Cells from the Adult Muscle Satellite Cell Niche. *Cell*, 122(2), pp.289–301.

Collins, C.A. & Zammit, P.S., 2009. Isolation and grafting of single muscle fibres. *Methods in Molecular Biology*, 482, pp.319–330.

Conboy, I.M. et al., 2003. Notch-Mediated Restoration of Regenerative Potential to

Aged Muscle. *Science*, 302(5650), pp.1575–1577.

Conboy, I.M. & Rando, T.A., 2002. The regulation of Notch signaling controls satellite cell activation and cell fate determination in postnatal myogenesis. *Developmental Cell*, 3(3), pp.397–409.

Cooper, W.G. & Konigsberg, I.R., 1961. Dynamics of myogenesisin vitro. *The Anatomical Record*, 140(3), pp.195–205.

Coppé, J.-P. et al., 2008. Senescence-Associated Secretory Phenotypes Reveal Cell-Nonautonomous Functions of Oncogenic RAS and the p53 Tumor Suppressor J. Downward, ed. *PLoS Biology*, 6(12), p.e301.

Coppé, J.-P. et al., 2010. The Senescence-Associated Secretory Phenotype: The Dark Side of Tumor Suppression. *Annual Review of Pathology: Mechanisms of Disease*, 5(1), pp.99–118.

Cornelison, D.D.W. et al., 2001. Syndecan-3 and Syndecan-4 Specifically Mark Skeletal Muscle Satellite Cells and Are Implicated in Satellite Cell Maintenance and Muscle Regeneration. *Developmental Biology*, 239(1), pp.79–94.

Corre, I., Niaudet, C. & Paris, F., 2010. Plasma membrane signaling induced by ionizing radiation. *Mutation Research - Reviews in Mutation Research*, 704(1–3), pp.61–67.

Cottle, B.J. et al., 2017. Skeletal muscle-derived interstitial progenitor cells (PICs) display stem cell properties, being clonogenic, self-renewing, and multi-potent in vitro and in vivo. *Stem cell research & therapy*, 8(1), p.158.

Counsell, J.R. et al., 2017. Lentiviral vectors can be used for full-length dystrophin gene therapy. *Scientific Reports*, 7(1), p.79.

d'Adda di Fagagna, F., 2008. Living on a break: cellular senescence as a DNA-damage

response. *Nature Reviews Cancer*, 8(7), pp.512–522.

D'Amours, D. & Jackson, S.P., 2002. The mre11 complex: at the crossroads of dna repair and checkpoint signalling. *Nature Reviews Molecular Cell Biology*, 3(5), pp.317–327.

Decary, S. et al., 2000. Shorter telomeres in dystrophic muscle consistent with extensive regeneration in young children. *Neuromuscular disorders : NMD*, 10(2), pp.113–20.

Dellavalle, A. et al., 2007. Pericytes of human skeletal muscle are myogenic precursors distinct from satellite cells. *Nature Cell Biology*, 9(3), pp.255–267.

Dellavalle, A. et al., 2011. Pericytes resident in postnatal skeletal muscle differentiate into muscle fibres and generate satellite cells. *Nature Communications*, 2, p.499.

Demaria, M. et al., 2014. An essential role for senescent cells in optimal wound healing through secretion of PDGF-AA. *Developmental cell*, 31(6), pp.722–33.

Desprez, P.Y. et al., 1998. A novel pathway for mammary epithelial cell invasion induced by the helix-loop-helix protein Id-1. *Molecular and cellular biology*, 18(8), pp.4577–88.

DeVita, V.T., Lawrence, T.S. & Rosenberg, S.A., 2015. *DeVita, Hellman, and Rosenberg's cancer: principles & practice of oncology, 10th edition* 10th Editi., Philadelphia, PA: Lippincott Williams & Wilkins.

DiMario, J. et al., 1989. Fibroblast growth factor in the extracellular matrix of dystrophic (mdx) mouse muscle. *Science (New York, N.Y.)*, 244(4905), pp.688–90.

DiMario, J. & Strohman, R.C., 1988. Satellite cells from dystrophic (mdx) mouse muscle are stimulated by fibroblast growth factor in vitro. *Differentiation;*

research in biological diversity, 39(1), pp.42–9.

Dobin, A. et al., 2013. STAR: ultrafast universal RNA-seq aligner. *Bioinformatics*, 29(1), pp.15–21.

Donato, A.L. et al., 2014. Caspase 3 promotes surviving melanoma tumor cell growth after cytotoxic therapy. *The Journal of investigative dermatology*, 134(6), pp.1686–92.

Du, C. et al., 2009. Mitochondrial ROS and radiation induced transformation in mouse embryonic fibroblasts. *Cancer biology & therapy*, 8(20), pp.1962–71.

Duddy, W. et al., 2015. Muscular dystrophy in the mdx mouse is a severe myopathy compounded by hypotrophy, hypertrophy and hyperplasia. , 5.

Dzierzak, E., 2005. The emergence of definitive hematopoietic stem cells in the mammal. *Current opinion in hematology*, 12(3), pp.197–202.

Ehrhardt, J. et al., 2007. Human muscle precursor cells give rise to functional satellite cells in vivo. *Neuromuscular disorders : NMD*, 17(8), pp.631–8.

Ehrhart, E.J. et al., 1997. Latent transforming growth factor beta1 activation in situ: quantitative and functional evidence after low-dose gamma-irradiation. *FASEB journal : official publication of the Federation of American Societies for Experimental Biology*, 11(12), pp.991–1002.

Elia, D. et al., 2007. Sonic hedgehog promotes proliferation and differentiation of adult muscle cells: Involvement of MAPK/ERK and PI3K/Akt pathways. *Biochimica et Biophysica Acta (BBA) - Molecular Cell Research*, 1773(9), pp.1438–1446.

Elyassaki, W. & Wu, S., 2006. Lipid Rafts Mediate Ultraviolet Light–induced Fas Aggregation in M624 Melanoma Cells. *Photochemistry and Photobiology*, 82(3),

p.787.

Fairclough, R.J., Bareja, A. & Davies, K.E., 2011. Progress in therapy for Duchenne muscular dystrophy. *Experimental Physiology*, 96(11), pp.1101–1113.

Fan, J.-B. & Zhang, D.-E., 2013. ISG15 regulates IFN-γ immunity in human mycobacterial disease. *Cell Research*, 23(2), pp.173–175.

Fan, Y. & Bergmann, A., 2008. Distinct mechanisms of apoptosis-induced compensatory proliferation in proliferating and differentiating tissues in the Drosophila eye. *Developmental cell*, 14(3), pp.399–410.

Fernando, P. et al., 2002. Caspase 3 activity is required for skeletal muscle differentiation. *Proceedings of the National Academy of Sciences of the United States of America*, 99(17), pp.11025–30.

Ferrari, G. et al., 1998. Muscle regeneration by bone marrow-derived myogenic progenitors. *Science (New York, N.Y.)*, 279(5356), pp.1528–30.

Finkel, R.S. et al., 2013. Phase 2a Study of Ataluren-Mediated Dystrophin Production in Patients with Nonsense Mutation Duchenne Muscular Dystrophy H. Sawada, ed. *PLoS ONE*, 8(12), p.e81302.

Flanagan, S.P., 1966. 'Nude', a new hairless gene with pleiotropic effects in the mouse. *Genetical Research*, 8(03), p.295.

Flandin, J.-F., Chano, F. & Descoteaux, A., 2006. RNA interference reveals a role for TLR2 and TLR3 in the recognition of Leishmania donovani promastigotes by interferon-gamma-primed macrophages. *European journal of immunology*, 36(2), pp.411–20.

Fogh, J. & Giovanella, B.C., 1978. *The Nude mouse in experimental and clinical research*, Academic Press.

Freeman, L.C., 1977. A Set of Measures of Centrality Based on Betweenness. *Sociometry*, 40(1), p.35.

Freeman, S.L. & MacNaughton, W.K., 2000. Ionizing radiation induces iNOS-mediated epithelial dysfunction in the absence of an inflammatory response. *American journal of physiology. Gastrointestinal and liver physiology*, 278(2), pp.G243-50.

Frost, R.A., Nystrom, G.J. & Lang, C.H., 2006. Multiple Toll-like receptor ligands induce an IL-6 transcriptional response in skeletal myocytes. *American journal of physiology. Regulatory, integrative and comparative physiology*, 290(3), pp.R773-84.

Fu, X. et al., 2015. Combination of inflammation-related cytokines promotes long-term muscle stem cell expansion. *Cell Research*, 25(6), pp.655–673.

Fujita, S. & Steenken, S., 1981. Pattern of hydroxyl radical addition to uracil and methyl- and carboxyl-substituted uracils. Electron transfer of hydroxyl adducts with N,N,N',N'-tetramethyl-p-phenylenediamine and tetranitromethane. *Journal of the American Chemical Society*, 103(10), pp.2540–2545.

Fukada, S. et al., 2007. Molecular Signature of Quiescent Satellite Cells in Adult Skeletal Muscle. *Stem Cells*, 25(10), pp.2448–2459.

Galliot, B. & Chera, S., 2010. The Hydra model: disclosing an apoptosis-driven generator of Wnt-based regeneration. *Trends in cell biology*, 20(9), pp.514–23.

Galloway, J.L. & Zon, L.I., 2003. Ontogeny of hematopoiesis: examining the emergence of hematopoietic cells in the vertebrate embryo. *Current topics in developmental biology*, 53, pp.139–58.

Gavrieli, Y., Sherman, Y. & Ben-Sasson, S.A., 1992. Identification of programmed cell death in situ via specific labeling of nuclear DNA fragmentation. *The Journal of*

Cell Biology, 119(3).

Gearhart, J.D. & Mintz, B., 1972. Clonal origins of somites and their muscle derivatives: Evidence from allophenic mice. *Developmental Biology*, 29(1), pp.27–37.

Gerstner, H.B., Lewis, R.B. & Richey, E.O., 1954. Early effects of high intensity x-radiation on skeletal muscle. *The Journal of general physiology*, 37(4), pp.445–59.

Giard, D.J. et al., 1973. In Vitro Cultivation of Human Tumors: Establishment of Cell Lines Derived From a Series of Solid Tumors2. *JNCI: Journal of the National Cancer Institute*, 51(5), pp.1417–1423.

Giardiello, F.M. et al., 1993. Treatment of Colonic and Rectal Adenomas with Sulindac in Familial Adenomatous Polyposis. *New England Journal of Medicine*, 328(18), pp.1313–1316.

Gnocchi, V.F. et al., 2009. Further Characterisation of the Molecular Signature of Quiescent and Activated Mouse Muscle Satellite Cells G. Parise, ed. *PLoS ONE*, 4(4), p.e5205.

Goessling, W. et al., 2008. APC mutant zebrafish uncover a changing temporal requirement for wnt signaling in liver development. *Developmental Biology*, 320(1), pp.161–174.

Goessling, W. et al., 2009. Genetic Interaction of PGE2 and Wnt Signaling Regulates Developmental Specification of Stem Cells and Regeneration. *Cell*, 136(6), pp.1136–1147.

Goldman, J.P. et al., 1998. Enhanced human cell engraftment in mice deficient in RAG2 and the common cytokine receptor gamma chain. *British Journal of*

Haematology, 103(2), pp.335–342.

Goodarzi, A.A. et al., 2008. ATM Signaling Facilitates Repair of DNA Double-Strand Breaks Associated with Heterochromatin. *Molecular Cell*, 31(2), pp.167–177.

Gorbunov, N. V et al., 2000. Activation of the nitric oxide synthase 2 pathway in the response of bone marrow stromal cells to high doses of ionizing radiation. *Radiation research*, 154(1), pp.73–86.

Goyenvalle, A. et al., 2011. Therapeutic approaches to muscular dystrophy. *Human molecular genetics*, 20(R1), pp.R69-78.

Grahn, D. & Hamilton, K.F., 1957. Genetic Variation in the Acute Lethal Response of Four Inbred Mouse Strains to Whole Body X-Irradiation. *Genetics*, 42(3), pp.189–98.

Le Grand, F. et al., 2009. Wnt7a Activates the Planar Cell Polarity Pathway to Drive the Symmetric Expansion of Satellite Stem Cells. *Cell Stem Cell*, 4(6), pp.535–547.

Gross, J.G. & Morgan, J.E., 1999. Muscle precursor cells injected into irradiated mdx mouse muscle persist after serial injury. *Muscle & Nerve*, 22(2), pp.174–185.

Grounds, M.D. & Yablonka-Reuveni, Z., 1993. Molecular and cell biology of skeletal muscle regeneration. In T. Partridge, ed. *Molecular and Cell Biology of Muscular Dystrophy*. Dordrecht: Springer Netherlands, pp. 210–256.

Le Guiner, C. et al., 2014. Forelimb treatment in a large cohort of dystrophic dogs supports delivery of a recombinant AAV for exon skipping in Duchenne patients. *Molecular therapy : the journal of the American Society of Gene Therapy*, 22(11), pp.1923–35.

Guiraud, S. et al., 2015. Second-generation compound for the modulation of utrophin

in the therapy of DMD. *Human Molecular Genetics*, 24(15), pp.4212–4224.

Gulati, A.K., 1987. The effect of X-irradiation on skeletal muscle regeneration in the adult rat. *Journal of the neurological sciences*, 78(1), pp.111–20.

Guo, Z. et al., 2010. ATM Activation by Oxidative Stress. *Science*, 330(6003), pp.517–521.

Gussoni, E., Blau, H.M. & Kunkel, L.M., 1997. The fate of individual myoblasts after transplantation into muscles of DMD patients. *Nature Medicine*, 3(9), pp.970–977.

Hacein-Bey-Abina, S. et al., 2003. LMO2-Associated Clonal T Cell Proliferation in Two Patients after Gene Therapy for SCID-X1. *Science*, 302(5644), pp.415–419.

Haertel, E., Werner, S. & Schäfer, M., 2014. Transcriptional regulation of wound inflammation. *Seminars in Immunology*, 26(4), pp.321–328.

Haimovitz-Friedman, A. et al., 1994. Ionizing radiation acts on cellular membranes to generate ceramide and initiate apoptosis. *The Journal of experimental medicine*, 180(2), pp.525–35.

Haimovitz-Friedman, A., 1994. Ionizing radiation acts on cellular membranes to generate ceramide and initiate apoptosis. *Journal of Experimental Medicine*, 180(2), pp.525–535.

Handgretinger, R. & Kuçi, S., 2013. CD133-Positive Hematopoietic Stem Cells: From Biology to Medicine. In *Advances in experimental medicine and biology*. pp. 99–111.

Hardee, J.P. et al., 2014. The effect of radiation dose on mouse skeletal muscle remodeling. *Radiology and oncology*, 48(3), pp.247–56.

Harley, C.B., Futcher, A.B. & Greider, C.W., 1990. Telomeres shorten during ageing of

human fibroblasts. *Nature*, 345(6274), pp.458–460.

Harris, J.B., 2003. Myotoxic phospholipases A2 and the regeneration of skeletal muscles. *Toxicon*, 42(8), pp.933–945.

Harrison, R.G., 1910. The outgrowth of the nerve fiber as a mode of protoplasmic movement. *Journal of Experimental Zoology*, 9(4), pp.787–846.

Härtlova, A. et al., 2015. DNA Damage Primes the Type I Interferon System via the Cytosolic DNA Sensor STING to Promote Anti-Microbial Innate Immunity. *Immunity*, 42(2), pp.332–343.

Hayflick, L., 1965. THE LIMITED IN VITRO LIFETIME OF HUMAN DIPLOID CELL STRAINS. *Experimental cell research*, 37, pp.614–36.

Hayflick, L. & Moorhead, P.S., 1961. The serial cultivation of human diploid cell strains. *Experimental Cell Research*, 25(3), pp.585–621.

Haynie, J.L. & Bryant, P.J., 1977. Roux's Archives of Developmental Biology The Effects of X-rays on the Proliferation Dynamics of Cells in the Imaginal Wing Disc of Drosophila melanogaster. , 85.

Heinrich, C., Spagnoli, F.M. & Berninger, B., 2015. In vivo reprogramming for tissue repair. *Nature Cell Biology*, 17(3), pp.204–211.

Hendry, J.H., 1979. *Radiobiology for the Radiologist*, Lippincott Williams & Wilkins.

Hensley, K. et al., 1996. Reactive Oxygen Species as Causal Agents in the Neurotoxicity of the Alzheimer's Disease-Associated Amyloid Beta Peptide. *Annals of the New York Academy of Sciences*, 786(1 Near-Earth Ob), pp.120–134.

Herranz, N. & Gil, J., 2018. Mechanisms and functions of cellular senescence. *Journal of Clinical Investigation*, 128(4), pp.1238–1246.

Heslop, L., Morgan, J.E. & Partridge, T.A., 2000. Evidence for a myogenic stem cell that is exhausted in dystrophic muscle. *Journal of cell science*, 113 (Pt 12), pp.2299–308.

High, K.A. et al., 1999. Long-term correction of canine hemophilia B by gene transfer of blood coagulation factor IX mediated by adeno-associated viral vector. *Nature Medicine*, 5(1), pp.56–63.

Hill, M. & Goldspink, G., 2003. Expression and Splicing of the Insulin-Like Growth Factor Gene in Rodent Muscle is Associated with Muscle Satellite (stem) Cell Activation following Local Tissue Damage. *The Journal of Physiology*, 549(2), pp.409–418.

Ho, A.T. V et al., 2017. Prostaglandin E2 is essential for efficacious skeletal muscle stem-cell function, augmenting regeneration and strength. *Proceedings of the National Academy of Sciences of the United States of America*, 114(26), pp.6675–6684.

Hoffman, E.P., Brown, R.H. & Kunkel, L.M., 1987. Dystrophin: The protein product of the duchenne muscular dystrophy locus. *Cell*, 51(6), pp.919–928.

Honda, K. & Taniguchi, T., 2006. IRFs: master regulators of signalling by Toll-like receptors and cytosolic pattern-recognition receptors. *Nature Reviews Immunology*, 6(9), pp.644–658.

Horsley, V. et al., 2001. Regulation of the growth of multinucleated muscle cells by an NFATC2-dependent pathway. *Journal of Cell Biology*, 153(2), pp.329–338.

Hsu, D.T., 2010. Cardiac manifestations of neuromuscular disorders in children. *Paediatric Respiratory Reviews*, 11(1), pp.35–38.

Huang, Q. et al., 2011. Caspase 3-mediated stimulation of tumor cell repopulation

during cancer radiotherapy. *Nature medicine*, 17(7), pp.860–6.

Huard, J. et al., 1994. Human myoblast transplantation in immunodeficient and immunosuppressed mice: Evidence of rejection. *Muscle & Nerve*, 17(2), pp.224–234.

Huh, J.R., Guo, M. & Hay, B.A., 2004. Compensatory Proliferation Induced by Cell Death in the Drosophila Wing Disc Requires Activity of the Apical Cell Death Caspase Dronc in a Nonapoptotic Role. *Current Biology*, 14(14), pp.1262–1266.

Hunt, L.C. et al., 2011. Alterations in the expression of leukemia inhibitory factor following exercise: comparisons between wild-type and mdx muscles. *PLoS Currents*, 3, p.RRN1277.

Irintchev, A. et al., 1994. Expression pattern of M-cadherin in normal, denervated, and regenerating mouse muscles. *Developmental Dynamics*, 199(4), pp.326–337.

Irwin, M.E. et al., 2011. Lipid raft localization of EGFR alters the response of cancer cells to the EGFR tyrosine kinase inhibitor gefitinib. *Journal of Cellular Physiology*, 226(9), pp.2316–2328.

Ishikawa, H., 1966. Electron microscopic observations of satellite cells with special reference to the development of mammalian skeletal muscles. *Zeitschrift für Anatomie und Entwicklungsgeschichte*, 125(1), pp.43–63.

Jansen, K.M. & Pavlath, G.K., 2006. Mannose receptor regulates myoblast motility and muscle growth. *The Journal of cell biology*, 174(3), pp.403–13.

Jobling, M.F. et al., 2006. Isoform-Specific Activation of Latent Transforming Growth Factor β (LTGF-β) by Reactive Oxygen Species. *Radiation Research*, 166(6), pp.839–848.

Joy, M.P. et al., 2005. High-Betweenness Proteins in the Yeast Protein Interaction Network. *Journal of Biomedicine and Biotechnology*, 2005(2), pp.96–103.

Jurdana, M., 2008. Radiation effects on skeletal muscle. *Radiology and Oncology*, 42(1), pp.15–22.

Kafri, T. et al., 1997. Sustained expression of genes delivered directly into liver and muscle by lentiviral vectors. *Nature Genetics*, 17(3), pp.314–317.

Katz, B., 1961. The Terminations of the Afferent Nerve Fibre in the Muscle Spindle of the Frog. *Philosophical Transactions of the Royal Society B: Biological Sciences*, 243(703), pp.221–240.

Kawai, T. et al., 2004. Interferon-α induction through Toll-like receptors involves a direct interaction of IRF7 with MyD88 and TRAF6. *Nature Immunology*, 5(10), pp.1061–1068.

Kelly, R. et al., 1995. Myosin light chain 3F regulatory sequences confer regionalized cardiac and skeletal muscle expression in transgenic mice. *The Journal of cell biology*, 129(2), pp.383–96.

Kennedy, C.L. et al., 2014. Differential role of MyD88 and Mal/TIRAP in TLR2-mediated gastric tumourigenesis. *Oncogene*, 33(19), pp.2540–2546.

Kergonou, J.-F., Braquet, M. & Rocquet, G., 1981. Influence of Whole-Body γ Irradiation upon Rat Liver Mitochondrial Fractions. *Source: Radiation Research*, 88(2), pp.377–384.

Kessler, P.D. et al., 1996. Gene delivery to skeletal muscle results in sustained expression and systemic delivery of a therapeutic protein. *Proceedings of the National Academy of Sciences of the United States of America*, 93(24), pp.14082–7.

Kim, B.-H. et al., 2016. Interferon-induced guanylate-binding proteins in inflammasome activation and host defense. *Nature Immunology*, 17(5), pp.481–489.

Kimura, E. et al., 2010. Dystrophin delivery to muscles of mdx mice using lentiviral vectors leads to myogenic progenitor targeting and stable gene expression. *Molecular therapy : the journal of the American Society of Gene Therapy*, 18(1), pp.206–13.

Kimura, K. et al., 2003. Role of ceramide in mediating apoptosis of irradiated LNCaP prostate cancer cells. *Cell Death & Differentiation*, 10(2), pp.240–248.

Kléber, M. & Sommer, L., 2004. Wnt signaling and the regulation of stem cell function. *Current Opinion in Cell Biology*, 16(6), pp.681–687.

Klein, L. et al., 2014. Positive and negative selection of the T cell repertoire: what thymocytes see (and don't see). *Nature reviews. Immunology*, 14(6), pp.377–91.

Kleopa, K.A. et al., 2006. Naturally occurring utrophin correlates with disease severity in Duchenne muscular dystrophy. *Human Molecular Genetics*, 15(10), pp.1623–1628.

Kobinger, G.P. et al., 2003. Correction of the Dystrophic Phenotype by *In Vivo* Targeting of Muscle Progenitor Cells. *Human Gene Therapy*, 14(15), pp.1441–1449.

Koleva, M. et al., 2005. Pleiotropic effects of sonic hedgehog on muscle satellite cells. *Cellular and molecular life sciences : CMLS*, 62(16), pp.1863–70.

Konigsberg, I.R., 1961. Some aspects of myogenesis in vitro. *Circulation*, 24(2), pp.447–57.

KONIGSBERG, I.R., 1963. Clonal analysis of myogenesis. *Science (New York, N.Y.)*,

140(3573), pp.1273–84.

Konigsberg, U.R., Lipton, B.H. & Konigsberg, I.R., 1975. The regenerative response of single mature muscle fibers isolated in vitro. *Developmental Biology*, 45(2), pp.260–275.

Krishnamurthy, J. et al., 2004. Ink4a/Arf expression is a biomarker of aging. *Journal of Clinical Investigation*, 114(9), pp.1299–1307.

Krtolica, A. et al., 2001. Senescent fibroblasts promote epithelial cell growth and tumorigenesis: A link between cancer and aging. *Proceedings of the National Academy of Sciences*, 98(21), pp.12072–12077.

Kuang, S. et al., 2007. Asymmetric Self-Renewal and Commitment of Satellite Stem Cells in Muscle. *Cell*, 129(5), pp.999–1010.

Kuang, S. & Rudnicki, M.A., 2008. The emerging biology of satellite cells and their therapeutic potential. *Trends in Molecular Medicine*, 14(2), pp.82–91.

Kurtova, A. V et al., 2015. Blocking PGE2-induced tumour repopulation abrogates bladder cancer chemoresistance. *Nature*, 517(7533), pp.209–13.

LaBarge, M.A. & Blau, H.M., 2002. Biological progression from adult bone marrow to mononucleate muscle stem cell to multinucleate muscle fiber in response to injury. *Cell*, 111(4), pp.589–601.

Lafreniere, J.-F. et al., 2009. Growth Factor Coinjection Improves the Migration Potential of Monkey Myogenic Precursors without Affecting Cell Transplantation Success. *Cell Transplantation*, 18(7), pp.719–730.

Landskron, G. et al., 2014. Chronic inflammation and cytokines in the tumor microenvironment. *Journal of immunology research*, 2014, p.149185.

Lang, C.H. et al., 2003. Endotoxin Stimulates In Vivo Expression of Inflammatory

Cytokines Tumor Necrosis Factor Alpha, Interleukin-1beta, -6, and High-Mobility-Group Protein-1 in Skeletal Muscle. *Shock*, 19(6), pp.538–546.

Langen, R.C. et al., 2001. Inflammatory cytokines inhibit myogenic differentiation through activation of nuclear factor-kappaB. *FASEB journal : official publication of the Federation of American Societies for Experimental Biology*, 15(7), pp.1169–80.

Langenbach, R. et al., 1995. Prostaglandin synthase 1 gene disruption in mice reduces arachidonic acid-induced inflammation and indomethacin-induced gastric ulceration. *Cell*, 83(3), pp.483–92.

Lapidos, K.A., Kakkar, R. & McNally, E.M., 2004. The dystrophin glycoprotein complex: signaling strength and integrity for the sarcolemma. *Circulation research*, 94(8), pp.1023–31.

Lareau, C.A. et al., 2015. Differential co-expression network centrality and machine learning feature selection for identifying susceptibility hubs in networks with scale-free structure. *BioData Mining*, 8(1), p.5.

Larochelle, N. et al., 2010. Modulation of coxsackie and adenovirus receptor expression for gene transfer to normal and dystrophic skeletal muscle. *The Journal of Gene Medicine*, 12(3), p.n/a-n/a.

Lavin, M.F. et al., 2015. ATM-Dependent Phosphorylation of All Three Members of the MRN Complex: From Sensor to Adaptor. *Biomolecules*, 5(4), pp.2877–902.

Leach, J.K. et al., 2001. Ionizing Radiation-induced, Mitochondria-dependent Generation of Reactive Oxygen/Nitrogen. *CANCER RESEARCH*, 61, pp.3894–3901.

Lee, M.N. et al., 2012. Identification of regulators of the innate immune response to

cytosolic DNA and retroviral infection by an integrative approach. *Nature Immunology*, 14(2), pp.179–185.

Lee, S.H. et al., 2010. ERK activation drives intestinal tumorigenesis in Apcmin/+ mice. *Nature Medicine*, 16(6), pp.665–670.

Lehnert, B.E., Goodwin, E.H. & Deshpande, A., 1997. Extracellular factor(s) following exposure to alpha particles can cause sister chromatid exchanges in normal human cells. *Cancer research*, 57(11), pp.2164–71.

Li, F. et al., 2010. Apoptotic Cells Activate the "Phoenix Rising" Pathway to Promote Wound Healing and Tissue Regeneration. *Science Signaling*, 3(110), pp.ra13-ra13.

Li, S. et al., 2005. Stable transduction of myogenic cells with lentiviral vectors expressing a minidystrophin. *Gene Therapy*, 12(14), pp.1099–1108.

Liberzon, A. et al., 2015. The Molecular Signatures Database Hallmark Gene Set Collection.

Liu, L. et al., 2004. Essential roles of S-nitrosothiols in vascular homeostasis and endotoxic shock. *Cell*, 116(4), pp.617–28.

Londhe, P. & Davie, J.K., 2011. Gamma Interferon Modulates Myogenesis through the Major Histocompatibility Complex Class II Transactivator, CIITA. *Molecular and Cellular Biology*, 31(14), pp.2854–2866.

Londhe, P. & Davie, J.K., 2013. Interferon- Resets Muscle Cell Fate by Stimulating the Sequential Recruitment of JARID2 and PRC2 to Promoters to Repress Myogenesis. *Science Signaling*, 6(305), pp.ra107-ra107.

Love, M.I., Huber, W. & Anders, S., 2014. Moderated estimation of fold change and dispersion for RNA-seq data with DESeq2. *Genome Biology*, 15.

Lu, Q.L. et al., 2005. Systemic delivery of antisense oligoribonucleotide restores dystrophin expression in body-wide skeletal muscles. *Proceedings of the National Academy of Sciences*, 102(1), pp.198–203.

Luiz Paiva-Oliveira, E. et al., 2012. TLR4 signaling protects from excessive muscular damage induced by Bothrops jararacussu snake venom. *Toxicon*, 60, pp.1396–1403.

Lyngdoh, R.H.D. & Schaefer, H.F., 2009. Elementary lesions in DNA subunits: Electron, hydrogen atom, proton, and hydride transfers. *Accounts of Chemical Research*, 42(4), pp.563–572.

Ma, H.-W. & Zeng, A.-P., 2003. The connectivity structure, giant strong component and centrality of metabolic networks. *Bioinformatics (Oxford, England)*, 19(11), pp.1423–30.

MacKenzie, T.C. et al., 2005. Transduction of satellite cells after prenatal intramuscular administration of lentiviral vectors. *The Journal of Gene Medicine*, 7(1), pp.50–58.

Madhala-Levy, D. et al., 2012. Cooperation between Shh and IGF-I in promoting myogenic proliferation and differentiation via the MAPK/ERK and PI3K/Akt pathways requires smo activity. *Journal of Cellular Physiology*, 227(4), pp.1455–1464.

Maere, S., Heymans, K. & Kuiper, M., 2005. BiNGO: a Cytoscape plugin to assess overrepresentation of Gene Ontology categories in Biological Networks. *Bioinformatics*, 21(16), pp.3448–3449.

Magli, A. et al., 2017. PAX7 Targets, CD54, Integrin α9β1, and SDC2, Allow Isolation of Human ESC/iPSC-Derived Myogenic Progenitors. *Cell Reports*, 19(13),

pp.2867–2877.

Malhotra, S. & Kincade, P.W., 2009. Wnt-Related Molecules and Signaling Pathway Equilibrium in Hematopoiesis. *Cell Stem Cell*, 4(1), pp.27–36.

von Maltzahn, J., Bentzinger, C.F. & Rudnicki, M.A., 2011. Wnt7a–Fzd7 signalling directly activates the Akt/mTOR anabolic growth pathway in skeletal muscle. *Nature Cell Biology*, 14(2), pp.186–191.

Manno, C.S. et al., 2003. AAV-mediated factor IX gene transfer to skeletal muscle in patients with severe hemophilia B. *Blood*, 101(8), pp.2963–72.

Martin, F.A., Perez-Garijo, A. & Morata, G., 2009. Apoptosis in Drosophila: compensatory proliferation and undead cells. *The International Journal of Developmental Biology*, 53(8-9–10), pp.1341–1347.

Martin, P. et al., 2003. *Wound Healing in the PU.1 Null Mouse—Tissue Repair Is Not Dependent on Inflammatory Cells*,

Mathes, A.L. & Lafyatis, R., 2011. Role for toll-like receptor 3 in muscle regeneration after cardiotoxin injury. *Muscle & Nerve*, 43(5), pp.733–740.

Mathieu, M.-E. et al., 2012. LIF-Dependent Signaling: New Pieces in the Lego. *Stem Cell Reviews and Reports*, 8(1), pp.1–15.

Mauro, A., 1961. Satellite cell of skeletal muscle fibers. *The Journal of biophysical and biochemical cytology*, 9(2), pp.493–495.

Mazurie, A. et al., 2010. Evolution of metabolic network organization. *BMC Systems Biology*, 4(1), p.59.

Mazurier, F. et al., 1999. A Novel Immunodeficient Mouse Model-RAG2 gamma Cytokine Receptor Chain Double Mutants-Requiring Exogenous Cytokine Administration for Human Hematopoietic Stem Cell Engraftment Common.

Journal of Interferon & Cytokine Research, 19(5), pp.533–541.

McDonald, C.M. et al., 2017. Ataluren in patients with nonsense mutation Duchenne muscular dystrophy (ACT DMD): a multicentre, randomised, double-blind, placebo-controlled, phase 3 trial. *The Lancet*, 390(10101), pp.1489–1498.

Melchionna, R. et al., 2010. Induction of myogenic differentiation by SDF-1 via CXCR4 and CXCR7 receptors. *Muscle & Nerve*, 41(6), pp.828–835.

Meller, S. et al., 2005. Ultraviolet radiation-induced injury, chemokines, and leukocyte recruitment: An amplification cycle triggering cutaneous lupus erythematosus. *Arthritis & Rheumatism*, 52(5), pp.1504–1516.

Mendell, J.R. et al., 2015. A Phase 1/2a Follistatin Gene Therapy Trial for Becker Muscular Dystrophy. *Molecular Therapy*, 23(1), pp.192–201.

Mendell, J.R., Campbell, K., et al., 2010. Dystrophin Immunity in Duchenne's Muscular Dystrophy. *New England Journal of Medicine*, 363(15), pp.1429–1437.

Mendell, J.R. et al., 2013. Eteplirsen for the treatment of Duchenne muscular dystrophy. *Annals of Neurology*, 74(5), pp.637–647.

Mendell, J.R. et al., 2012. Evidence-based path to newborn screening for duchenne muscular dystrophy. *Annals of Neurology*, 71(3), pp.304–313.

Mendell, J.R. et al., 2016. Longitudinal effect of eteplirsen versus historical control on ambulation in Duchenne muscular dystrophy. *Annals of Neurology*, 79(2), pp.257–271.

Mendell, J.R. et al., 1995. Myoblast Transfer in the Treatment of Duchenne's Muscular Dystrophy. *New England Journal of Medicine*, 333(13), pp.832–838.

Mendell, J.R., Rodino-Klapac, L.R., et al., 2010. Sustained alpha-sarcoglycan gene expression after gene transfer in limb-girdle muscular dystrophy, type 2D.

Annals of Neurology, 68(5), pp.629–638.

Meng, J., Adkin, C.F., et al., 2011. Contribution of Human Muscle-Derived Cells to Skeletal Muscle Regeneration in Dystrophic Host Mice M. Rota, ed. *PLoS ONE*, 6(3), p.e17454.

Meng, J. et al., 2014. Human Skeletal Muscle–derived CD133+ Cells Form Functional Satellite Cells After Intramuscular Transplantation in Immunodeficient Host Mice. *Molecular Therapy*, 22(5), pp.1008–1017.

Meng, J. et al., 2015. The effect of the muscle environment on the regenerative capacity of human skeletal muscle stem cells. *Skeletal muscle*, 5, p.11.

Meng, J., Muntoni, F. & Morgan, J.E., 2011. Stem cells to treat muscular dystrophies - Where are we? *Neuromuscular Disorders*, 21(1), pp.4–12.

Mercuri, E. & Muntoni, F., 2013. Muscular dystrophies. *The Lancet*, 381(9869), pp.845–860.

von Mering, C. et al., 2003. STRING: a database of predicted functional associations between proteins. *Nucleic acids research*, 31(1), pp.258–61.

Merkle, D. et al., 2002. The DNA-dependent protein kinase interacts with DNA to form a protein-DNA complex that is disrupted by phosphorylation. *Biochemistry*, 41(42), pp.12706–14.

Michael, J.M., Lavin, M.F. & Watters, D.J., 1997. Resistance to radiation-induced apoptosis in Burkitt's lymphoma cells is associated with defective ceramide signaling. *Cancer research*, 57(16), pp.3600–5.

Miller, R.G. et al., 1997. Myoblast implantation in Duchenne muscular dystrophy: the San Francisco study. *Muscle & nerve*, 20(4), pp.469–78.

Miller, S.C. et al., 1988. Tumor necrosis factor inhibits human myogenesis in vitro.

Molecular and cellular biology, 8(6), pp.2295–301.

Minasi, M.G. et al., 2002. The meso-angioblast: a multipotent, self-renewing cell that originates from the dorsal aorta and differentiates into most mesodermal tissues. *Development (Cambridge, England)*, 129(11), pp.2773–83.

Mintz, B. & Baker, W.W., 1967. Normal mammalian muscle differentiation and gene control of isocitrate dehydrogenase synthesis. *Proceedings of the National Academy of Sciences of the United States of America*, 58(2), pp.592–598.

Mitchell, K.J. et al., 2010. Identification and characterization of a non-satellite cell muscle resident progenitor during postnatal development. *Nature Cell Biology*, 12(3), p.ncb2025.

Moat, S.J. et al., 2013. Newborn bloodspot screening for Duchenne Muscular Dystrophy: 21 years experience in Wales (UK). *European Journal of Human Genetics*, 21(10), pp.1049–1053.

Moens, P.D., Van-Schoor, M.C. & Maréchal, G., 1996. Lack of myoblasts migration between transplanted and host muscles of mdx and normal mice. *Journal of muscle research and cell motility*, 17(1), pp.37–43.

Monahan, P. et al., 1998. Direct intramuscular injection with recombinant AAV vectors results in sustained expression in a dog model of hemophilia. *Gene Therapy*, 5(1), pp.40–49.

Montarras, D. et al., 2005. Direct isolation of satellite cells for skeletal muscle regeneration. *Science (New York, N.Y.)*, 309(5743), pp.2064–7.

Mootha, V.K. et al., 2003. PGC-1α-responsive genes involved in oxidative phosphorylation are coordinately downregulated in human diabetes. *Nature Genetics*, 34(3), pp.267–273.

Morgan, J.E. et al., 1993. Long-term persistence and migration of myogenic cells injected into pre-irradiated muscles of mdx mice. *Journal of the Neurological Sciences*, 115(2), pp.191–200.

Morgan, J.E. et al., 1994. Myogenic Cell Lines Derived from Transgenic Mice Carrying a Thermolabile T Antigen: A Model System for the Derivation of Tissue-Specific and Mutation-Specific Cell Lines. *Developmental Biology*, 162(2), pp.486–498.

Morgan, J.E. et al., 2002. Myogenic cell proliferation and generation of a reversible tumorigenic phenotype are triggered by preirradiation of the recipient site. *The Journal of Cell Biology*, 157(4), pp.693–702.

Morgan, J.E., Hoffman, E.P. & Partridge, T.A., 1990. Normal myogenic cells from newborn mice restore normal histology to degenerating muscles of the mdx mouse. *The Journal of cell biology*, 111(6 Pt 1), pp.2437–49.

Moss, F.P. & Leblond, C.P., 1971. Satellite cells as the source of nuclei in muscles of growing rats. *The Anatomical Record*, 170(4), pp.421–435.

Mothersill, C. & Seymour, C., 1997. Medium from irradiated human epithelial cells but not human fibroblasts reduces the clonogenic survival of unirradiated cells. *International journal of radiation biology*, 71(4), pp.421–7.

Muir, A.R., Kanji, A.H. & Allbrook, D., 1965. The structure of the satellite cells in skeletal muscle. *Journal of anatomy*, 99(Pt 3), pp.435–44.

Müller, A.-K., Meyer, M. & Werner, S., 2012. The roles of receptor tyrosine kinases and their ligands in the wound repair process. *Seminars in Cell & Developmental Biology*, 23(9), pp.963–970.

Muñoz-Cánoves, P. et al., 2013. Interleukin-6 myokine signaling in skeletal muscle: A double-edged sword? *FEBS Journal*, 280(17), pp.4131–4148.

Munro, T.R., 1970. The site of the target region for radiation-induced mitotic delay in cultured mammalian cells. *Radiat.Res.*, 44(3), pp.748–757.

Muntoni, F., Bushby, K.D. & van Ommen, G., 2008. 149th ENMC International Workshop and 1st TREAT-NMD Workshop on: "Planning Phase I/II Clinical trials using Systemically Delivered Antisense Oligonucleotides in Duchenne Muscular Dystrophy." *Neuromuscular Disorders*, 18(3), pp.268–275.

Muzyczka, N., 1992. Use of adeno-associated virus as a general transduction vector for mammalian cells. *Current topics in microbiology and immunology*, 158, pp.97–129.

Nagata, Y. et al., 2006. Entry of muscle satellite cells into the cell cycle requires sphingolipid signaling. *The Journal of cell biology*, 174(2), pp.245–53.

Nallamilli, B.R.R. et al., 2014. Molecular Diagnosis of Duchenne Muscular Dystrophy. In *Current Protocols in Human Genetics*. Hoboken, NJ, USA: John Wiley & Sons, Inc., p. 9.25.1-9.25.29.

Narayanan, P.K., Goodwin, E.H. & Lehnert, B.E., 1997. Alpha particles initiate biological production of superoxide anions and hydrogen peroxide in human cells. *Cancer research*, 57(18), pp.3963–71.

Naugler, W.E. et al., 2007. Gender Disparity in Liver Cancer Due to Sex Differences in MyD88-Dependent IL-6 Production. *Science*, 317(5834), pp.121–124.

Negroni, E. et al., 2009. In vivo myogenic potential of human CD133+ muscle-derived stem cells: a quantitative study. *Molecular therapy : the journal of the American Society of Gene Therapy*, 17(10), pp.1771–8.

Newman, M.E.J., 2010. *Networks. An introduction*,

Newman, M.R. et al., 2014. The Methylation of DNA Repeat Elements is Sex-

Dependent and Temporally Different in Response to X Radiation in Radiosensitive and Radioresistant Mouse Strains. *Radiation Research*, 181(1), pp.65–75.

O'Neill, L.A.J. & Bowie, A.G., 2007. The family of five: TIR-domain-containing adaptors in Toll-like receptor signalling. *Nature reviews. Immunology*, 7(5), pp.353–64.

Ochi, T. et al., 2015. PAXX, a paralog of XRCC4 and XLF, interacts with Ku to promote DNA double-strand break repair. *Science*, 347(6218), pp.185–188.

Okabe, M. et al., 1997. 'Green mice' as a source of ubiquitous green cells. *FEBS Letters*, 407(3), pp.313–319.

Oshima, M. et al., 1996. Suppression of intestinal polyposis in Apc delta716 knockout mice by inhibition of cyclooxygenase 2 (COX-2). *Cell*, 87(5), pp.803–9.

Otto, A. et al., 2008. Canonical Wnt signalling induces satellite-cell proliferation during adult skeletal muscle regeneration. *Journal of Cell Science*, 121(17), pp.2939–2950.

Ouchi, M. & Ouchi, T., 2008. Role of IFI16 in DNA damage and checkpoint. *Frontiers in bioscience : a journal and virtual library*, 13, pp.236–9.

Ozgur, A. et al., 2008. Identifying gene-disease associations using centrality on a literature mined gene-interaction network. *Bioinformatics*, 24(13), pp.i277–i285.

Pagel, C.. & Partridge, T.., 1999. Covert persistence of mdx mouse myopathy is revealed by acute and chronic effects of irradiation. *Journal of the Neurological Sciences*, 164(2), pp.103–116.

Pagel, C.N. & Partridge, T.A., 1999. Covert persistence of mdx mouse myopathy is revealed by acute and chronic effects of irradiation. *Journal of the neurological*

sciences, 164(2), pp.103–16.

Pantelouris, E.M. & Hair, J., 1970. Thymus dysgenesis in nude (nu nu) mice. *Development*, 24(3).

Pantelouris, E.M.E.M., 1968. Absence of Thymus in a Mouse Mutant. *Nature*, 217(5126), pp.370–1.

Parker, R.P., Smith, P.H.S. & Taylor, D.M., 1978. *Basic Science of Nuclear Medicine*, Edinburgh London And New York: Churchill Livingstone.

Partridge, T.A. et al., 1989. Conversion of mdx myofibres from dystrophin-negative to -positive by injection of normal myoblasts. *Nature*, 337(6203), pp.176–179.

Partridge, T.A., Grounds, M. & Sloper, J.C., 1978. Evidence of fusion between host and donor myoblasts in skeletal muscle grafts. *Nature*, 273(5660), pp.306–308.

Pasut, A., Jones, A.E. & Rudnicki, M.A., 2013. Isolation and Culture of Individual Myofibers and their Satellite Cells from Adult Skeletal Muscle. *Journal of Visualized Experiments*, (73), pp.e50074–e50074.

Pateras, I.S. et al., 2015. The DNA damage response and immune signaling alliance: Is it good or bad? Nature decides when and where. *Pharmacology & Therapeutics*, 154, pp.36–56.

Pazhanisamy, S.K. et al., 2011. NADPH oxidase inhibition attenuates total body irradiation-induced haematopoietic genomic instability. *Mutagenesis*, 26(3), pp.431–435.

Pichavant, C. et al., 2011. Current Status of Pharmaceutical and Genetic Therapeutic Approaches to Treat DMD. *Molecular Therapy*, 19(5), pp.830–840.

Podsakoff, G., Wong, K.K. & Chatterjee, S., 1994. Efficient gene transfer into nondividing cells by adeno-associated virus-based vectors. *Journal of virology*,

68(9), pp.5656–66.

Pola, R. et al., 2003. Postnatal recapitulation of embryonic hedgehog pathway in response to skeletal muscle ischemia. *Circulation*, 108(4), pp.479–85.

Pollard, M. & Luckert, P.H., 1981. Effect of indomethacin on intestinal tumors induced in rats by the acetate derivative of dimethylnitrosamine. *Science (New York, N.Y.)*, 214(4520), pp.558–9.

Pollard, M. & Luckert, P.H., 1980. Indomethacin treatment of rats with dimethylhydrazine-induced intestinal tumors. *Cancer treatment reports*, 64(12), pp.1323–7.

Ponnaiya, B., Cornforth, M.N. & Ullrich, R.L., 1997. Radiation-induced chromosomal instability in BALB/c and C57BL/6 mice: the difference is as clear as black and white. *Radiation research*, 147(2), pp.121–5.

Pradere, J.-P., Dapito, D.H. & Schwabe, R.F., 2014. The Yin and Yang of Toll-like receptors in cancer. *Oncogene*, 33(27), pp.3485–3495.

Prise, K.M. et al., 1998. Studies of bystander effects in human fibroblasts using a charged particle microbeam. *International journal of radiation biology*, 74(6), pp.793–8.

Quinlan, J.G. et al., 1995. Radiation inhibition of mdx mouse muscle regeneration: Dose and age factors. *Muscle & Nerve*, 18(2), pp.201–206.

Quinlan, J.G. et al., 1997. Regeneration-blocked mdx muscle: in vivo model for testing treatments. *Muscle & Nerve*, 20(8), pp.1016–1023.

Rakoff-Nahoum, S. & Medzhitov, R., 2007. Regulation of Spontaneous Intestinal Tumorigenesis Through the Adaptor Protein MyD88. *Science*, 317(5834), pp.124–127.

Raper, S.E. et al., 2003. Fatal systemic inflammatory response syndrome in a ornithine transcarbamylase deficient patient following adenoviral gene transfer. *Molecular Genetics and Metabolism*, 80(1–2), pp.148–158.

Ratikan, J.A. et al., 2015. Radiation takes its Toll. *Cancer Letters*, 368(2), pp.238–245.

Reinig, A.M., Mirzaei, S. & Berlau, D.J., 2017. Advances in the Treatment of Duchenne Muscular Dystrophy: New and Emerging Pharmacotherapies. *Pharmacotherapy: The Journal of Human Pharmacology and Drug Therapy*, 37(4), pp.492–499.

Reisz, J.A. et al., 2014. Effects of ionizing radiation on biological molecules--mechanisms of damage and emerging methods of detection. *Antioxidants & redox signaling*, 21(2), pp.260–92.

Relaix, F. & Zammit, P.S., 2012. Satellite cells are essential for skeletal muscle regeneration: the cell on the edge returns centre stage. *Development*, 139(16), pp.2845–2856.

Reuter, S. et al., 2010. Oxidative stress, inflammation, and cancer: How are they linked? *Free Radical Biology and Medicine*, 49(11), pp.1603–1616.

Revesz, L., 1956. Effect of Tumour Cells killed by X-rays upon the Growth of Admixed Viable Cells. *Nature*, 178, pp.1391–1392.

Ricotti, V. et al., 2016. Safety, Tolerability, and Pharmacokinetics of SMT C1100, a 2-Arylbenzoxazole Utrophin Modulator, following Single- and Multiple-Dose Administration to Pediatric Patients with Duchenne Muscular Dystrophy I. Choonara, ed. *PLOS ONE*, 11(4), p.e0152840.

Robbins, M.E. et al., 2002. Radiation-induced kidney injury: a role for chronic oxidative stress? *Micron (Oxford, England : 1993)*, 33(2), pp.133–41.

Robertson, T.A., Grounds, M.D. & Papadimitriou, J.M., 1992. Elucidation of aspects of murine skeletal muscle regeneration using local and whole body irradiation. *Journal of anatomy*, 181 (Pt 2)(Pt 2), pp.265–76.

Roderick, T.H., 1963. The Response of Twenty-Seven Inbred Strains of Mice to Daily Doses of Whole-Body X-Irradiation. *Radiation Research*, 20(4), p.631.

Rodier, F. et al., 2009. Persistent DNA damage signalling triggers senescence-associated inflammatory cytokine secretion. *Nature Cell Biology*, 11(8), pp.973–979.

Rosenblatt, J.D. & Parry, D.J., 1993. Adaptation of rat extensor digitorum longus muscle to gamma irradiation and overload. *Pflugers Archiv : European journal of physiology*, 423(3–4), pp.255–64.

Le Roux, I. et al., 2015. Numb is required to prevent p53-dependent senescence following skeletal muscle injury. *Nature Communications*, 6(1), p.8528.

Rybalko, V. et al., 2015. The Development of Macrophage-Mediated Cell Therapy to Improve Skeletal Muscle Function after Injury A. Musaro, ed. *PLOS ONE*, 10(12), p.e0145550.

Ryoo, H.D., Gorenc, T. & Steller, H., 2004. Apoptotic Cells Can Induce Compensatory Cell Proliferation through the JNK and the Wingless Signaling Pathways. *Developmental Cell*, 7(4), pp.491–501.

Rzeszowska-Wolny, J. et al., 2009. X-irradiation and bystander effects induce similar changes of transcript profiles in most functional pathways in human melanoma cells. *DNA Repair*, 8(6), pp.732–738.

Sacco, A. et al., 2008. Self-renewal and expansion of single transplanted muscle stem cells. *Nature*, 456(7221), pp.502–506.

Saha, B. et al., 2010a. Gene modulation and immunoregulatory roles of Interferon?? *Cytokine*, 50(1), pp.1–14.

Saha, B. et al., 2010b. Gene modulation and immunoregulatory roles of Interferonγ. *Cytokine*, 50(1), pp.1–14.

Sampaolesi, M. et al., 2003. Cell Therapy of -Sarcoglycan Null Dystrophic Mice Through Intra-Arterial Delivery of Mesoangioblasts. *Science*, 301(5632), pp.487–492.

Sampaolesi, M. et al., 2006. Mesoangioblast stem cells ameliorate muscle function in dystrophic dogs. *Nature*, 444(7119), pp.574–579.

Santana, P. et al., 1996. Acid sphingomyelinase-deficient human lymphoblasts and mice are defective in radiation-induced apoptosis. *Cell*, 86(2), pp.189–99.

Sauer, J.-D. et al., 2011. The N-Ethyl-N-Nitrosourea-Induced Goldenticket Mouse Mutant Reveals an Essential Function of Sting in the In Vivo Interferon Response to Listeria monocytogenes and Cyclic Dinucleotides. *Infection and Immunity*, 79(2), pp.688–694.

Scardoni, G. & Laudanna, C., 2012. Network centralities for Cytoscape Centralities. *Bioinformatics*, pp.1–8.

Scardoni, G., Petterlini, M. & Laudanna, C., 2009. Analyzing biological network parameters with CentiScaPe. *Bioinformatics (Oxford, England)*, 25(21), pp.2857–9.

Schiechl, G. et al., 2011. Tumor development in murine ulcerative colitis depends on MyD88 signaling of colonic F4/80+CD11bhighGr1low macrophages. *Journal of Clinical Investigation*, 121(5), pp.1692–1708.

Schuster-Gossler, K., Cordes, R. & Gossler, A., 2007. Premature myogenic

differentiation and depletion of progenitor cells cause severe muscle hypotrophy in Delta1 mutants. *Proceedings of the National Academy of Sciences of the United States of America*, 104(2), pp.537–42.

Seale, P. et al., 2000. Pax7 is required for the specification of myogenic satellite cells. *Cell*, 102(6), pp.777–786.

Serrano, A.L. et al., 2008. Interleukin-6 Is an Essential Regulator of Satellite Cell-Mediated Skeletal Muscle Hypertrophy. *Cell Metabolism*, 7(1), pp.33–44.

Shan, Y.-X. et al., 2007. Ionizing radiation stimulates secretion of pro-inXammatory cytokines: dose–response relationship, mechanisms and implications. *Radiat Environ Biophys*, 46, pp.21–29.

Sharpless, N.E. & Sherr, C.J., 2015. Forging a signature of in vivo senescence. *Nature Reviews Cancer*, 15(7), pp.397–408.

Shelton, D.N. et al., 1999. Microarray analysis of replicative senescence. *Current Biology*, 9(17), pp.939–945.

Sherwood, R.I. et al., 2004. Isolation of adult mouse myogenic progenitors: Functional heterogeneity of cells within and engrafting skeletal muscle. *Cell*, 119(4), pp.543–554.

Shiloh, Y., 2006. The ATM-mediated DNA-damage response: taking shape. *Trends in Biochemical Sciences*, 31(7), pp.402–410.

Silva-Barbosa, S.D. et al., 2008. Human Myoblast Engraftment Is Improved in Laminin-Enriched Microenvironment. *Transplantation*, 85(4), pp.566–575.

da Silva, M.R., Hongwu Ma & An-Ping Zeng, 2008. Centrality, Network Capacity, and Modularity as Parameters to Analyze the Core-Periphery Structure in Metabolic Networks. *Proceedings of the IEEE*, 96(8), pp.1411–1420.

Singh, A. & Singh, H., 1983. Time-scale and nature of radiation-biological damage: Approaches to radiation protection and post-irradiation therapy. *Progress in Biophysics and Molecular Biology*, 39(C), pp.69–107.

Skuk, D. et al., 2006. Dystrophin Expression in Muscles of Duchenne Muscular Dystrophy Patients After High-Density Injections of Normal Myogenic Cells. *Journal of Neuropathology and Experimental Neurology*, 65(4), pp.371–386.

Skuk, D. et al., 2004. Dystrophin expression in myofibers of Duchenne muscular dystrophy patients following intramuscular injections of normal myogenic cells. *Molecular therapy : the journal of the American Society of Gene Therapy*, 9(3), pp.475–82.

Skuk, D. et al., 2007. First test of a "high-density injection" protocol for myogenic cell transplantation throughout large volumes of muscles in a Duchenne muscular dystrophy patient: eighteen months follow-up. *Neuromuscular Disorders*, 17(1), pp.38–46.

Snijders, A.M. et al., 2012. Genetic Differences in Transcript Responses to Low-Dose Ionizing Radiation Identify Tissue Functions Associated with Breast Cancer Susceptibility Y. Li, ed. *PLoS ONE*, 7(10), p.e45394.

Snow, M.H., 1978. An autoradiographic study of satellite cell differentiation into regenerating myotubes following transplantation of muscles in young rats. *Cell and tissue research*, 186(3), pp.535–40.

Spychalowicz, A. et al., 2012. Novel therapeutic approaches in limiting oxidative stress and inflammation. *Current pharmaceutical biotechnology*, 13(13), pp.2456–66.

Srivastava, D. & DeWitt, N., 2016. In Vivo Cellular Reprogramming: The Next

Generation. *Cell*, 166(6), pp.1386–1396.

Stark, G., 1991. The effect of ionizing radiation on lipid membranes. *Biochimica et Biophysica Acta (BBA)-Reviews on …*, 1071(2), pp.103–122.

Stevens, C. & La Thangue, N.B., 2004. The emerging role of E2F-1 in the DNA damage response and checkpoint control. *DNA Repair*, 3(8–9), pp.1071–1079.

Stewart, G.S. et al., 1999. The DNA double-strand break repair gene hMRE11 is mutated in individuals with an ataxia-telangiectasia-like disorder. *Cell*, 99(6), pp.577–87.

Stockdale, F.E. & Holtzer, H., 1961. DNA synthesis and myogenesis. *Experimental Cell Research*, 520(3), pp.508–520.

Storek, K.M. et al., 2015. cGAS and Ifi204 Cooperate To Produce Type I IFNs in Response to *Francisella* Infection. *The Journal of Immunology*, 194(7), pp.3236–3245.

Straface, G. et al., 2009. Sonic hedgehog regulates angiogenesis and myogenesis during post-natal skeletal muscle regeneration. *Journal of cellular and molecular medicine*, 13(8B), pp.2424–35.

Subramanian, A. et al., 2005. Gene set enrichment analysis: a knowledge-based approach for interpreting genome-wide expression profiles. *Proceedings of the National Academy of Sciences of the United States of America*, 102(43), pp.15545–50.

Summermatter, S. et al., 2017. Blockade of Metallothioneins 1 and 2 Increases Skeletal Muscle Mass and Strength. *Molecular and Cellular Biology*, 37(5), pp.e00305-16.

Sun, H. et al., 2007. Stra13 regulates satellite cell activation by antagonizing Notch

signaling. *The Journal of cell biology*, 177(4), pp.647–57.

Surh, C.D. & Sprent, J., 1994. T-cell apoptosis detected in situ during positive and negative selection in the thymus. *Nature*, 372(6501), pp.100–103.

Swann, J.B. et al., 2008. Demonstration of inflammation-induced cancer and cancer immunoediting during primary tumorigenesis. *Proceedings of the National Academy of Sciences of the United States of America*, 105(2), pp.652–6.

Szklarczyk, D. et al., 2015. STRING v10: protein-protein interaction networks, integrated over the tree of life. *Nucleic Acids Research*, 43(D1), pp.D447–D452.

Szklarczyk, D. et al., 2017. The STRING database in 2017: quality-controlled protein–protein association networks, made broadly accessible. *Nucleic Acids Research*, 45(D1), pp.D362–D368.

Tabeta, K. et al., 2004. Toll-like receptors 9 and 3 as essential components of innate immune defense against mouse cytomegalovirus infection. *Proceedings of the National Academy of Sciences of the United States of America*, 101(10), pp.3516–21.

Tanaka, S.S. et al., 2000. The mouse homolog of Drosophila Vasa is required for the development of male germ cells. *Genes & development*, 14(7), pp.841–53.

Tanaka, Y. & Chen, Z.J., 2012. STING specifies IRF3 phosphorylation by TBK1 in the cytosolic DNA signaling pathway. *Science signaling*, 5(214), p.ra20.

Teresa Pinto, A. et al., 2016. Ionizing radiation modulates human macrophages towards a pro-inflammatory phenotype preserving their pro-invasive and pro-angiogenic capacities. *Scientific reports*, 6, p.18765.

Thakali, K.M. et al., 2012. *Muscle: Fundamental Biology and Mechanisms of Disease* 1st ed. K. K. Griendling et al., eds., Academic Press.

Thaper, D. et al., 2017. Targeting Lyn regulates Snail family shuttling and inhibits metastasis. *Oncogene*, 36(28), pp.3964–3975.

Thompson, L.H., 2012. Recognition, signaling, and repair of DNA double-strand breaks produced by ionizing radiation in mammalian cells: The molecular choreography. *Mutation Research - Reviews in Mutation Research*, 751(2), pp.158–246.

Tidball, J.G., 2017. Regulation of muscle growth and regeneration by the immune system. *Nature Publishing Group*, 17.

Tinsley, J. et al., 1998. Expression of full-length utrophin prevents muscular dystrophy in mdx mice. *Nature Medicine*, 4(12), pp.1441–1444.

Tinsley, J.M. et al., 2011. Daily Treatment with SMTC1100, a Novel Small Molecule Utrophin Upregulator, Dramatically Reduces the Dystrophic Symptoms in the mdx Mouse P. Dent, ed. *PLoS ONE*, 6(5), p.e19189.

Torrente, Y. et al., 2004. Human circulating AC133+ stem cells restore dystrophin expression and ameliorate function in dystrophic skeletal muscle. *Journal of Clinical Investigation*, 114(2), pp.182–195.

Toth, K.G. et al., 2011. IL-6 induced STAT3 signalling is associated with the proliferation of human muscle satellite cells following acute muscle damage J. Smith, ed. *PLoS ONE*, 6(3), p.e17392.

Tremblay, J.P. et al., 1993. Results of a triple blind clinical study of myoblast transplantations without immunosuppressive treatment in young boys with Duchenne muscular dystrophy. *Cell Transplantation*, 2(2), pp.99–112.

Tseng, A.-S. et al., 2007. Apoptosis is required during early stages of tail regeneration in Xenopus laevis. *Developmental biology*, 301(1), pp.62–9.

Tsuboi, K., Sugimoto, Y. & Ichikawa, A., 2002. Prostanoid receptor subtypes. *Prostaglandins and Other Lipid Mediators*, 68–69, pp.535–556.

Turrens, J.F. et al., 1991. Mitochondrial generation of oxygen radicals during reoxygenation of ischemic tissues. *Free radical research communications*, 12–13 Pt 2, pp.681–9.

Uronis, J.M. et al., 2009. Modulation of the Intestinal Microbiota Alters Colitis-Associated Colorectal Cancer Susceptibility S. Bereswill, ed. *PLoS ONE*, 4(6), p.e6026.

Vasyutina, E. et al., 2007. RBP-J (Rbpsuh) is essential to maintain muscle progenitor cells and to generate satellite cells. *Proceedings of the National Academy of Sciences*, 104(11), pp.4443–4448.

Venable, J.H., 1966. Morphology of the cells of normal, testosterone-deprived and testosterone-stimulated levator ani muscles. *American Journal of Anatomy*, 119(2), pp.271–301.

Vénéreau, E., Ceriotti, C. & Bianchi, M.E., 2015. DAMPs from cell death to new life. *Frontiers in Immunology*, 6(AUG), p.422.

Volonte, D., Liu, Y. & Galbiati, F., 2004. The modulation of caveolin-1 expression controls satellite cell activation during muscle repair.

Waddell, W.R. & Loughry, R.W., 1983. Sulindac for polyposis of the colon. *Journal of surgical oncology*, 24(1), pp.83–7.

Wakeford, S., Watt, D.J. & Partridge, T.A., 1991. X-Irradiation improves mdx mouse muscle as a model of myofiber loss in DMD. *Muscle & Nerve*, 14(1), pp.42–50.

Waltes, R. et al., 2009. Human RAD50 Deficiency in a Nijmegen Breakage Syndrome-like Disorder. *The American Journal of Human Genetics*, 84(5), pp.605–616.

Wang, X. et al., 2008. Effects of Interleukin-6, Leukemia Inhibitory Factor, and Ciliary Neurotrophic Factor on the Proliferation and Differentiation of Adult Human Myoblasts. *Cellular and Molecular Neurobiology*, 28(1), pp.113–124.

Ward, J.F., 1994. DNA Damage as the Cause of Ionizing Radiation-induced Gene Activation. *J. F. Ward Source: Radiation Research RADIATION RESEARCH*, 138(138), pp.85–88.

Welch, E.M. et al., 2007. PTC124 targets genetic disorders caused by nonsense mutations. *Nature*, 447(7140), pp.87–91.

Weller, B. et al., 1991. Major alteration of the pathological phenotype in gamma irradiated mdx soleus muscles. *Journal of neuropathology and experimental neurology*, 50(4), pp.419–31.

Wen, Z., Zhong, Z. & Darnell, J.E., 1995. Maximal Activation of Transcription by Statl and Stat3 Requires Both Tyrosine and Serine Phosphorylation. *Cell*, 82, pp.241–250.

White, J., Davies, M. & Grounds, M., 2001. Leukaemia inhibitory factor increases myoblast replication and survival and affects extracellular matrix production: combined in vivo and in vitro studies in post-natal skeletal muscle. *Cell and Tissue Research*, 306(1), pp.129–141.

Wozniak, A.C. & Anderson, J.E., 2007. Nitric oxide-dependence of satellite stem cell activation and quiescence on normal skeletal muscle fibers. *Developmental dynamics : an official publication of the American Association of Anatomists*, 236(1), pp.240–50.

Wu, J. & Chen, Z.J., 2014. Innate Immune Sensing and Signaling of Cytosolic Nucleic Acids. *Annu. Rev. Immunol*, 32, pp.461–88.

Xiao, F. et al., 2011. Oncostatin M inhibits myoblast differentiation and regulates muscle regeneration. *Cell Research*, 21(2), pp.350–364.

Yaffe, D. & Feldman, M., 1965. The formation of hybrid multinucleated muscle fibers from myoblasts of different genetic origin. *Developmental Biology*, 11(2), pp.300–317.

Yaffe, D. & Saxel, O., 1977. Serial passaging and differentiation of myogenic cells isolated from dystrophic mouse muscle. *Nature*, 270(5639), pp.725–727.

Yamamori, T. et al., 2012. Ionizing radiation induces mitochondrial reactive oxygen species production accompanied by upregulation of mitochondrial electron transport chain function and mitochondrial content under control of the cell cycle checkpoint. *Free Radical Biology and Medicine*, 53(2), pp.260–270.

Yang, H. et al., 2011. Oxidative stress and diabetes mellitus. *Clinical chemistry and laboratory medicine*, 49(11), pp.1773–82.

Yokoyama, U. et al., 2013. The prostanoid EP4 receptor and its signaling pathway. *Pharmacological reviews*, 65(3), pp.1010–52.

Yu, L., Wang, L. & Chen, S., 2010. Endogenous toll-like receptor ligands and their biological significance. *Journal of Cellular and Molecular Medicine*, 14(11), pp.2592–2603.

Zammit, P.S. & Beauchamp, J.R., 2001. The skeletal muscle satellite cell: stem cell or son of stem cell? *Differentiation*, 68(4–5), pp.193–204.

Zhang, W. et al., 2016. Role of Metallothionein in Post-Burn Inflammation. *Inflammation*, 39(2), pp.768–774.

Zhao, X. et al., 2006. Caspase-3-dependent activation of calcium-independent phospholipase A 2 enhances cell migration in non-apoptotic ovarian cancer

cells. *Journal of Biological Chemistry*, 281(39), pp.29357–29368.

Zietman, A.L. et al., 1991. A comparative study on the xenotransplantability of human solid tumors into mice with different genetic immune deficiencies. *International Journal of Cancer*, 47(5), pp.755–759.

Zotenko, E. et al., 2008. Why Do Hubs in the Yeast Protein Interaction Network Tend To Be Essential: Reexamining the Connection between the Network Topology and Essentiality B. Rost, ed. *PLoS Computational Biology*, 4(8), p.e1000140.

Appendix

Appendix 4.1

Appendix 4.1: Enriched GO-Terms for the top network regulators in Control vs Grafted			
GO-ID	Description	Genes in test set	corr p-value
2376	immune system process	IL10|CXCL10|IL6|PTPRC|ITGAM|CCL5|IRF1|CCL2|TLR4	1.21 E-10
6952	defense response	IL10|CXCL10|IL6|PTPRC|CCL5|CCL2|TLR4|CD44	1.81 E-10
48522	positive regulation of cellular process	IL10|CXCL10|IL6|PTPRC|STAT1|CCL5|IRF1|CCL2|TLR4|CD44	9.79 E-10
6955	immune response	IL10|CXCL10|IL6|PTPRC|CCL5|CCL2|TLR4	2.01 E-09
48518	positive regulation of biological process	IL10|CXCL10|IL6|PTPRC|STAT1|CCL5|IRF1|CCL2|TLR4|CD44	2.01 E-09
2682	regulation of immune system process	IL10|CXCL10|IL6|PTPRC|CCL5|TLR4|CD44	2.46 E-09
48583	regulation of response to stimulus	IL10|CXCL10|IL6|PTPRC|CCL5|TLR4|CD44	6.00 E-09
6954	inflammatory response	CXCL10|IL6|CCL5|CCL2|TLR4|CD44	9.85 E-09
50896	response to stimulus	IL10|CXCL10|IL6|PTPRC|ITGAM|STAT1|CCL5|CCL2|TLR4|CD44	2.47 E-08
51239	regulation of multicellular organismal process	IL10|CXCL10|IL6|PTPRC|CCL5|IRF1|CCL2|TLR4	4.46 E-08

42127	regulation of cell proliferation	IL10|CXCL10|IL6|PTPRC|STAT1|CCL2|TLR4	7.74 E-08
6950	response to stress	IL10|CXCL10|IL6|PTPRC|CCL5|CCL2|TLR4|CD44	1.18 E-07
9611	response to wounding	CXCL10|IL6|CCL5|CCL2|TLR4|CD44	1.18 E-07
8284	positive regulation of cell proliferation	CXCL10|IL6|PTPRC|STAT1|CCL2|TLR4	1.44 E-07
42035	regulation of cytokine biosynthetic process	IL10|IL6|IRF1|TLR4	2.34 E-07
50730	regulation of peptidyl-tyrosine phosphorylation	IL6|PTPRC|TLR4|CD44	3.11 E-07
43410	positive regulation of MAPKKK cascade	IL6|PTPRC|TLR4|CD44	6.44 E-07
51707	response to other organism	IL10|IL6|PTPRC|STAT1|TLR4	1.12 E-06
10647	positive regulation of cell communication	IL6|PTPRC|CCL2|TLR4|CD44	1.12 E-06
43065	positive regulation of apoptosis	IL10|PTPRC|STAT1|TLR4|CD44	1.62 E-06
43068	positive regulation of programmed cell death	IL10|PTPRC|STAT1|TLR4|CD44	1.63 E-06
10942	positive regulation of cell death	IL10|PTPRC|STAT1|TLR4|CD44	1.72 E-06
42981	regulation of apoptosis	IL10|IL6|PTPRC|STAT1|TLR4|CD44	1.78 E-06

43067	regulation of programmed cell death	IL10|IL6|PTPRC|STAT1|TLR4|CD44	1.85 E-06
10941	regulation of cell death	IL10|IL6|PTPRC|STAT1|TLR4|CD44	1.88 E-06
10740	positive regulation of intracellular protein kinase cascade	IL6|PTPRC|TLR4|CD44	1.88 E-06
70374	positive regulation of ERK1 and ERK2 cascade	IL6|TLR4|CD44	1.88 E-06
6935	chemotaxis	CXCL10|ITGAM|CCL5|CCL2	1.88 E-06
42330	taxis	CXCL10|ITGAM|CCL5|CCL2	1.88 E-06
32655	regulation of interleukin-12 production	IL10|IRF1|TLR4	1.99 E-06
9607	response to biotic stimulus	IL10|IL6|PTPRC|STAT1|TLR4	1.99 E-06
9605	response to external stimulus	CXCL10|ITGAM|STAT1|CCL5|CCL2	2.72 E-06
43408	regulation of MAPKKK cascade	IL6|PTPRC|TLR4|CD44	3.66 E-06
40011	locomotion	CXCL10|ITGAM|CCL5|CCL2|CD44	3.67 E-06
51704	multi-organism process	IL10|IL6|PTPRC|STAT1|TLR4	3.71 E-06
45428	regulation of nitric oxide biosynthetic process	IL10|IL6|TLR4	3.71 E-06
70372	regulation of ERK1 and ERK2 cascade	IL6|TLR4|CD44	3.71 E-06
30595	leukocyte chemotaxis	ITGAM|CCL5|CCL2	3.71 E-06

60326	cell chemotaxis	ITGAM|CCL5|CCL2	4.37 E-06
10604	positive regulation of macromolecule metabolic process	IL10|IL6|PTPRC|IRF1|TLR4|CD44	4.37 E-06
1817	regulation of cytokine production	IL10|IL6|IRF1|TLR4	4.76 E-06
9967	positive regulation of signal transduction	IL6|PTPRC|TLR4|CD44	5.02 E-06
51249	regulation of lymphocyte activation	IL10|IL6|PTPRC|TLR4	5.04 E-06
23056	positive regulation of signaling process	IL6|PTPRC|TLR4|CD44	5.05 E-06
30888	regulation of B cell proliferation	IL10|PTPRC|TLR4	5.50 E-06
32101	regulation of response to external stimulus	IL10|CXCL10|CCL5|TLR4	6.85 E-06
9893	positive regulation of metabolic process	IL10|IL6|PTPRC|IRF1|TLR4|CD44	6.85 E-06
2694	regulation of leukocyte activation	IL10|IL6|PTPRC|TLR4	6.85 E-06
48247	lymphocyte chemotaxis	CCL5|CCL2	6.87 E-06
1932	regulation of protein amino acid phosphorylation	IL6|PTPRC|TLR4|CD44	6.88 E-06
50865	regulation of cell activation	IL10|IL6|PTPRC|TLR4	7.39 E-06

50731	positive regulation of peptidyl-tyrosine phosphorylation	IL6|TLR4|CD44	7.59E-06
7610	behavior	CXCL10|IL6|ITGAM|CCL5|CCL2	7.59E-06
10627	regulation of intracellular protein kinase cascade	IL6|PTPRC|TLR4|CD44	9.45E-06
50900	leukocyte migration	ITGAM|CCL5|CCL2	9.55E-06
35468	positive regulation of signaling pathway	IL6|PTPRC|TLR4|CD44	1.35E-05
31399	regulation of protein modification process	IL6|PTPRC|TLR4|CD44	1.46E-05
50776	regulation of immune response	IL10|IL6|PTPRC|TLR4	1.54E-05
42221	response to chemical stimulus	CXCL10|ITGAM|STAT1|CCL5|CCL2|TLR4	1.56E-05
48584	positive regulation of response to stimulus	CXCL10|PTPRC|CCL5|TLR4	1.63E-05
50864	regulation of B cell activation	IL10|PTPRC|TLR4	1.75E-05
45321	leukocyte activation	PTPRC|ITGAM|IRF1|TLR4	1.81E-05
2684	positive regulation of immune system process	CXCL10|IL6|PTPRC|TLR4	2.00E-05
80134	regulation of response to stress	IL10|CCL5|TLR4|CD44	2.07E-05

7626	locomotory behavior	CXCL10|ITGAM|CCL5|CCL2	2.14 E-05
70887	cellular response to chemical stimulus	ITGAM|STAT1|CCL5|CCL2	2.47 E-05
1775	cell activation	PTPRC|ITGAM|IRF1|TLR4	2.47 E-05
45348	positive regulation of MHC class II biosynthetic process	IL10|TLR4	2.47 E-05
51240	positive regulation of multicellular organismal process	IL6|CCL5|CCL2|TLR4	2.51 E-05
16477	cell migration	ITGAM|CCL5|CCL2|CD44	2.51 E-05
50794	regulation of cellular process	IL10|CXCL10|IL6|PTPRC|STAT1|CCL5|IRF1|CCL2|TLR4|CD44	2.82 E-05
32103	positive regulation of response to external stimulus	CXCL10|CCL5|TLR4	2.85 E-05
45346	regulation of MHC class II biosynthetic process	IL10|TLR4	3.23 E-05
51716	cellular response to stimulus	ITGAM|STAT1|CCL5|CCL2|TLR4	3.72 E-05
51674	localization of cell	ITGAM|CCL5|CCL2|CD44	3.86 E-05
48870	cell motility	ITGAM|CCL5|CCL2|CD44	3.86 E-05
32689	negative regulation of interferon-gamma production	IL10|TLR4	4.08 E-05

50789	regulation of biological process	IL10|CXCL10|IL6|PTPRC|STAT1|CCL5|IRF1|CCL2|TLR4|CD44	4.16E-05
23036	initiation of signal transduction	IL6|STAT1|CCL2	4.43E-05
23038	signal initiation by diffusible mediator	IL6|STAT1|CCL2	4.43E-05
23049	signal initiation by protein/peptide mediator	IL6|STAT1|CCL2	4.43E-05
19221	cytokine-mediated signaling pathway	IL6|STAT1|CCL2	4.43E-05
32944	regulation of mononuclear cell proliferation	IL10|PTPRC|TLR4	5.06E-05
50670	regulation of lymphocyte proliferation	IL10|PTPRC|TLR4	5.06E-05
1934	positive regulation of protein amino acid phosphorylation	IL6|TLR4|CD44	5.06E-05
70663	regulation of leukocyte proliferation	IL10|PTPRC|TLR4	5.34E-05
50727	regulation of inflammatory response	IL10|CCL5|TLR4	6.17E-05
65007	biological regulation	IL10|CXCL10|IL6|PTPRC|STAT1|CCL5|IRF1|CCL2|TLR4|CD44	6.73E-05
32844	regulation of homeostatic process	PTPRC|CCL5|CD44	6.77E-05

32268	regulation of cellular protein metabolic process	IL6|PTPRC|TLR4|CD44	6.77E-05
32720	negative regulation of tumor necrosis factor production	IL10|TLR4	6.77E-05
51251	positive regulation of lymphocyte activation	IL6|PTPRC|TLR4	6.96E-05
31325	positive regulation of cellular metabolic process	IL6|PTPRC|IRF1|TLR4|CD44	7.58E-05
42325	regulation of phosphorylation	IL6|PTPRC|TLR4|CD44	7.58E-05
42036	negative regulation of cytokine biosynthetic process	IL10|IL6	7.78E-05
48585	negative regulation of response to stimulus	IL10|PTPRC|CD44	7.88E-05
2696	positive regulation of leukocyte activation	IL6|PTPRC|TLR4	7.92E-05
42327	positive regulation of phosphorylation	IL6|TLR4|CD44	7.92E-05
60255	regulation of macromolecule metabolic process	IL10|IL6|PTPRC|STAT1|IRF1|TLR4|CD44	7.92E-05

31401	positive regulation of protein modification process	IL6|TLR4|CD44	7.92 E-05
10562	positive regulation of phosphorus metabolic process	IL6|TLR4|CD44	7.92 E-05
45937	positive regulation of phosphate metabolic process	IL6|TLR4|CD44	7.92 E-05
61138	morphogenesis of a branching epithelium	IL10|IL6|CD44	7.92 E-05
19220	regulation of phosphate metabolic process	IL6|PTPRC|TLR4|CD44	7.92 E-05
51174	regulation of phosphorus metabolic process	IL6|PTPRC|TLR4|CD44	7.92 E-05
6928	cellular component movement	ITGAM|CCL5|CCL2|CD44	8.01 E-05
10646	regulation of cell communication	IL6|PTPRC|CCL2|TLR4|CD44	8.13 E-05
23052	signaling	CXCL10|IL6|PTPRC|ITGAM|STAT1|CCL2|TLR4|CD44	8.13 E-05
50867	positive regulation of cell activation	IL6|PTPRC|TLR4	8.13 E-05
48519	negative regulation of biological process	IL10|CXCL10|IL6|PTPRC|TLR4|CD44	8.71 E-05
42110	T cell activation	PTPRC|ITGAM|IRF1	8.84 E-05

51179	localization	CXCL10|IL6|PTPRC|ITGAM|CCL5|CCL2|CD44	9.82E-05
32642	regulation of chemokine production	IL6|TLR4	1.04E-04
51246	regulation of protein metabolic process	IL6|PTPRC|TLR4|CD44	1.05E-04
33138	positive regulation of peptidyl-serine phosphorylation	IL6|CD44	1.16E-04
7159	leukocyte cell-cell adhesion	PTPRC|ITGAM	1.16E-04
31323	regulation of cellular metabolic process	IL10|IL6|PTPRC|STAT1|IRF1|TLR4|CD44	1.18E-04
1763	morphogenesis of a branching structure	IL10|IL6|CD44	1.21E-04
31347	regulation of defense response	IL10|CCL5|TLR4	1.51E-04
32270	positive regulation of cellular protein metabolic process	IL6|TLR4|CD44	1.59E-04
7165	signal transduction	CXCL10|IL6|PTPRC|STAT1|CCL2|TLR4|CD44	1.60E-04
19222	regulation of metabolic process	IL10|IL6|PTPRC|STAT1|IRF1|TLR4|CD44	1.73E-04
30593	neutrophil chemotaxis	ITGAM|CCL2	1.73E-04
71222	cellular response to lipopolysaccharide	STAT1|TLR4	1.89E-04

51247	positive regulation of protein metabolic process	IL6|TLR4|CD44	2.02E-04
33135	regulation of peptidyl-serine phosphorylation	IL6|CD44	2.05E-04
9966	regulation of signal transduction	IL6|PTPRC|TLR4|CD44	2.13E-04
45429	positive regulation of nitric oxide biosynthetic process	IL6|TLR4	2.19E-04
23051	regulation of signaling process	IL6|PTPRC|TLR4|CD44	2.19E-04
23060	signal transmission	CXCL10|IL6|PTPRC|STAT1|CCL2|TLR4|CD44	2.40E-04
23046	signaling process	CXCL10|IL6|PTPRC|STAT1|CCL2|TLR4|CD44	2.40E-04
35467	negative regulation of signaling pathway	PTPRC|TLR4|CD44	2.40E-04
9617	response to bacterium	IL10|STAT1|TLR4	2.46E-04
31644	regulation of neurological system process	IL10|IL6|CCL2	2.56E-04
71219	cellular response to molecule of bacterial origin	STAT1|TLR4	2.69E-04
30890	positive regulation of B cell proliferation	PTPRC|TLR4	2.86E-04
46635	positive regulation of alpha-beta T cell activation	IL6|PTPRC	2.86E-04

46649	lymphocyte activation	PTPRC|ITGAM|IRF1	2.96 E-04
42098	T cell proliferation	PTPRC|ITGAM	3.49 E-04
9987	cellular process	CXCL10|IL6|PTPRC|ITGAM|STAT1|CCL5|IRF1|CCL2|TLR4|CD44	3.75 E-04
10628	positive regulation of gene expression	IL6|IRF1|TLR4|CD44	3.84 E-04
1818	negative regulation of cytokine production	IL10|TLR4	3.87 E-04
32680	regulation of tumor necrosis factor production	IL10|TLR4	3.87 E-04
45859	regulation of protein kinase activity	IL6|PTPRC|TLR4	3.89 E-04
10468	regulation of gene expression	IL10|IL6|STAT1|IRF1|TLR4|CD44	4.01 E-04
45935	positive regulation of nucleobase, nucleoside, nucleotide and nucleic acid metabolic process	IL6|PTPRC|IRF1|TLR4	4.11 E-04
51171	regulation of nitrogen compound metabolic process	IL10|IL6|PTPRC|STAT1|IRF1|TLR4	4.20 E-04
43549	regulation of kinase activity	IL6|PTPRC|TLR4	4.33 E-04
45582	positive regulation of T cell differentiation	IL6|PTPRC	4.39 E-04

46634	regulation of alpha-beta T cell activation	IL6|PTPRC	4.39 E-04
32649	regulation of interferon-gamma production	IL10|TLR4	4.39 E-04
51173	positive regulation of nitrogen compound metabolic process	IL6|PTPRC|IRF1|TLR4	4.48 E-04
10557	positive regulation of macromolecule biosynthetic process	IL10|IL6|IRF1|TLR4	4.50 E-04
35466	regulation of signaling pathway	IL6|PTPRC|TLR4|CD44	4.58 E-04
51338	regulation of transferase activity	IL6|PTPRC|TLR4	4.58 E-04
45621	positive regulation of lymphocyte differentiation	IL6|PTPRC	4.73 E-04
42108	positive regulation of cytokine biosynthetic process	IRF1|TLR4	4.73 E-04
2009	morphogenesis of an epithelium	IL10|IL6|CD44	4.73 E-04
10648	negative regulation of cell communication	PTPRC|TLR4|CD44	4.85 E-04
42592	homeostatic process	IL6|PTPRC|CCL2|TLR4	4.85 E-04

50777	negative regulation of immune response	IL10|PTPRC	4.87 E-04
23014	signal transmission via phosphorylation event	PTPRC|STAT1|TLR4	5.30 E-04
7243	intracellular protein kinase cascade	PTPRC|STAT1|TLR4	5.30 E-04
2700	regulation of production of molecular mediator of immune response	PTPRC|TLR4	5.30 E-04
8283	cell proliferation	IL6|PTPRC|ITGAM	5.42 E-04
9891	positive regulation of biosynthetic process	IL10|IL6|IRF1|TLR4	5.47 E-04
50871	positive regulation of B cell activation	PTPRC|TLR4	5.47 E-04
48523	negative regulation of cellular process	IL10|IL6|PTPRC|TLR4|CD44	5.54 E-04
45597	positive regulation of cell differentiation	IL6|PTPRC|CCL5	5.54 E-04
46651	lymphocyte proliferation	PTPRC|ITGAM	5.88 E-04
51054	positive regulation of DNA metabolic process	IL6|PTPRC	5.88 E-04
32943	mononuclear cell proliferation	PTPRC|ITGAM	6.12 E-04
9628	response to abiotic stimulus	PTPRC|STAT1|CCL2	6.19 E-04

70661	leukocyte proliferation	PTPRC|ITGAM	6.33 E-04
51971	positive regulation of transmission of nerve impulse	IL6|CCL2	6.54 E-04
50795	regulation of behavior	CXCL10|IL6	6.54 E-04
50729	positive regulation of inflammatory response	CCL5|TLR4	6.79 E-04
50793	regulation of developmental process	CXCL10|IL6|PTPRC|CCL5	7.23 E-04
31646	positive regulation of neurological system process	IL6|CCL2	7.26 E-04
71216	cellular response to biotic stimulus	STAT1|TLR4	7.26 E-04
45580	regulation of T cell differentiation	IL6|PTPRC	7.48 E-04
34097	response to cytokine stimulus	STAT1|CCL5	7.48 E-04
80090	regulation of primary metabolic process	IL6|PTPRC|STAT1|IRF1|TLR4|CD44	7.98 E-04
48729	tissue morphogenesis	IL10|IL6|CD44	8.42 E-04
187	activation of MAPK activity	PTPRC|TLR4	8.59 E-04
6469	negative regulation of protein kinase activity	IL6|PTPRC	9.53 E-04
44057	regulation of system process	IL10|IL6|CCL2	9.81 E-04